

**Applications of Small Heterocycles: Oxetanes as Additives and
Cosolvents *and* Oxazolines as Linkers for Controlled Release from
Silica Nanoparticles**

by

Melissa Margaret Sprachman

B.S., The College of William and Mary, 2006

Submitted to the Graduate Faculty of

The Kenneth P. Dietrich School of Arts and Sciences in partial fulfillment

of the requirements for the degree of

Doctor of Philosophy

University of Pittsburgh

2012

UNIVERSITY OF PITTSBURGH
DIETRICH SCHOOL OF ARTS AND SCIENCES

This dissertation was presented

by

Melissa Margaret Sprachman

It was defended on

November 12, 2012

and approved by

Dr. Dennis P. Curran, Distinguished Service Professor and Bayer Professor, Department of
Chemistry

Dr. Craig S. Wilcox, Professor, Department of Chemistry

Dr. Judith C. Yang, Nickolas A. DeCecco Professor, Department of Chemical and Petroleum
Engineering

Dissertation Advisor: Dr. Peter Wipf, Distinguished University Professor, Department of
Chemistry

Copyright © by Melissa Margaret Sprachman

2012

**Applications of Small Heterocycles: Oxetanes as Additives and Cosolvents *and*
Oxazolines as Linkers for Controlled Release from Silica Nanoparticles**

Melissa Margaret Sprachman, PhD

University of Pittsburgh, 2012

In the first chapter of this dissertation, the design and synthesis of bifunctional additives and cosolvents containing an oxetane moiety are described. The use of dimeric oxetanes as additives for reactions involving organometallic agents—namely, organolithium, organozirconium, and organomagnesium reagents was studied. A dimeric bisoxetanyl ether showed promise for solvating organolithium aggregates, but dimeric oxetanyl ethers were not useful additives in hydrozirconation reactions. A bisoxetanyl sulfide is being investigated further as an additive for Grignard reactions. A bisoxetanyl sulfoxide (MMS350) was developed as a dimethylsulfoxide substitute that showed utility for enhancing the aqueous solubility of small organic molecules.

In the second chapter, efforts toward the development of agents for protection and mitigation of ionizing radiation damage are outlined. It was discovered that administration of MMS350 prolonged survival in irradiated mice. Moreover, mice given MMS350 in their drinking water had lower incidences of pulmonary fibrosis. Additional analogs of MMS350 were synthesized for further investigation of the molecular and structural requirements for successful sulfoxide-containing radiation protectors.

In the third chapter, the design and proof-of-concept study of using an oxazoline linker for functionalization and pH-dependent release of reactive oxygen species (ROS) scavengers from silica nanoparticles is discussed. pH-Dependent hydrolysis of model oxazolines was

achieved by modulating the substitution on the oxazoline moiety. Moreover, functionalized silica nanoparticles were successfully endocytosed by macrophages. Our studies have laid the groundwork for the design of covalently modified nanoparticles for delivery of ROS.

ACKNOWLEDGEMENTS

I extend my gratitude to Professor Peter Wipf for giving me the opportunity to undertake stimulating and rewarding multidisciplinary research projects. I feel quite fortunate to work for an advisor who pushes his students to their highest potential but is also accommodating of the different skills and aspirations his students possess; I admire his dedication to producing excellent science and scientists.

I would like to thank Professor Dennis Curran, Professor Craig Wilcox, and Professor Judith Yang for serving on my thesis committee—I place great value on the feedback I have received during my years in this program. I also thank Professor W. Seth Horne for serving as my proposal mentor.

During my time at the University of Pittsburgh, I have been fortunate to work with several collaborators. I thank Dr. Joel Greenberger, Dr. Michael Epperly, and Ms. Julie Goff for a successful and exciting project involving the use of bisoxetanyl sulfoxides as radiation mitigators. I also thank Dr. Erin Skoda for her role in facilitating our collaboration and for her advice and encouragement.

I am grateful to Dr. Andreas Vogt for the cellular toxicity data of MMS350 and Dr. Manuj Tandon and Dr. Q. Jane Wang for data regarding the use of MMS350 in the radiometric PKD1 inhibition assays.

I thank Dr. Amir Faraji for his preliminary studies involving the synthesis and characterization of nitroxide-functionalized silica nanoparticles. I also thank Dr. Donna Stolz

and Ms. Ming Sun at the University of Pittsburgh Center for Biological Imaging and Dr. Joel Gillespie (Director of the Department of Chemistry Materials Characterization Facility) for their assistance in characterizing silica nanoparticles. I am grateful to Dr. Valerian Kagan, Dr. Vladimir Tyurin, and Dr. Wei-Hong Feng for the EPR spectroscopy measurements and biological evaluation of the nitroxide-functionalized silica nanoparticles.

I would also like to thank Dr. Steven Geib for obtaining X-Ray structures of MMS350, Dr. Damodaran Krishnan and Ms. Sage Bowser for their excellent upkeep of the NMR facilities, and Dr. John Williams and Dr. Bhaskar Godugu for their work in the department's mass spectroscopy facilities.

I feel blessed to have worked in a stimulating and pleasant work environment. I am particularly appreciative of the helpful critiques from Dr. Maciej Walczak, who helped me hone my laboratory skills as well as my critical thinking skills. I also thank Dr. Bryan Wakefield for his help during my first years in the program. I am very much indebted to all Wipf group members (past and present) for helping to shape my experiences as both a colleague and a researcher.

I am fortunate to have worked in a lab where research runs smoothly thanks to the excellent work of dedicated staff members including Mr. Peter Chambers, Ms. Courtney Vowell, Ms. Kayla Lloyd, and Ms. Michelle Paul.

I also extend my appreciation to my first research advisor, Professor Robert Hinkle, who gave me my first laboratory opportunities at The College of William and Mary. I would not have pursued this career path if it had not been for his encouragement. Lastly, I thank my friends and my family for their unconditional love and support.

TABLE OF CONTENTS

1.0	OXETANES AS ADDITIVES AND COSOLVENTS	1
1.1	INTRODUCTION	2
1.1.1	Physical Properties of Solvents	2
	1.1.1.1 The EPD-EPA Interaction: Measures of Donating Ability	2
	1.1.1.2 Physical Properties of Oxetanes	8
1.1.2	Solvent Effects in Organometallic Reactions	10
	1.1.2.1 Consequences of Aggregation and Generation of Activated Anions	10
	1.1.2.2 The Effect of Ion-Pairing	11
	1.1.2.3 Aggregation of Organolithium Species.....	14
	1.1.2.4 .Spectroscopic Investigations of Interactions with Organolithium Species	16
1.1.3	Hydrozirconation: Solvent Effects and Mechanistic Considerations	18
	1.1.3.1 Mechanism of the Hydrozirconation of Alkenes	19
	1.1.3.2 Effect of Solvent on the Hydrozirconation of Alkenes	19
	1.1.3.3 Effect of Ethereal Solvents on Reactions Involving Organomagnesium Reagents	23

1.1.4	Solubility Enhancement Using Oxetanes: Applications in Medicinal Chemistry.....	26
1.1.5	Preparation and Toxicological Properties of Oxetanes.....	28
1.1.5.1	Synthesis of Oxetanes	28
1.1.5.2	Intramolecular Cyclization Reactions	28
1.1.5.3	Pyrolysis of Cyclic Carbonates.....	29
1.1.5.4	Synthesis of 2-Substituted Oxetanes	30
1.1.5.5	Synthesis and Functionalization of Oxetan-3-one	30
1.1.6	Toxicity and Carcinogenicity of Oxetanes.....	31
1.2	RESULTS AND DISCUSSION: OXETANES IN ORGANOMETALLIC REACTIONS	33
1.2.1	3,3-Disubstituted Dimeric Oxetanyl Ethers as Additives and Cosolvents.	33
1.2.2	Synthesis of Dimeric Oxetanes.....	34
1.2.3	Use of Dimeric Oxetanes in Reactions Involving Organolithium Reagents.....	37
1.2.4	Effect of Oxetane-Based Additives on the Rate of Hydrozirconation of Alkenes	39
1.2.4.1	Hydrozirconation in Aromatic and Chlorinated Solvents.....	40
1.2.4.2	Reactions in Ethereal Solvents	40
1.2.5	Synthesis of Alternative Bisoxetanyl Ethers.....	44
1.2.5.1	Synthesis of 2,2'-Oxybis(methylene)dioxetane.....	44

1.2.5.2	Synthesis of Enantiopure Oxetanes to Generate a Diastereomerically and Enantiomerically Pure Bisoxetanyl Dimer.	46
1.2.5.3	Synthesis of 3,3'-Oxybis(methylene)dioxetane.....	47
1.2.6	Synthesis of Bisoxetanyl Ethers—Conclusions	49
1.2.7	Synthesis and Application of Bisoxetanylsulfides and Sulfoxides	50
1.2.7.1	Preliminary Investigations of Grignard Additions	51
1.2.7.2	Grignard Additions to Ketones	52
1.2.7.3	Use of Sulfide 1-69 to Attenuate Grignard Reagent Reactivity.....	56
1.2.7.4	Effect of Sulfide 1-69 on the Anionic Schlenk Equilibrium.....	61
1.2.7.5	Additional Reactions Involving Grignard Reagents	62
1.2.7.6	Conclusions for Use of Oxetanes as Additives in Organometallic Reactions.....	65
1.3	RESULTS AND DISCUSSION: USE OF MMS350 FOR AQUEOUS SOLUBILITY ENHANCEMENT OF SMALL ORGANIC MOLECULES.....	66
1.3.1.1	Oxidation Reactions Using MMS350 as a DMSO Substitute.....	67
1.3.2	MMS350—A Dimethylsulfoxide Substitute for Aqueous Solubility Enhancement of Small Organic Molecules	71
1.3.2.1	Problems with Compound Storage in DMSO	72
1.3.2.2	Initial Compound Solubility Measurements	73
1.3.2.3	Applicability of MMS350 to <i>in vitro</i> and <i>in vivo</i> Assays.....	80
1.3.2.4	MMS350 for Compound Storage—Hygroscopicity and Other Implications	83
1.3.2.5	Toxicity of MMS350	84

1.3.2.6	Conclusions for MMS350 as a DMSO Substitute.....	87
1.4	CONCLUSIONS.....	87
2.0	SMALL MOLECULES AS PROTECTORS AND MITIGATORS AGAINST IONIZING RADIATION.....	89
2.1	INTRODUCTION	90
2.1.1	Ionizing Radiation: Generation of ROS	90
2.1.1.1	ROS Scavenging by Endogenous Enzymes	91
2.1.2	TEMPO as an SOD Mimic.....	92
2.1.3	Strategies for Developing ROS Scavenging Agents	94
2.1.4	Targeted Delivery of Nitroxides to the Mitochondria	95
2.1.5	Sulfoxides as ROS Scavengers	96
2.1.5.1	DMSO as a Radioprotector	98
2.2	RESULTS AND DISCUSSION.....	99
2.2.1	MMS350—An Effective Radiation Mitigator?	99
2.2.1.1	MMS350 is Both Radioprotective and Mitigating.....	100
2.2.2	Ongoing and Future Studies of MMS350.....	102
2.2.2.1	Control Studies with MMS399	103
2.2.2.2	Azetidines as Modules in Medicinal Chemistry.....	104
2.2.2.3	MMS350 Analog Synthesis—Toward Bis-azetidines	105
2.2.3	Calculated Membrane Permeabilities of MMS350 and Analogs	110
2.3	CONCLUSIONS.....	113
3.0	NITROXIDE FUNCTIONALIZATION OF SILICA NANOPARTICLES USING AN OXAZOLINE LINKER	116

3.1	INTRODUCTION	117
3.1.1	Nanoparticles in Drug Delivery	117
3.1.1.1	Silica Nanoparticles for Drug Delivery	117
3.1.1.2	Biocompatibility of Silica Nanoparticles	119
3.1.1.3	Biodistribution of Silica Nanoparticles.....	121
3.1.1.4	Endocytosis of Silica Nanoparticles	121
3.1.1.5	Use of Nanoparticles to Deliver Antioxidants	123
3.1.2	Stimuli-Responsive Nanoparticles and Strategies for pH-Mediated Release	124
3.1.2.1	General Strategies for pH-Mediated Release.....	124
3.1.2.2	pH Responsive Polymers.....	125
3.1.2.3	pH-Mediated Release via Cleavage of Covalent Bonds	126
3.1.2.4	pH Responsive Nanoparticles for Delivery of Nitroxides	127
3.1.3	Oxazolines as pH-Controllable Linkers.....	128
3.1.3.1	Oxazolines in Medicinal Chemistry and Use as Prodrugs.....	129
3.1.3.2	Methods for Preparation of Oxazolines.....	130
3.1.3.3	Oxazolines as Acid-Cleavable Protecting Groups and Linkers ...	130
3.2	RESULTS AND DISCUSSION	134
3.2.1	Nanoparticle Design.....	134
3.2.2	Synthesis of Benzylic Chloride 3-44	135
3.2.3	Assays for Determining the Loading of the Imidothiolate Particles	141
3.2.3.1	Reductive Cleavage and Loading Quantification	143
3.2.4	Efforts to Increase Nanoparticle Loading	147

3.2.5	Click Chemistry Approach for Nanoparticle Functionalization	150
3.2.5.1	Ugi Approach	155
3.2.6	Oxazoline Hydrolysis of Model Systems	156
3.2.7	Functionalization of Controlled-Pore-Glass (CPG).....	160
3.2.7.1	General Strategy for Functionalization of Porous Glass	160
3.2.7.2	Synthesis of Precursors and Functionalization of CPG	161
3.3	CONCLUSIONS AND FUTURE DIRECTIONS.....	166
4.0	EXPERIMENTAL SECTION	168
	APPENDIX A: SELECTED ¹ H NMR AND ¹³ C NMR SPECTRA	268
	APPENDIX B: X-RAY DATA FOR MMS350	291
	APPENDIX C: DATA FOR MACROPHAGE UPTAKE OF IMIDOTHIOATE FUNCTIONALIZED SILICA NANOPARTICLES	303

LIST OF TABLES

Table 1-1. Physical parameters for selected solvents.	4
Table 1-2. Equilibrium constants for the interaction of ethers with <i>p</i> -chlorophenol.....	5
Table 1-3. Hydrogen bond basicity of selected Lewis basic moieties.....	6
Table 1-4. Physical properties of cyclic ethers	7
Table 1-5. Effect of alkyl substitution on the EPD-ability of oxetanes.....	10
Table 1-6. Effect of solvent on the dissociation of sodium malonate oligomers.....	11
Table 1-7. Effect of solvent on cyanohydrin additions.....	12
Table 1-8. Effect of solvent on dithiane additions.....	12
Table 1-9. Effect of solvent on lithium enolate stabilization.....	16
Table 1-10. Relative K_{solv} values for a chelated organolithium reagent determined by ^{31}P NMR titrations.	17
Table 1-11. Effect of solvent on the aggregation of LiHMDS solvates.	18
Table 1-12. Effect of solvent on the hydrozirconation of 1-hexene.	20
Table 1-13. Effect of concentration on the rate of hydrozirconation of 1-hexene.....	21
Table 1-14. Effect of solvent on the hydrozirconation of amides.....	22
Table 1-15. Effect of solvent on the rate of racemization of an organomagnesium cyanocyclopropane.	24

Table 1-16. Mg/Br exchange reactions of 4-bromoanisole using <i>i</i> -PrMgCl-LiCl and various additives.....	25
Table 1-17. Selected data showing the consequences of substitution at the benzylic position with a <i>gem</i> -dimethyl group or an oxetanyl group. ⁶	27
Table 1-18. Results from using dimeric oxetanes in dithiane additions to 2-cyclohexen-1-one..	37
Table 1-19. Results from using oxetane additives to enhance dianion solubility.....	38
Table 1-20. Hydrozirconation of 1-hexene using ethereal solvents.	41
Table 1-21. Effect of dimeric oxetane additives on the hydrozirconation of 1-hexene.....	43
Table 1-22. Additions of methylmagnesium bromide to benzaldehyde in presence of sulfide 1-69	53
Table 1-23. Addition of EtMgBr to <i>p</i> -trifluoromethylbenzoyl chloride in the presence of additives.....	58
Table 1-24. Mg/I exchange reactions in the presence of BDMAEE and sulfide 1-69	59
Table 1-25. Asymmetric additions of Grignard reagents to benzaldehyde in the presence of additives.....	60
Table 1-26. Effect of additives on the Mg/Br exchange of 4-bromoanisole.	62
Table 1-27. Addition of EtMgBr to benzonitrile in the presence of sulfide 1-69	63
Table 1-28. Conjugate addition reactions in the presence of sulfide 1-69	64
Table 1-29. Selected physical properties of MMS350 and DMSO.	66
Table 1-30. Kornblum oxidation of α -bromoacetophenone in the presence of sulfoxides.	70
Table 1-31. Solubility of estrone in solutions of pH 9.0 buffer, NMP, and sulfoxide.....	78
Table 1-32. Solubility of selected compound in solutions of sulfoxide MMS350 in 0.01 M pH 7.0 phosphate buffer.....	79

Table 1-33. Kinetic solubility measurements of carbendazim and griseofulvin after dilution with phosphate buffered saline.	80
Table 1-34. Comparative water absorption measurements of possible compound storage media.	84
Table 1-35. Brine shrimp assay results: toxicity of sulfoxide MMS350.	85
Table 2-1. Selected data showing the effect of radioprotective agents on irradiation survival of CB MNC.	101
Table 2-2. Calculated membrane permeabilities for DMSO, MMS350, and related analogs.	112
Table 3-1. Thiourea alkylation of a model system.	139
Table 3-2. Click chemistry reactions using azide 3-50 and a model alkyne.	152
Table 3-3. Nitroxide content of particles suspended in phosphate buffer.	154
Table 3-4. Nitroxide content of particles after both sonication and centrifugation.	155
Table 3-5. Synthesis of model oxazolines.	159
Table 4-1. Tabulated elemental analysis data for imidothiolate-functionalized silica nanoparticles.	225
Table 4-2. Loadings of 3-aminopropyl functionalized CPG.	259
Table 4-3. Loadings of succinylated CPG.	260
Table 4-4. Loadings of CPG esterified with triazole 3-95	262
Table B-1. Crystal data and structure refinement for MMS350.	291
Table B-2. Atomic coordinates ($\times 10^4$) and equivalent isotropic displacement parameters ($\text{\AA}^2 \times 10^3$) for MMS350.	292
Table B-3. Bond lengths [\AA] and angles [$^\circ$] for MMS350.	293

Table B-4. Anisotropic displacement parameters ($\text{\AA}^2 \times 10^3$) for sprach3a. The anisotropic ... 300

Table B-5. Hydrogen coordinates ($\times 10^4$) and isotropic displacement parameters ($\text{\AA}^2 \times 10^3$) 301

LIST OF FIGURES

Figure 1-1. Structural parameters for a) cyclobutane, b) oxetane, and c) 3,3-disubstituted oxetane.	8
Figure 1-2. The effect of contact ion-pairing in a) addition of dithianes to enones and b) addition of cyanohydrins to enones.	13
Figure 1-3. Structures derived from crystallographic data on lithium enolates and amides: a) Dimeric lithium enolate of <i>N, N</i> -dimethylcycloheptatrienecarboxamide, crystallized from THF. b) Dimeric lithium diisopropylamide, obtained as the [LDA] ₂ •(THF) ₂ complex.	15
Figure 1-4. Diastereomeric solvates of a chelated organolithium reagent.....	17
Figure 1-5. Representation of possible functional groups for which oxetane may serve as a bioisostere.	26
Figure 1-6. Examples of ethereal ionophores.	34
Figure 1-7. Dimeric oxetane additives for initial solvent effect screens.	34
Figure 1-8. Strategies for generating analogs of bisoxetanyl ether 1-37	50
Figure 1-9. GC trace of the reaction reported in Table 1-22, entry 4.	54
Figure 1-10. Additives and substrates used for studying the Mg/I exchange reaction of aryl iodides.	58
Figure 1-11. X-ray structure of MMS350.....	67

Figure 1-12. Space-filling model of MMS350.	67
Figure 1-13. DMSO substitutes for aqueous solubility enhancement of lipophilic compounds. .	73
Figure 1-14. Test set of poorly aqueous soluble compounds.....	74
Figure 1-15. Solubility of quinine 1-100 in aqueous solutions with MMS350 and DMSO	75
Figure 1-16. Solubility of naproxen 1-101 in aqueous solutions with MMS350 and DMSO	75
Figure 1-17. Solubility of carbendazim 1-102 in aqueous solutions with MMS350 and DMSO	76
Figure 1-18. Solubility of griseofulvin 1-103 in aqueous solutions with MMS350 and DMSO..	76
Figure 1-19. Compounds assayed for PKD1 inhibitory activity.....	81
Figure 1-20. Plot of PKD1 activity with compound concentrations of 1 μ M.	82
Figure 1-21. Plot of PKD1 activity with compound concentrations of 10 μ M.	82
Figure 1-22. Toxicity of MM350 and DMSO against a HepG2 cell line.	86
Figure 1-23. Toxicity of MMS350 and DMSO against a MDA-MB-231 cell line.	86
Figure 2-1. Gramicidin S and hemigramicidin S TEMPO conjugates for mitochondria-targeted delivery.	95
Figure 2-2. Survival curves of mice injected with 20 mg/kg MMS350 in PBS or JP4-039.....	100
Figure 2-3. General structure of azetidine analogs of MMS350.	104
Figure 2-4. Comparative aqueous solubility and lipophilicity data for spirocyclic azetidines and the corresponding monocyclic scaffolds.....	104
Figure 2-5. Comparison of the conformation of azetidine (a) and oxetane (b).	105
Figure 2-6. Compounds compared for calculated membrane permeabilities.	111
Figure 3-1. Main types of silica nanoparticles.....	118
Figure 3-2. General endocytotic pathways for nanoparticles in mammalian cells.	122
Figure 3-3. Example antioxidant molecules delivered using nanoparticle systems.	123

Figure 3-4. Examples of polymers used for construction of pH-responsive nanoparticles.	125
Figure 3-5. pH-Responsive cleavage of boronate esters for release of therapeutics.	126
Figure 3-6. pH-Responsive polymeric nanoparticles for selective delivery of nitroxides.	127
Figure 3-7. General structure of an oxazoline.	128
Figure 3-8. Natural products containing oxazolines or prepared by reactions of oxazolines.	128
Figure 3-9. Oxazolines, oxazolidines and oxazolidinones studied as potential pro-drugs.	129
Figure 3-10. General strategy for nanoparticle functionalization.	134
Figure 3-11. TEM image of 3-aminopropyl silica nanoparticles.	138
Figure 3-12. General strategy for loading assays using UV/VIS spectroscopy.	144
Figure 3-13, Typical design of succinylated CPG for oligonucleotide synthesis.	160
Figure C-1. Macrophage uptake by imidothiolate-functionalized silica nanoparticles.	303

LIST OF SCHEMES

Scheme 1-1. Ring-opening of oxetanes using nucleophilic lithium reagents.....	9
Scheme 1-2. Equilibrium and reaction pathways for contact and solvent-separated ion pairs.....	14
Scheme 1-3. General mechanism for the hydrozirconation of alkenes.	19
Scheme 1-4. General description of the kinetics of the hydrozirconation of 1-hexene.....	21
Scheme 1-5. General mechanism for the addition of Grignard reagents to carbonyl compounds.	23
Scheme 1-6. General description of the Schlenk equilibrium.	24
Scheme 1-7. General depiction of the anionic Schlenk equilibrium in the presence of 1,4- dioxane.....	25
Scheme 1-8. Synthesis of oxetanes via intramolecular cyclization reactions.....	29
Scheme 1-9. Synthesis of oxetanes via pyrolysis of cyclic carbonates.	29
Scheme 1-10. Oxetane synthesis via the Paterno-Büchi reaction.....	30
Scheme 1-11. Synthesis of oxetanes via ring expansion of epoxides.....	30
Scheme 1-12. Scaleable synthesis of oxetan-3-one.....	31
Scheme 1-13. Example methods for functionalizing oxetan-3-one.....	31
Scheme 1-14. Synthesis of dimeric ether 1-37	35
Scheme 1-15. Attempted preparation of 2,6-dioxaspiro[3.3]heptane.....	35
Scheme 1-16. Independent synthesis of bromide 1-42 and ethyl ether 1-43	36

Scheme 1-17. Optimized protocol for synthesis of spirocycle 1-38 .	36
Scheme 1-18. Synthetic plan for the synthesis of bisoxetanyl ethers.	44
Scheme 1-19. Synthesis of alcohol <i>rac</i> - 1-48 .	45
Scheme 1-20. Synthesis of dimeric oxetane 1-47 .	45
Scheme 1-21. Attempted synthesis of 1-47 via a double methylene transfer reaction.	46
Scheme 1-22. Synthesis of diastereomerically and enantiomerically pure (<i>S,S</i>)- 1-47 .	47
Scheme 1-23. Synthesis of 1-50 via a mono-benzylated triol.	48
Scheme 1-24. Synthesis of alcohol 1-50 via a symmetrical triol.	48
Scheme 1-25. Synthesis of bisoxetanyl ether 1-49 .	49
Scheme 1-26. Synthesis of sulfur-functionalized bisoxetanyl dimers.	51
Scheme 1-27. Mechanism of the magnesium-Oppenauer oxidation.	54
Scheme 1-28. Synthesis of ketones from acid chlorides using BDMAEE-Grignard complexes.	56
Scheme 1-29. Halogen/Mg exchange reactions of aromatic halides using deactivated Grignard reagents.	57
Scheme 1-30. Asymmetric addition of Grignard reagents to aldehydes.	57
Scheme 1-31. Reaction of <i>i</i> -PrMgCl and 4-bromoanisole, proceeding through an anionic Schlenk equilibrium.	61
Scheme 1-32. Example utility of using a shift in the Schlenk equilibrium for favorable reactivity.	65
Scheme 1-33. Reactions where DMSO is used an oxidant.	68
Scheme 1-34. Mechanism of A) the Swern oxidation and B) the Kornblum oxidation.	68
Scheme 1-35. Proposed Kornblum oxidation using MMS350 as an oxidant.	69
Scheme 1-36. Reaction of cyanuric chloride and MMS350 for attempted oxidation reactions.	71

Scheme 2-1. Enzymatic reactions that mitigate ROS.	91
Scheme 2-2. Mechanism for dismutation of superoxide by superoxide dismutase.	92
Scheme 2-3. Mechanisms for nitroxide-catalyzed dismutation of superoxide.	93
Scheme 2-4. General reaction of hydroxyl radicals with sulfoxides.	97
Scheme 2-5. Hydroxyl radical scavenging assay based on the rapid reaction of DMSO with hydroxyl radical.	98
Scheme 2-6. Synthesis of MMS350.	99
Scheme 2-7. Synthesis of control sulfoxide MMS399.	103
Scheme 2-8. Strategy for the synthesis of bis-azetidines.	106
Scheme 2-9. Initial route toward synthesis of bis-azetidines.	106
Scheme 2-10. Synthesis of bis-azetidines from sulfide 1-69	108
Scheme 2-11. Synthesis of bis-azetidines using a tetrabrosylated sulfide.	108
Scheme 2-12. Sulfide oxidation and future plans for protecting group removal.	109
Scheme 2-13. Synthesis of bis-azetidines with tosyl and benzyl substituents.	109
Scheme 2-14. Precedented methods for functionalizing azetidines.	110
Scheme 2-15. Proposed mechanisms for scavenging of ROS by MMS350.	115
Scheme 3-1. Typical modification of a silica surface by condensation with trialkoxysilanes. ..	118
Scheme 3-2. General methods for oxazoline synthesis using cyclodehydration methods.	130
Scheme 3-3. Acidic cleavage of oxazolines to afford carboxylic acids.	131
Scheme 3-4. Selective hydrolysis of a 2-alkyl-substituted oxazoline in the presence of a 2-aryl-substituted oxazoline.	131
Scheme 3-5. Hydrolysis of oxazolines and subsequent <i>O-N</i> acyl shift.	132
Scheme 3-6. Oxazolines as polystyrene-supported linkers for synthesis of acids and esters.	133

Scheme 3-7. Thiourea alkylation approach for nanoparticle functionalization.....	135
Scheme 3-8. Synthesis of benzylic chloride 3-44	136
Scheme 3-9. Synthesis of TEMPO-coupled benzylic azide 3-50	137
Scheme 3-10. Amide bond formation using halotripyrrolidinophosphonium hexafluorophosphates.	137
Scheme 3-11. Synthesis of thiourea-functionalized silica nanoparticles.....	138
Scheme 3-12. Alkylation of thiourea particles with benzylic chloride 3-44	141
Scheme 3-13. Proposed thioether cleavage strategy for loading determination.....	142
Scheme 3-14. Imidothiolate cleavage using Raney Ni on a solution-phase model system.....	142
Scheme 3-15. Reduction of benzylic chloride 3-44 ; synthesis of standards for LC-MS analysis	143
Scheme 3-16. Synthesis of benzylic chlorides bearing chromophores.....	144
Scheme 3-17. Synthesis of chromophore-labeled imidothiolate.	145
Scheme 3-18. Control reductive cleavage experiments to validate the loading quantification experiments.....	146
Scheme 3-19. Synthesis of benzylic alcohol for leaving group studies.....	148
Scheme 3-20. Synthesis of model substrates for variation of the benzylic leaving group.	149
Scheme 3-21. General strategy for functionalization using click chemistry.	150
Scheme 3-22. Synthesis of model alkyne.	151
Scheme 3-23. Synthesis of alkyne-functionalized nanoparticles and click chemistry using 4- bromobenzylazide.	153
Scheme 3-24. TEMPO-functionalization of silica nanoparticles using click chemistry.	153
Scheme 3-25. Ugi reaction on a model system.....	156

Scheme 3-26. Synthesis of model oxazoline 3-86	157
Scheme 3-27. Hydrolysis of model oxazoline.....	157
Scheme 3-28. Strategy for functionalization of porous glass.....	161
Scheme 3-29. Synthesis of alcohol 3-95	161
Scheme 3-30. Functionalization of CPG with triazole 3-95	162
Scheme 3-31. Saponification of CPG-ester for loading determination.....	163
Scheme 3-32. Validation of the saponification assay for determination of loading on CPG.....	164
Scheme 3-33. Subjection of CPG-ester 3-94 to acidic conditions.....	165
Scheme 3-34. Synthesis of serine adducts as standards.....	166

LIST OF ABBREVIATIONS

Ac	Acetyl
AMT	2-Amino-6-methylthiazone
BDMAEE	Bis[2-(<i>N,N</i> -dimethylamino)ethyl] ether
Bn	Benzyl
BOM	Benzyloxymethyl
Bs	<i>p</i> -Bromobenzenesulfonyl
<i>n</i> -Bu	<i>n</i> -Butyl
<i>t</i> -Bu	<i>tert</i> -Butyl
Bz	Benzoyl
Cp	Cyclopentadienyl
CPG	Controlled-pore glass
CSD	Cambridge Structural Database
D ₀	Dose of radiation that reduces a population by 67%
DAST	Diethylaminosulfur trifluoride
DBU	1,8-Diazabicycloundec-7-ene
DIPEA	Diisopropylethylamine
DMAP	4-Dimethylaminopyridine
DME	1,2-Dimethoxyethane
DMF	<i>N,N</i> -Dimethylformamide
DMPU	<i>N,N</i> -Dimethylpropyleneurea
DMS	Dimethylsulfide
DMSO	Dimethylsulfoxide
DOPC	1,2-Dioleoyl- <i>sn</i> -glycero-3-phosphocholine
DOPS	1,2-Dioleoyl- <i>sn</i> -glycero-3-[phospho-L-serine](sodium salt)
DPPA	Diphenylphosphoryl azide
EDC	1-Ethyl-3-(3-dimethylaminopropyl)carbodiimide
Et	Ethyl

Fmoc	Fluorenylmethyloxycarbonyl
GC	Gas Chromatography
GI ₅₀	Growth Inhibitory Concentration (50%)
Gy	Gray: absorption unit (J/kg) of ionizing radiation
HATU	2-(1 <i>H</i> -7-Azabenzotriazol-1-yl)--1,1,3,3-tetramethyl uronium hexafluorophosphate
HBC	2-Hydroxypropyl- β -cyclodextrin
HESI	Heated Electrospray Ionization
HMDS	Hexamethyldisilazane
HMPA	Hexamethylphosphoramide
HOBT	Hydroxybenzotriazole
HPLC	High Performance Liquid Chromatography
<i>i</i> -Pr	<i>iso</i> -Propyl
LAH	Lithium Aluminum Hydride
LDA	Lithium Diisopropylamide
<i>m</i> -CPBA	<i>m</i> -Chloroperbenzoic Acid
Me	Methyl
PMP	<i>p</i> -Methoxyphenyl
MSN	Mesoporous silica nanoparticle
MTBE	Methyl <i>tert</i> -butyl ether
NBP	<i>p</i> -Nitrobenzylpyridine
NMP	<i>N</i> -Methylpyrrolidone
NMR	Nuclear Magnetic Resonance
PBS	Phosphate buffered saline
PEG	Polyethylene glycol
PKD1	Protein Kinase D, isoform 1
<i>n</i> -Pr	<i>n</i> -Propyl
Ph	Phenyl
PTC	Phase-Transfer Catalyst
Pyr	Pyridine

RNS	Reactive nitrogen species
ROS	Reactive oxygen species
rt	Room temperature
Ser	Serine
SOD	Superoxide dismutase
TBAF	Tetrabutylammonium fluoride
TBA-RS	Thiobarbituric acid reactive substance
TBS	<i>tert</i> -Butyldimethylsilyl
TBDPS	<i>tert</i> -Butyldiphenylsilyl
TEMPO	2,2,6,6,-Tetramethylpiperidine(1-oxyl)
TEOS	Tetraethoxysilane
THF	Tetrahydrofuran
THP	Tetrahydropyran
TMS	Trimethylsilyl
Ts	<i>p</i> -Toluenesulfonyl
UV/VIS	Ultraviolet/Visible

In his introduction to *Solvents and Solvent Effects in Organic Chemistry*, Christian Reichardt states, “The development of our knowledge of solutions reflects to some extent the development of chemistry itself.”¹ Although a number of solvents and cosolvents with varying polarities, electron-donating and accepting properties, and boiling points are available, the development of new reaction media can advance the scope of our synthetic capabilities. Moreover, environmental and health concerns regarding solvent toxicity prompt the exploration of new media, particularly in the case of process chemistry² and biological applications. In the 1980’s, the desire to replace carcinogenic HMPA led to the introduction of more benign DMPU.³ Similar movements for solvent replacement currently exist, and the definition of a “green”^{4,5} solvent varies depending on the application; there is a need for the continuous development of new solvents and additives to address the ever-changing demands of both academia and industry.

Among common ethereal solvent scaffolds, oxetanes have not been extensively used as solvents. Yet, oxetanes, particularly 3,3-disubstituted oxetanes, have favorable solvolytic properties. Moreover, Carreira and Müller have introduced the oxetane as a replacement for carbonyl or *gem*-dimethyl groups in medicinally relevant molecules.^{6,7} Many of the attributes (e.g., enhanced hydrogen-bond affinity, large polar surface area) that make oxetanes attractive moieties in drug discovery translate to their potential application as solvents.

To examine the feasibility of using oxetanes as additives or cosolvents, I generated bifunctional molecules wherein oxetanes were appended to common solvent motifs including ethers and sulfides. I tested the effect of adding the bifunctional compounds to reactions involving organometallic reagents—namely organolithium, organozirconium, and

organomagnesium reagents. I then shifted my focus to the utility of a bifunctional sulfoxide as a dimethyl sulfoxide substitute for applications including chemical storage and biological assays.

1.1 INTRODUCTION

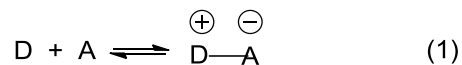
In this section, important physical properties for Lewis basic solvents are highlighted, and emphasis is placed on the known physical properties of cyclic ethers and oxetanes. Key factors leading to observed solvent effects in reactions involving organometallic reagents are detailed, and key precedents for using oxetanes in reactions involving organolithium and organozirconium reagents are addressed. Methods by which oxetanes can be prepared and elaborated are then discussed. Finally, issues regarding toxicity and mutagenicity of oxetanes are addressed.

1.1.1 Physical Properties of Solvents

“Solvent effect” is a general term referring to differences in reaction rate, regioselectivity, chemoselectivity, diastereoselectivity, or enantioselectivity observed upon changing reaction media. The properties of solvents, notably bulk permittivity (dielectric constant, ϵ), dipole moment (μ), and electron-donating and accepting properties can have an important role in dictating the relative stabilities of the starting materials, activated complex, and reaction products.⁸

1.1.1.1 The EPD-EPA Interaction: Measures of Donating Ability

Ethereal solvents are often used in reactions involving organometallic reagents because they exhibit low reactivity and have the ability to coordinate and solvate cations; the donor-acceptor interaction of coordinating ethereal solvents with organometallic species can be modeled as a Lewis acid/Lewis base interaction (eq 1).



As outlined by Reichardt,¹ electron-pair donors (EPDs) are classified according to the energetically highest orbitals as *n*-EPDs (e.g., ethers, tertiary amines), σ -EPDs (e.g., cyclopropane, dichloromethane) and π -EPDs (e.g., alkenes, alkylbenzenes). Electron-pair acceptors (EPAs) are classified according to the energetically lowest unoccupied orbitals as υ -EPAs (e.g., metal cations, boron trihalides), σ -EPAs (e.g., Br₂), and π -EPAs (e.g., unsaturated compounds with electron-withdrawing substituents such as tetracyanoethane).¹ In the case of interactions between ethereal solvents and organometallic reagents, the *n*-donor-to- υ -acceptor relationship is of consequence.

Due to the importance of coordinating solvents in metal-mediated reactions, researchers have developed scales of relative donating ability. Gutmann established the concept of Donor Number (DN), which is the enthalpy of reaction of an electron donating solvent with SbCl₅ correlated to dichloroethane as a reference solvent (eq 2).⁹ Gal and Maria have developed a similar scale based on measurements of reaction enthalpy for the reaction between boron trifluoride and a donating organic species (eq 3).¹⁰ Along with donating ability, the solvating power of solvents depends on the dielectric constant (ϵ), which is an indication of solvent polarity and dissociating ability. As indicated by the tabulation of solvent data (Table 1-1), donor number and ionizing ability are not necessarily correlated.

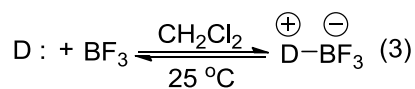
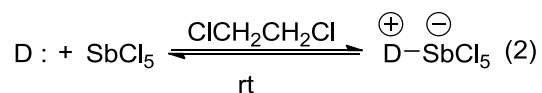


Table 1-1. Physical parameters for selected solvents.

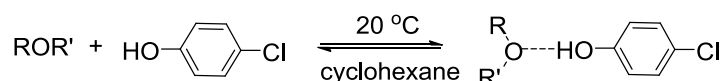
Entry	Solvent	ϵ (25 °C) ¹¹	DN (kcal/mol) ⁹	$-\Delta H_{\text{BF}_3}^0$ (kcal/mol) ¹⁰
1	nitromethane	35.87	2.7	8.99
2	1,4-dioxane	2.22	14.8	17.71
3	ethyl acetate	6.02	17.1	18.06
4	acetone	20.56	17.0	18.17
5	diethyl ether	4.27	19.2	18.83
6	tetrahydropyran	5.66	22	20.40
7	tetrahydrofuran	7.52	20.0	21.61 (19.6) ^a
8	oxetane	<i>b</i>	<i>c</i>	<i>d</i> (20.3) ^a
9	dimethylsulfoxide	46.45	29.8	25.18
10	hexamethylphosphoramide	29.30	38.8	28.08
11	pyridine	12.91	33.1	30.61

^aGas-phase BF_3 -affinities calculated at the MP3 level of theory.¹² ^bThe dielectric constant of oxetane has not been measured. ^c DN for oxetane has not been reported. ^dThe BF_3 -affinity of oxetane has not been measured experimentally; McLaughlin et al. report polymerization of oxetane when attempting to determine the stability of oxetane- BF_3 addition compounds.¹³

Ethereal solvents are better n -EPDs than esters and ketones (entries 3-4) but poorer donors than sulfoxides (entry 9), amines (entry 11), and phosphoramides (entry 10). Although ether (entry 5) and tetrahydrofuran (entry 7) have similar experimental Lewis basicities, additional studies indicate that tetrahydrofuran has significantly higher proton affinity. By nature of their constrained geometry, cyclic ethers have larger exposed surface areas at the

coordinating oxygen, which enhances hydrogen-bonding capabilities and, consequently, aqueous solubility.¹⁴ Bellon demonstrated the effect of cyclization on hydrogen-bonding by measuring equilibrium constants for the interaction of ethers with *p*-chlorophenol (Table 1-2).¹⁵

Table 1-2. Equilibrium constants for the interaction of ethers with *p*-chlorophenol.



Entry	Acyclic ether	K (10^{-2})	Cyclic ether	K (10^{-2})	$K_{\text{cyclic}}/K_{\text{acyclic}}$
1	MeOEt	---- ^a	oxetane	5.8 ± 0.2	2.3^b
2	EtOEt	2.49 ± 0.08	THF	5.1 ± 0.2	2.1 ± 0.1
3	EtO- <i>n</i> -Pr	2.08 ± 0.06	THP	4.4 ± 0.1	2.1 ± 0.1
4	EtO- <i>i</i> -Pr	2.49 ± 0.08	2-MeTHF	6.2 ± 0.2	2.5 ± 0.1
5	EtO- <i>t</i> -Bu	2.71 ± 0.09	2,2-Me ₂ THF	6.6 ± 0.2	2.5 ± 0.1
6	<i>n</i> -PrO- <i>n</i> -Pr	2.84 ± 0.09	oxepane	5.0 ± 0.2	3.0 ± 0.2

^aThe value was not obtained because MeOEt is a gas at 20 °C.¹⁵ ^bThe ratio was estimated based on the known gas-phase basicity of MeOEt.

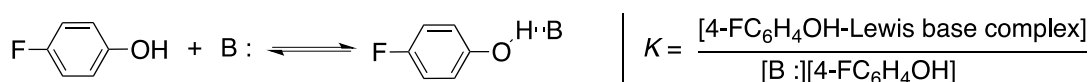
The data shown in Table 1-2 support that cyclic ethers are superior hydrogen-bond acceptors, which can be rationalized both by steric arguments (the oxygen of acyclic ethers may be crowded by freely rotating alkyl groups) and the higher bulk permittivities and dipole moments of the cyclic ethers (compare THF: $\epsilon = 7.52$, $\mu = 1.75$ D to diethyl ether: $\epsilon = 4.27$, $\mu = 1.15$ D). Another aspect of the data is the greater basicity of 2-substituted tetrahydrofurans, indicating that substitution at the 2-position of cyclic ethers enhances donating ability. Among

unsubstituted cyclic ethers, oxetane has the greatest basicity, which Bellon attributes both to its smaller size and larger dipole moment (See Table 1–4, entry 2).

More recently, the pK_{BHX} scale¹⁶ has become popular for measuring hydrogen bond basicity—the values are based on formation of a complex between the acceptor (e.g., an ether) and 4-fluorophenol. Representative values for a range of Lewis bases are tabulated in Table 1–3.

The data indicate a similar trend as observed in the case of association constants with *p*-chlorophenol. These data also corroborate the trend observed in the case of donor numbers (Table 1-1) wherein cyclic ethers (e.g., oxetane, THF) have higher hydrogen-bonding affinities than ketones (e.g., acetone) and acyclic ethers (e.g., diethyl ether).

Table 1-3. Hydrogen bond basicity of selected Lewis basic moieties.



Solvent	Me ₃ PO	Me ₂ SO	morpholine	oxetane	THF	(CH ₃) ₂ O	EtOEt
pK_{BHX}	3.53	2.54	1.78	1.36	1.28	1.18	1.01

Computational studies indicate that the gas-phase basicity of oxetane is 2.6 kcal/mol higher than for methyl ethyl ether, whereas the gas-phase basicities of tetrahydrofuran and diethyl ether are comparable. Bordeje et al. postulate that the difference results from lengthening of C–O bonds upon protonation, which alleviates ring strain. Protonation of less strained tetrahydrofuran would not facilitate comparable strain relief as protonation of oxetane.¹⁷ Although gas-phase Brønsted basicities are often not indicative of solution-phase behavior, the result suggests a

superior coordinating ability of oxetane due to the structural differences (namely angular strain) in the four- and five-membered rings.

Because oxetane may exhibit enhanced basicity due to its small size and strain, epoxides might also be considered viable coordinating solvents; however, oxiranes are typically too reactive for use as reaction media. Although oxetane and oxirane have similar strain energies (Table 1-4, entries 1 and 2), computational models¹⁸ indicate that oxirane is greater than 10^6 times more susceptible to nucleophilic addition than oxetane. Furthermore, the cleavage of an aziridinium triflate in acetonitrile using DIPEA is 10^3 times faster than cleavage of the corresponding azetidinium salt.¹⁹ The enhanced reactivity of epoxides may result from the difference in hybridization when compared with oxetane (Table 1–4, entries 1 and 2); oxirane is almost sp^2 -hybridized, which may facilitate faster ring-opening than in the case of oxetanes.

Table 1-4. Physical properties of cyclic ethers

Entry	Ether	Strain Energy (kcal/mol) ²⁰	Hybridization ²¹ (%s character of C-H bonds)	Dipole Moment ¹¹ (D)
1	oxirane	26.8	30 ^a	1.89 ± 0.01
2	oxetane	25.2	26 ^a	1.94 ± 0.01 ²²
3	tetrahydrofuran	5.9	25 ^b	1.75 ± 0.01
4	tetrahydropyran	0.5	25 ^b	1.58 ± 0.03
5	1,4-dioxane	3.3	25 ^b	

^aThe %s character was measured using C-H coupling constants.

^bThe hybridization is assumed based on the absence of geometrical deviation from typical sp^3 -hybridized carbons.

1.1.1.2 Physical Properties of Oxetanes

As discussed, oxetanes are constrained cyclic ethers; the lone pairs are more exposed as hydrogen bond acceptors. The enhanced hydrogen bonding affinity of oxetanes led us to hypothesize that oxetanes would also coordinate strongly to positively charged organometallic reagents; indeed, the coordinating ability of oxetane for small cations (e.g., Li^+) has been demonstrated experimentally and is discussed in detail in section 1.1.2.4.^{23,24}

Unlike cyclobutane,²¹ oxetane has a minimal inversion barrier and a relatively flat (unpuckered) geometry (Figure 1-1), which make oxetanes relatively flat. These properties have led to the use of oxetanes as isosteric replacements for the carbonyl moiety. Carrier and Müller have recently reported an averaged structure of 3,3-disubstituted oxetanes.⁶ In this case, it was shown that there is slight puckering due to eclipsing interactions, but that the ring puckering angle is relatively small (*ca.* 10°) (Figure 1-1, c).

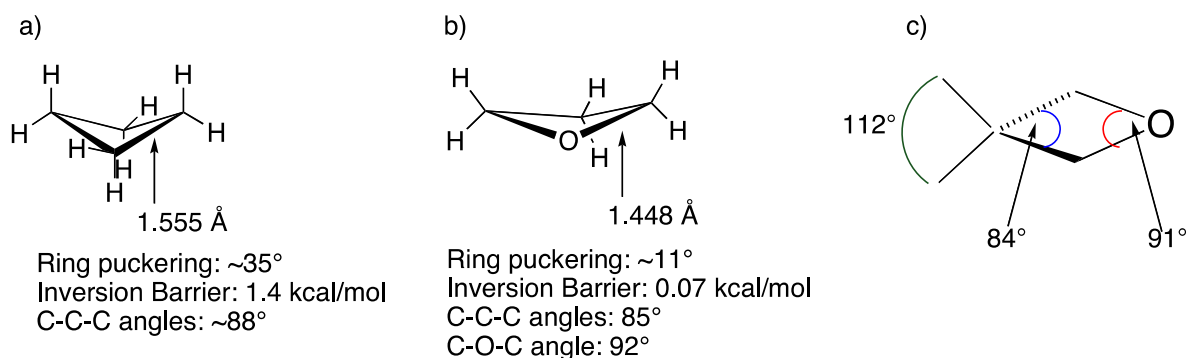
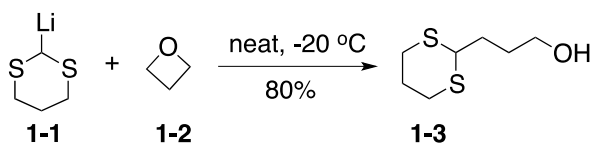


Figure 1-1. Structural parameters for a) cyclobutane, b) oxetane, and c) 3,3-disubstituted oxetane. The parameters in c) represent averaged structural parameters from data taken from the CSD (adapted from reference 6).

Although oxetanes are less susceptible to ring-opening than epoxides, nucleophilic addition to trimethylene oxide is well-established.²⁵ An example is the addition of (1,3-dithian-2-yl)lithium to oxetane (Scheme 1-1).²⁶

Scheme 1-1. Ring-opening of oxetanes using nucleophilic lithium reagents.



3,3-Disubstituted oxetanes are more stable than their unsubstituted counterparts due to steric hindrance and the Thorpe-Ingold effect.²⁷ Carreira and Müller²⁸ demonstrated that 3,3-disubstituted oxetanes are stable to stirring in aqueous buffers over a pH range of 1-10; in contrast, trimethylene oxide is readily susceptible to hydrolysis under acidic conditions.²⁹

Searles et al.³⁰ catalogued the electron-donating properties of several substituted oxetanes based on the CH₃OD spectra (Table 1–5). The data indicate that substitution at the 3-position of oxetane (entry 2) renders the oxygen moiety less donating whereas substitution at the 2-position enhances donating ability (entry 3). The latter result is readily explained by increased electron-donation by alkyl substitution. The decreased donation from the 3,3-disubstituted oxetane can be explained by the Thorpe-Ingold effect; geminal substitution at the 3-position decreases the internal angles, consequently decreasing the overall electron-availability. Searles also demonstrated that the donating-ability of the oxetane has a positive correlation with its proclivity toward reductive cleavage with LAH in THF at reflux.³⁰ Although 2-substituted oxetanes may have superior donating ability, 3-substituted oxetanes have the optimal combination of donating ability *and* stability.

Table 1-5. Effect of alkyl substitution on the EPD-ability of oxetanes.

Entry	Oxetane	O-D shift (cm ⁻¹) ^a
1	oxetane	120
2	3,3-diethyloxetane	115
3	2,2-diethyloxetane	125

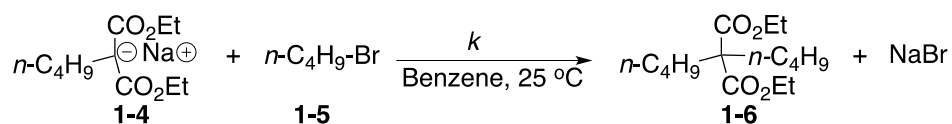
^aThe O-D shift refers to the difference in the O-D band frequency in the infrared spectrum of a 0.1 M solution of methanol-*d* in an ether (e.g., oxetane) versus a 0.1 M solution of methanol-*d* in a reference solvent (in this case, CCl₄).³⁰ The Lewis basicity of ethers has been positively correlated to the magnitude of the O-D shift.³¹

1.1.2 Solvent Effects in Organometallic Reactions

1.1.2.1 Consequences of Aggregation and Generation of Activated Anions

In the case of reactions involving organometallic reagents, the principles governing solvent effects are complicated by ion-pairing and aggregation. For example, the alkylation of sodium malonate **1-4** with *n*-butyl bromide **1-5** (Table 1-6) is significantly accelerated when electron-donating solvents are used as additives.^{32,33} The observation indicates that dissociation of sodium malonate oligomers produces kinetically active lower-order aggregates. Generation of activated anions is generally achieved by 1) increasing the size of the cation to effectively cause an electrostatic “mismatch” (e.g., the “cesium effect”), 2) using electron-pair-donating solvents that interact with cations or 3) using ligands designed for specific cation solvation (e.g., crown ethers).¹

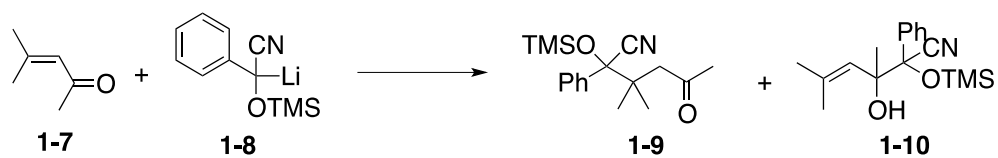
Table 1-6. Effect of solvent on the dissociation of sodium malonate oligomers.



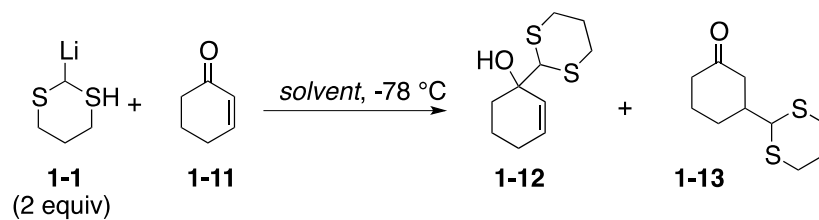
Additive (5 equiv)	None	THF	DME	1,4-dioxane	DMF	HMPA
<i>k</i> (rel.)	1	1.1	6.4	18	19	54

1.1.2.2 The Effect of Ion-Pairing

The presence of contact versus solvent-separated ion pairs can impact the chemoselectivity of chemical transformations. Examples include the addition of lithium carbanions to enones (Tables 1-7 and 1-8). The addition of benzaldehyde *O*-(trimethylsilyl)-cyanohydrin **1-8** to enone **1-7** proceeds via 1,4-addition in ether but predominantly 1,2-addition in DME or THF (Table 1-7).³⁴ Conversely, the addition of electron-donating media (e.g., HMPA) to the reaction between (1,3-dithian-2-yl)lithium **1-1** and 2-cyclohexen-1-one **1-10** led to formation of the 1,4-addition product (Table 1-8).³⁵ Both results can be explained by the presence or absence of ion-pairing. The dithiane addition results are explained by the presence or absence of lithium cation in carbonyl activation (Figure 1-2, a); the cyanohydrin addition results are explained by chelation from both the carbonyl and the nitrile (Figure 1-2, b). In electron-donating solvents, the chelation to nitrogen is impeded, and 1,2-addition is the operative pathway when the reaction is kinetically controlled. Warming the reaction performed in THF from -78 °C to 0 °C had no effect on the product ratio of **1-9** to **1-10**.

Table 1-7. Effect of solvent on cyanohydrin additions.³⁴

Entry	Solvent	Ratio 1-9 : 1-10	Combined yield of 1-9 and 1-10 (%)
1	Et ₂ O	> 95:5	84
2	DME	22:78	98
3	THF	25:75	Not reported

Table 1-8. Effect of solvent on dithiane additions.

Entry	Solvent	Ratio 1-12 : 1-13
1	THF or Et ₂ O	> 99: 1
2	THF, HMPA (2 equiv)	< 5:95

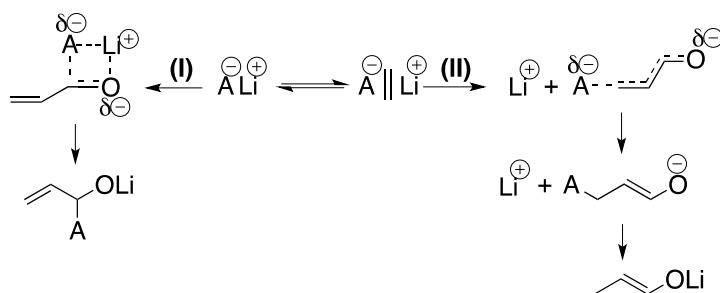


Figure 1-2. The effect of contact ion-pairing in a) addition of dithianes to enones and b) addition of cyanohydrins to enones.

Cohen et al.³⁶ proposed that 1,2- versus 1,4-selectivity results from a rapid equilibrium between contact and solvent-separated ion pairs (Scheme 1-2). 1,2-Addition to enones has a low activation barrier and proceeds from the contact ion pair via a four-center transition state (pathway I). Under kinetic control, *solvent-separated* ion pairs add at the 4-carbon (pathway II), regardless of the nature of the nucleophile. In the case of an early transition state, kinetic 1,4-addition is favored because the 4-carbon in acrolein has a larger LUMO coefficient than the carbonyl carbon. In the case of a late transition state, the relative stabilities of the enolate anion and the oxyanion must be taken into account, with the enolate anion being more stable (again, 1,4-addition would be favored).

Curtin-Hammett limitations prevented Sikorski and Reich³⁵ from determining if the product distributions of the 2-lithio-1,3-dithiane additions (Table 1-8) could be correlated to the ground state populations of contact and solvent-separated ion pairs; the equilibrium between the contact-ion pairs (observed spectroscopically) and the solvent-separated ion pairs was too rapid for measurement.³⁵ Nevertheless, the observed regioselectivities suggest that the kinetic reaction product distribution is governed by the presence or absence of ion-pairing. Under thermodynamic conditions, the 1,2-addition of 2-lithio-2-phenyl-1,3-dithiane has been shown to be reversible, with the 1,4-addition product being formed upon warming reaction mixtures from $-78\text{ }^{\circ}\text{C}$ to rt regardless of solvent system.³⁷

Scheme 1-2. Equilibrium and reaction pathways for contact and solvent-separated ion pairs.



1.1.2.3 Aggregation of Organolithium Species

Lithium enolates typically exist as aggregates of the lithium-coordinated enolates or as mixed aggregates of the lithium enolate with solvent molecules or additives (e.g., HMPA, DMPU). Bulky lithium amides (e.g., LDA, LiHMDS) typically exist as disolvated dimers (Figure 1-3).³⁸

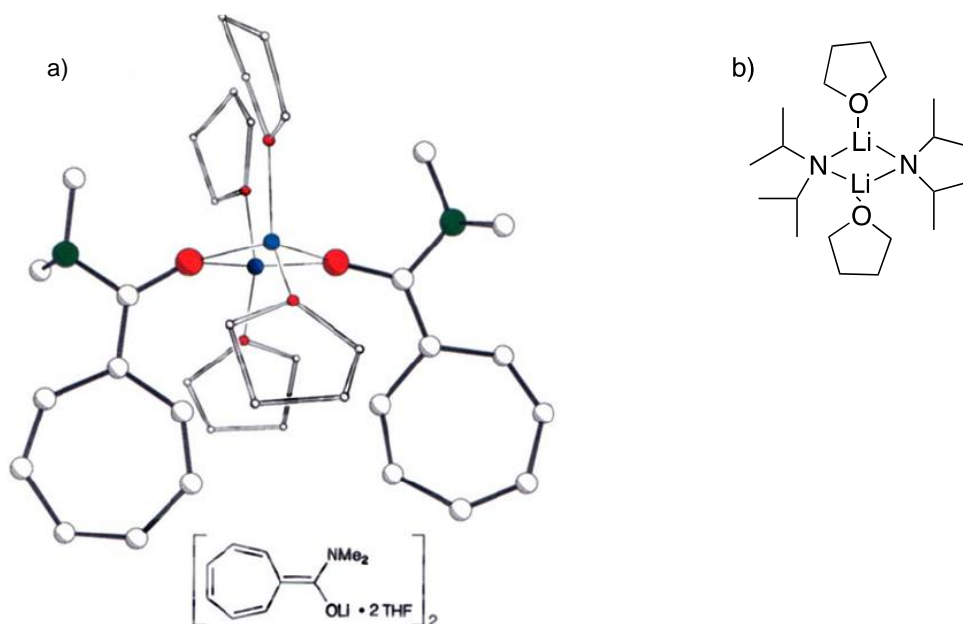
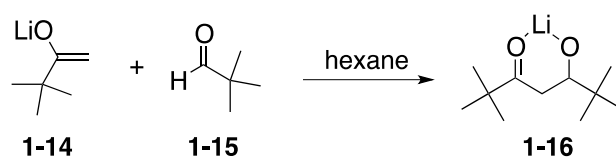


Figure 1-3. Structures derived from crystallographic data on lithium enolates and amides: a) Dimeric lithium enolate of *N, N*-dimethylcycloheptatrienecarboxamide, crystallized from THF. b) Dimeric lithium diisopropylamide, obtained as the $[LDA]_2 \cdot (THF)_2$ complex.

Figure 1-3 a) Seebach, D. Structure and Reactivity of Lithium Enolates. From Pinacolone to Selective C-Alkylations of Peptides. Difficulties and Opportunities Afforded by Complex Structures. *Angew. Chem. Int. Ed. Engl.* **1988**, 27, 1624-1654. Copyright Wiley-VCH Verlag GmbH & Co. KGaA. Reproduced with Permission.

A major consequence of lithium enolate aggregation is the change in reactivity that occurs upon stabilization of the lithium ion by solvent molecules. For example, the aldol reaction between lithium pinacolonate **1-14** and pivaldehyde **1-15** is highly exothermic in hexane but 12 kcal/mol less exothermic when the lithium pinacolonate aggregate is stabilized by THF (Table 1-9).^{39,40}

Table 1-9. Effect of solvent on lithium enolate stabilization.

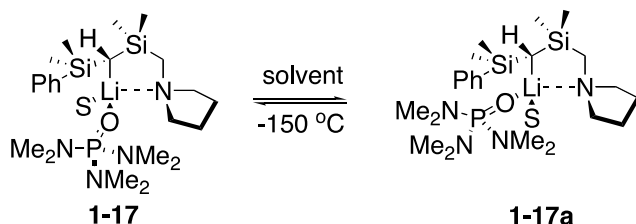


	No additive	1 equiv TMEDA	1 equiv DME	1 equiv THF
ΔH_{aldol} (kcal/mol)	-30.2	-20.9	-19.0	-17.9

^aHeat of reaction data were obtained by calorimetric measurements of the reaction between 1 equiv lithium pinacolonate and 1 equiv electrophile.⁴⁰

1.1.2.4 .Spectroscopic Investigations of Interactions with Organolithium Species

Studies regarding the low-temperature solution structure of lithium amides have revealed the superior ligating properties of oxetane in comparison to THF. Reich et al.²⁴ determined the relative coordinating ability of donating solvents using ³¹P NMR titrations of the chiral organolithium reagent **1-17** (Figure 1-4). It was discovered that the relative donor strength toward lithium was correlated with the rate exchange of the solvated diastereomers. The rate of diastereomeric exchange was faster in the presence of weakly coordinating solvents (e.g., Me₂O), than in stronger donor solvents (e.g., oxetane). In fact, in the presence of 6 equiv of oxetane, an ~1:1 ratio of solvated diastereomers was observed at -150 °C (by ³¹P NMR spectroscopy). Furthermore, by integration of phosphorus signals, the equilibrium constant for solvent exchange with dimethyl ether (Table 1-10) was calculated, yielding relative K_{solv} values at -150 °C (Table 1-10). Interestingly, no solvent coordination was observed upon addition of 2-methyloxirane (up to 28 equiv).



S = Me₂O, THF, 3,3-dimethyloxetane, oxetane, pyridine, or HMPA

Figure 1-4. Diastereomeric solvates of a chelated organolithium reagent.

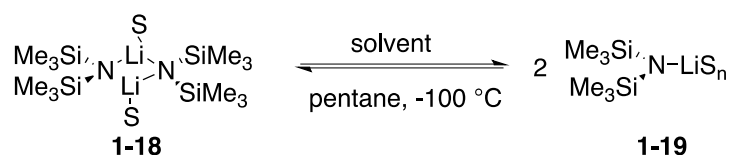
Table 1-10. Relative K_{solv} values for a chelated organolithium reagent determined by ³¹P NMR titrations.



Solvent	Me ₂ O	THF	3,3-dimethyloxetane	oxetane	pyridine	HMPA
K_{solv} (rel.)	1	7	13	16	100	2000

Collum and coworkers studied the effects of ethereal solvents on the equilibrium between dimeric aggregate **1-18** and n-solvated monomer **1-19** (Table 1-11).²³ The studies indicated that the LiHMDS monomer **1-19** appeared at unusually low concentrations of oxetane (5.0 equiv per Li), and the concentration of **1-19** increased more rapidly upon addition of oxetane than upon addition of THF. Furthermore, addition of just 20 equiv oxetane shifted the equilibrium toward the monomeric species (Table 1-11, entry 5), whereas addition of up to 40 equiv THF still favored the dimer (Table 1-11, entry 4). Collum has also noted the superior coordinating properties of oxetane versus THF or Et₂O regarding solvation of LDA⁴¹ and lithium diethylamide.⁴²

Table 1-11. Effect of solvent on the aggregation of LiHMDS solvates.



Entry	Solvent	Ratio 1-18 : 1-19
1	ether ^a	49:1
2	2,2-dimethyltetrahydrofuran ^a	1:34
3	2,2,5,5-tetramethyltetrahydrofuran ^a	>50:1
4	tetrahydrofuran ^a	2.6:1
5	oxetane ^b	1:42

^a40 equiv solvent were used. ^b20 equiv solvent were used.

Another outcome of Collum's studies on the dimer/monomer equilibrium of LiHMDS is the importance of substitution on the cyclic ether ligand. Among a series of substituted tetrahydrofurans, 2,2-dimethyltetrahydrofuran proved the most efficient at dissociation of LiHMDS dimers, likely due to unfavorable steric interactions between the solvent ligand and the trimethylsilyl groups on the amide. 2,2,5,5-Tetramethyltetrahydrofuran was a poor solvent for dimer dissociation, likely due to severe solvent-solvent steric interactions on the monomer **1-19**, driving the equilibrium back toward the dimeric aggregate **1-18**.

1.1.3 Hydrozirconation: Solvent Effects and Mechanistic Considerations

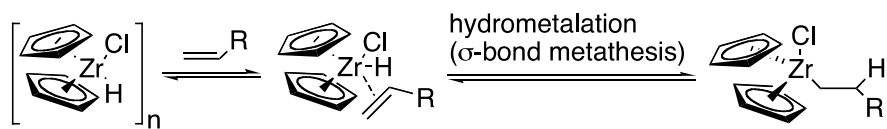
Zirconium hydrides were first prepared by Wailes et al. in 1970,⁴³ and their utility in organic synthesis was first systematically explored by Schwartz in the mid 1970's.^{44,45} Since

then, Schwartz reagent ($\text{Cp}_2\text{Zr(H)Cl}$) has been used in many important C-C bond forming transformations involving π -systems—most commonly alkynes.⁴⁶

1.1.3.1 Mechanism of the Hydrozirconation of Alkenes

Based on calculations performed by Endo et al.,⁴⁷ the mechanism of hydrozirconation of simple olefins proceeds via alkene coordination followed by hydrometalation (Scheme 1-3). The calculated activation barrier for hydrozirconation of ethylene is 15.0 kcal/mol at the RHF level of theory, with most of the activation energy coming from a distortion of the metal complex to allow for coordination of the alkene. According to Endo's model, alkene coordination is rate-limiting, with the subsequent hydrometalation having little to no calculated barrier.

Scheme 1-3. General mechanism for the hydrozirconation of alkenes.

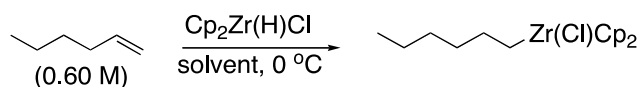


1.1.3.2 Effect of Solvent on the Hydrozirconation of Alkenes

The effect of solvent on the rate of hydrozirconation of 1-hexene was studied (Table 1-12), and from these preliminary screenings oxetane appeared to increase the rate of reaction when used as either a solvent or cosolvent.⁴⁶ The order of reaction in both THF and oxetane was also determined by varying the equivalents of Schwartz reagent and 1-hexene (Table 1-13). In both solvents, doubling the concentration of 1-hexene decreases the half-life approximately 2-fold, indicating the reaction is first-order in 1-hexene. Doubling the concentration of Schwartz reagent has no effect on the rate of reaction in THF, whereas the rate of reaction increases by 1.5-fold in oxetane. Based on this preliminary evaluation, it appears hydrozirconation of 1-

hexene is zeroth order in Schwartz reagent when the reaction is performed in THF but first-order in Schwartz reagent when the reaction is performed in oxetane.

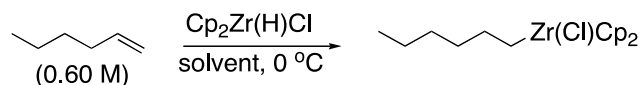
Table 1-12. Effect of solvent on the hydrozirconation of 1-hexene.



Entry	Solvent	Half-life of 1-hexene (min) ^a
1	benzene	2210
2	benzene/oxetane, 9:1 (v/v)	545
3	tetrahydrofuran	113
4	tetrahydrofuran/oxetane, 9:1 (v/v)	95
5	tetrahydrofuran/oxetane, 3:1 (v/v)	60
6	oxetane	37

^aHalf-life refers to the time to reach 50% conversion of 1-hexene to n-hexane when 1 equiv of 1-hexene is mixed with 1 equiv of Schwartz reagent.

Table 1-13. Effect of concentration on the rate of hydrozirconation of 1-hexene.

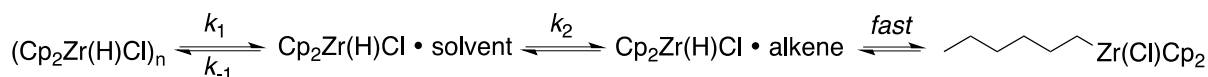


Entry	Solvent	Equiv 1-hexene	Equiv Cp ₂ Zr(H)Cl	Half-life of 1-hexene (min) ^a
1	tetrahydrofuran	1	1	113
2	tetrahydrofuran	2	1	58
3	tetrahydrofuran	1	2	105
4	oxetane	1	1	37
5	oxetane	2	1	24
6	oxetane	1	2	22

^aHalf-life refers to the time to reach 50% conversion of 1-hexene when 1 equiv of 1-hexene is mixed with 1 equiv of Schwartz reagent.

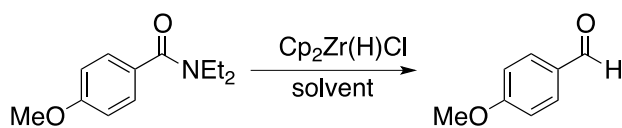
From these preliminary screenings, a general description of the kinetics of hydrozirconation of 1-hexene was generated (Scheme 1-4). Dissociation of the oligomeric Schwartz reagent to form the kinetically active species is likely operable based on the observed solvent effect.

Scheme 1-4. General description of the kinetics of the hydrozirconation of 1-hexene.



Spletsoser et al.⁴⁸ have also noted the solvolytic properties of oxetane when using Schwartz reagent to convert amides to aldehydes (Table 1-14). Use of donating ethers such as oxetane and THF (entries 1 and 2) provided rapid reagent dissolution and subsequent high reaction yields. Using pyridine, a better electron donor, facilitated faster dissolution but poor chemical yields. The authors speculate that pyridine actually occupies a coordination sphere on the zirconium, forming a species that is too stable for the necessary exchange with the amide substrates.

Table 1-14. Effect of solvent on the hydrozirconation of amides.



Entry	Solvent	Yield (%)	t _{diss} (min) ^a
1	oxetane	95	2-3
2	tetrahydrofuran	99	15
3	1,4-dioxane	15	<i>b</i>
4	pyridine	15	1
5	toluene	15	<i>b</i>
6	chloroform	0	<i>b</i>

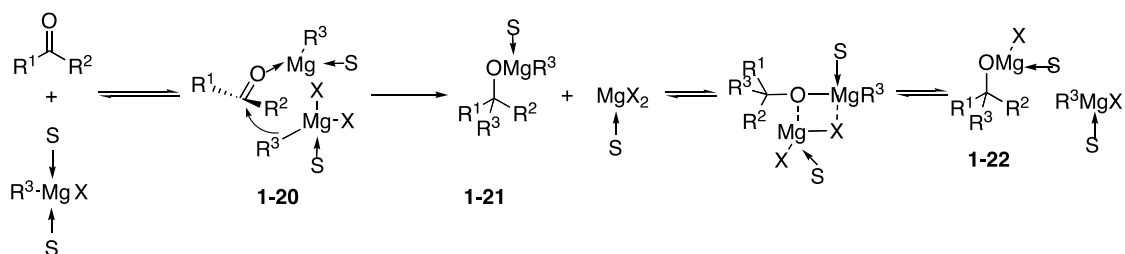
^aTime of dissolution refers to a qualitative observation of the time the solution became homogeneous.

^bComplete dissolution (homogeneity) was not observed.

1.1.3.3 Effect of Ethereal Solvents on Reactions Involving Organomagnesium Reagents

Reactions involving organomagnesium (Grignard) are typically performed in ethereal solvents. Ethereal solvents are sufficiently coordinating to solubilize the organomagnesium reagents while also being inert to Grignard reactivity. An example of the prototypical Grignard reaction—the addition of organomagnesium reagents to ketones, is shown in Scheme 1-5.⁴⁹ It has been established (via kinetic studies) that addition of Grignard reagents to ketones is 2nd order in Grignard reagent, leading to a proposed mechanism involving a bimetallic intermediate **1-20** which, upon delivery of an alkyl or aryl group to the ketone, generates the alkoxide **1-21** and a magnesium dihalide. The complex **1-21** and dihalide are in equilibrium with complex **1-22** and the Grignard reagent.

Scheme 1-5. General mechanism for the addition of Grignard reagents to carbonyl compounds.

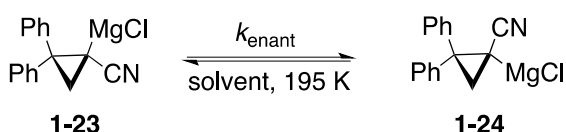


It has been shown that solvent basicity has dramatic effects on the outcome of Grignard reactions. For example, Lewis and Wright found that using strongly basic solvents (e.g., pyridine) afforded only trace amounts of product when ethylmagnesium bromide was added to benzophenone.⁵⁰ In contrast, using weakly basic solvents (e.g., ether, anisole) led to more rapid reactions and higher product yields. This phenomenon is typical of Grignard additions to ketones—more basic solvents coordinate more strongly to the magnesium reagents, thus attenuating the reactivity of the reagents.

Additionally, solvent effects have been observed in the case of racemization of configurationally stable Grignard reagents. Patwardhan and coworkers showed that the rate of racemization of cyanocyclopropane **1-23** increased when switching solvents from ether to 2-

methyltetrahydrofuran to tetrahydrofuran; however, the rate of epimerization with 2-MeTHF and THF does appear comparable within the reported experimental error (Table 1-15).⁵¹ Nevertheless, the relationship between racemization and donating ability is indicative of a mechanism whereby association of solvent is followed by cleavage of the Mg-C bond.

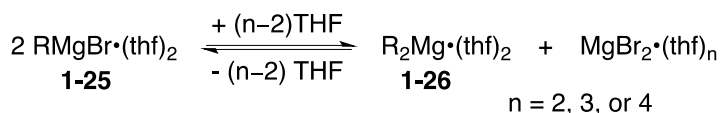
Table 1-15. Effect of solvent on the rate of racemization of an organomagnesium cyanocyclopropane.



Solvent	Et ₂ O	THF	2-MeTHF
$K_{\text{enant}} (\text{s}^{-1})$	$20.8 \times 10^6 \pm 3.3$	150.1 ± 4.2	175.3 ± 32.5

Reactions involving Grignard reagents are further complicated by the existence of the Schlenk equilibrium (Scheme 1-6) in the case of ethereal solvents. In general, the equilibrium lies to the left in the case of acyclic dialkyl ethers (e.g, diethyl ether, methyl *tert*-butyl ether), but the equilibrium is shifted to the right in the case of cyclic ethers (e.g., THF, 1,4-dioxane). A general equation (Scheme 1-6) showing the Schlenk equilibrium for Grignard reagents in the presence of THF is depicted below.

Scheme 1-6. General description of the Schlenk equilibrium.



The consequence of the Schlenk equilibrium is a differing reactivity of the organomagnesium halide **1-25** and the diorganomagnesium reagent **1-26**. Knochel and coworkers have performed extensive studies detailing the effect of additives (e.g., 1,4-dioxane) on the *anionic* Schlenk equilibrium (Scheme 1-7).⁵² One outcome of their studies was that additives with sufficient coordination to MgCl₂ (e.g., [15]-crown-5 or 1,4-dioxane) facilitated the Mg/Br exchange reaction of electron-rich aromatic bromides (Table 1-16).

Scheme 1-7. General depiction of the anionic Schlenk equilibrium in the presence of 1,4-dioxane.

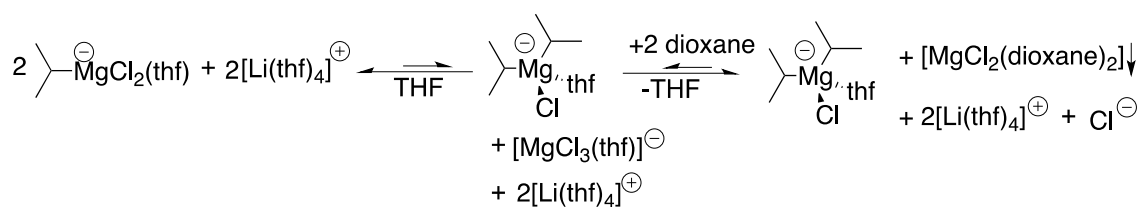
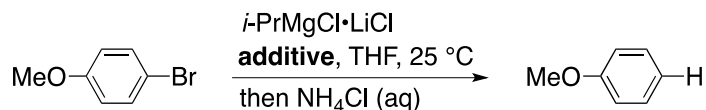


Table 1-16. Mg/Br exchange reactions of 4-bromoanisole using *i*-PrMgCl-LiCl and various additives.



Entry	Additive (amount)	Conversion (GC, %) ^a
1	none	31
2	DMPU (10% v/v)	60
3	Me(OCH ₂ CH ₂) ₄ OMe (10% v/v)	60
4	1,4-dioxane (10% v/v)	100 ^b
5	[15]-crown-5 (1 equiv)	100 ^c

^aConversion was determined after 24 h. ^bConversion was determined after 10 h. ^cConversion was determined after 6 h.

1.1.4 Solubility Enhancement Using Oxetanes: Applications in Medicinal Chemistry

In recent years, interest in the oxetane moiety has surged, mostly due to discovery initiatives pioneered by Müller and Carreira.²⁸ It was first postulated that an oxetane could replace a *gem*-dimethyl group as a metabolically robust subunit that decreases the lipophilicity of the modified molecule (Figure 1-5). The hypothesis was based on the similar partial molar volumes of oxetane (61.4 cm³/mol at 25 °C) and propane (75 cm³/mol at 25 °C) in water; therefore, substituting the *gem*-dimethyl groups with an oxetane increases polar surface area without changing the overall molecular size and conformation. Results from screening a range of oxetanes derived from oxetane-3-one revealed that oxetanes bearing aromatic substituents were stable across a broad pH range. A report by the same group⁵³ suggests that, rather than being a substitute for the *gem*-dimethyl group, the oxetane moiety may be a substitute for the carbonyl group. In this case, the molar volume of oxetane is larger than formaldehyde; yet, the structural analogy comes from a similar disposition of the oxygen lone pairs. An oxetane-for-carbonyl substitution maintains Lewis basicity and polar surface area while disrupting conjugation (e.g., in the case of enones or amides). The consequences of oxetane-for-carbonyl bioisosterism may therefore be the creation of metabolically stable analogs with more acceptable toxicity profiles.

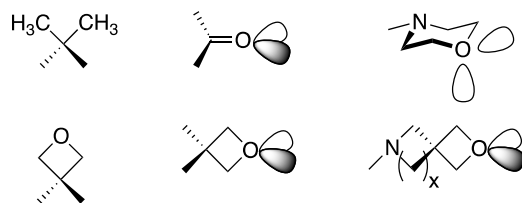
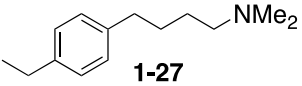
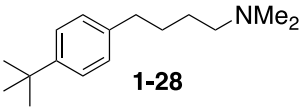
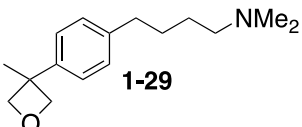


Figure 1-5. Representation of possible functional groups for which oxetane may serve as a bioisostere (adapted from reference 6).

The aqueous solubility enhancement as well as gain in metabolic stability from introduction of an oxetane was well demonstrated in the case of substrate **1-27** (Table 1-17). Substitution of the methylene group with a *gem*-dimethyl group (**1-28**) increased metabolic stability at the

expense of aqueous solubility (Table 1-17, entry 2). Substitution of the methylene group with an oxetane group (**1-29**) enhanced both metabolic stability and aqueous solubility (Table 1-17, entry 3).

Table 1-17. Selected data showing the consequences of substitution at the benzylic position with a *gem*-dimethyl group or an oxetanyl group.⁶

Entry	Compound	logD ^a	Solubility (μmol/L)	Intrinsic clearance (min ⁻¹ /mg/μL) _{protein} human (mouse)
1	 1-27	1.8	250	37 (520)
2	 1-28	2.5	< 4	16 (240)
3	 1-29	0.8	18,000	0 (43)

^aLogD represents the logarithm of the *n*-octanol/water distribution coefficient at pH 7.4. ^bMolar solubility of the neutral base, measured as an experimental thermodynamic solubility in 50 mM phosphate buffer at pH 9.9 at 22.5 ± 1 °C. ^cPseudo-first-order rate constants of intrinsic clearance, measured in human and mouse microsomes.

1.1.5 Preparation and Toxicological Properties of Oxetanes

In order for oxetanes to be widely used as additives or cosolvents, affordable, scalable syntheses of oxetanes must be possible. Moreover, the compounds should have relatively low toxicity and mutagenicity. In this section, general methods for oxetane synthesis and a “building block” approach toward 3,3-disubstituted oxetanes recently developed by Carreira are reviewed. Reported studies of the toxicity and alkylating abilities of oxetanes are discussed.

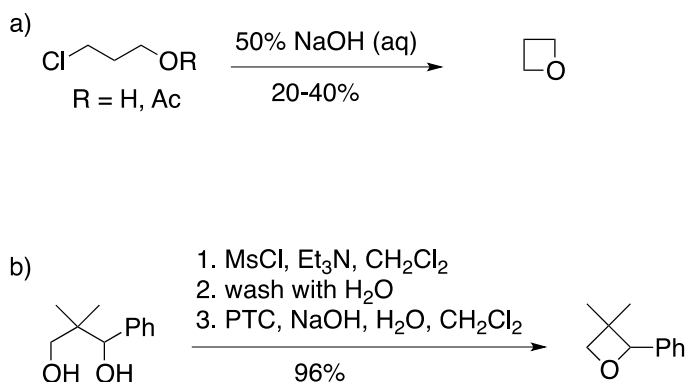
1.1.5.1 Synthesis of Oxetanes

The first reported synthesis of trimethylene oxide was reported by Reboul in 1878,⁵⁴ and an *Organic Synthesis* protocol⁵⁵ for its preparation via saponification and cyclization of 3-chloropropyl acetate was submitted by Noller in 1949. In recent years, interest in oxetanes has laid mostly with polymer chemists.⁵⁶ Synthetic chemists have used oxetanes as precursors for substituted alcohols,^{25,57,58} larger heterocycles,^{59,60} or as precursors to complex crown ether networks.^{61,62} Oxetanes are also components of natural products (notably Taxol⁶³⁻⁶⁵), and recently a surge in the synthesis and manipulation of oxetane-bearing substrates has stemmed from a medicinal interest in these molecules.^{28,53,66} A summary of methods for oxetane preparation is provided in this section.

1.1.5.2 Intramolecular Cyclization Reactions

The most general method for the synthesis of oxetanes is via intramolecular displacement reactions. Typically, the precursors are 3-halogenated alcohols or acetates (for intramolecular Williamson ether synthesis, Scheme 1-8a),⁶⁷⁻⁷⁰ or 1,3-diols. In the latter case, one-pot mono-derivatization/cyclization procedures have been developed (e.g., Scheme 1-8b).^{71,72} Although the intramolecular displacement reaction often leads to the desired oxetane products, yields are typically modest, primarily due to polymerization of the substrates and side reactions (elimination and Wharton fragmentation reactions).^{73,74} A solid-support synthesis of oxetanes has been reported as one method for avoiding side-product formation.⁷⁵ The diastereoselective synthesis of oxetanes substituted at C-2 using Mitsunobu conditions has also been reported.⁷⁶

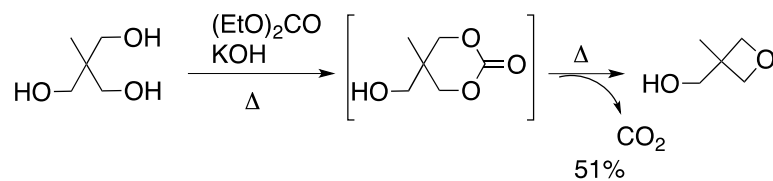
Scheme 1-8. Synthesis of oxetanes via intramolecular cyclization reactions.



1.1.5.3 Pyrolysis of Cyclic Carbonates

An alternative route to oxetane products is the pyrolytic decomposition of cyclic carbonates (Scheme 1-9), first reported by Pattison in 1957.⁷⁷ The one-pot procedure involves generation of the carbonate (generally via reaction of the starting diol and a dialkyl carbonate) followed by extrusion of carbon dioxide. The procedure is scaleable (a 200 g scale), and the product oxetanes can often be collected by distillation from the reaction mixture. This synthesis has been completed in our laboratories as part of our program to scale-up dimeric oxetanyl additives and cosolvents.

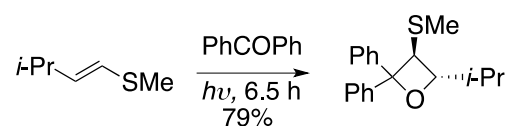
Scheme 1-9. Synthesis of oxetanes via pyrolysis of cyclic carbonates.



1.1.5.4 Synthesis of 2-Substituted Oxetanes

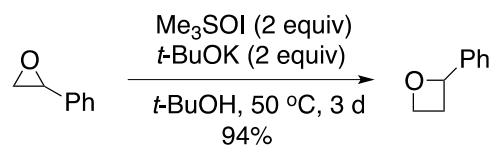
One of the earliest reports of oxetane formation was the discovery of the Paterno-Büchi reaction (e.g., Scheme 1-10) in 1909 and 1954.⁷⁸ The reaction typically proceeds with excellent regio- and stereoselectivity but in modest yields. Moreover, the reactions are limited in that there must be at least one substituent at the 2-position.

Scheme 1-10. Oxetane synthesis via the Paterno-Büchi reaction.



2-Substituted oxetanes can also be synthesized via methylene transfer (Corey-Chaykovsky protocol) to ketones or epoxides (Scheme 1-11).^{79,80} Generally, the yields are high, and the only drawback is the long reaction time (typically 3 d).

Scheme 1-11. Synthesis of oxetanes via ring expansion of epoxides.

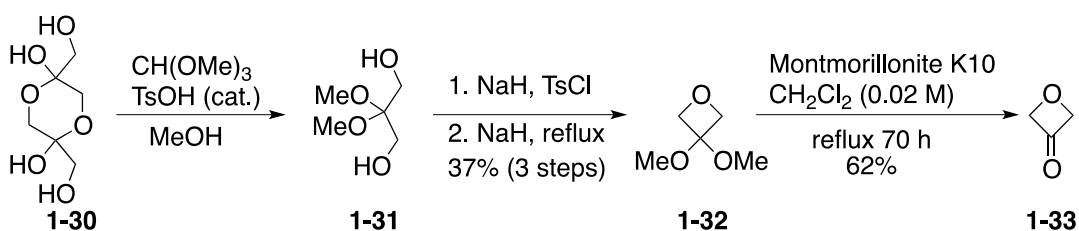


1.1.5.5 Synthesis and Functionalization of Oxetan-3-one

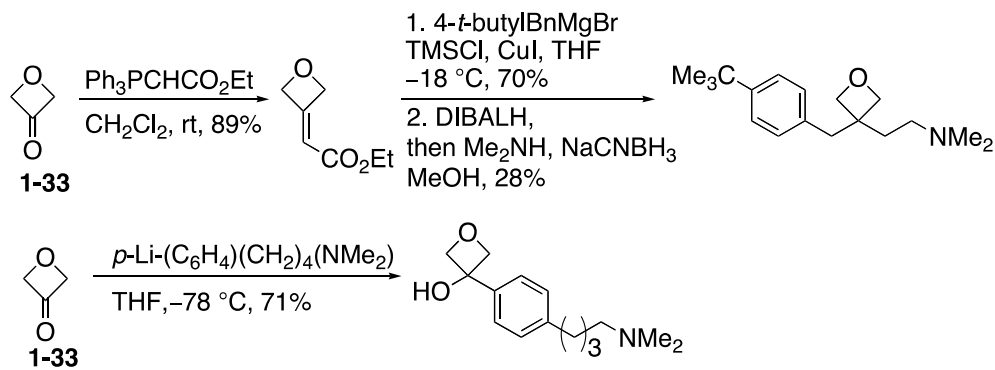
To facilitate incorporation of oxetanes onto medicinally interesting scaffolds, Carreira and coworkers developed a scaleable route to a useful building block, oxetan-3-one (Scheme 1-12).^{7,27} Acetalization of 1,3-dihydroxy acetone dimer **1-30** to afford acetal **1-31** was followed by mono-tosylation (NaH, TsCl) and ring closure to afford oxetane **1-32** in 37% yield over three steps. The authors reported difficulty cleaving the acetal due to substrate polymerization under acidic conditions. Nevertheless, treatment of a dilute solution of **1-32** with Montmorillonite K-

10 provided oxetane-3-one **1-33** in acceptable yield. Oxetan-3-one **1-33** can be derivatized using Wittig reactions, and nucleophilic addition to the resulting enones affords 3,3-disubstituted oxetanes (Scheme 1-13). Oxetan-3-one **1-33** can also be functionalized via addition of organometallic reagents (Scheme 1-13) and Strecker reactions.

Scheme 1-12. Scaleable synthesis of oxetan-3-one.



Scheme 1-13. Example methods for functionalizing oxetan-3-one.



1.1.6 Toxicity and Carcinogenicity of Oxetanes

Due to the high strain energy of the oxetane ring (25.2 kcal/mol),⁸¹ oxetanes are regarded as electrophiles, thus, there are many concerns that oxetanes will exhibit similar toxicity and mutagenicity profiles as other strained, heterocyclic alkylating agents (e.g., oxiranes, β -lactones). Animal studies performed in 1963⁸² and 1970⁸³ showed that oxetane and 3,3-

dimethyloxetane induced tumor formation when injected into rats; yet, these data are equivocal, and the cause of tumors may have been from sources other than oxetanes (i.e., impurities).

Recently, Gómez-Bomarelli et al. performed an extensive study regarding the alkylating potential and toxicity of oxetanes.⁸⁴ They screened a set of simple, commercially available oxetanes—trimethylene oxide, 3,3-dimethyloxetane, and 3-methyl-3-oxetanemethanol. All three substrates showed no indication of being mutagenic (Ames test) or genotoxic (BTC *E. coli* test). Additionally, when subjected to a comet assay, the results from using the three compounds were not statistically different than that of the negative control, indicating that the oxetanes are not capable of producing DNA strand breaks.

The authors also tested cell viability in the presence of oxetanes using an MTT assay (using Chinese hamster lung fibroblast cells). The oxetanes did not exhibit toxicity toward the cells even at the highest concentration tested (30 mM). It can be implied that the oxetanes and any metabolites were not toxic to the cell line used in this study.

A final and important experiment performed as part of this study was the kinetic NBP test, which is an *in vitro*, chemical assay that examines the reactivity of electrophiles toward 4-(*p*-nitrobenzyl)pyridine (NBP). NBP has similar nucleophilicity to DNA bases, and this assay can be used to predict DNA-alkylating ability of electrophiles. Alkylation only occurred at acidic pH, and the half-reaction time for the alkylation of NBP by trimethylene oxide was ~1 month; the values were 10-fold to 40-fold higher in the case of the more sterically hindered, 3,3-substituted substrates. The data are corroborated by the previously discussed work regarding the metabolic stability of 3,3-disubstituted oxetanes (section 1.1.4).

1.2 RESULTS AND DISCUSSION: OXETANES IN ORGANOMETALLIC REACTIONS

I began an exploration of using oxetanes as additives or cosolvents by testing them in reactions involving organolithium, organozirconium, and organomagnesium reagents. Herein, I detail the design and synthesis of our oxetane-containing additives and describe results obtained from a series of selected test reactions with known solvent effects.

1.2.1 3,3-Disubstituted Dimeric Oxetanyl Ethers as Additives and Cosolvents

I synthesized possible additives or cosolvents bearing multiple oxetane functionalities. Although oxetane is commercially available, it is a costly solvent (typically \$8–10/mL) and has high volatility (bp = 50 °C). Furthermore, the ring strain of oxetane renders it susceptible to reacting under nucleophilic conditions; generating 3,3-disubstituted oxetanes substitute would attenuate reactivity while still preserving sufficient donating ability. The overall goal was to generate more robust alternatives that would be used in lower quantities.

As a basis for designing additives and solvents containing oxetanes, inspiration was drawn from known metal chelating agents such as crown ethers (e.g., [18]-crown-6 (**1-34**)) and podands (e.g., **1-35**) (Figure 1-6). These additives contain oxygens in an appropriate special orientation for chelation and sequestering of metal ions. Additionally, use of cyclic ethers for metal ion chelation has been demonstrated by Paquette and coworkers. For example, the tris (2,2',2'')-tetrahydrofuran **1-36** had an association constant for Li⁺ that was comparable to that of [15]-crown-5.⁸⁵

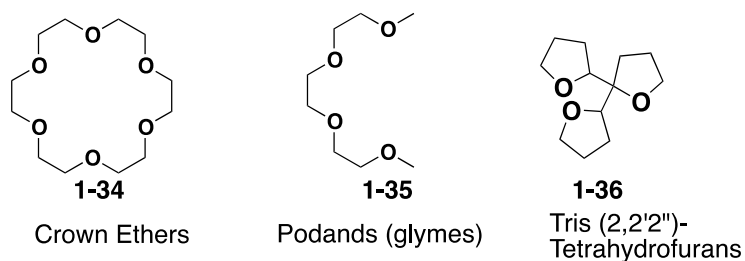


Figure 1-6. Examples of ethereal ionophores.

1.2.2 Synthesis of Dimeric Oxetanes

Previously reported compounds **1-37**⁶² and **1-38**⁷³ were first explored because they are accessible in 1–2 steps from commercially available materials (Figure 1-7). Using **1-37** would allow for investigation of a flexible ether with oxygens that are appropriately positioned for possible chelation of metal ions. Spirocycle **1-38** could be considered as a more stable analog of oxetane itself.

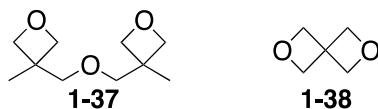
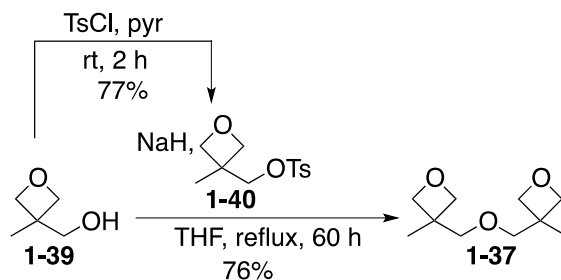


Figure 1-7. Dimeric oxetane additives for initial solvent effect screens.

The synthesis of ether **1-37** was accomplished by treatment of commercially available alcohol **1-39** with known tosylate **1-40**⁸⁶ and sodium hydride (Scheme 1-14).⁶² Heating at reflux for an extended reaction time (60 h) in THF was required for acceptable conversion; the requirement for a long reaction time likely comes from the difficulty in reacting a neopentyl nucleophile with a neopentyl electrophile.

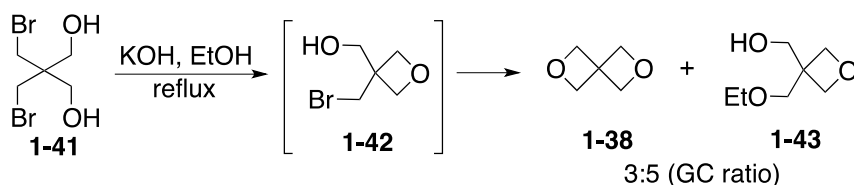
Scheme 1-14. Synthesis of dimeric ether **1-37**.



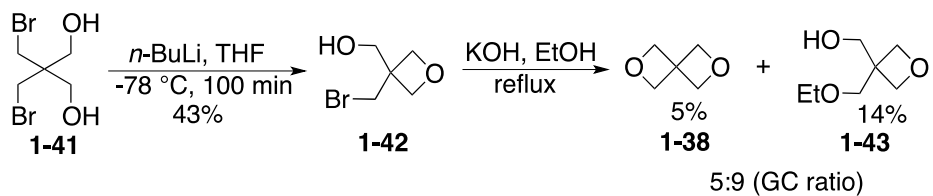
It should be noted that the starting alcohol **1-39** can be prepared on multi-gram scale by treating inexpensive 1,1,1-tris(hydroxymethyl)ethane with dimethyl carbonate and catalytic amounts of KOH and methanol.^{87,88} Alcohol **1-39** is distilled from the reaction mixture, thus obviating the need for additional purification steps; **1-39** is therefore a feasible starting material that can be purchased or prepared in sufficient quantities for use as a solvent precursor.

Synthesis of spirocycle **1-38** was more problematic; initial attempts to reproduce the literature procedure⁷² by treating 2,2 bis(bromomethyl)-1,3-propanediol **1-41** with KOH and EtOH resulted in trace amounts of the desired product (Scheme 1-15). Ethyl ether **1-43** was isolated as the major product—it is reasonable that **1-43** is formed from an initial intramolecular Williamson ether reaction of **1-41** to form bromide **1-42**, followed by an *intermolecular* Williamson ether reaction between EtOH and the neopentyl bromide **1-42**. This hypothesis was confirmed by the independent synthesis of mono-cyclized bromide **1-42** by treatment of **1-41** with *n*-BuLi in THF (Scheme 1-16). Bromide **1-42** was subjected to the reaction conditions (KOH, EtOH, reflux); indeed, ethyl ether **1-43** was formed as the major product, albeit in low yield.

Scheme 1-15. Attempted preparation of 2,6-dioxaspiro[3.3]heptane.

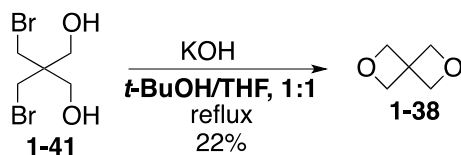


Scheme 1-16. Independent synthesis of bromide **1-42** and ethyl ether **1-43**.



It was reasoned that attenuating solvent nucleophilicity would prevent the undesired intermolecular substitution reaction. After screening many commercially available alcohols, it was determined that *t*-BuOH was the optimal choice for both efficient solvation of the starting diol and sufficient suppression of the undesired side reaction. Although a reproducible method for the formation of **1-38** was developed, the yield was low due to the problems with isolating the spirocycle, which sublimates at atmospheric pressure. To isolate spirocycle **1-38**, solvent was removed by distillation. Spirocycle **1-38** was collected by sublimation from the resulting residue after gentle heating ($60\text{ }^\circ\text{C}$) at atmospheric pressure. Due to the need to remove large volumes of solvent by distillation, the protocol was modified, and a binary mixture of *t*-BuOH and lower boiling THF was used; the optimized conditions are shown in Scheme 1-17. Attempts to improve the isolation protocol (and consequently the isolated yield) included distilling the product from high-boiling, hindered alcoholic solvents (e.g., 2,2,4-trimethyl-1,3-pentandiol and (1*R*)-endo-(+)-fenchyl alcohol); however, the desired product was not collected using this distillation protocol.

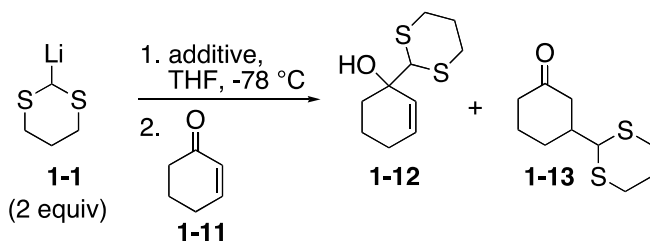
Scheme 1-17. Optimized protocol for synthesis of spirocycle **1-38**.



1.2.3 Use of Dimeric Oxetanes in Reactions Involving Organolithium Reagents.

Because studies by Collum and Reich (Section 1.1.2.4) indicated that oxetane-solvated lithium aggregates to a greater extent than THF, it was worthwhile to screen reactions dependent on solvent interactions with organolithium species. The addition of (1,3-dithian-2-yl)lithium **1-1** to 2-cyclohexenone **1-11** (Table 1-18) was tested. Using dimeric oxetanyl ether **1-37** (up to 4 equiv) afforded only the 1,2-addition product **1-13** (entry 3). Spirocycle **1-38** was used in large excess, but, again, only the kinetic, 1,2-addition product **1-13** (entry 4) was formed. Because the 1,2-addition product has been shown to be formed when contact ion-pairing is operable,³⁵ the results indicate that **1-37** and **1-38** were ineffective at providing the cation solvation necessary for disruption of the carbonyl-lithium interaction.

Table 1-18. Results from using dimeric oxetanes in dithiane additions to 2-cyclohexen-1-one.

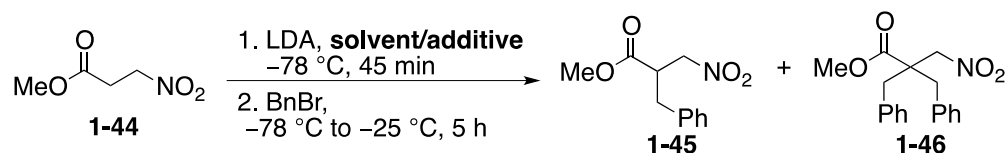


Entry	Additive	Ratio 1-12 : 1-13 ^a	Yield (%)
1	none	> 95:5	74
2	HMPA (2 equiv)	16:84 ^b	67
3	1-37 (4 equiv)	> 95:5	56
4	1-38 (30 equiv)	>95:5	78

^aRatios were determined by crude ¹H NMR analysis. ^bReich reported a ratio of <5:95.³⁵

The ability of the oxetane additives to solvate lithium aggregates was investigated by examining the solubility of the lithium dianion of methyl 3-nitropropanoate **1-44**. Literature reports document that the dianion precipitated from THF solutions but was well-solvated by addition of electron-donating solvents such as HMPA and DMPU.⁸⁹ Dianion solubility correlated directly with the yield from alkylation with electrophiles. For example, yields ranging from 0–8% have been reported when THF was used as a solvent. Yields as high as 85% were reported when 5 equiv HMPA (and a THF/HMPA, 5:1 v/v ratio) were employed.⁹⁰ Therefore, the alkylation of the dianion of methyl 3-nitropropanoate was a suitable test system for the dimeric oxetane additives. Results from testing this alkylation reaction are summarized in Table 1-19.

Table 1-19. Results from using oxetane additives to enhance dianion solubility.



Entry	Solvent	Yield of 1-45	Yield of 1-46
1	THF	<5%	--
2	DMPU (10 equiv)	63%	4%
3	THF, HMPA (5 equiv), 5:1 (v/v)	58% ^a	9%
4	THF/oxetane, 5:1 (v/v)	--	--
5	THF, 1-37 (5 equiv)	36–42% ^b	0–2%
6	THF, 1-38 (5 equiv)	0% ^b	--

^aThree trials were performed; yields of **1-45** were consistent (55–58%). ^bIn a separate trial, **1-45** was isolated in 14% yield.

The results (Table 1-19) indicated that dimer **1-37** indeed solvated the dianion because the alkylated product was isolated in modest yield. Although the reaction mixture became heterogeneous when the dianion was formed in THF, it remained homogeneous when using 5 equiv of dimer **1-37**. Heterogeneity was observed when spirocycle **1-38** was used as an additive.

Spirocycle **1-38**, although stable toward nucleophilic attack, has a rigid structure. Conformational changes that would accompany electron-donation to metal cations may not be operable on this additive. Conversely, dimer **1-37** has a more flexible framework and would be capable of undergoing conformational changes upon electronic donation to cations. Moreover, the ability to form 6-membered chelates or possibly bidentate complexes makes the system of interest, particularly given the promising preliminary result in this dianion solubility screen.

1.2.4 Effect of Oxetane-Based Additives on the Rate of Hydrozirconation of Alkenes

As discussed in section 1.1.3, solvent has an effect on the rate of hydrozirconation of alkenes. More specifically, electron-donating solvents are postulated to disrupt aggregation of polymeric Schwartz reagent, thus generating the kinetically active monomeric zirconocene species.

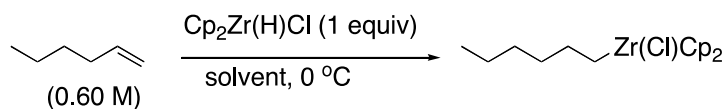
Based on the preliminary results reported in the Wipf group,⁴⁶ the effect of solvent on the rate of hydrozirconation of 1-hexene was explored further. A range of solvents with varying donating abilities and bulk permittivities was screened. The study was limited to ethers, aromatic hydrocarbons, and chlorinated hydrocarbons; carbonyl-bearing solvents (e.g., acetone, ethyl acetate), dimethyl sulfoxide, hexamethylphosphoramide, acetonitrile, and nitromethane are incompatible with Schwartz reagent.

1.2.4.1 Hydrozirconation in Aromatic and Chlorinated Solvents

To expand the table of previously reported results (Table 1-12), the rate of hydrozirconation in aromatic hydrocarbons and chlorinated hydrocarbons was measured. In the case of aromatic hydrocarbons, poor conversion was observed in toluene, and little to no improvement was seen upon moving to more polar aromatic hydrocarbons such as chlorobenzene or α,α,α -trifluorotoluene. In corroboration with observations noted in the case of hydrozirconation of alkynes, the reaction proceeds fastest in methylene chloride ($t_{1/2} = 40$ min). My interest, however, was in examining the effect of increasing the electron-donating ability of ethereal solvents, and a range of ethers was first screened to establish the solvent scope.

1.2.4.2 Reactions in Ethereal Solvents

A series of ethereal solvents in the hydrozirconation of 1-hexene (Table 1-20) was screened. Oxetane was found to be the superior solvent (Table 1-20, entry 3). Moreover, addition of oxetane to other ethereal solvents enhanced the rate of hydrozirconation. For example, the rate of hydrozirconation in THF was increased when oxetane was added in a 50% v/v ratio (entry 5), yet it appears the effect of additional oxetane has a threshold—no significant improvement was made upon increasing the oxetane percentage to a 75% v/v solution (entry 6).

Table 1-20. Hydrozirconation of 1-hexene using ethereal solvents.

Entry	Solvent	Half-life (min) ^a
1	tetrahydropyran	1200
2	tetrahydrofuran	120
3	oxetane	52 ± 4 ^b
4	tetrahydrofuran/oxetane, 3:1	112 ± 3 ^c
5	tetrahydrofuran/oxetane, 1:1	69
6	tetrahydrofuran/oxetane, 1:3	65
7	tetrahydropyran/oxetane, 3:1	320
8	dimethoxymethane	no conversion
9	dimethoxyethane	870
10	2-methyltetrahydrofuran	< 5% conversion ^d
11	2,5-dimethyltetrahydrofuran	no conversion ^d
12	3,3-dimethyloxetane	< 5% conversion ^d
13	diethyl ether	no conversion ^d

^aHalf-lives of 1-hexene were calculated based on GC measurements (after an aqueous quench) of the relative concentrations of 1-hexene and n-hexane over time. ^bThe data represents an average of three trials. ^cThe data represents and average of four trials. ^dMinimal or no conversion was observed after a period of 2 h.

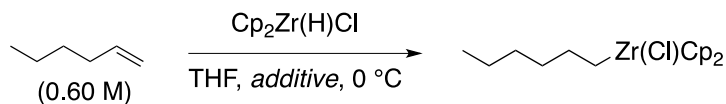
When the hydrozirconation reaction was performed using substituted ethereal heterocycles (Table 1-20, entries 10-12) as solvents, little to no conversion was observed. The donor number of 2-methyltetrahydrofuran is 18 kcal/mol, which does not differ substantially from that of THF (20.0 kcal/mol). Furthermore, rate retardation or no reaction was observed in solvents with similar or higher donor numbers than THF such as ether (Table 1-20, entry 13, $DN = 19.2$ kcal/mol) and THP (Table 1-20, entry 1, $DN = 22$ kcal/mol). Interestingly, using 3,3-dimethyloxetane (Table 1-20, entry 12) as a solvent also resulted in poor conversion of 1-hexene.

Clearly, donicity alone cannot explain the trend in rate differences for the hydrozirconation of 1-hexene. Because Schwartz reagent contains two bulky cyclopentadienyl units per zirconium atom, the lack of reactivity of substituted cyclic ethers may be rationalized by a steric effect—the substituents prevent solvent coordination and dissociation of the oligomeric reagent into kinetically active monomers.

I also examined the outcome of the hydrozirconation of 1-hexene using dimeric oxetane additives **1-37** and **1-38** with THF as a parent solvent (Table 1-21). The data indicated that spirocycle **1-38** had no effect on the rate of reaction when up to 5 equiv were added (Table 1-21, entry 4). Dimer **1-37** appeared to have a detrimental effect on the rate of hydrozirconation—higher relative concentrations of dimer slowed the reaction to a greater extent. The reaction rate was higher when 1-hexene was used at lower concentration (0.40 M) in a 2:1 v/v solution of THF/**1-37** than when a more concentrated (0.60 M) solution of 1-hexene in a 1:1 v/v solution of THF/**1-38** (Table 1-21, entry 6) was used.

I postulate that dimer **1-37** competes with THF for coordination to zirconium oligomers; however, dimer **1-37** does not have the same dissociating capabilities as THF. This competitive coordination would inhibit production of kinetically active zirconium monomers. A simpler explanation may be that dimer **1-37** is not a sufficient solvent for deaggregation of Schwartz reagent—increasing the concentration of **1-37** would effectively decrease the concentration of THF. This second hypothesis is corroborated by the fact that no hydrozirconation is observed when the reaction is performed in neat **1-37** at 0 °C (Table 1-21, entry 7).

Table 1-21. Effect of dimeric oxetane additives on the hydrozirconation of 1-hexene.



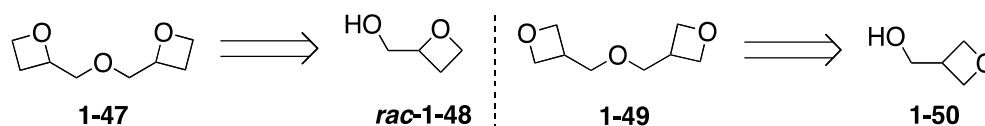
Entry	Additive	Half-life (min) ^a
1	none	120
2	20% oxetane (5 equiv)	120
3	1-38 (1.8 equiv)	130
4	1-38 (5 equiv)	110
5 ^b	1-37 (5 equiv) (1-37 /THF, 2:1 v/v)	220
6	1-37 (5 equiv) (1:1 v/v)	690
7	1-37 (neat)	no conversion

^aHalf-lives of 1-hexene were measured in the manner described in the footnote of Table 14. Reported values are the result of a single trial. ^b1-Hexene was added in an initial concentration of 0.40 M.

1.2.5 Synthesis of Alternative Bisoxetanyl Ethers

Despite the modest success observed when using dimer **1-37** for enhancement of lithium dianion solubility (Table 1-19), I had not yet discovered an optimal oxetane-substituted additive for use in organometallic reactions. I decided to develop synthetic routes for additional bisoxetanyl ethers **1-47** and **1-49** (Scheme 1-18). These compounds could be generated from the corresponding oxetanols **1-48** and **1-50**.

Scheme 1-18. Synthetic plan for the synthesis of bisoxetanyl ethers.



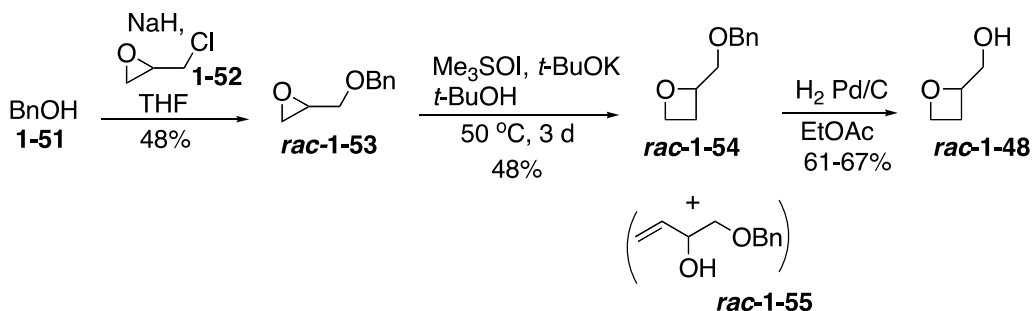
Although the target compounds do not have the stabilization of being 3,3-disubstituted oxetanes, two effects would be probed using these structures. In the case of substrate **1-47**, the oxygen atoms have a different topography in comparison to the original dimeric oxetane **1-37**; the different special orientation may provide access to alternative modes of metal chelation. In the case of substrate **1-49**, the structure is less sterically encumbered due to absence of the methyl group at the 3-position. Moreover, incorporation of an ethereal linkage (analogous to **1-37**) may enhance chelation properties and solubilizing ability, as in the case of dimethoxyethane in comparison to diethyl ether.^{91,92}

1.2.5.1 Synthesis of 2,2'-Oxybis(methylene)dioxetane

The 2-substituted oxetanol **rac-1-48** was synthesized using a modified version of a literature protocol⁸⁰ wherein the alcohol was protected as an ethoxy-ether moiety (Scheme 1-19). A benzyl group was used instead of the ethoxy-ether to avoid aqueous workup of water-soluble alcohol **rac-1-48**. Benzyl glycidol ether **rac-1-53** was readily prepared via alkylation of benzyl alcohol with epichlorohydrin—the product was purified by distillation. **rac-1-54** was obtained

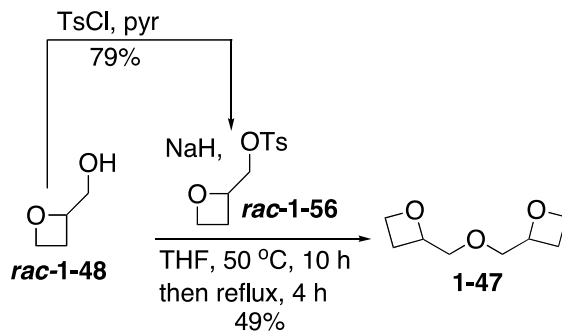
via methylene-transfer methodology using trimethylsulfoxonium iodide in *t*-BuOK and *t*-BuOH.⁹³ The modest yield was due to formation of 1-(benzyloxy)but-3-en-2-ol; presumably, the ylide adds into the epoxide, but E2 elimination of dimethylsulfoxide occurs competitively with the S_N2-type oxetane formation. The benzyl group was removed by hydrogenation to afford alcohol **rac-1-48**.

Scheme 1-19. Synthesis of alcohol **rac-1-48**.



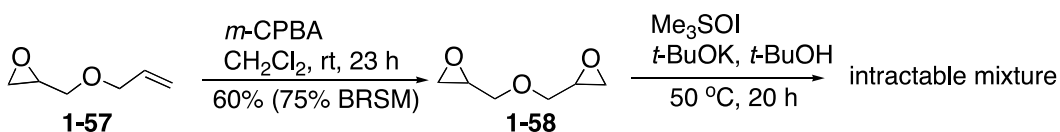
Bisoxetanyl dimer **1-47** was prepared using a standard etherification procedure (Scheme 1-20). Tosylate **1-56** was prepared by treatment of **rac-1-48** with TsCl in pyridine. Reaction of alcohol **rac-1-48** with sodium hydride and tosylate **rac-1-56** and heating in THF for 14 h afforded the desired dimer **1-47** as a mixture of *dl*- and *meso*- diastereomers.

Scheme 1-20. Synthesis of dimeric oxetane **1-47**.



I attempted to shorten the synthesis of dimer **1-47** by performing a double methylene transfer reaction on diglycidyl ether **1-58**, which was accessed from epoxidation of allyl glycidol ether (Scheme 1-21). The reaction yielded a complex mixture of oxetane-containing and olefinic products, and this route was therefore abandoned.

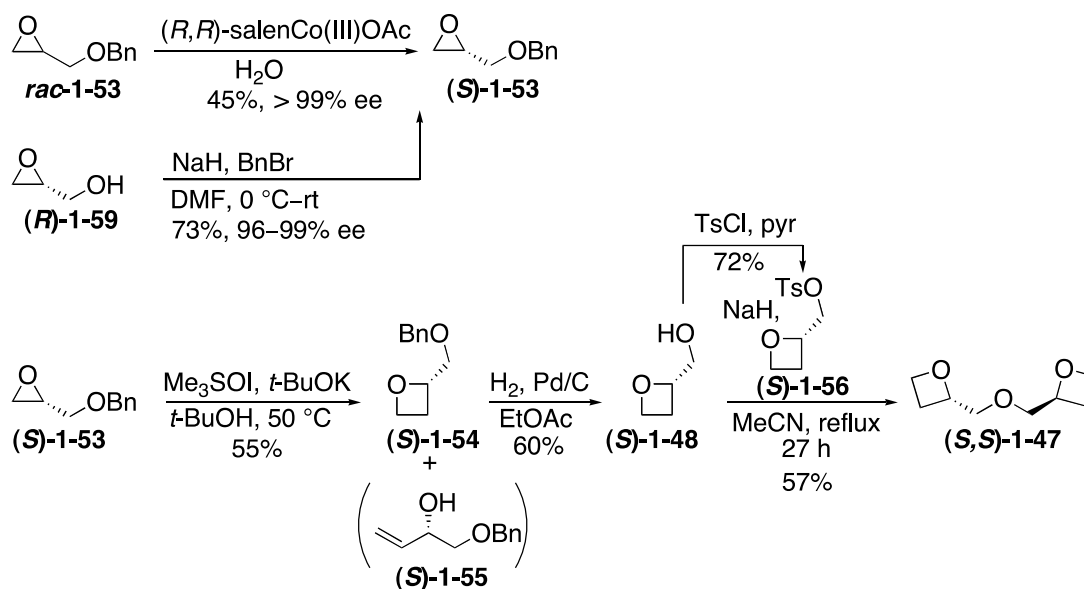
Scheme 1-21. Attempted synthesis of **1-47** via a double methylene transfer reaction.



1.2.5.2 Synthesis of Enantiopure Oxetanes to Generate a Diastereomerically and Enantiomerically Pure Bisoxetanyl Dimer.

1-47 was synthesized as a mixture of *dl*- and *meso*- diastereomers; a diastereomerically and enantiomerically pure variant was synthesized for characterization (Scheme 1-22). Enantiomerically enriched (*S*)-**1-53** was generated either by benzylation of commercially available (*R*)-glycidol (*R*)-**1-59** or *via* hydrolytic kinetic resolution of racemic benzyl glycidyl ether *rac*-**1-53**⁹⁴ (Scheme 1-22). The synthesis was performed in analogous fashion to that of **1-147**—ring expansion of (*S*)-**1-53** followed by debenylation afforded oxetanol (*S*)-**1-48**. Tosylation of (*S*)-**1-48** and etherification (in this case, using MeCN as solvent) afforded (*S,S*)-**1-47** as a single diastereomer (as evidenced by ¹H NMR analysis).

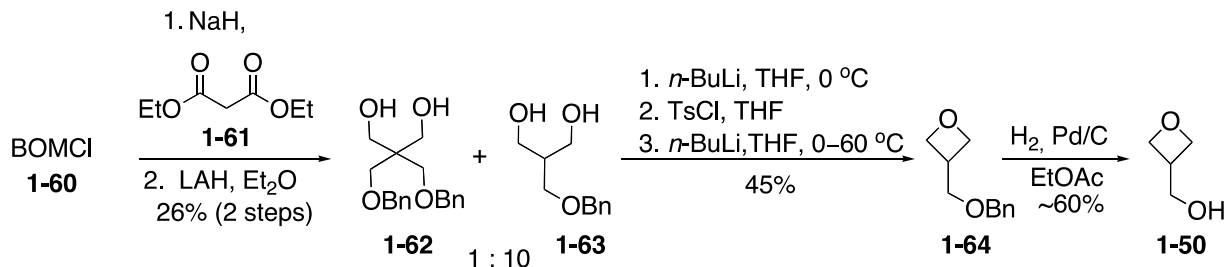
Scheme 1-22. Synthesis of diastereomerically and enantiomerically pure (*S,S*)-**1-47**.



1.2.5.3 Synthesis of 3,3'-Oxybis(methylene)dioxetane

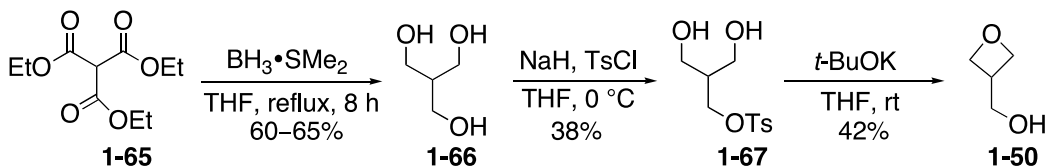
Having completed the synthesis of (*S,S*)-**1-47**, I developed a route to dimeric ether **1-49** via the corresponding oxetanol **1-50**. Synthesis of the alcohol **1-50** was first attempted using a one-pot monotosylation-cyclization procedure (Scheme 1-23). Alkylation of diethyl malonate **1-61** with BOMCl (**1-60**) afforded a mixture of mono- and di-alkylated esters. Reduction of the mixture with LAH led to a 10:1 mixture of desired diol **1-63** and byproduct **1-62**; the diols were separable by chromatography on SiO₂. Diol **1-63** was mono-tosylated and cyclized to afford oxetane **1-64** in modest yield. Debenzylation of **1-64** afforded **1-50** in comparable yield to the debenzylations of *rac*- and (*S*)-**1-54**. Although the oxetane formation proceeded in respectable yield, the inefficiency of the synthesis of diol **1-63** prompted development of a new approach.

Scheme 1-23. Synthesis of **1-50** via a mono-benzylated triol.



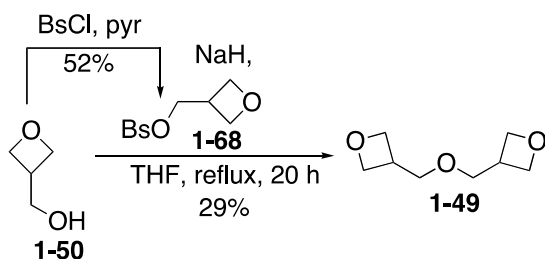
It was hypothesized that alcohol **1-50** could be synthesized directly from mono-tosylated triol **1-67** (Scheme 1-24). Triol **1-66** was generated via reduction of triethyl methanetricarboxylate **1-65**,⁹⁵ which is commercially available or readily prepared by alkylation of diethyl malonate with ethyl chloroformate.⁹⁶ Triol **1-66** was monotosylated to afford **1-67**, which, upon drop-wise addition to a dilute, basic THF solution afforded alcohol **1-50** in modest yield (Scheme 1-24). This pathway was a more atom-economical approach because it obviated the need for a protecting group on the triol.

Scheme 1-24. Synthesis of alcohol **1-50** via a symmetrical triol.



With alcohol **1-50** in hand, the formation of bisoxetanyl ether **1-49** (Scheme 1-25) was attempted. Mindful of the sluggish alkylation in the case of synthesizing dimer **1-37**, alcohol **1-50** was converted to the corresponding brosylate **1-68**; brosylates are more electrophilic than the corresponding tosylates due to the electron-withdrawing nature of the *p*-bromo substituent on the aromatic ring. Etherification by treating alcohol **1-50** with sodium hydride and brosylate **1-68** and refluxing the reaction mixture in THF provided the desired dimeric oxetane **1-49** in low yield.

Scheme 1-25. Synthesis of bisoxetanyl ether **1-49**.



1.2.6 Synthesis of Bisoxetanyl Ethers—Conclusions

Dimeric oxetanyl ethers **1-37** and **1-38** were synthesized, and their ability to induce solvent effects in reactions involving organolithium and organozirconium reagents was tested. In the case of additions of (1,3-dithian-2-yl)lithium to cyclohexen-1-one, neither **1-37** nor **1-38** affected a change in selectivity in comparison to reactions when no additive was used. It was demonstrated that dimeric oxetanyl ether **1-37** improved the solubility of the lithium dianion of methyl 3-nitropropanoate, and this result may be pursued further in due course.

Dimeric oxetanyl ethers were also tested as additives in the reaction of Schwartz reagent with 1-hexene. No effect was observed when spirocycle **1-38** was used as an additive in THF solutions. Use of dimeric oxetanyl ether **1-37** as an additive in THF solutions actually led to a *decrease* in reaction rate, which was indicative of either a) competitive chelation with THF but lack of dissociating power or b) an effective decrease in concentration of THF, which is the coordinating solvent capable of dissociating the polymeric Schwartz reagent.

Three additional bisoxetanyl dimers **1-47**, (*S,S*)-**1-47**, and **1-49** were synthesized. In all cases, low yields during the synthetic sequences made scale-up difficult. I refrained from testing these additives in our set of organometallic test reactions until more favorable results were obtained with the readily accessible oxetanyl dimers.

Due to the difficulty in generating large quantities of bisoxetanyl ether analogs of **1-37**, I instead decided to replace the linking heteroatom with sulfur (Figure 1-8). The synthesis and experiments performed with these new analogs are discussed in the next section.

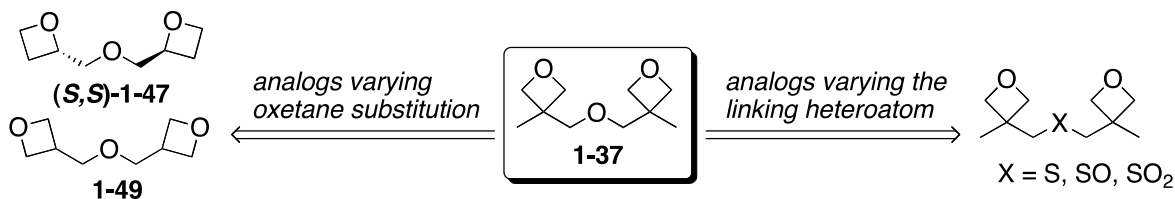


Figure 1-8. Strategies for generating analogs of bisoxetanyl ether **1-37**.

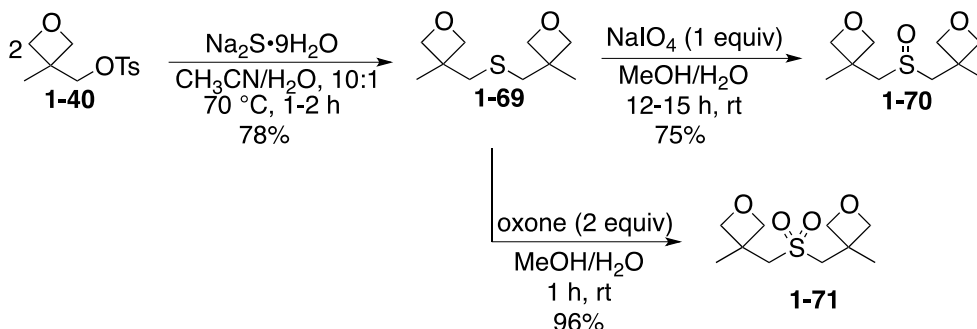
1.2.7 Synthesis and Application of Bisoxetanylsulfides and Sulfoxides

I decided to pursue sulfur-containing analogs of **1-37** because a sulfide provides internal stabilization toward peroxide generation due to preferential oxidation at the sulfur versus C-H abstraction. Additionally, simply changing the oxidation state of the sulfur can generate analogs with different physical properties.

Syntheses of sulfur-based analogs of bisoxetanyl ether **1-37** (Scheme 1-26) were developed. Tosylate **1-40** was dimerized to the symmetrical sulfide **1-69** using disodium sulfide. Initially, oxidation of sulfide **1-69** was attempted with *m*-CPBA in CH₂Cl₂, but only low yields (*ca.* 30%) of sulfoxide **1-70** were obtained. It was discovered that the low yields were due to the aqueous solubility of **1-70**, resulting in loss of material in the aqueous layer during workup. Back-extracting the aqueous layers multiple times increased the yield to 78%; however, this protocol would not translate well to scale-up. Using NaIO₄ in H₂O/MeOH effectively oxidized **1-69** to **1-70**. In this case, sulfoxide **1-70** was isolated after filtration of the resultant NaIO₃, removal of MeOH and H₂O in *vacuo*, and desalting of crude **1-70** prior to further purification by

recrystallization. To confirm the structural assignment of **1-70**, sulfide **1-69** was oxidized to the corresponding sulfone **1-71** using oxone in MeOH/H₂O.

Scheme 1-26. Synthesis of sulfur-functionalized bisoxetanyl dimers.



Sulfide **1-69** is a high boiling liquid (bp = 140 °C at 15 Torr), whereas sulfoxide **1-70** is a crystalline solid (mp = 92–94 °C). It was proposed that sulfide **1-69** could be used as an additive in reactions involving organometallic reagents. Oxidative workup would convert sulfide **1-69** to water-soluble sulfoxide **1-70** and facilitate removal of the additive from reaction mixtures.

1.2.7.1 Preliminary Investigations of Grignard Additions

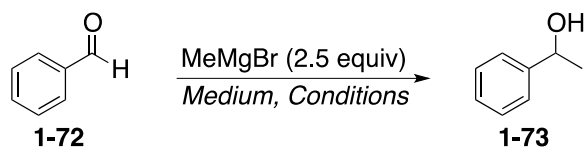
Sulfide **1-69** was tested as an additive for addition of 1,2-dithianyllithium to 2-cyclohexenone (i.e., Table 1-18), but only the 1,2-addition product **1-12** was observed by crude ¹H NMR analysis. I turned my attention to using organomagnesium reagents (Grignard reagents). Grignard reagents have a wide utility for functionalizing organic scaffolds, yet, it is difficult to translate Grignard reactions to process scale. In 2011, the ACS Green Chemistry Institute cited issues regarding the exothermicity of Grignard reactions as well as the *dependence on the ethereal solvents diethyl ether and THF* as primary reasons for the difficulty in translating Grignard reactions to a commercial scale. Moreover, many Grignard reagents are commercially available or readily prepared by reacting Mg metal with the corresponding halides, and reactions

involving Grignard reagents typically have uncomplicated experimental setups. The reported need for finding diethyl ether and THF replacements coupled with an ability to rapidly screen several reactions provided the motivation for studying these reactions.

1.2.7.2 Grignard Additions to Ketones

The addition of MeMgBr to benzaldehyde (Table 1-22) was studied; reactions were performed by adding an ethereal solution of MeMgBr to a solution of benzaldehyde in various solvent mixtures. When sulfide **1-69** was used neat or as a 10–20% (v/v) solution in heptane (entries 4–7), incomplete conversion of benzaldehyde to 1-phenylethanol **1-73** was observed (GC analysis). In contrast, the reaction proceeded quickly in THF, solutions of **1-69** in THF (entries 1–2), and heptane alone (entry 3).

Table 1-22. Additions of methylmagnesium bromide to benzaldehyde in presence of sulfide **1-69**.



Entry	Medium	Conditions	Ratio 1-73 : 1-72 (GC)
1	100% THF	0 °C, < 5 min	only 1-73
2	10% 1-69 /THF (v/v)	0 °C, < 5 min	99 : 1
3	100% heptane	rt, 90 min	only 1-73
4	10% 1-69 /heptane (v/v)	rt, 90 min	0.96 : 1
5	10% 1-69 /heptane (v/v)	0 °C, 25 min, rt 90 min	2.2 : 1
6	20% 1-69 /heptane (v/v)	0 °C, 25 min, rt 90 min	1.9 : 1
7	100% 1-69	0 °C 30 min, rt 30 min	1.9 : 1

In the case of reactions where sulfide **1-69** was used as an additive or cosolvent in heptane (Table 1-22, entries 4–6), additional product peaks were observed in the GC traces of the reaction mixtures (Figure 1-9). The products were identified as benzyl alcohol **1-74**, acetophenone **1-75**, and 2-phenylpropane-2-ol **1-76**. The formation of these products can be explained by invoking a magnesium-Oppenauer oxidation (Scheme 1-27).

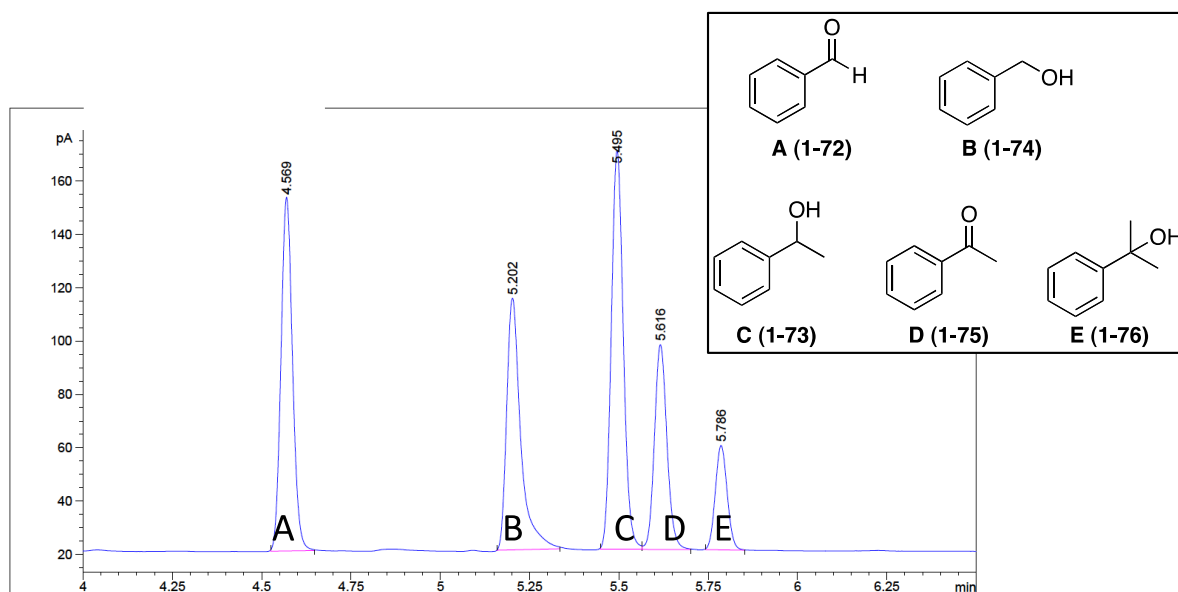
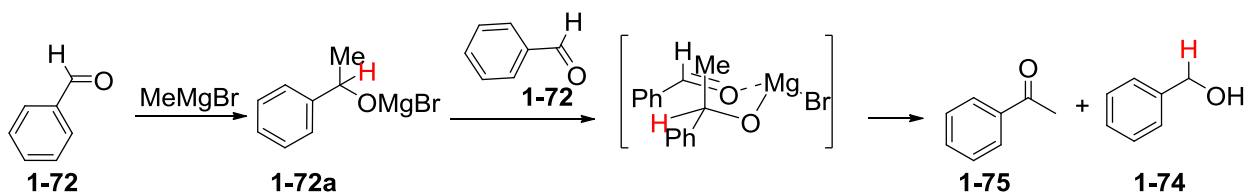


Figure 1-9. GC trace of the reaction reported in Table 1-22, entry 4.

Scheme 1-27. Mechanism of the magnesium-Oppenauer oxidation.



The results (Table 1-22) may be explained by an effective complexation and solubilization of alkoxides **1-72a** by sulfide **1-69**. Enhancing the solubility of the alkoxides would render them more reactive to a hydride transfer process. Moreover, the starting aldehyde **1-72** does not undergo complete conversion in the **1-69**/heptane solvents, but complete consumption of **1-72** is observed using THF, **1-69**/THF or heptane as solvents. These results also support a strong complexation of sulfide **1-69** with magnesium; we hypothesize that the bisoxetanyl sulfide may also attenuate the reactivity of the methylmagnesium bromide for the carbonyl addition reaction.

Reports of solvent effects on the magnesium-Oppenauer oxidation have been documented. Byrne and Karras have studied the effect of solvent on the magnesium-Oppenauer oxidation.⁹⁷ In the case of addition of *n*-BuMgBr to benzaldehyde, they observed good conversion to 1-phenylpentan-1-one (83% yield within 1 h at rt) when dibutyl ether was used as the solvent. The ketone yield decreased when the length of the alkyl chain on the ethereal solvent was decreased; the yields in *i*-Pr₂O and Et₂O were 67% and 33%, respectively. Furthermore, they found that using THF as a solvent or a cosolvent led to poor conversion to the magnesium-Oppenauer products. They reasoned that the trend in yield resulted from stronger Lewis bases coordinating to the magnesium alkoxide (analogous to **1-72a**), thus preventing complexation with the hydride acceptor (analogous to **1-72**).⁹⁷ Their results were corroborated by a report that using Bu₂O and *t*-BuOMe led to increased yields of byproducts from magnesium Oppenauer oxidations in the case of a process-scale synthesis of a phosphodiesterase IV isoenzyme inhibitor.⁹⁸

Kloetzing et al. showcased the utility of the magnesium-Oppenauer oxidation for the synthesis of aryl metallocenyl ketones.⁹⁹ They noted the importance of using additives such as LiCl or DMPU to effectively solubilize the magnesium alcoholates.

In the case of using **1-69** as an additive in the Grignard addition (Table 1-22), it was also observed that the reaction mixtures became cloudy immediately upon addition of the Grignard reagent. The precipitate was assumed to be MgBr₂, and it was postulated that additive **1-69** was shifting the Schlenk equilibrium toward the diorganomagnesium reagents. The incomplete conversion of benzaldehyde **1-72** to reaction products may also be due to a lack of reactivity with the diorganomagnesium species.

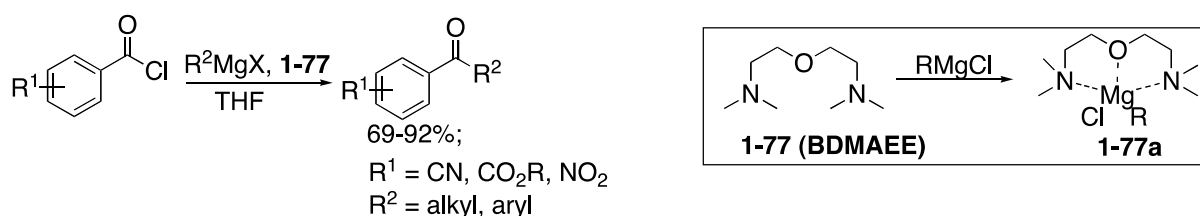
A simple reaction was studied—the addition of methylmagnesium bromide to benzaldehyde. From this study, two key observations were made regarding the use of sulfide **1-69** as a cosolvent in nonpolar solvents (e.g., heptane) or as neat solvent: a) magnesium Oppenauer oxidation products were formed and b) precipitate (MgBr₂) was observed, likely due to a shift in the Schlenk equilibrium.

In the next sections, experiments that were designed to evaluate the hypotheses that sulfide **1-69** complexes with Grignard reagents or organomagnesium intermediates and that sulfide **1-69** effects the Schlenk equilibrium are discussed.

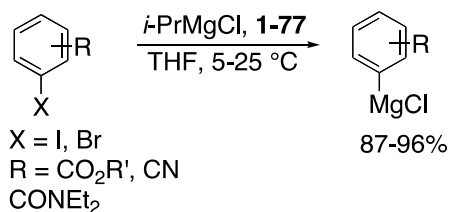
1.2.7.3 Use of Sulfide **1-69** to Attenuate Grignard Reagent Reactivity

It was hypothesized that sulfide **1-69** interacts with Grignard reagents; its utility was evaluated in reactions where decreased reactivity of Grignard reagents is desirable (Schemes 1-28, 1-29, and 1-30). I identified previous cases where use of the multi-functional chelating additive bis[2-(*N,N*-dimethylamino)ethyl]ether (BDMAEE) **1-77** in reactions involving Grignard reagents has led to increased yields or enantioselectivities. Examples include ketone synthesis via additions of Grignard reagents to aryl acyl chlorides¹⁰⁰ (Scheme 1-28) and I/Br-Mg exchange of aromatic halides¹⁰¹ with sensitive functional groups (Scheme 1-29). Addition of **1-77** led to enhanced enantioselectivities in the case of the asymmetric addition of alkyl Grignard reagents to aldehydes (Scheme 1-30).^{102,103} In all cases, the superior yields and enantioselectivities could be explained by chelation of **1-77** to the Grignard reagents (i.e., to form **1-77a**), thus attenuating the reactivity.

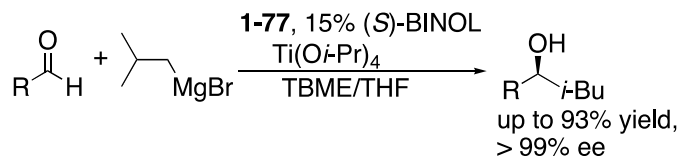
Scheme 1-28. Synthesis of ketones from acid chlorides using BDMAEE-Grignard complexes.



Scheme 1-29. Halogen/Mg exchange reactions of aromatic halides using deactivated Grignard reagents.

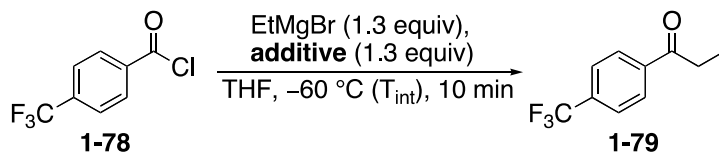


Scheme 1-30. Asymmetric addition of Grignard reagents to aldehydes.



The use of sulfide **1-69** was first investigated in Grignard additions to electron deficient acyl chlorides—namely, addition into 4-(trifluoromethyl)benzoyl chloride **1-78** (Table 1-23). Some variability in yield was observed in reactions where sulfide **1-69** was used as an additive (entry 3); in general, the yield was only slightly improved in comparison to the case with no additive, whereas use of BDMAEE **1-77** resulted in a noticeably higher yield (entry 2). Because **1-69** did not induce a noticeable effect on the reaction outcome, other examples where additives affect the results of organomagnesium reagent-mediated reactions were studied.

Table 1-23. Addition of EtMgBr to *p*-trifluoromethylbenzoyl chloride in the presence of additives.



Entry	Additive (1.3 equiv)	Yield (GC) ^a
1	none	31%
2	BDMAEE 1-77	58%
3	sulfide 1-69	36%, 40%, 45%

^aYields were determined after quenching the reaction mixtures with saturated aqueous NH_4Cl and extracting with ether. The ethereal solutions were spiked with dodecane and analyzed by GC. Yields were determined using a previously generated calibration curve relating the area ratios of **1-79**:dodecane to the mmol ratios of **1-79**:dodecane. A standard sample of **1-79** was prepared by converting **1-78** to the corresponding Weinreb amide followed by addition of EtMgBr.

The use of sulfide **1-69** was also tested in the noncryogenic Mg/I exchange reaction of aromatic substrates with sensitive functional groups. Three substrates, **1-80**, **1-81**, and **1-82** (Figure 1-10) were studied, and the results are shown in Table 1-24.

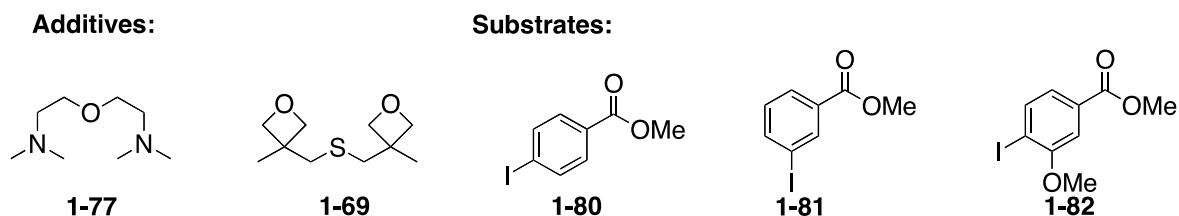


Figure 1-10. Additives and substrates used for studying the Mg/I exchange reaction of aryl iodides.

Table 1-24. Mg/I exchange reactions in the presence of BDMAEE and sulfide **1-69**.
$$\text{Additive (1.2 equiv)} + i\text{-PrMgCl (1.2 equiv)} \xrightarrow[15\text{ }^\circ\text{C, 20 min}]{\text{THF}} \text{Ar-I} \xrightarrow[\text{then NH}_4\text{Cl}]{\text{rt, 10 min}} \text{Ar-H}$$

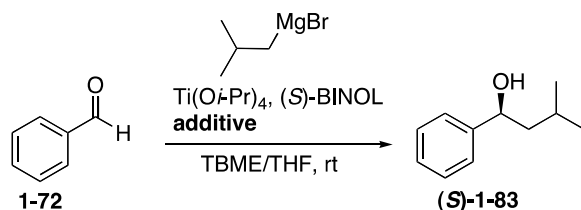
Entry	Substrate (Ar-I)	Additive	Yield ^a	Reported yield ¹⁰¹
1	1-80	none	80%	87%
2	1-80	1-77	84%	96%
3	1-80	1-69	71%	NA
4	1-81	none	51%	61%
5	1-81	1-77	76%	87%
6	1-81	1-69	54%	NA
7	1-82	none	59%	43%
8	1-82	1-77	86%	95%
9	1-82	1-69	49%	NA

^a Yields were determined by GC analysis and are based on area ratios of the product methyl benzoates and an external standard (dodecane).

The same trends in yield as reported by Wang et al.¹⁰¹ were observed. A comparative increase in yield when using BDMAEE as an additive was observed. In the case of using sulfide **1-69** as an additive, either comparable or lower yields than in reactions where no additive was used were obtained. Therefore, sulfide **1-69** is not an effective additive for use these in Mg/I exchange reactions.

Finally, sulfide **1-69** was tested as an additive in the asymmetric addition of Grignard reagents to aldehydes.¹⁰² I first explored the reaction reported to generate products with the highest enantiomeric excess—the addition of *iso*-butylmagnesium bromide to benzaldehyde (Table 1-25). Although products were obtained in high enantiomeric ratios, I could not reproduce the yields reported in the literature. By using ¹H NMR and GC analyses, I determined that formation of benzyl alcohol was the major side reaction. It was reasoned that the alcohol may originate from hydride transfer from the *iso*-butylmagnesium bromide. Therefore, other Grignard reagents (e.g., *n*-butylmagnesium bromide) that would be less prone to hydride transfer reactions were used; however, isolated yields of *ca.* 20% were also obtained from these reactions.

Table 1-25. Asymmetric additions of Grignard reagents to benzaldehyde in the presence of additives.



Entry	Additive	Enantiomeric ratio ^a	Yield
1	none	ND ^b	ND ^b
2	sulfide 1-69	97.5 : 2.5	~20%
3	BDMAEE 1-77	99.5 : 0.5	~20%

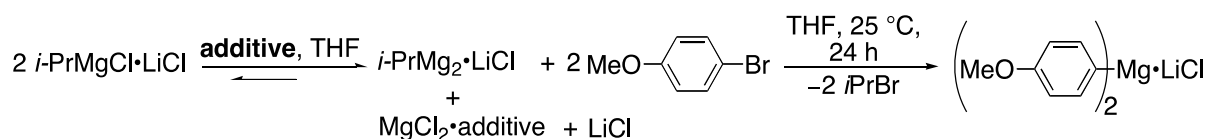
^aEnantiomeric excess was determined by HPLC analysis using a chiral OD-1 column. ^bYield and e.r. were not determined because benzyl alcohol was the major product (GC analysis).

Because a high enantiomeric ratio was obtained when sulfide **1-69** was used, I was interested in modifying the reaction parameters to obtain better yields. I studied the reaction of methylmagnesium bromide with alternative titanium reagents. Methylmagnesium bromide was used as the Grignard reagent to eliminate the possibility of hydride transfer from the Grignard reagent. It was hypothesized that the reduced products may also result from Meerwein-Ponndorf-Verley reductions—that is, the hydride source was the *iso*-propanol ligand on the titanium complex. Therefore, reactions using Ti(*O**t*-Bu)₄, and Ti(NMe)₄ as substitutes for Ti(*O**i*-Pr)₄ were performed. Unfortunately, only starting material or the reduction product (i.e., benzyl alcohol) was observed in both cases.

1.2.7.4 Effect of Sulfide 1-69 on the Anionic Schlenk Equilibrium

The effect of sulfide **1-69** was next investigated using a model reaction known to depend on the *anionic* Schlenk equilibrium (Scheme 1-31).⁵² Knochel and coworkers postulated that strong σ donors (e.g., chelating ethers) coordinate to MgCl₂ and form an MgCl₂•additive precipitate, causing a shift in the Schlenk equilibrium and forming *i*-Pr₂Mg•LiCl *in situ*. The *in situ* formed reagent exhibits good reactivity toward the Br/Mg exchange reaction of electron-rich aromatic bromides (e.g., 4-bromoanisole).⁵²

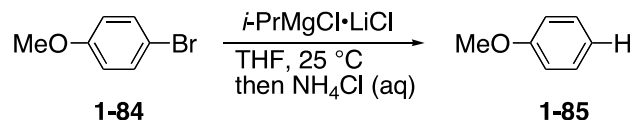
Scheme 1-31. Reaction of *i*-PrMgCl and 4-bromoanisole, proceeding through an anionic Schlenk equilibrium.



Solutions of *i*-PrMgCl•LiCl were treated with 4-bromoanisole followed by an additive; the results are shown in Table 1-26. When no additive was used, the reaction mixture remained homogeneous; when additives (e.g., 1,4-dioxane) were added, the mixtures immediately became cloudy. The conversion in the case of using sulfide **1-69** (entry 4) as an additive was comparable

to using 1,4-dioxane (entry 3). Therefore, sulfide **1-69** may be a substitute for 1,4-dioxane or other coordinating ethers in reactions that proceed via an anionic Schlenk equilibrium.

Table 1-26. Effect of additives on the Mg/Br exchange of 4-bromoanisole.



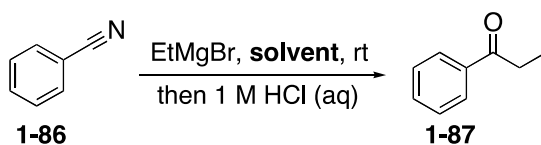
Entry	Additive (1 equiv)	Conversion (yield) ^b	Reaction appearance
1	none	28% (38%) ^c	homogeneous
2	[15]-crown-5	57% ^d	heterogeneous
3	1,4-dioxane (10% v/v)	86% (89%) ^e	heterogeneous
4	sulfide 1-69	72–86% (80–88%)	heterogeneous

^aAliquots (100 μL) were quenched with saturated aqueous NH_4Cl after 24 h. The quenched aliquot was partitioned into ether, and the ethereal layer was analyzed by GC. ^bConversion is based on the ratio of anisole:4-bromoanisole. Yields were calculated using dodecane as an external standard. ^cA conversion of 31% was reported by Krasovskiy et al.⁵² ^dA conversion of 100% after 6 h was reported by Krasovskiy et al. ^eA conversion of 100% after 10 h was reported by Krasovskiy et al.

1.2.7.5 Additional Reactions Involving Grignard Reagents

I also explored the reactivity of Grignard reagents in the presence of sulfide **1-69** in two additional reactions—the addition of ethylmagnesium bromide to benzonitrile (Table 1-27) and the conjugate addition reaction under copper-catalyzed (Kharash) conditions (Table 1-28).

Table 1-27. Addition of EtMgBr to benzonitrile in the presence of sulfide **1-69**.



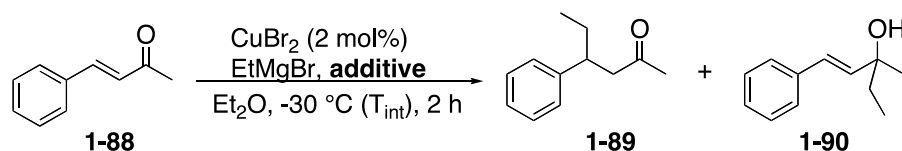
Entry	Solvent	Ratio 1-86 : 1-87 at t = 3 h ^a	Ratio 1-86 : 1-87 at t = 15 h ^a
1	ether	1.9 : 1	0.05 : 1
2	10% 1-69 /ether (v/v)	5.1 : 1	2.6 : 1
3	20% 1-69 /ether (v/v)	6.4 : 1	3.1 : 1

^aReported ratios were determined by GC analysis of aliquots. Ratios are corrected for instrument response based on an independently generated calibration curve.

In the case of adding Grignard reagents to benzonitrile, using sulfide **1-69** slows the rate of reaction; furthermore, increasing the amount of **1-69** from 10% v/v (Table 1-27, entry 2) to 20% v/v (Table 1-27, entry 3) did not have a substantial impact on the outcome. I hypothesize that sulfide **1-69** may outcompete the nitrile for coordination to the Grignard reagent, thus attenuating the Grignard reagent reactivity.

Finally, the conjugate addition of EtMgBr to enone **1-88** (Table 1-28) was tested. When EtMgBr was added to a solution of sulfide **1-69** and **1-88** in ether, a slightly improved selectivity for the 1,4-addition product was observed (Table 1-28, entry 2); however, the isolated product yield decreased in comparison to the case with no additive (entry 1). Use of substoichiometric amounts of sulfide (entry 3) or premixing sulfide **1-69** with the Grignard reagent (entry 4) afforded the same ratio of 1,2- to 1,4-addition products as the control case (entry 1). Moreover, decreased product yields and more complex reaction profiles were observed when sulfide **1-69** was used as an additive.

Table 1-28. Conjugate addition reactions in the presence of sulfide **1-69**.



Entry	Additive	Ratio 1-89 : 1-90	Isolated Yield (combined 1-89 + 1-90)
1	none	2 : 1	73%
2	sulfide 1-69 (2 equiv) ^a	1.1 : 1	42%
3	sulfide 1-69 (0.2 equiv) ^a	2 : 1	50%
4	sulfide 1-69 (2 equiv) ^b	2 : 1	ND

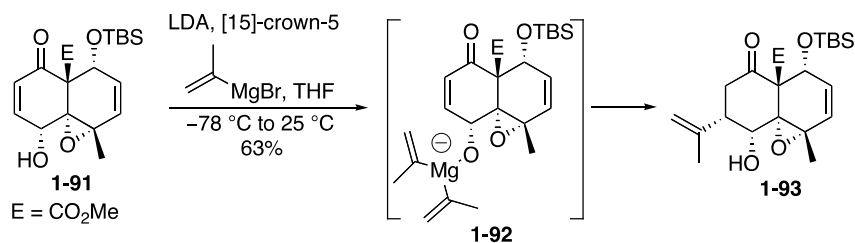
^aA solution of EtMgBr in Et₂O was added to a solution of CuBr₂, **1-88**, and **1-69** at -30 °C *via* syringe pump. ^bEtMgBr and sulfide **1-69** were pre-mixed in Et₂O and added to a solution of CuBr₂ and **1-88** *via* syringe pump.

The decreased product yields may be attributed to a shift in the Schlenk equilibrium toward the diorganomagnesium species. The effect of solvent on conjugate additions has been noted in the literature; Harutyunyan et al. observed that the copper-catalyzed enantioselective conjugate addition of Grignard reagents to enones proceeds well in TBME or Et₂O but that using THF was detrimental to the reaction efficiency.¹⁰⁴ Moreover, they found that adding 1,4-dioxane or the diorganomagnesium reagents decreased the reaction rate. Their results supported their hypothesis that the shift in Schlenk equilibrium was the cause of the decreased rates—the diorganomagnesium reagents were less reactive than a monoalkylmagnesium species (e.g., RMgBr•OEt₂) in the 1,4-addition reactions. The lower isolated yields in cases where sulfide **1-69** was used as an additive may also be explained by a shift in the Schlenk equilibrium.

1.2.7.6 Conclusions for Use of Oxetanes as Additives in Organometallic Reactions

Using sulfide **1-69** as an additive or solvent in reactions involving Grignard reagents likely causes a shift in the Schlenk equilibrium. This hypothesis was supported by the fact that **1-69** showed comparable effects to 1,4-dioxane when used for the Mg/Br exchange reaction of 4-bromoanisole. Moreover, when **1-69** was used a cosolvent in conjugate addition reactions, decreased yields were obtained; this observation can also be attributed to a shift in the Schlenk equilibrium. For future work, the effect of sulfide **1-69** will be studied in reactions where using the diorganomagnesium reagents results in favorable reaction outcomes. One example is the intramolecular delivery of alkyl groups through formation of an ate complex; this approach was used in the total synthesis of (\pm)-euonyminol (Scheme 1-32).¹⁰⁵ The effects of bisoxetanyl ether **1-37** in Grignard reactions will also be studied to determine the significance of the heteroatom tethering the two oxetanes.

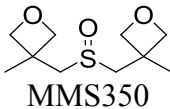
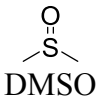
Scheme 1-32. Example utility of using a shift in the Schlenk equilibrium for favorable reactivity.



1.3 RESULTS AND DISCUSSION: USE OF MMS350 FOR AQUEOUS SOLUBILITY ENHANCEMENT OF SMALL ORGANIC MOLECULES

The bifunctional sulfoxide **1-70** (MMS350) was tested for use as a DMSO substitute. A comparison of the physical properties of DMSO and MMS350 is shown in Table 1-29. MMS350 is a crystalline solid, whereas DMSO is a viscous, hygroscopic liquid. MMS350 may be an attractive DMSO alternative in terms of compound handling. Moreover, MMS350 was synthesized in three steps from commercially available material (Scheme 1-17). The synthesis was amenable to scale, and no chromatography was required. The noted aqueous solubility ($\log P = -0.87$) would facilitate the removal of MMS350 during workup.

Table 1-29. Selected physical properties of MMS350 and DMSO.

Entry	Property	 MMS350	 DMSO
1	melting point	93–94 °C	16–19 °C
2	boiling point	NA	189 °C
3	LogP	-0.87 ^a	-1.3 ¹²¹

^aThe logP (log of the octanol/water partition coefficient) value for MMS350 was determined using the shake-flask method. The reported value represents an average of 3 independent experiments.

X-ray structural data for MMS350 (Figures 1-11 and 1-12) was obtained.¹⁰⁶ The smallest asymmetric unit consists of two MMS350 molecules with the oxetanyl moieties packed to minimize intermolecular dipoles. Interestingly, the oxetane moieties and the sulfoxide oxygen are oriented in a manner that may promote cation chelation.

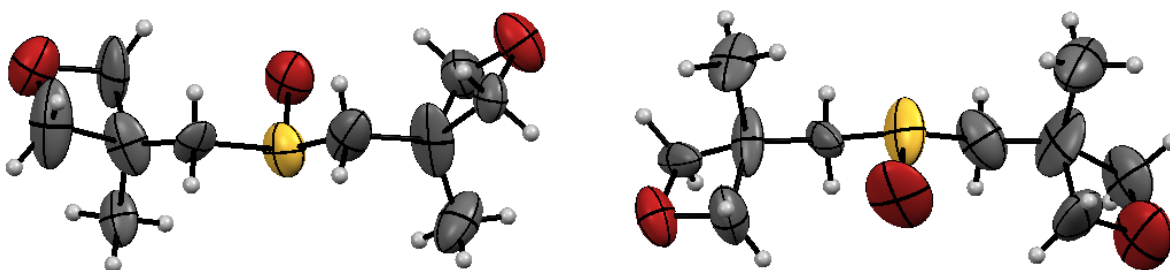


Figure 1-11. X-ray structure of MMS350.

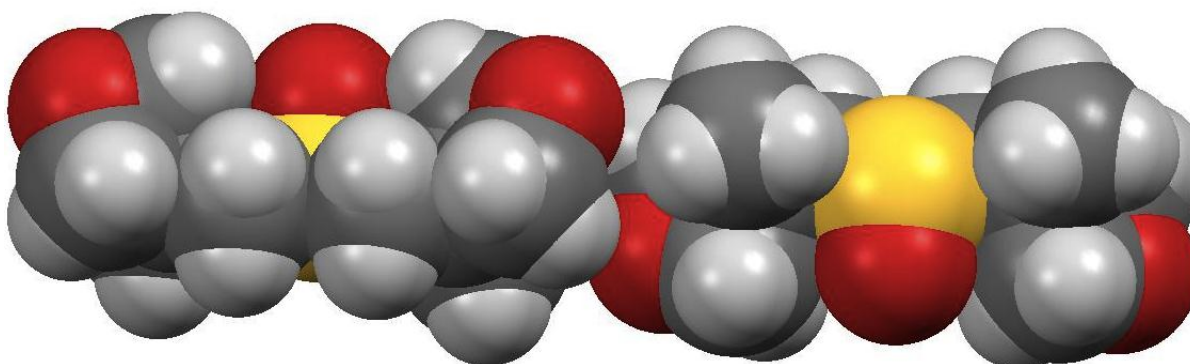


Figure 1-12. Space-filling model of MMS350.

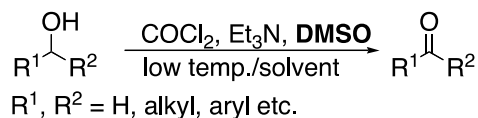
1.3.1.1 Oxidation Reactions Using MMS350 as a DMSO Substitute

DMSO is widely used as an oxidant for alcohols and halides, affording the corresponding aldehydes (Scheme 1-33).¹⁰⁷ These reactions are known as the Swern and Kornblum oxidations (Scheme 1-33). The mechanisms of the standard Swern and Kornblum oxidations are depicted in Scheme 1-34. Notable features of both mechanisms include a) nucleophilic addition of a sulfoxide (DMSO) b) deprotonation of an alpha-methylene hydrogen to form an intermediate

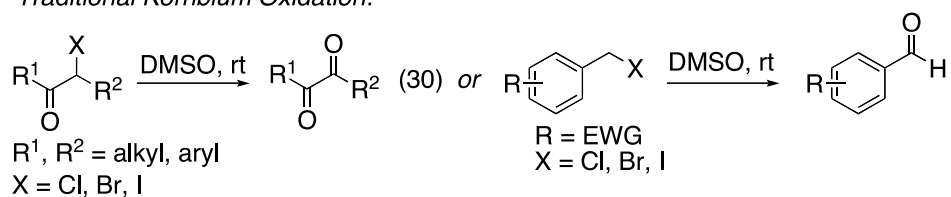
ylide, and c) intramolecular hydride transfer to the ylide and subsequent expulsion of dimethyl sulfide.

Scheme 1-33. Reactions where DMSO is used as an oxidant (adapted from reference 107).

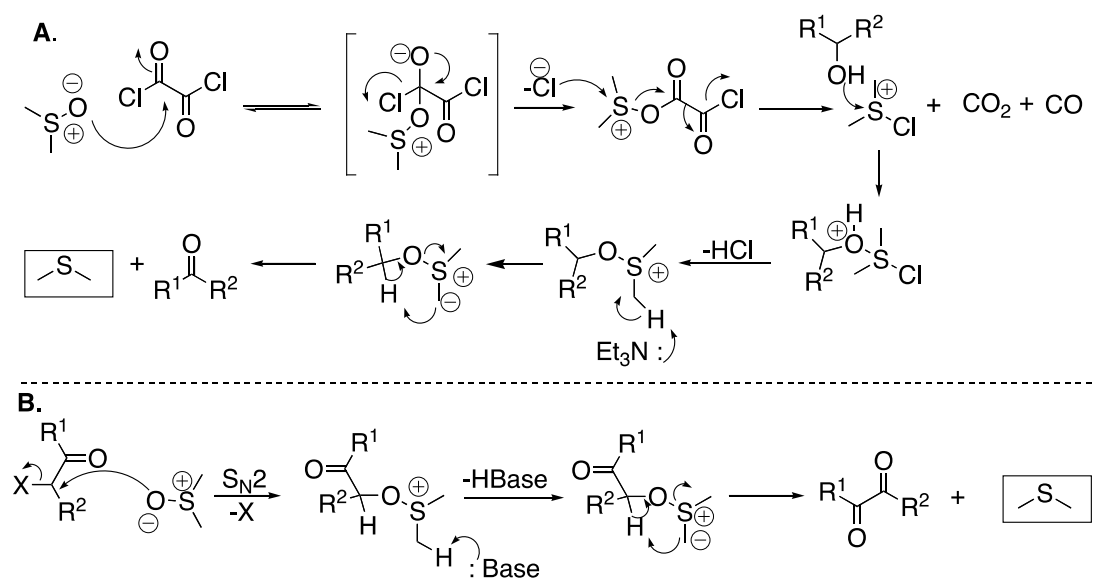
Traditional Swern Oxidation:



Traditional Kornblum Oxidation:

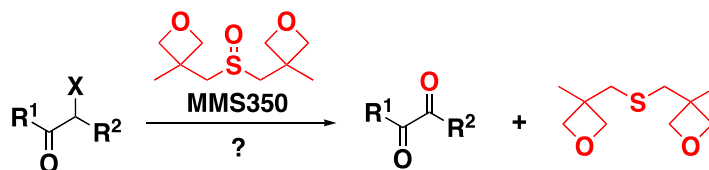


Scheme 1-34. Mechanism of A) the Swern oxidation and B) the Kornblum oxidation (adapted from reference 107).



Although DMSO has widespread utility as an oxidant, a major drawback to the Swern and Kornblum oxidation is the stoichiometric production of dimethylsulfide (DMS), which is a volatile, odorous liquid (bp = 35–41 °C). On laboratory scale, the production of DMS is easily handled by good laboratory practices (e.g., use of fume hoods and washing glassware with bleach); however, on an industrial scale, evolution of DMS is problematic. It was postulated that MMS350 may be a suitable substitute for DMSO that would generate the more tractable byproduct sulfide **1-69** (Scheme 1-35).

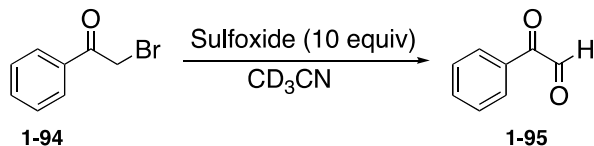
Scheme 1-35. Proposed Kornblum oxidation using MMS350 as an oxidant.



To explore the possibility of using sulfoxide MMS350 in Kornblum oxidations, the conversion of benzyl bromide to benzaldehyde was investigated. Mixing MMS350, benzyl bromide, and KHCO₃ and performing the reaction as a melt (under either thermal or microwave conditions) resulted in decomposition of the sulfoxide. Heating a solution of MMS350 and benzyl bromide in acetonitrile at 75 °C did affect ~30% (by ¹H NMR analysis) conversion to benzaldehyde; however, this reaction was not reproducible. Moreover, attempted oxidations of *p*-nitrobenzylbromide with MMS350 in acetonitrile solutions were unsuccessful. To quickly gauge the reactivity of MMS350 in comparison to DMSO, the oxidation of α -bromoacetophenone **1-94** in CD₃CN (Table 1-30) was explored. In the case of using DMSO (10 equiv) as the oxidant, conversion of **1-94** was apparent within 60 h, and ~96% conversion was observed after

84 h; however, α -bromoacetophenone was stable to MMS350 even after 2 weeks of standing in CD_3CN .

Table 1-30. Kornblum oxidation of α -bromoacetophenone in the presence of sulfoxides.



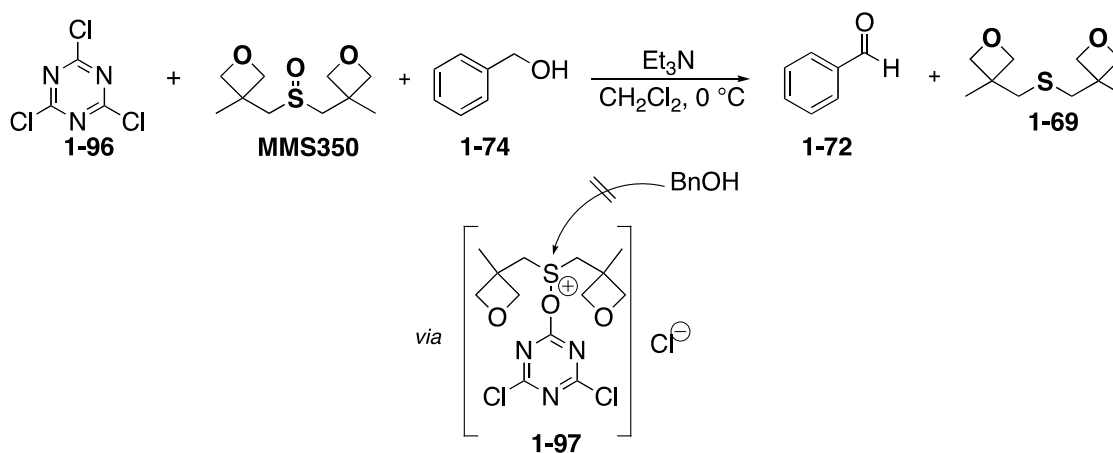
Entry	Sulfoxide	Result
1	DMSO	~96% conversion after 84 h ^a
2	MMS350	no conversion after > 2 weeks

^aConversion was determined by ¹H NMR analysis.

MMS350 was also tested in modified Swern oxidations in which cyanuric chloride **1-96**¹⁰⁸ (Scheme 1-36) was substituted for oxalyl chloride. Benzyl alcohol was used as the substrate, and only recovered benzyl alcohol and deoxygenated sulfoxide (sulfide **1-69**) were observed by analysis of the crude ¹H NMR spectrum.

The results of the above experiments indicate that MMS350 does not have the same oxidizing properties as DMSO. In the case of the Kornblum oxidation, MMS350 may be too sterically encumbered for effective nucleophilic attack of the α -bromoketone or benzylic bromide. In the case of the modified Swern oxidations, the formation of sulfide **1-69** may indicate that MMS350 does indeed react with cyanuric chloride; however, the resulting complex or chlorosulfonium salt **1-97** may again be too sterically hindered for addition of the alcohol to occur (Scheme 1-36).

Scheme 1-36. Reaction of cyanuric chloride and MMS350 for attempted oxidation reactions.



MMS350 was not an effective DMSO substitute for the Kornblum and modified Swern reactions; the lack of reactivity may be a positive attribute—another application of DMSO is its use as a solvent in biological assays and for compound storage libraries. In these cases, a *less reactive* DMSO analog may be a useful substitute. I thus switched my focus to exploring the use of MMS350 as a DMSO substitute for applications related to compound storage and high-throughput screening. The experiments and findings are discussed in the next section.

1.3.2 MMS350—A Dimethylsulfoxide Substitute for Aqueous Solubility Enhancement of Small Organic Molecules

Note: The tables, figures, and text in this section were adapted (with permission) from reference [122], in *ASSAY and Drug Development Technologies* ©2012 Mary Ann Liebert, Inc.

1.3.2.1 Problems with Compound Storage in DMSO

Compound libraries designated for high-throughput screening assays are often plated and stored in DMSO. The storage period can last for several months to even years;¹⁰⁹ during this time, compound degradation due to hydrolysis, oxidation, isomerization, and other chemical reactions can occur.¹¹⁰ There have been several studies¹¹¹ documenting compound degradation in DMSO storage solutions; in general, it can be estimated that ~50% of samples degrade after 12 months of storage. Moreover, compound precipitation from stored DMSO solutions can occur—in one study, there was qualitative precipitation of compounds in 26% of test plates.¹¹²

For use in high-throughput screening assays, compounds stored in DMSO stock solutions are diluted in aqueous buffers. Many libraries are composed of high molecular weight, hydrophobic compounds designed to have enhanced membrane permeabilities.¹¹³ The trend toward designing lipophilic compounds results in libraries of materials with lower intrinsic aqueous solubilities. It is currently estimated that 30%–50% of compounds in screening libraries have aqueous solubilities of less than 10 μM .¹¹⁴ Compounds with low aqueous solubilities often precipitate upon dilution in the assay media. When compound concentrations in assay media fall below the calculated concentrations, flawed conclusions regarding structure-activity-relationships, toxicity, or efficacy are drawn.¹¹³ Additionally, compounds reported to be “clean” after counter-screens for off-target activities may, in fact, simply have poor solubility in the screening assays.¹¹⁵

Methods for optimizing *in vitro* assays to address solubility issues include limiting aqueous dilutions, using organic solvents for serial dilutions, using cosolvents, and performing screens at lower concentrations. Solubilizing agents such as 2-hydroxypropyl- β -cyclodextrin (HBC), surfactants, and commonly used pharmaceutical excipients are now frequently incorporated into assay plates.¹¹⁵ Aqueous dissolution of problematic compounds can also be enhanced by pH adjustment,¹¹⁶ salt formation,¹¹⁷ or chemical modification of the substrate (formation of pro-drugs).¹¹⁷ Cosolvents including glycerin,¹¹² *N*-methyl pyrrolidone (NMP),¹¹⁸ and low-molecular-weight polyethylene glycols (PEGs, e.g., PEG 400)¹¹³ can also be used.

Solubilizing agents based on DMSO have been developed. For example, poly-*L*-methionine **1-98** (Figure 1-13) was shown to increase solubility of lipophilic molecules in PBS solutions (phosphate buffered saline).¹¹⁹ Due to the stability and hydrophilicity of MMS350, it was reasoned that it may also function as a DMSO substitute for aqueous solubility enhancement of lipophilic molecules; therefore, MMS350 was tested as a solubilizer and compound storage additive. In the following subsections, findings regarding the use of MMS350 in chemical storage applications are described. The toxicity and applicability of MMS350 to cellular and *in vivo* bioassays is discussed.

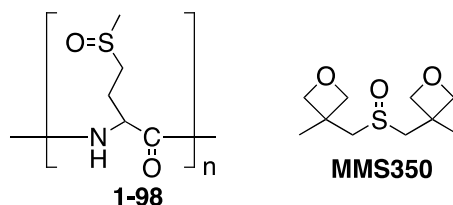


Figure 1-13. DMSO substitutes for aqueous solubility enhancement of lipophilic compounds.

1.3.2.2 Initial Compound Solubility Measurements

To evaluate the utility of MMS350 as a solubilizing agent, a test set of poorly aqueous-soluble compounds (Figure 1-14) was chosen. The solubility enhancement of curcumin **1-99** was first examined. Curcumin is a promising lead for treatment of several disorders (e.g., colon cancer), but its bioavailability and utility as a therapeutic agent are limited by its severely low aqueous solubility (0.6 $\mu\text{g}/\text{mL}$ at ambient temperature, up to 7.4 $\mu\text{g}/\text{mL}$ upon heating).^{120,121} UV/VIS spectroscopy was used to measure the solubility of curcumin in a 25 wt% solution of MMS350 in water. After equilibration at ambient temperature for 20 h in an end-over-end rotator, the measured solubility was $60 \pm 20 \mu\text{g}/\text{mL}$. Although the solubility remained low, the noticeable increase was encouraging.¹²² Moreover, curcumin is yellow in color, and I observed that solutions prepared in 25 wt% MMS350/water had a yellow color whereas aqueous solutions remained colorless.

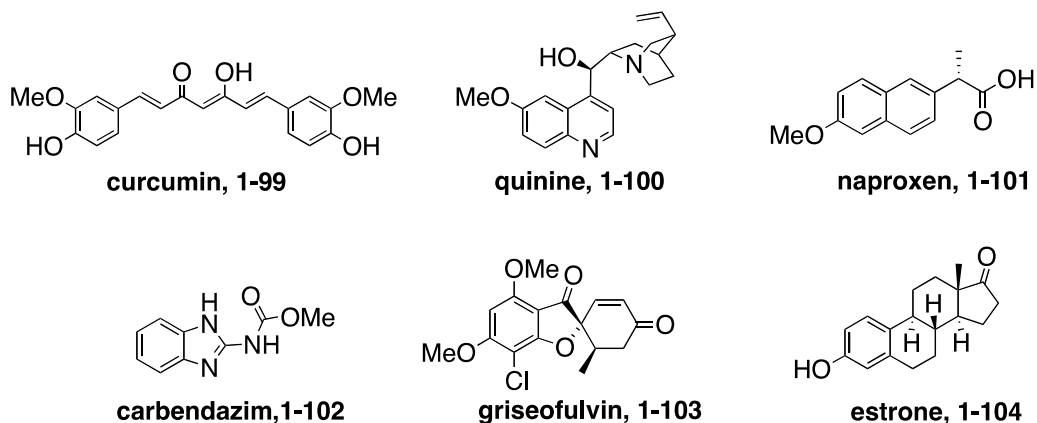


Figure 1-14. Test set of poorly aqueous soluble compounds.

Encouraged by this result, we tested a diverse set of compounds including amines, acids, and non-ionizable motifs (e.g., griseofulvin). The results are shown in Figures 15–18. Each experiment was performed in duplicate, and the solubilization efficacy with varying wt% solutions of MMS350 was compared with that of DMSO. Up to 10-fold increases in solubility were observed using 25 wt% solutions of MMS350 in water. Furthermore, up to two-fold enhancements were observed in comparison to using the equivalent wt% solutions of DMSO in water.¹²²

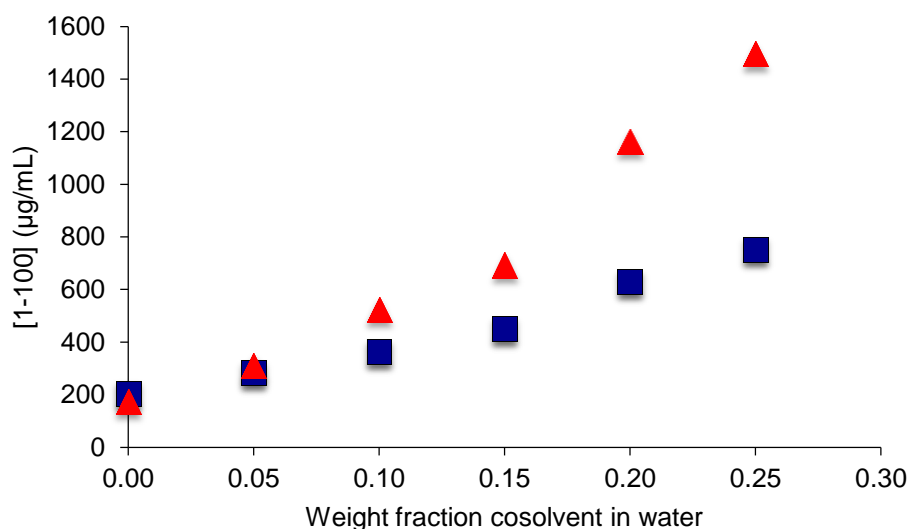


Figure 1-15. Solubility of quinine **1-100** in aqueous solutions with MMS350 (σ) and DMSO (ν) as cosolvents.

Each trial was run in duplicate and each point represents the average of the duplicate trials. In the case of MMS350, the pH varied from 8.7 (with no additive) to 9.4 (with a 0.25 weight fraction additive). In the case of DMSO, the pH varied from 8.9 (with no additive) to 9.5 (with a 0.25 weight fraction additive).

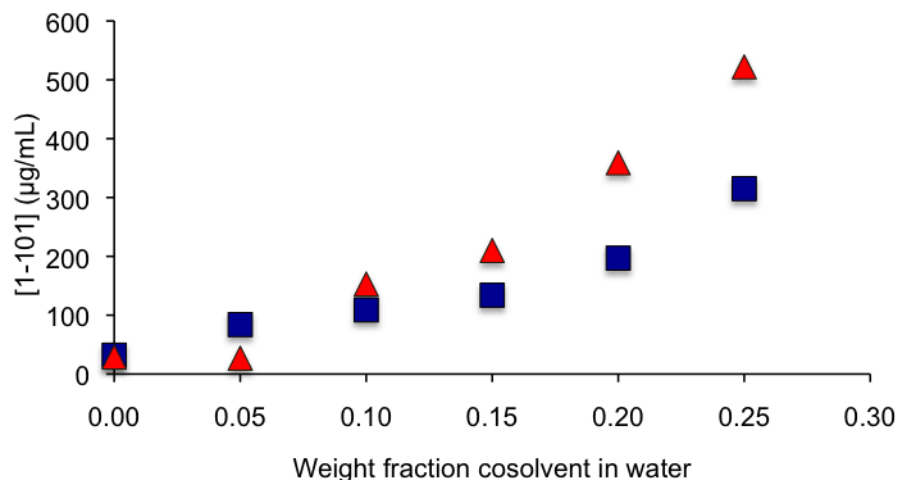


Figure 1-16. Solubility of naproxen **1-101** in aqueous solutions with MMS350 (σ) and DMSO (ν) as cosolvents.

Each trial was run in duplicate and each point represents the average of the duplicate trials. In the case of MMS350, the pH varied from 4.6 (with no additive) to 4.2 (with a 0.25 weight fraction additive). In the case of the DMSO, the pH varied from 4.8 to 4.4.

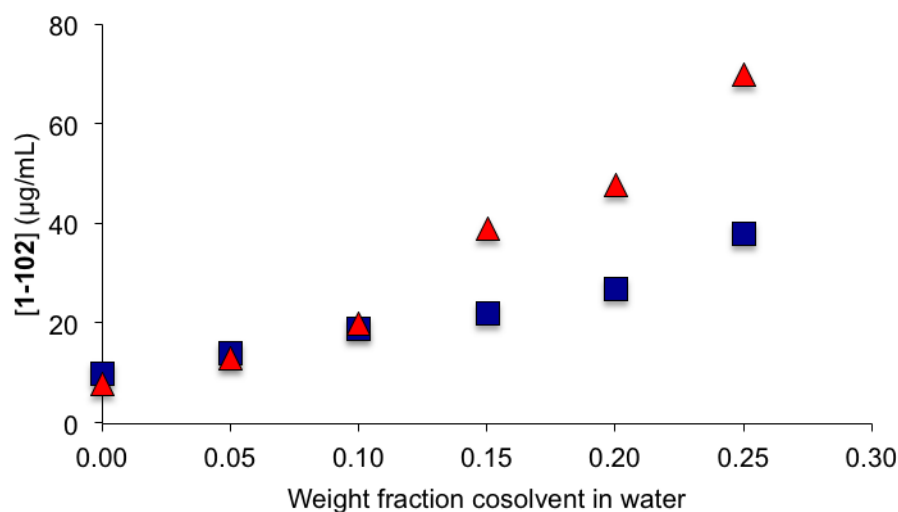


Figure 1-17. Solubility of carbendazim **1-102** in aqueous solutions with MMS350 (σ) and DMSO (ν) as cosolvents.

Each trial was run in duplicate and each point represents the average of the duplicate trials. In the case of MMS350, the pH varied from 6.7 (with no additive) to 7.0 (with a 0.15 weight fraction additive). In the case of DMSO, the pH varied from 6.8 (with no additive) to 7.4 (with a 0.25 weight fraction additive).

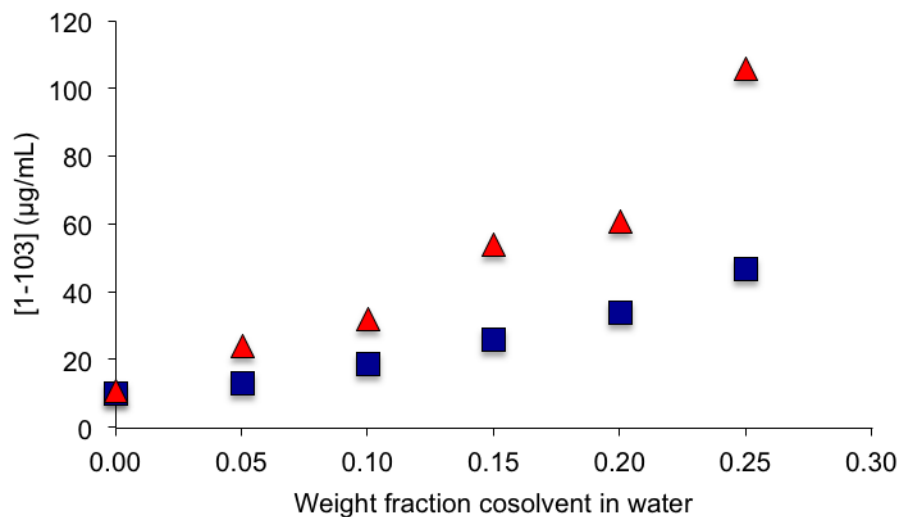


Figure 1-18. Solubility of griseofulvin **1-103** in aqueous solutions with MMS350 (σ) and DMSO (ν) as cosolvents.

Each trial was run in duplicate and each point represents the average of the duplicate trials. In the case MMS350, the pH varied from 6.3 (with no additive) to 6.8 (with a 0.20 weight fraction additive). In the case of DMSO, the pH varied from 6.3 (with no additive) to 6.8 (with a 0.20 weight fraction additive).

It was hypothesized that DMSO and MMS350 function as cosolvents rather than complexing agents. Yalkowsky has developed a model (eq 4) for solubilization in cosolvent mixtures showing that observed solubility increases exponentially with increasing volume fraction of cosolvent.^{116,118} His model is shown in equation 14; S_{mix} and S_w are the solubility of the solute in the cosolvent mixture and water, respectively, σ is the solubilizing efficacy of the cosolvent, and f_c is the volume fraction of cosolvent. The slope of a semi-log plot (σ) is related to the cosolvent's ability to disrupt the intermolecular hydrogen bond network of water and form a less polar solvent mixture. The higher solubilizing efficacy of MMS350 in comparison to DMSO can be rationalized by comparing the logP of MMS350 (-0.87) to that of DMSO (-1.3).¹²³ Because MMS350 is slightly more lipophilic, the resulting solvent mixture may be effectively less polar.

$$\text{Log } S_{\text{mix}} = \text{log}S_w + \sigma f_c \quad (4)$$

The solubilization of a steroid in aqueous media was also tested. Estrone **104** was chosen because it has a chromophore, thus its solubility could be measured using UV/VIS spectroscopy. The reported aqueous solubility of estrone is quite low (0.8 $\mu\text{g/mL}$),^{124,125} and we had difficulty quantifying the solubility by UV/VIS ($\epsilon = 2000$), even when using a 25 wt% solution of MMS350 in water. Ternary mixtures of pH 9.0 buffer (Borax), NMP, and sulfoxide were tested (Table 1-31). In this case, noticeable differences in in solubility were measured, and the solubility in the ternary mixture of pH 9.0 buffer, NMP, and DMSO was optimal (Table 1-31, entry 4). It should be noted a noticeable improvement in solubility using a 3:1:1 pH 9.0 buffer/NMP/MMS350 was still observed (Table 1-31, entry 3).

Table 1-31. Solubility of estrone in solutions of pH 9.0 buffer, NMP, and sulfoxide.

Entry	Medium	Solubility ($\mu\text{g/mL}$) ^a
1	3:1 pH 9.0 buffer/MMS350	30 \pm 10
2	3:1 pH 9.0 buffer/NMP	63 \pm 5
3	3:1:1 pH 9.0 buffer/NMP/MMS350	160 \pm 20
4	3:1:1 pH 9.0 buffer/NMP/DMSO	230 \pm 30

^aSolubility was determined after equilibration for 20 h at 30.0 °C. Data were obtained by UV/VIS analysis of the saturated solutions and were confirmed by analysis of independently prepared estrone standards. Each entry represents a mean solubility \pm standard deviation (n = 3).

Because several of the compounds in the test set contain ionizable functionalities (e.g., quinine, naproxen, carbendazim), the solubilization in buffered media (0.01 M pH 7.0 phosphate buffer) was examined (Table 1-32). The solubility of quinine **1-100** was higher in the buffer (Table 1-34, entries 1–3) than in HPLC-grade water (Figure 1-15), and a correlation between wt. fraction MMS350 and solubility was observed. In the case of naproxen (pK_a *ca* 4.8), the molecule is ionized at pH 7.0, and therefore little effect is observed upon increasing the wt% of the sulfoxide in pH 7.0 buffer (Table 1-32, entries 4–6). The solubility of carbendazim (Table 1-32, entries 7–9) was consistent with that in solutions prepared in HPLC-grade water (Figure 1-17). This is not surprising given that the pK_a of the benzimidazole is *ca.* 4, and therefore the molecule is not ionized at pH 7.0.

Table 1-32. Solubility of selected compound in solutions of sulfoxide MMS350 in 0.01 M pH 7.0 phosphate buffer.

Entry	Compound	Weight percent MMS350 in pH 7.0 buffer	Solution pH ^a	Measured solubility (µg/mL) ^b
1	1-100	0	7.6	1100 (780) ^d
2	1-100	10	8.0	1900 (1300) ^d
3	1-100	25	8.2	6200 (3900) ^d
4	1-101	0	6.0	950 ^c
5	1-101	10	5.8	1100
6	1-101	25	5.2	1400
7	1-102	0	6.8	10
8	1-102	10	6.9	34
9	1-102	25	7.1	77

^aThe pH was measured electrochemically after excess compound was filtered from the solution.

^bMeasurements were performed in duplicate unless otherwise noted. ^cAverage of 5 trials. ^dThe two numbers represent data from separate trials where entries 1-3 were run in parallel. There was some variability in the results from the two trials.

Up to this point, the *thermodynamic solubility* of the test set of compounds (i.e., the equilibrium solubility after 20 h) was measured. The *kinetic solubility* (i.e., the solubility of a compound after dilution of a stock solution in buffer) is often a better measure of the how the media will affect compound solubility in terms of high-throughput screening assays. The kinetic solubility of carbendazim **1-102** and griseofulvin **1-103** was determined (Table 1-33). Stock solutions (10 mM) of **1-102** and **1-103** in DMSO, NMP, or a 25% MMS350/NMP solution were

prepared, and aliquots (10 μ L) were added directly to pH 7.4 PBS solutions, and the solubilities were measured. Across the three test media, the measured kinetic solubilities were consistent. It should be noted that the observed kinetic solubility of griseofulvin was higher than previously reported,¹²⁶ and it approached the threshold solubility of 200 μ M. However, the data were used to establish a general trend, and I observed no difference in kinetic solubility when using the three different media for stock solution preparation.

Table 1-33. Kinetic solubility measurements of carbendazim and griseofulvin after dilution with phosphate buffered saline.

Entry	Compound	Medium of stock solution	Kinetic solubility (μ M) ^a
1	1-102	DMSO	140 \pm 13 ^b
2	1-102	NMP	160 \pm 5
3	1-102	25% MMS350/NMP	150 \pm 9
4	1-103	DMSO	170 \pm 16
5	1-103	NMP	180 \pm 13
6	1-103	25% MMS350/NMP	190 \pm 7

^aData are reported as mean \pm standard deviation (n = 3). ^bData are reported as mean \pm standard deviation (n = 5).

1.3.2.3 Applicability of MMS350 to *in vitro* and *in vivo* Assays

MMS350 was evaluated as a cosolvent for solutions that would be used in *in vitro* assays. The use of MMS350/NMP solutions was compared to both 100% NMP solutions and 100% DMSO solutions. NMP was needed as a cosolvent because MMS350 is a solid at room temperature and thus must be mixed with an appropriate cosolvent for use in preparation of compound stock solutions. NMP is thermally stable, has low toxicity, and has solubilizing

power superior to that of ethanol and propylene glycol. Moreover, there are precedents for using NMP in bioassays and commercial pharmaceutical applications.^{118,127}

The radiometric PKD1 inhibition assay was used to test the effect MMS350 would have on biological assays. The synthesis and biological evaluation of a series of structures (Figure 1-19) showing nanomolar to micromolar inhibitory activity toward PKD1 was disclosed by the Wipf group.¹²⁸⁻¹³⁰ Several compounds evaluated in this study, especially pyrimidine-containing structures, exhibited poor solubility not only in aqueous solutions but also in DMSO.

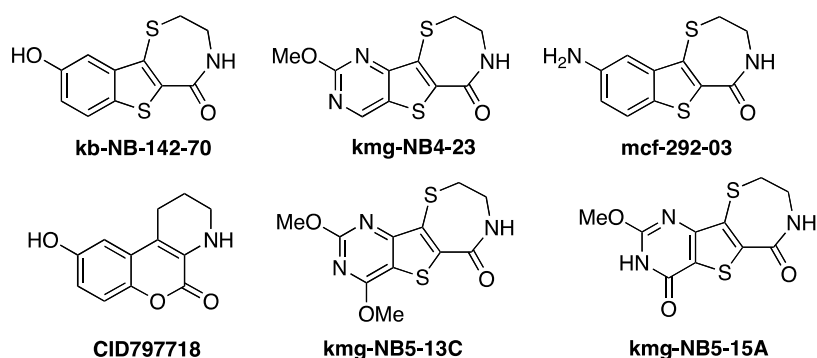


Figure 1-19. Compounds assayed for PKD1 inhibitory activity.

Stock solutions of the 6 PKD1 inhibitors (Figure 1-19) at 10 mM concentrations in DMSO, NMP, and 25 wt% MMS350/NMP were prepared. The solutions were used in the radiometric PKD1 assay to test inhibitor activity at both 1 μ M and 10 μ M concentrations.¹³¹ Graphs comparing the PKD1 activity are shown in Figures 1-20 and 1-21. In the case of NMP, less inhibitory activity was generally observed, especially in the case of mcf-292-03 at inhibitor concentrations of 10 μ M. In general, comparable results were observed when both DMSO and 25 wt% MMS350/NMP were used for compound solution preparation. In the case of the standard PKD1 inhibitory assay, use of MMS350 did not interfere with PKD1 inhibition or the read-out of results.

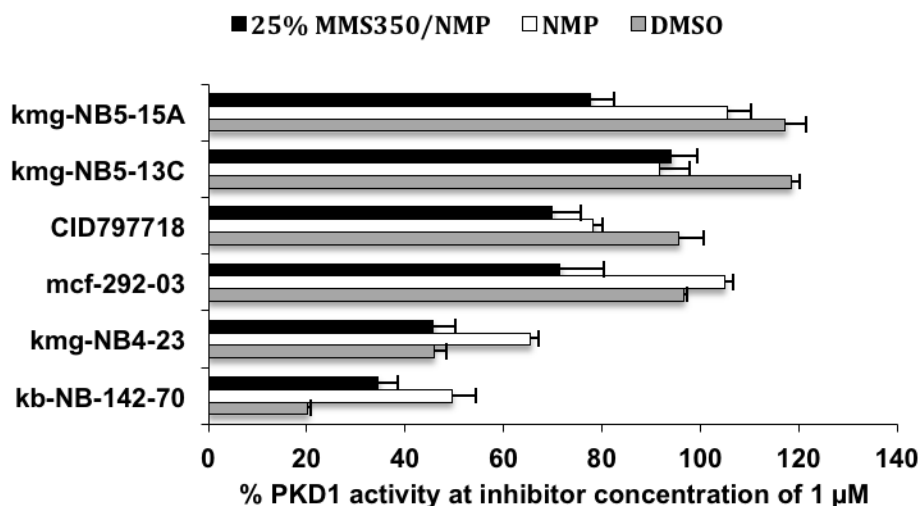


Figure 1-20. Plot of PKD1 activity with compound concentrations of 1 μM.

Stock solutions were prepared in three different media at concentrations of 10 mM, and dilutions were performed using the same media. The % PKD 1 activity is reported as the mean, and error bars represent SEM (n = 3). The % PKD1 activity was determined as previously described.¹²⁹

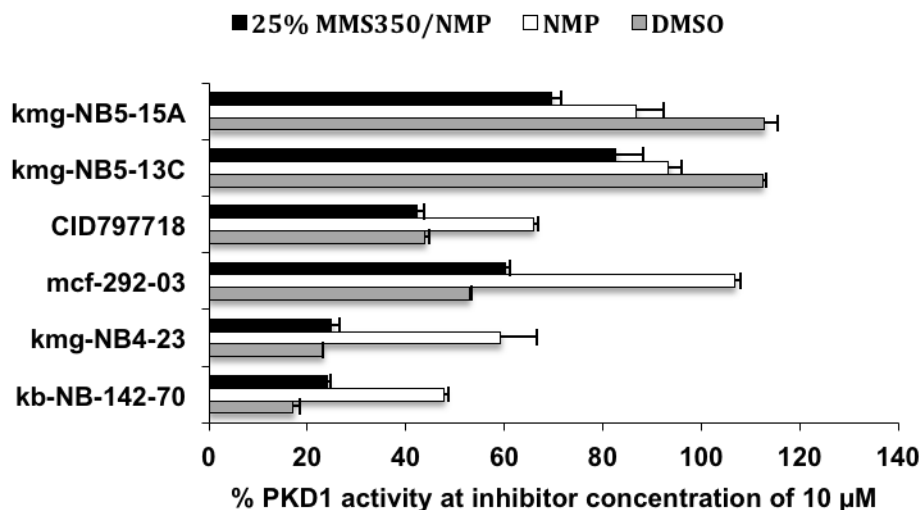


Figure 1-21. Plot of PKD1 activity with compound concentrations of 10 μM.

Stock solutions were prepared in three different media at concentrations of 10 mM, and dilutions were performed using the same media. The % PKD 1 activity is reported as the mean, and error bars represent SEM (n = 3). The % PKD1 activity was determined as previously described.¹²⁹

1.3.2.4 MMS350 for Compound Storage—Hygroscopicity and Other Implications

It was envisioned that solutions of MMS350 in an appropriate cosolvent (e.g., NMP) can be used for compound storage solutions. The test set of compounds (Figure 1-14) was stored in 25 wt% solutions of MMS350/NMP for 6 weeks at -20 °C. It was noted that MMS350 partially precipitated from the solutions at -20 °C, but no change in model compound concentrations were observed after thawing the storage vessels.

Water absorption by storage media is a significant factor for the lifetime of library compounds stored in solutions. Zitha-Bovens and coworkers designed a study to construct a predictive model of the lifetime of compounds in DMSO solution storage solutions.¹¹⁰ Libraries comprising 1000 to 10,000 compounds were examined for compound stability across a broad range of temperatures in both DMSO and H₂O/DMSO (20% v/v). In general, more compound degradation was observed in compounds stored in H₂O/DMSO; however, a small percentage of compound (~3%) actually decomposed in neat DMSO while maintaining stability in wet DMSO. A study¹³² performed at Abbott also indicated that water absorption induced more compound degradation than oxygen exposure.

The degree of water absorption in 25% w/w MMS350/NMP solutions was ascertained. I monitored DMSO, NMP, and 25% w/w MMS350/NMP for one week at ambient temperature (Table 1-34). Although significant water absorption was observed (*ca.* 7000 ppm over the course of 7 days), the MMS350/NMP solution absorbed less water than NMP alone. The result indicates that the hygroscopicity of MMS350 is low relative to NMP.

Table 1-34. Comparative water absorption measurements of possible compound storage media.

Entry	Medium	Water content at t = 0 (ppm) ^a	Water content at t = 7 d (ppm) ^a
1	DMSO	160, 170 ^b	1080, 1130 ^b
2	NMP	150, 130 ^c	12,090, 17,000 ^c
3	25% MMS350/NMP (w/w)	160, 200 ^c	6500, 8600 ^c

^aWater content was analyzed by Karl Fischer titration. The two values listed represent individual vessels, the first value in each column corresponding to the same vessel at each time-point. ^bAverage of 3 measurements. ^cAverage of 2 measurements.

1.3.2.5 Toxicity of MMS350

Because MMS350 showed promising properties for aqueous solubility enhancement and possible compound storage, studies to validate the hypothesis that the compound could also be useful in cellular and *in vivo* assays were undertaken. It was necessary to ensure that MMS350 was not prohibitively toxic to living organisms and cell lines. Brine shrimp assays were performed, and the results are shown in Table 1-35.

Brine shrimp floating in water containing concentrations of MMS350 up to 20 mg/mL showed <10% mortality after 48 h. Shrimp incubated in water containing 50 mg/mL of MMS350 had 85% mortality after 24 h and 100% mortality within 48 h. The data indicate an LC₅₀ of approximately 32 mg/mL (147 mM). In comparison, shrimp treated with DMSO at the same concentrations showed no mortality after 24 h and only 15% mortality after 48 h at 50 mg/mL of DMSO. The cellular toxicity of MMS350 was tested against a breast cancer cell line

(MDA-MB-231) and a liver cell line (HepG2) (Figures 1-22 and 1-23).¹³³ In both cases, the 50% growth inhibitory concentration (GI₅₀) for MMS350 was ~200 mM, whereas the GI₅₀ for DMSO was ~800 mM. The same concentration threshold observed in the case of brine shrimp was also observed; in the case of both cell lines, MMS350 had limited toxicity at concentrations up to ~100 mM. The results indicate that MMS350 may be tolerated in biological assays in concentrations of up to 2% (by mass).

Table 1-35. Brine shrimp assay results: toxicity of sulfoxide MMS350.

Entry	Compound	Concentration (mg/mL)	% Mortality ^a after 24 h	% Mortality ^a after 48 h
1	MMS350	0	<10	10
2	MMS350	1	0	0
3	MMS350	5	0	0
4	MMS350	20	0-10	0-10
5	MMS350	50	85	100
6	DMSO	0	<10	10
7	DMSO	1	0	0-10
8	DMSO	5	0	0-6
9	DMSO	20	0	0
10	DMSO	50	0	15

^aPercent mortality was determined for an average of 5 trials. Percent mortality was determined by estimating the number of shrimp showing no motility after several minutes of observation.

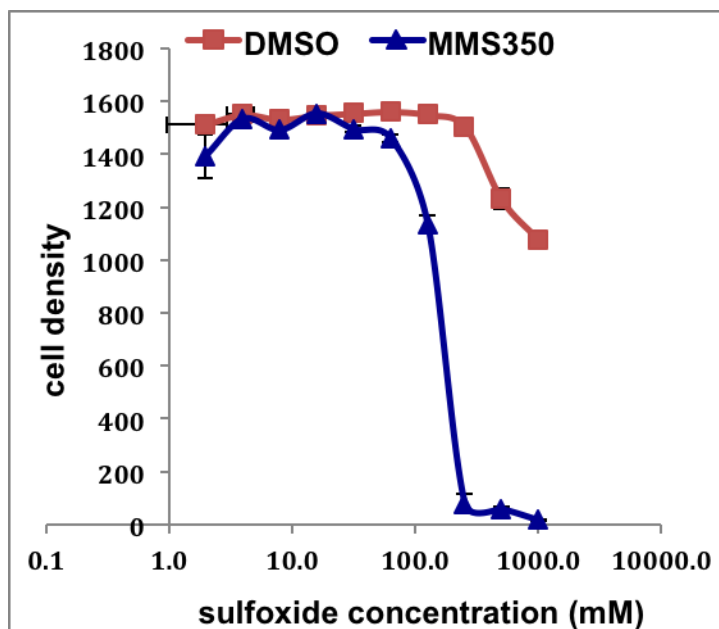


Figure 1-22. Toxicity of MM350 and DMSO against a HepG2 cell line.

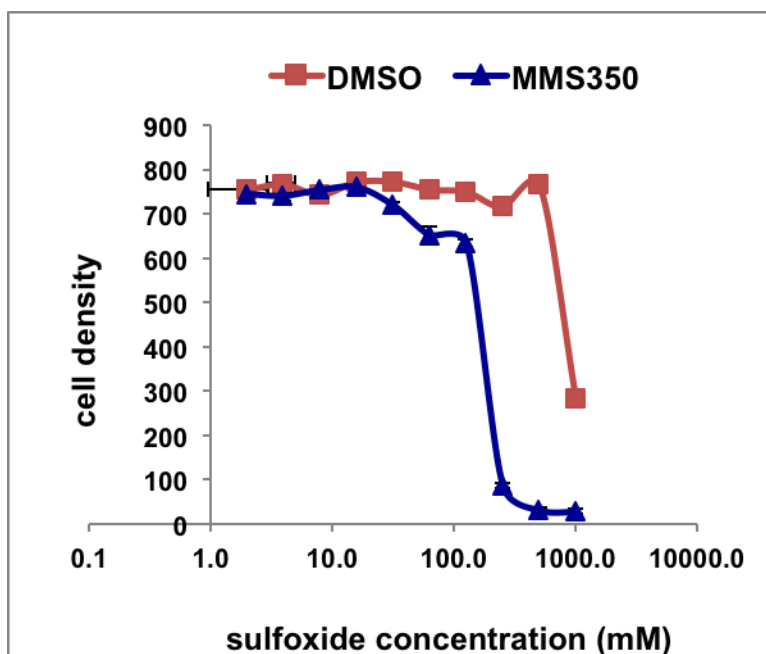


Figure 1-23. Toxicity of MMS350 and DMSO against a MDA-MB-231 cell line.

1.3.2.6 Conclusions for MMS350 as a DMSO Substitute

The utility of MMS350 for enhancing the aqueous solubility of small organic molecules has been demonstrated. Advantages to using MMS350 as a DMSO replacement include its lower reactivity in oxidation reactions. Moreover, MMS350 was used in an enzymatic assay without affecting the readout of results. Although MMS350 exhibited higher toxicity than DMSO in the brine shrimp and cellular assays, the toxicity was sufficiently low to permit use of MMS350 for cellular and *in vivo* assay development in concentrations up to 2%.

Use of MMS350 as a cosolvent for aqueous solubility enhancement showcases the utility of the oxetanyl moiety as a solvent scaffold. Incorporating oxetanes onto the DMSO backbone generated a more lipophilic cosolvent that still maintained good aqueous miscibility. This study prompts further development of using oxetanes in the design of new additives and cosolvents.

1.4 CONCLUSIONS

The donating ability and compact structure of oxetanes make them viable candidates as additives and cosolvents. Oxetanes have a high strain energy, yet their reactivity can be attenuated by substitution at the 3-position. Bisoxetanyl ether **1-37** and bisoxetanyl sulfide **1-69** showed promising solvent effects when used as cosolvents in organolithium- and organomagnesium-mediated reactions, respectively. Notably, the oxetanyl additives were stable in the presence of the organometallic reagents studied. Further experimentation with these compounds is warranted in order to identify key areas where oxetanes can be used to solvate cations.

A bisoxetanyl sulfoxide MMS350 was evaluated as a DMSO substitute. It was shown that MMS350 does not have utility as an oxidizing agent. I took advantage of this property and demonstrated that MMS350 can be used as a cosolvent for aqueous solubility enhancement of

lipophilic compounds. The low toxicity and stability of MMS350 make this sulfoxide suited for use in pharmaceutical formulations.

These studies show that oxetanes are promising moieties for incorporation into solvents and ligand scaffolds. Future work may involve design of oxetane-based ligands for transition-metal mediated reactions. I did explore the use of MMS350 as a substitute for DMSO ligands in the palladium-catalyzed aerobic dehydrogenation of ketones;¹³⁴ yet, I observed no reaction. It may still be worthwhile to explore other palladium or related transition-metal mediated reactions where sulfoxide-based ligands are typically used.

2.0 SMALL MOLECULES AS PROTECTORS AND MITIGATORS AGAINST IONIZING RADIATION

Ionizing radiation causes many physiological conditions ranging from mild nausea to severe health complications (e.g., sepsis) or death.¹³⁵ The biological consequences of ionizing radiation include induction of nuclear DNA single- and double- strand breaks and a molecular damage response that ultimately results in cell death.^{136,137} Reactive nitrogen species (RNS) and reactive oxygen species (ROS) are implicated in a large part of the damage imparted by ionizing radiation.

Chemical substances that are effective ROS scavengers can counteract the harmful effects of ionizing radiation. The identification of agents that are *protectors* (administered prior to radiation exposure) has direct application for patients receiving clinical radiation exposure. The identification of agents that *mitigate* the effects of systemic radiation exposure is of importance to military efforts, disaster relief, and counter-terrorism measures.¹³⁸ In our design of radioprotective or radiation mitigating agents, we focused on two classes of ROS scavengers—sulfoxides and nitroxides. MMS350, a bifunctional, water-soluble dimethylsulfoxide analog, was shown to protect against and mitigate whole-body radiation damage in mice. We have also undertaken a strategy for a nanoparticle-based delivery of nitroxides, which is described in Chapter 3.

Herein, the consequences of unregulated generation of ROS and the endogenous mechanisms for scavenging ROS are described. Two strategies for developing chemical radiation countermeasures are discussed, followed by the results obtained when using MMS350 for radiation protection/mitigation. Finally, there is a description of the synthesis of MMS350

analogs that will be used for studying the mechanism of action of MMS350 and for investigating the SAR of the bifunctional sulfoxide-containing molecules.

2.1 INTRODUCTION

2.1.1 Ionizing Radiation: Generation of ROS

Ionizing radiation has an associated energy that is much greater than the bond energies of many molecules; therefore, homolytic bond scission can occur when ionizing radiation is absorbed. Primary radiolysis products come from homolytic bond cleavage of water, generating hydroxyl radicals, H atoms, and solvated electrons. These species have short life times (10^{-10} to 10^{-9} s);¹³⁹ often, they react rapidly to form secondary radicals, which have longer lifetimes (10^{-6} s). Secondary radicals can react with and damage biomolecules such as DNA, lipids, and proteins.

A consequence of ionizing radiation damage is overproduction of ROS, which include hydroxyl radical (HO^\bullet), hydrogen peroxide (H_2O_2), and superoxide radical anion ($\text{O}_2^{\bullet-}$). It should be noted that reactive oxygen species are, in fact, produced as part of endogenous processes, mostly due to electron transport. It has been estimated that *ca.* 90% of these endogenously generated ROS are produced in the mitochondria as a consequence of oxidative phosphorylation.¹⁴⁰ There are several innate mechanisms for the efficient scavenging of ROS. Yet, as a result of age, pathological processes, or environmental stressors (e.g., ionizing radiation), the production of ROS may exceed the limitations of intrinsic scavenging mechanisms.¹³⁸

One pathway by which ROS affect cell death involves the mitochondria-specific phospholipid cardiolipin (CL).¹⁴¹⁻¹⁴⁴ ROS-mediated oxidation of CL initiates migration of CL

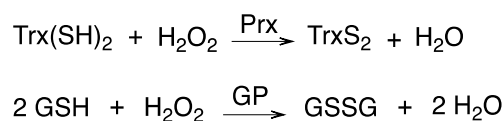
from the inner to the outer mitochondrial membrane. At this point, cytochrome *c*, a heme protein with a critical role in the electron transport chain, forms a complex with CL that acts as a CL-specific oxygenase/oxidase. Oxidation of CL leads to detachment of cyt *c* from the mitochondrial membranes and ultimately the release of pro-apoptotic factors into the cytosol.¹⁴¹⁻¹⁴³ Thus, chemical agents that react with ROS can, in effect, shut down the CL-mediated cell death pathway.

Several natural and unnatural antioxidants, which include DMSO, EtOH, vitamin C, vitamin E, and ubiquinol, are effective for scavenging radiolysis products and ROS.¹⁴³ Chemical reagents can be designed based on these nonspecific ROS scavengers. Another strategy involves specific targeting of the mitochondria due to its role in both ROS production and ROS-mediated cell death pathways.^{140,145} In the following sections, the endogenous mechanisms for ROS elimination are discussed, and strategies based on both mitochondria-targeted and nonspecific ROS scavengers are detailed.

2.1.1.1 ROS Scavenging by Endogenous Enzymes

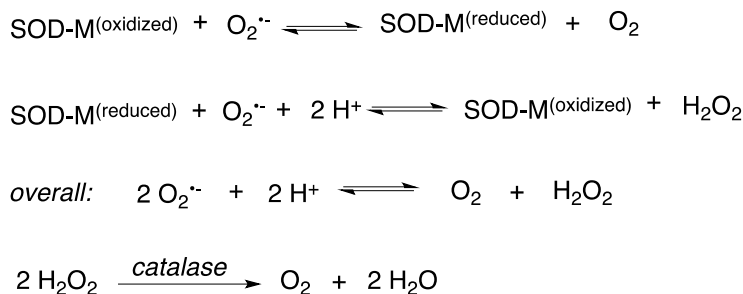
Several enzymes are involved in the continuous scavenging of ROS; examples are depicted in Scheme 2-1. Typical ROS scavenging mechanisms involve peroxidase-mediated redox chemistry of sulfide bonds and H₂O₂. For example, the thioredoxin-thioredoxin reductase system operates via oxidation of thiols in the thioredoxin active site, forming TrxS₂ and water.¹⁴⁶ Similarly, glutathione peroxidase catalyzes the reaction between glutathione and H₂O₂, again generating the disulfide and water (Scheme 2-1).¹⁴⁰

Scheme 2-1. Enzymatic reactions that mitigate ROS (adapted from reference [140]). Prx = peroxiredoxin; GP = glutathione peroxidase; Trx = thioredoxin; GSH = glutathione.



Superoxide dismutases (SODs) (Scheme 2-2) have a different mechanism of ROS scavenging. SODs catalyze the dismutation of superoxide to oxygen and hydrogen peroxide—a general mechanism is shown in Scheme 2-2.^{147,148} There are several families of SOD known, and each is dependent on redox-active metal cofactors including Mn, Fe, Cu, and Ni. Members of the manganese superoxide dismutase (MnSOD) family are critical for the “shuffling” of mitochondrial ROS species. In eukaryotes, these enzymes typically exist as tetramers; in the enzyme active site, a manganese atom catalyzes the conversion of superoxide to hydrogen peroxide. A general mechanism for SOD-mediated disproportionation of superoxide is shown in Scheme 2-2. Briefly, the SOD-oxidized metal cofactor complex is reduced by superoxide with concomitant generation of oxygen. The SOD complex (with a reduced cofactor) can be oxidized by superoxide with resultant formation of H₂O₂. Overall, SODs convert two molecules of superoxide to molecular oxygen and hydrogen peroxide—the resultant hydrogen peroxide is further reduced by a catalase to oxygen and water.^{140,147,148}

Scheme 2-2. Mechanism for dismutation of superoxide by superoxide dismutase (M = Mn, Cu, Fe, Ni).



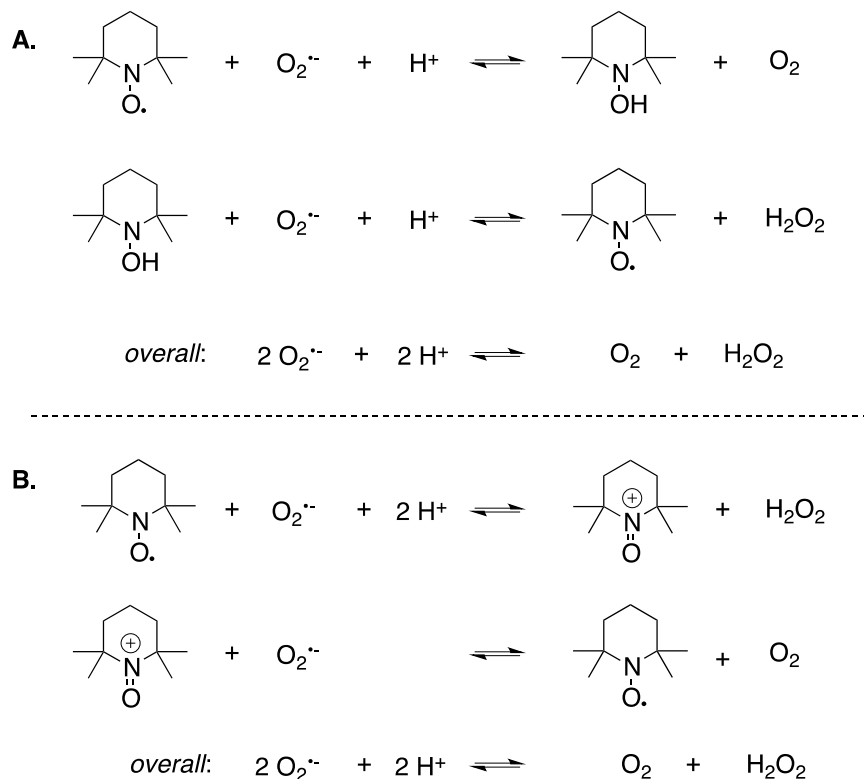
2.1.2 TEMPO as an SOD Mimic

Small molecules bearing stable nitroxyl radicals have been demonstrated to be effective mitigators of ROS.^{138,140,145,149-152} The nitroxyl radical (e.g., in (2,2,6,6-tetramethylpiperidin-1-yl)oxyl, TEMPO) mimics the redox activity of SOD by catalyzing dismutation of superoxide by one of two pathways (Scheme 2-3). One proposal is that superoxide reduces the nitroxide to the hydroxylamine, generating molecular oxygen. The hydroxylamine is then reoxidized to the

nitroxide by an additional molecule of superoxide, generating hydrogen peroxide (Scheme 2-3, **A**). In an alternative pathway, the nitroxide is first oxidized to the *N*-oxoammonium cation followed by subsequent reduction of the *N*-oxoammonium cation back to the nitroxide with concomitant production of molecular oxygen (Scheme 2-3, **B**). In both cases, two molecules of superoxide are ultimately disproportionated to molecular oxygen and H₂O₂.¹⁵³

Additionally, the *N*-oxoammonium cation can be reduced to the corresponding hydroxylamine by ascorbate in biofluids or by cellular NAD(P)-H-mediated electron transport.¹⁴³ Nitroxides are also easily reduced to hydroxylamines by electron transporting enzymes and ascorbate. These hydroxylamines act as reducing agents; single electron transfer regenerates the nitroxides and ROS are scavenged by hydrogen transfer.¹⁴³ Therefore, stabilized nitroxyl radicals can both catalyze dismutation of superoxide *and* act as precursors to other biologically active ROS scavengers.

Scheme 2-3. Mechanisms for nitroxide-catalyzed dismutation of superoxide.



2.1.3 Strategies for Developing ROS Scavenging Agents

The Wipf group and collaborators have undertaken two general strategies for development of ROS scavenging agents. One major research focus is the development of agents that *specifically target* the mitochondria. It has been established that lipid peroxidation of *mitochondria-specific* phospholipid CL is associated with the deleterious effects of ionizing radiation. Moreover, it has been demonstrated that mitochondrial localization of endogenous ROS scavenging enzymes (e.g., SOD) is correlated with successful mitigation of radiation-induced cellular damage.¹⁵⁴

One method of mitochondria-specific targeting is the use of manganese superoxide dismutase-plasmid liposomes (MnSOD-PL).^{138,155} Using this method (in mouse models), a plasmid containing the transgene for MnSOD expression was administered (via a liposomal delivery system) to the esophagus. Alternatively, the liposomes were delivered to the lungs by intra-tracheal injection or inhalation. In all cases, a decrease in both acute and chronic symptoms of radiation was observed. Although the use of the antioxidative transgene products was shown to be *radioprotective*, the time-course of administration (several hours for *in vivo* gene expression) renders it unrealistic to use this strategy in radiation *mitigation*.¹³⁷

An alternative to the MnSOD transgene approach is the use of small molecules specifically designed to target the mitochondria.¹⁴⁵ Strategies for delivery of antioxidants to the mitochondria involve tethering ROS scavengers (e.g., TEMPO, section 2.1.3) to delivery vehicles. Examples of effective vehicles include lipophilic cations^{145,156} such as triphenylphosphine-based conjugates,^{145,157} which take advantage of the negative membrane potential of the inner mitochondrial membrane. A major research focus in the Wipf group has been the conjugation of TEMPO to Gramicidin S conjugates. In the next sections, delivery vehicles designed for mitochondria-specific delivery of TEMPO are described.

2.1.4 Targeted Delivery of Nitroxides to the Mitochondria

A current strategy for targeted delivery of nitroxides to mitochondria involves conjugation of nitroxides to hemigramicidin-S mimics (Figure 2-1). The design was based on the antibiotic Gramicidin S, which has high permeability for bacterial cell membranes. Because bacterial cell membranes are structurally similar to mitochondrial membranes, delivery systems based on Gramicidin S were postulated to be selectively permeable to mitochondrial membranes. To generate delivery systems with lower susceptibilities to protease degradation, the *E*-alkene peptide isosteres (e.g., XJB-5-131) were synthesized.¹⁵⁸ It has been shown that the hemigramicidin-TEMPO conjugate XJB-5-131 localizes in mitochondria of mouse embryonic cells (MECs); furthermore, cells treated with XJB-5-131 were protected from an actinomycin D-induced increase of superoxide production.¹⁵²

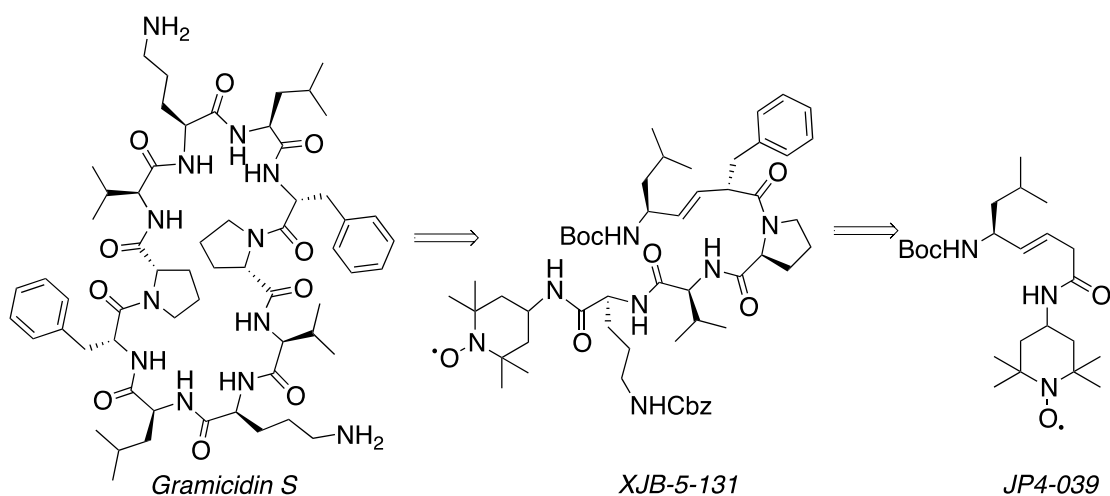


Figure 2-1. Gramicidin S and hemigramicidin S TEMPO conjugates for mitochondria-targeted delivery.

The radioprotective effects of XJB-5-131 and related analogs were also demonstrated. It was shown that these targeting peptides directed either 4-amino-TEMPO or 2-amino-6-methylthiazone (AMT, a nitric oxide synthase antagonist) to the mitochondria, which effectively induced radioprotective effects.¹⁵¹ The simplified *E*-alkene isostere JP4-039 (Figure 2-1) has

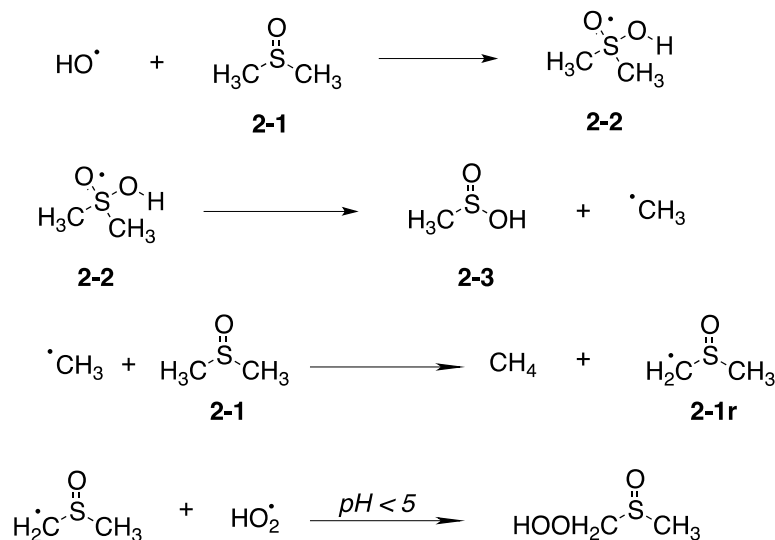
shown promise in mitochondrial targeting and radioprotective initiatives. For example, JP4-039 exhibited both radioprotective and radiation mitigating effects against Fanconi anemia (FA) cell lines, which have enhanced sensitivity to DNA crosslinking agents and show enhanced radiosensitivity. Furthermore, use of a fluorescently labeled BODIPY-JP4-039 gave additional evidence that the molecule does localize to the mitochondria. JP4-039 showed improved radioresistance in comparison to 4-hydroxy-TEMPO (TEMPOL), which does not have a mechanism for mitochondrial localization.¹⁴⁹

One drawback to the TEMPO-hemigramicidin S conjugates is their low aqueous solubility (JP4-039, 0.5 mg/mL; XJB-5-131, 0.04 mg/mL).¹⁵⁹ Ongoing efforts toward developing suitable formulations for these compounds is in progress. I also explored new TEMPO delivery systems involving pH-mediated release from nanoparticles; these systems are discussed in Chapter 3.

2.1.5 Sulfoxides as ROS Scavengers

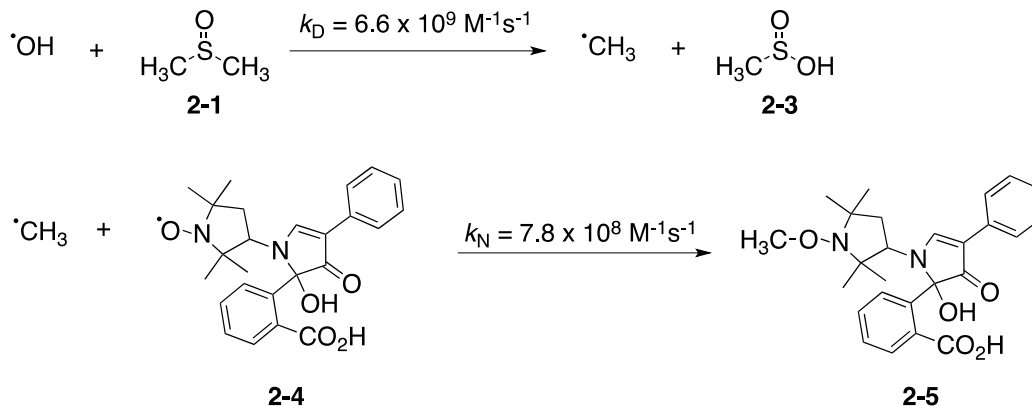
An alternative strategy to using mitochondria-targeted scavengers is to use nonspecific scavengers that are easy to administer (i.e., no vehicle is necessary). DMSO and other sulfoxides typically have favorable aqueous solubility and have long been recognized as having protective properties against ionizing radiation.¹⁶⁰⁻¹⁶² It is hypothesized that DMSO prevents lipid peroxidation, likely by scavenging reactive oxygen species, particularly $\bullet\text{OH}$. The reaction of sulfoxides with hydroxyl radicals is well-studied.¹⁶³ Sulfoxides react with hydroxyl radicals to generate intermediate sulfur radical species **2-2** (Scheme 2-4) that react further to generate methyl radical and methanesulfinic acid **2-3**. Methyl radical can abstract hydrogen from another molecule of DMSO (or methanesulfonic acid) to generate methane and a stabilized dimethyl sulfoxide radical **2-1r** (Scheme 2-4).¹⁶⁴ Possible chain termination steps involve reaction with superoxide radical anion (in the case of the mechanism in Scheme 2-4, at acidic pH) to generate hydroperoxy(methylsulfinyl)methane.¹⁶³

Scheme 2-4. General reaction of hydroxyl radicals with sulfoxides.



DMSO is also used in analytical assays for quantitative detection of hydroxyl radicals (Scheme 2-5).¹⁶⁵ Rapid reaction of DMSO with hydroxyl radical generates methyl radicals, which react with the fluorescamine-derivatized nitroxide **2-4**, generating the *O*-methylhydroxylamine product **2-5**. Product **2-5** can be analyzed and quantified by reverse-phase HPLC using fluorometric detection. These assays have been used for evaluating the extent of hydroxyl radical formation by anti-cancer drugs (e.g., quinone-containing compounds).¹⁶⁵ It should be noted that DMSO also reacts with superoxide and carbonate radicals to produce methyl radicals; thus, assays such as those depicted in Scheme 2-5 cannot be used as unambiguous determination of *hydroxyl* radicals in solution. Yet, for the purposes of our studies, the coupling of the hydroxyl radical scavenging reaction with the nitroxide methylation is a viable precedent for generating synergistic therapeutic agents incorporating both sulfoxides and nitroxides.

Scheme 2-5. Hydroxyl radical scavenging assay based on the rapid reaction of DMSO with hydroxyl radical.



2.1.5.1 DMSO as a Radioprotector

DMSO has shown radioprotective properties in both cellular assays and *in vivo* experiments. For example, it was demonstrated that golden hamster embryos (GHEs) pre-treated with DMSO were protected from the damaging effects of γ -radiation; moreover, the D_0 value (dose of radiation that reduces a population by 67%) increased with increased DMSO concentrations.¹⁶⁶ Additionally, DMSO pretreatment prevented γ -ray induced DNA single-strand breaks (SSBs) and reduced the occurrence of chromatid aberrations, also in a concentration-dependent manner.¹⁶⁶ In a separate study, it was shown that the 30-days lethality of mice pre-treated with DMSO and subjected to 9 Gy radiation was 16%; the 30-days lethality of the control, untreated group was 44%.¹⁶⁷

Ueda and coworkers examined the role of DMSO in preventing mouse liver lipid peroxidation.¹⁶⁷ The authors used precedented assays wherein the extent of lipid peroxidation was determined as thiobarbituric acid reactive substance (TBA-RS); an increase in TBA-RS levels was observed after mice were subjected to 9 Gy whole-body irradiation, whereas mice pre-treated with DMSO (0.11 g, i.p. injection 30 min prior to irradiation) exhibited similar levels of TBA-RS as the control (non-irradiated) group. The authors also noted that SOD activity

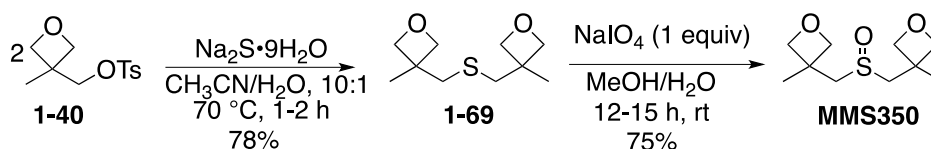
decreased in irradiated mice 10 days after irradiation, but SOD activity of DMSO-treated mice stayed consistent with that of mice not subjected to radiation. A final observation from this study was that the mitochondria and endoplasmic reticulum of liver cells from irradiated mice exhibited swelling; these effects were not observed in livers from mice that were pre-treated with DMSO.

2.2 RESULTS AND DISCUSSION

2.2.1 MMS350—An Effective Radiation Mitigator?

Although the mitochondrial targeted reagents are promising radioprotectors, they are limited in regard to aqueous solubility. Based on the precedents for dimethylsulfoxide being radioprotective, we decided to test bifunctional dimethylsulfoxide analog MMS350 due to its low toxicity, high aqueous solubility, and ease of synthesis—MMS350 can be prepared in 3 steps from commercially available materials without the need for chromatography (see section 1.2.7). The synthesis is reproduced in Scheme 2-6. Tosylate **1-40** (synthesized from commercially available 3-methyl-3-oxetanemethanol) was treated with disodium sulfide followed by oxidation with sodium periodate to afford MMS350.

Scheme 2-6. Synthesis of MMS350.



2.2.1.1 MMS350 is Both Radioprotective and Mitigating

MMS350 was first tested in a screening experiment wherein 32D cl 3 cells were irradiated at doses of irradiation up to 7 Gy and then treated with mitigating compounds at 10 μ M. MMS350 had efficacy similar to JP4-039.¹⁶⁸ Because the initial screen was encouraging, the compound was tested for use as a radiation mitigator in C57Bl/6/HNsd mice. Mice treated with MMS350 had a 40-days lethality of 50% whereas 50% of the untreated mice died by day 13 (Figure 2-2). It was also encouraging that using MMS350 showed similar results to using the known radiation protector/mitigator JP4-039.¹⁶⁸

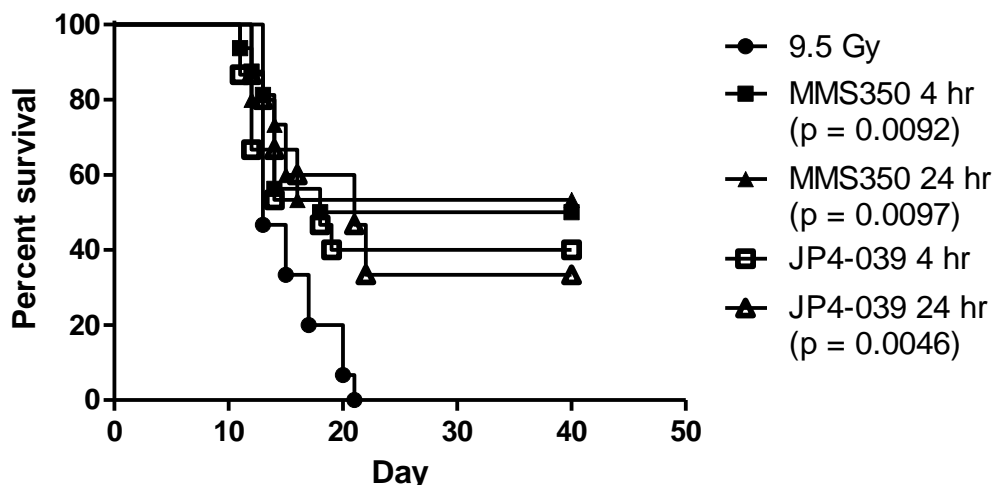


Figure 2-2. Survival curves of mice injected with 20 mg/kg MMS350 in PBS or JP4-039 in cremphor el and ethanol at 4 h or 24 h after irradiation.

In the course of their work toward identifying useful radiation protectors or mitigators for human use, Goff and coworkers discovered that some agents are highly effective in mice but ultimately have no human efficacy. They have since developed an assay wherein umbilical cord blood progenitor cells are irradiated and treated with potential protectors/mitigators either before or after irradiation.¹⁶⁹ Representative data are shown in Table 2-1. MMS350 was protective of cord blood cells (colony-forming unit granulocyte macrophage (CFU-GM)) at concentrations of 200 μ M (D_0 2.3 ± 0.09 ; control 1.85 ± 0.35 , DMSO treated pre-treated cells 1.93 ± 0.15). MMS350 was also protective in the case of burst-forming unit erythroid (BFU-E)—the D_0 value

for cells pre-treated with MMS350 (50 μ M) was 1.79 ± 0.27 , which was an improvement over the D_0 value found for cells pre-treated with DMSO (1.34 ± 0.33).¹⁶⁹

Table 2-1. Selected data showing the effect of radioprotective agents on irradiation survival of CB MNC.^a

Entry	Conditions	D_0 value
1	Cells only	1.49 ± 0.23
2	DMSO	1.72 ± 0.15
3	XJB-5-131 (10 μ M)	1.93 ± 0.13 (p = 0.044)
4	JP4-039 (10 μ M)	1.99 ± 0.13 (p = 0.029)
5	MMS350 (200 μ M)	2.3 ± 0.09^b (p = 0.023)

^aData are for cells (CFU-GM) pre-treated with the agents before irradiation. Pairwise comparisons were made with the two-side two sample t-test; p-values represent comparisons between the treated cells and the cells-only group. ^bA different “cells-only” group was used with a D_0 value of 1.85 ± 0.35 .

MMS350 showed similar efficacy as mitochondrial targeting agents XJB-5-131 and JP4-039 in the *in vitro* and *in vivo* assays; however the aqueous solubility of MMS350 makes it an attractive candidate for further testing due to ease of administration during *in vivo* assays. The straightforward synthesis and relatively low cost for production of MMS350 make it feasible to design experiments requiring large amounts of material (i.e., for animal studies).

MMS350 was also tested for its effectiveness in preventing the late-stage side effects of radiation, in particular, fibrosis.¹⁷⁰ It has been demonstrated that pulmonary fibrosis comes from bone marrow stromal cells, which migrate to the lungs via the circulatory system. Two mouse

models of fibrosis were used to test the effectiveness of MMS350 for protective effects against late-stage irradiation symptoms. One model used C57BL/6 mice that were irradiated to 10 Gy and then transplanted intravenously with luciferase positive C57BL/6J mouse bone marrow. The mice were periodically injected with luciferin and imaged. A second model involved the use of clonal bone marrow stromal cell lines established from long-term bone marrow cultures of luciferase positive mice. After irradiation of the thoracic cavity to 20 Gy, mice were administered (i.p.) luc+ cells. Radiation fibrosis was indicated by an increase in luciferase activity in the lungs. In the case of both studies, mice administered MMS350 in the drinking water showed lower degrees of luciferase activity in the lungs, which is indicative of a lower incidence of radiation fibrosis. Preliminary data indicate that MMS350 is “downregulating the expression of VEGF and vWF, specifically in pulmonary endothelial cells.”^{171,172} Current research efforts are focused on gaining a better understanding of how MMS350 attenuates pulmonary fibrosis.

2.2.2 Ongoing and Future Studies of MMS350

We and our collaborators are planning more studies to elucidate the role of MMS350 in radiation protection and mitigation. We will study the impact of MMS350 on DNA repair; in this regard, we are pursuing a collaboration with Bevin Engelward at MIT, who has developed the CometChip, a high-throughput DNA repair analysis system.

Testing of MMS350 on Fanconi D2 -/- mice is also planned. We hope that the protective effects of MMS350 will translate to a decrease in side effects from radiation therapy on patients with impaired DNA repair mechanisms.

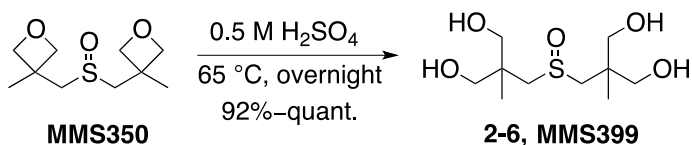
As an extension of the work, MMS350 will be explored as an agent for reducing osteopenia. Julie Glowacki at Brigham and Women’s Hospital developed a mouse model for wound healing. The model involves administration of ionizing radiation to the legs of normal C57BL6 mice, which leads to delayed bone healing (likely due to reduced antioxidant reserves). It was shown that using JP4-039 was beneficial to wound healing in this mouse model. Because

MMS350 showed similar efficacy in the radioprotective assays as JP4-039, it seems feasible that MMS350 could be useful for wound healing. Successful results with MMS350 would be beneficial to military efforts because MMS350 can be administered in drinking water.

2.2.2.1 Control Studies with MMS399

I also developed a control analog to ascertain the need for MMS350 versus other sulfoxide-containing compounds. Tetrol **2-6** (MMS399) was generated by heating MMS350 with aqueous sulfuric acid (Scheme 2-7). This compound did not show radioprotective effects relative to DMSO or the control (untreated) cells in the 32D cl 3 survival assay. Recently, however, it was demonstrated that MMS399 is not a true negative control *in vivo*. It should be noted that DMSO itself is not a radioprotector or mitigator for cultured cells.

Scheme 2-7. Synthesis of control sulfoxide MMS399.



One hypothesis for the difference in activity between MMS350, MMS399, and DMSO is that the membrane permeabilities of the analogs lead to differing degrees of efficacy. I decided to generate analogs of MMS350 to develop an understanding of the physical properties and structural requirements for radioprotection or mitigation of these bifunctional sulfoxide derivatives. I turned to the synthesis of azetidine analogs **2-7** (Figure 2-3); variation would be introduced at the nitrogen in the 4-membered rings, thus altering the physical properties without making major changes to the overall conformation.

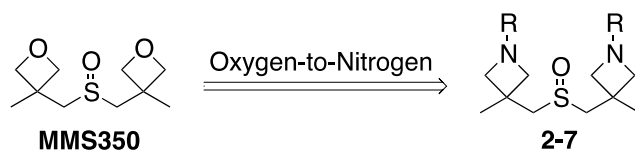
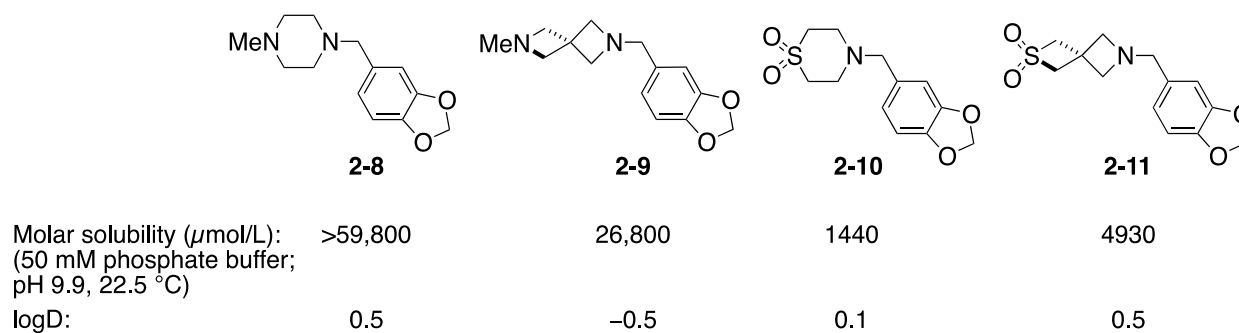


Figure 2-3. General structure of azetidine analogs of MMS350.

2.2.2.2 Azetidines as Modules in Medicinal Chemistry

Along with oxetanes, azetidines have become an increasingly explored structural motif for use as bioisosteres. Notably, Müller and Carreira have demonstrated the utility of spirocyclic azetidines as replacements for piperazines, piperidines, morpholines, and thiomorpholines (Figure 2-4).¹⁷³ For example, the spirocyclic compound **2-9** exhibits lower intrinsic aqueous solubility and but also a lower logD (*n*-octanol/water distribution coefficient at pH 7.4) than the corresponding *N*-methylpiperazine **2-8**. Interesting, the analogous sulfone-containing compounds show a reversal in this trend, wherein the spirocyclic compound still has an improved aqueous solubility but also has a high logD value. It was also demonstrated that replacing the piperazynl moiety on ciprofloxacin with a spirocyclic azetidine led to improved metabolic stability in human microsomal assays.¹⁷³ The authors postulate that the more polar spirocyclic azetidine compounds may have fewer interactions with membrane-bound oxidizing enzymes (e.g., cytochrome P450), thus leading to less metabolic degradation.



The replacement of the oxetanes of MMS350 with azetidines (i.e., Figure 2-5, **2-7**) has

Figure 2-4. Comparative aqueous solubility and lipophilicity data for spirocyclic azetidines and the corresponding monocyclic scaffolds.

several implications. Azetidines introduce basic amine functions, and the basicity can be modulated by introduction of different *N*-substituents. The pKa of azetidine is reported to be 11.29, making azetidine essentially identical in basicity to pyrrolidine (pKa = 11.27) and more basic than dimethylamine (pKa 10.73).¹⁷⁴ The pKa of azetidines is influenced by substituents; for example, the measured pKa of **2-11** is 6.7 whereas the pKa of the corresponding 6-membered analog **2-10** is 4.0.¹⁷³ However, the pKa values of the spirocyclic and piperidinyl analogs of **2-10** and **2-11** wherein the sulfone was replaced for a methylene group were identical (both 9.6).¹⁷⁰ Furthermore, variation of the nitrogen substituents will allow for changes in the intrinsic aqueous solubility and membrane permeability. Geometrically, azetidines have puckering angles similar to cyclobutane (35°),^{175,176} the azetidine analogs will therefore differ spacially from the relatively unpuckered oxetanes.

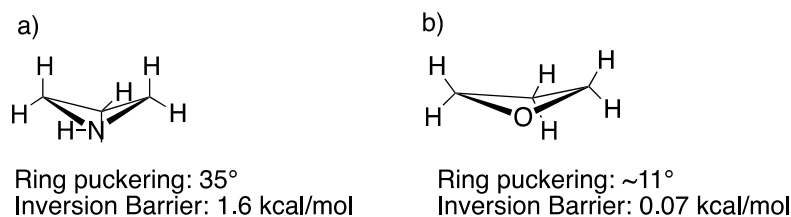
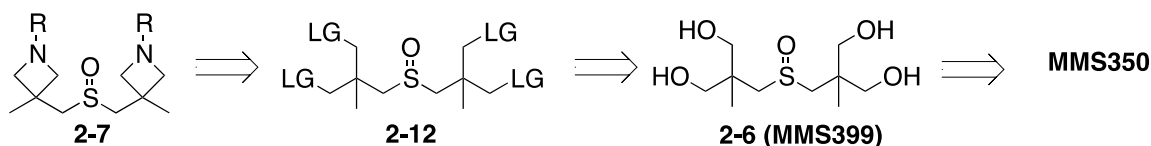


Figure 2-5. Comparison of the conformation of azetidine (a) and oxetane (b).

2.2.2.3 MMS350 Analog Synthesis—Toward Bis-azetidines

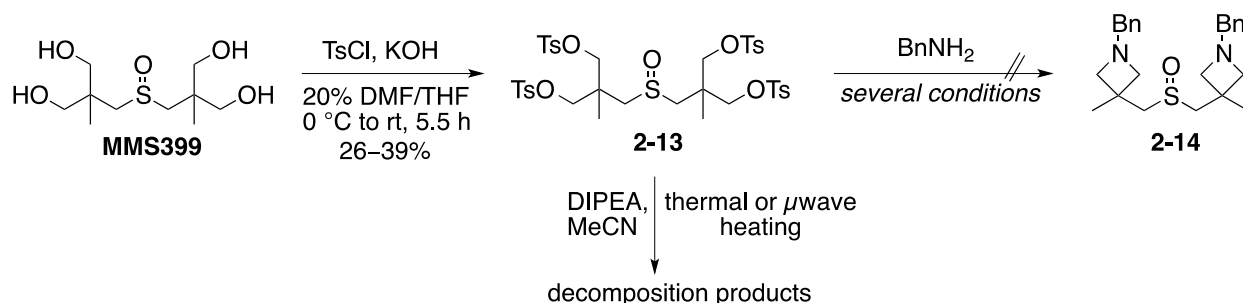
It was envisioned that bis-azetidines **2-7** could be obtained by reaction of activated tetrol **2-12** with amines (Scheme 2-8). The activated tetrol **2-12** would be generated from **2-6** (MMS399), which is synthesized from MMS350. As part of a strategy for convergent analog generation, the plan included synthesis of a common structure **2-7** where “R” would be a readily cleavable protection group (e.g., benzyl). Analogs would be generated by alkylation or reductive amination.

Scheme 2-8. Strategy for the synthesis of bis-azetidines.



Starting from tetrol **2-6** (MMS399), tetratosylate **2-13** was synthesized in modest but usable yield (Scheme 2-9). Reacting tetratosylate **2-13** with benzylamine using reported conditions (e.g., DIPEA or K_2CO_3 in polar, aprotic solvents such as MeCN, DMSO, or DMF with thermal or microwave heating) did not lead to isolation of bisazetidine **2-14**. Instead, formation of a new, unidentified product that decomposed rapidly upon concentration in $CDCl_3$ was observed. I tested whether the product came from intramolecular reactions of sulfoxide **2-13** versus an intermolecular reaction with benzylamine; the tetratosylate was subjected to representative reaction conditions (DIPEA, MeCN, thermal or microwave heating) in the absence of benzylamine. In this case, conversion of **2-13** to similar, unidentified products was observed (Scheme 2-9).

Scheme 2-9. Initial route toward synthesis of bis-azetidines.



I reasoned that the instability of tetratosylate **2-13** may be due to the presence of the sulfoxide functional group. Intramolecular reaction of the sulfoxide and the activated methylene groups to generate 5-membered intermediates is possible. Additionally, the α -protons adjacent to

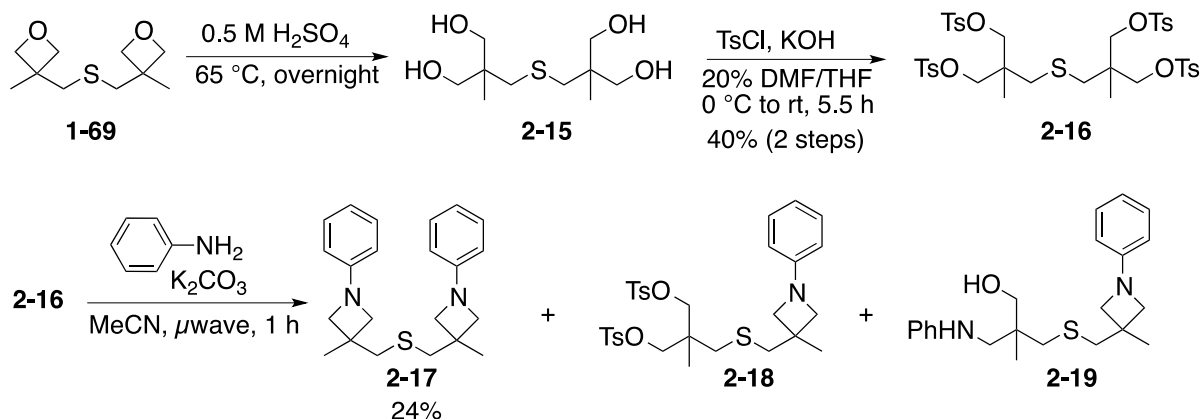
the sulfoxide are acidic—Pummerer-type rearrangements may occur. Therefore I hypothesized that starting from the corresponding sulfide would be a viable alternative.

The corresponding tetratosylated sulfide **2-15** (Scheme 2-10) was synthesized using by acid-mediated opening of bisoxetanyl sulfide **1-69** followed by global tosylation to afford tetratosylate **2-16** in moderate yield. Subjecting **2-16** to representative reaction conditions (DIPEA, MeCN, microwave heating) in the absence of amine afforded starting material, indicating that sulfide **2-16** is stable to the basic, thermal conditions.

At this point, I changed strategies and use anilines rather than primary amines in the initial condition screening for bis-azetidine formation. I reasoned that the corresponding azetidine products would be more stable to standard purification conditions (e.g., silica-gel chromatography). I also envisioned using the *p*-methoxyphenyl group as a protecting group that would be cleaved under oxidizing conditions (e.g., CAN or H₅IO₆).¹⁷⁷

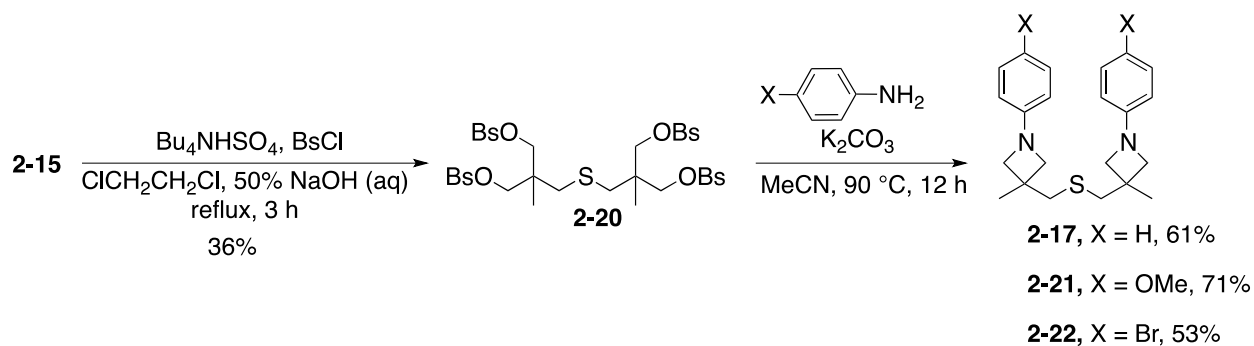
The synthesis of azetidines from sulfide **2-16** is shown in Scheme 2-10. Sulfide **2-16** was treated with K₂CO₃ and aniline and subjected to microwave heating in acetonitrile at 140 °C for 1 h. Gratifyingly, the desired bis-azetidine sulfide was isolated in 24% yield. Byproducts including the corresponding mono-azetidine and a hydrolyzed azetidine were also identified (by LCMS analysis of the crude reaction mixture). Performing the same reaction under thermal conditions (MeCN, 100 °C, overnight) also afforded the desired product **2-17** in 13% yield.

Scheme 2-10. Synthesis of bis-azetidines from sulfide **1-69**.



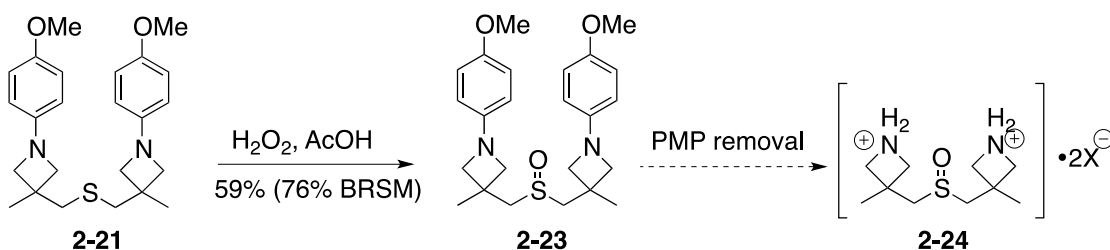
The yield of the bis-azetidine formation was improved by increasing the electrophilicity of the neopentyl- methylene groups (Scheme 2-11). Initially, tetrabrosylated sulfide **2-20** was synthesized using the same conditions as the tetratosylation protocols (BsCl, KOH, 20% DMF/THF); however, these conditions afforded the tetrabrosylate **2-20** in consistently low yield (*ca.* 20%). After screening alternative conditions, I found that phase-transfer conditions afforded the tetrabrosylate **2-20** in 36% yield (Scheme 2-11). Reaction of the tetrabrosylate with aniline provided the desired bis-azetidine in 61% yield. The *p*-methoxy- and *p*-bromo- analogs **2-21** and **2-22** were also synthesized with the intent of further derivatizing the bis-azetidine scaffolds.

Scheme 2-11. Synthesis of bis-azetidines using a tetrabrosylated sulfide.



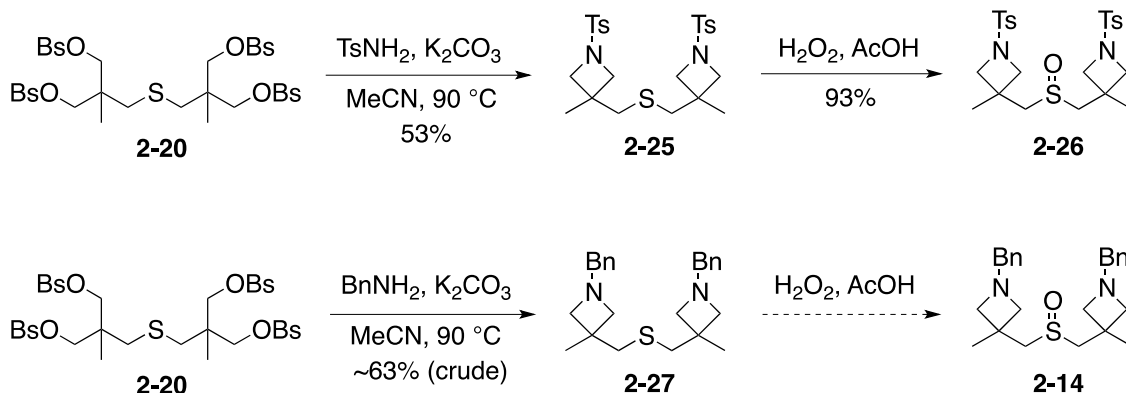
I planned to use *p*-methoxyphenyl (PMP)-protected bis-azetidine **2-21** for further diversification of the scaffold. Sulfide **2-21** was oxidized to the corresponding sulfoxide **2-23** with H₂O₂ in acetic acid (Scheme 2-12). Optimization of the sulfide oxidation protocol is in progress. Conditions for removal of the PMP-group will be screened.

Scheme 2-12. Sulfide oxidation and future plans for protecting group removal.



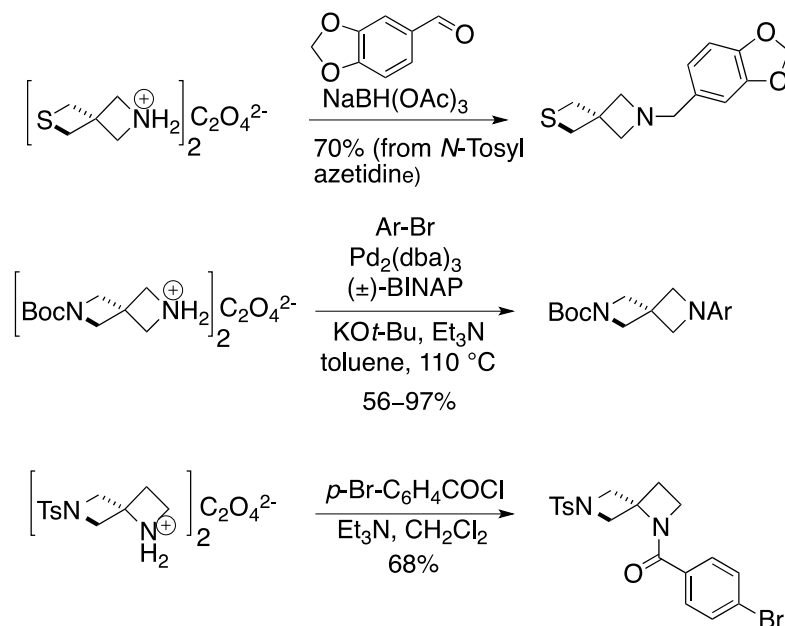
Bis-azetidine formation was also accomplished using benzylamine and *p*-toluenesulfonamide as nucleophiles (Scheme 2-13). In the case of *p*-toluenesulfonyl-substituted azetidines, sulfide **2-25** was smoothly oxidized to the corresponding sulfoxide **2-26** and isolated in good yield after an aqueous workup with NaHCO₃. In the case of the alkyl (benzyl) substituted sulfide **2-27**, oxidation afforded sulfoxide **2-14** in low yields due to loss of material in the aqueous layer. Further optimization of the workup protocol (e.g., using aqueous NaOH instead of aqueous NaHCO₃) to facilitate isolation of **2-14** is in progress. In the case of either **2-26** or **2-14**, deprotection of the bis-azetidines by detosylation of **2-26** or debenzylation of **2-14** would allow for access to common intermediate **2-24**.

Scheme 2-13. Synthesis of bis-azetidines with tosyl and benzyl substituents.



Carreira and coworkers have demonstrated that the oxalate salts of azetidines are easily derivatized by reductive amination,¹⁷³ Buchwald-Hartwig cross-coupling reactions,¹⁷⁸ or acylation reactions¹⁷⁹ (Scheme 2-14). These reactions may be used to introduce diversity into the scaffold of bis-azetidine **2-24**.

Scheme 2-14. Precedented methods for functionalizing azetidines.



2.2.3 Calculated Membrane Permeabilities of MMS350 and Analogs

The therapeutic efficacy of DMSO, MMS350, and related analogs may depend on both cellular and mitochondrial membrane permeability. To gain an understanding of the relationship between analog structure and membrane permeability, calculations were performed using QikProp software (Table 2-2). The permeability of DMSO, MMS350, MMS399, and a series of bis-azetidinyll MMS350 analogs (Figure 2-6) were compared, and the results are shown in Table 2-2.

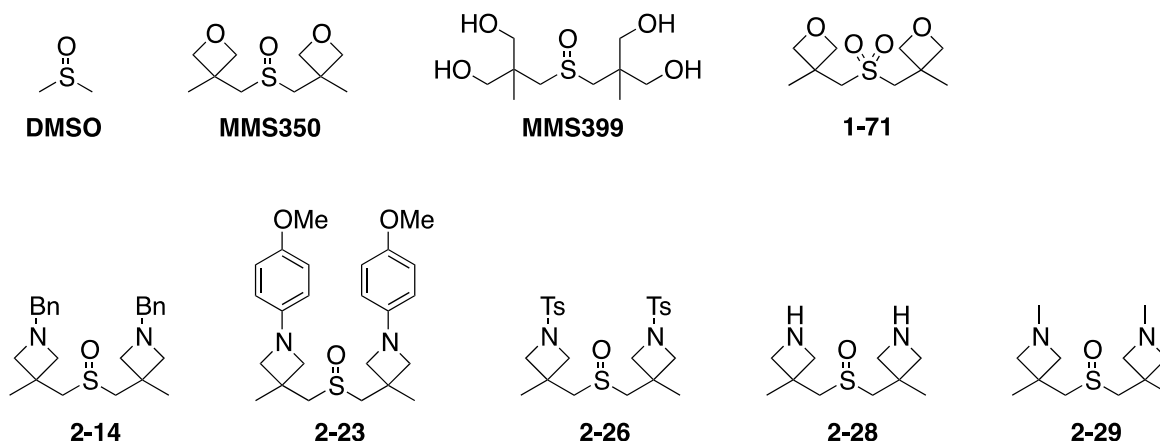


Figure 2-6. Compounds compared for calculated membrane permeabilities.

Based on these calculations, it is apparent that MMS350 is slightly more permeable than DMSO, whereas the permeability of the corresponding sulfone **1-71** is calculated to be significantly better in the case of Caco-2 cell permeability but comparable to MMS350 and related analogs in the case of MDCK cell permeability. As expected, the permeabilities of tetrol MMS399 and bis-tosylate **2-26** are much lower than those of DMSO, MMS350, and the related bis-azetidine analogs. It should be noted that the samples were all calculated as neutral molecules, and therefore the differences in pKa and consequent differences in protonation state of the aniline-based azetidine **2-23** and bis-benzylated azetidine **2-14** were not taken into account. It is notable that the free bis-azetidine **2-28** has lower calculated permeabilities than MMS350 and the substituted bis-azetidines. These values may be used (in conjunction with relevant experimental data) as a means of rationalizing differences in experimental efficacies among vastly different functional groups (e.g., free azetidine versus alkyl azetidine versus tosylated azetidine versus oxetane). The calculated values do not indicate that any large differences in membrane permeabilities are achieved by varying the substituents on the bis-azetidine sulfoxide analogs.

Table 2-2. Calculated membrane permeabilities for DMSO, MMS350, and related analogs.

Entry	Compound	QPPCaco (nm/s) ^{a,b}	QPPMDCK (nm/s) ^{a,c}
1	DMSO	146	2860
2	MMS350	246	3589
3	MMS399	6	71
4	1-71	4248	2362
5	2-14	243	3564
6	2-23	232	3341
7	2-26	22	264
8	2-28	54	711
9	2-29	184	2638

^aData were generated using QikProp, version 3.1, Schrödinger, LLC, New York, NY, 2008. The following parameters were used for structure minimization:

Forcefield: OPLS; solvent: water; electrostatic treatment: constant dielectric; dielectric constant: 1.0; Method: PRCG, 500 iterations, converged on energy.

Further explanations of the QikProp calculations¹⁸⁰ and correlations between experimental and predicted values¹⁸¹ are documented in the literature.

^bThe calculations represent predicted Caco-2 cell permeability, which is typically used to model passage through the blood-gut barrier.¹⁸²

^cThe calculations represent predicted MDCK (Mdin-Darby canine kidney) cell permeability, which is typically used as a general model to predict passive diffusion through cell membranes.¹⁸³

2.3 CONCLUSIONS

The Wipf group has developed effective small molecules for radiation protection and mitigation. Efforts have focused on the design of *E*-alkene isostere hemigramicidin S conjugates for the targeted delivery of nitroxides to the mitochondria. The bifunctional sulfoxide MMS350 was also tested in both cellular and animal studies for its efficacy as a radiation protector/mitigator. MMS350 was both protecting and mitigating in cord blood assays and *in vivo* mouse studies. Irradiated mice that were administrated MMS350 in their drinking water showed lower incidences of pulmonary fibrosis, a late-stage side effect of ionizing radiation damage. The low toxicity and high aqueous solubility make MMS350 an attractive candidate for further studies.

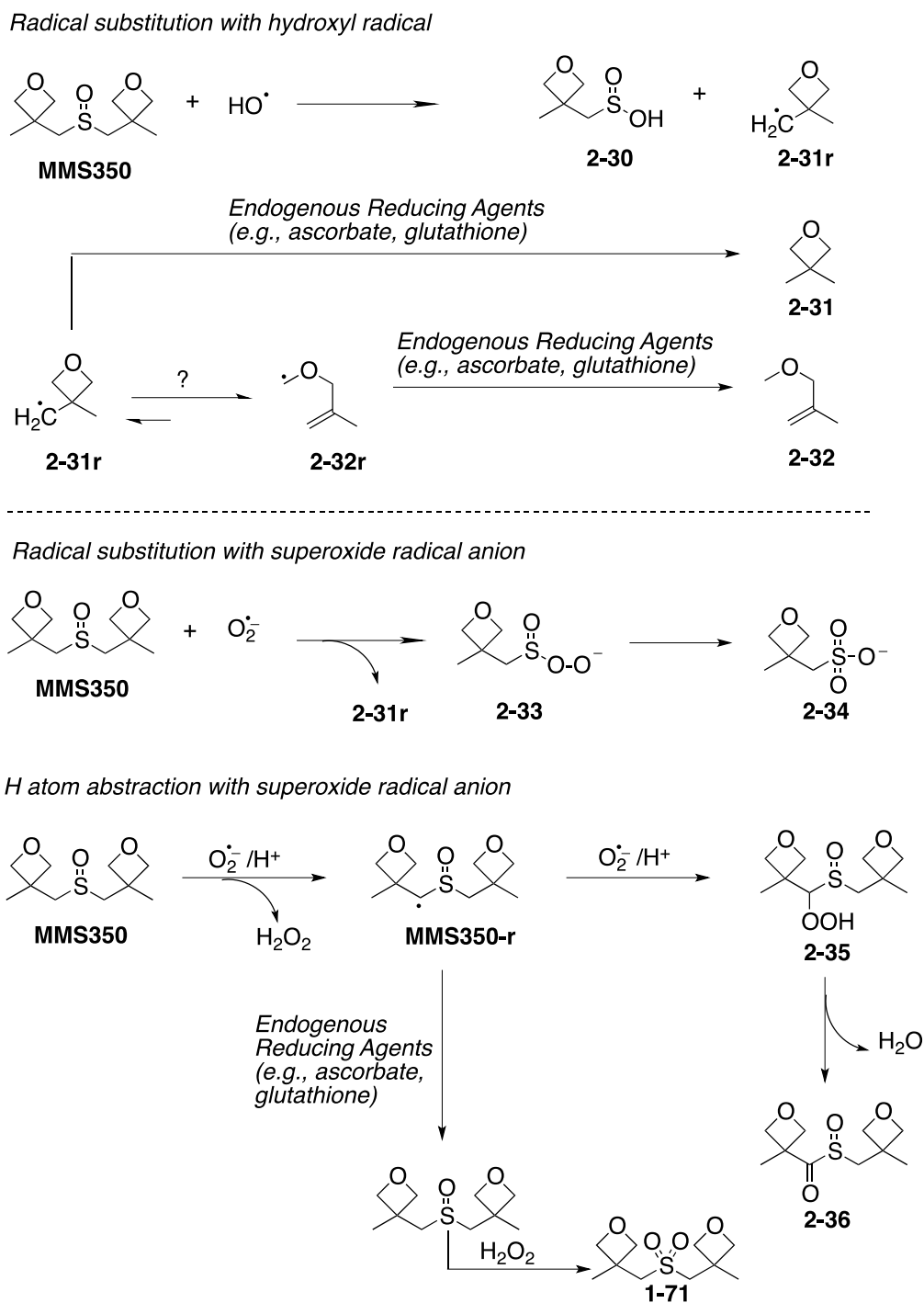
Currently, it is hypothesized that MMS350 is a nonspecific radiation protector/mitigator that prevents lipid peroxidation in the same manner as DMSO and other sulfoxides—that is, by scavenging ROS, particularly hydroxyl radicals. The favorable effects of MMS350 may result from enhanced membrane permeability (relative to DMSO). Current efforts are focused on understanding the mechanism of action of MMS350 as well as in the design and study of bis-azetidiny sulfoxide analogs.

Possible mechanisms for the scavenging effects of MMS350 under physiological conditions are shown in Scheme 2-15. Reaction of MMS350 with hydroxyl radical (analogous to the reaction with DMSO shown in Scheme 2-4) would generate the corresponding sulfinic acid **2-30** and a radical **2-31r**. It is feasible that radical **2-31r** may rearrange to form the corresponding captodatively stabilized methyl ether radical **2-32r**; both **2-31r** and **2-32r** may be quenched with endogenous reducing agents (e.g., ascorbate or glutathione) to generate 3,3-dimethyloxetane **2-31** or 3-methoxy-2-methylprop-1-ene **2-32**. Radical substitution with superoxide radical anion may also occur, resulting in radical **2-31r** (and consequently the proposed **2-32r**) and sulfonoperoxide **2-33**. Sulfonoperoxide **2-33** may undergo an internal oxidation and rearrange to generate sulfonate **2-34**.

Alternatively, reaction of MMS350 with superoxide radical anion may occur via an hydrogen atom abstraction pathway, generating alpha-sulfoxy radical **MMS350-r** and H₂O₂. Reduction with endogenous reducing agents would regenerate MMS350, which can react again with hydroxyl radical or superoxide radical anion. MMS350 may also react with the hydrogen peroxide generated to produce sulfone **1-71**. Lastly, the alpha-sulfoxy radical **MMS350-r** may react with a second molecule of superoxide radical anion, generating peroxide **2-35** which can rearrange to form **2-36** and water.

It would be useful to perform studies to a) ascertain if radical species such as those proposed in Scheme 2-15 are generated by reaction of MMS350 with ROS and b) determine the identity of the radical species formed. Performing analogous assays to those described in Scheme 2-5 wherein MMS350 is substituted for DMSO may be a useful method for determining the nature of the species formed in the reaction of MMS350 and hydroxyl radicals. Trapping studies with stabilized nitroxides (e.g., **2-4**, Scheme 2-5) and analysis by mass spectroscopy would facilitate identification of the radical species formed.

Scheme 2-15. Proposed mechanisms for scavenging of ROS by MMS350.



3.0 NITROXIDE FUNCTIONALIZATION OF SILICA NANOPARTICLES USING AN OXAZOLINE LINKER

This section focuses on the design of covalently modified silica nanoparticles for the pH-mediated release of nitroxides. In Chapter 2, the use of hemigracidin S conjugates was discussed, namely the use of XJB-5-131 and JP4-039 in the mitochondria-targeted delivery of nitroxides to the mitochondria. Herein, an alternative and perhaps complementary approach that relies on environmental stimuli (i.e., pH) for controlled release of nitroxides is described.

A pH-responsive release mechanism is of interest for two reasons. Nanomaterials typically cross the cell membrane by phagocytosis or receptor-mediated endocytosis. At this point, the nanomaterials undergo a number of biological processes involving vesicular coating, endosome development, and lysosome degradation. Each stage is accompanied by changes in pH, providing an opportunity for pH-stimulated release of therapeutics.¹⁸⁴

Additionally, a pH-responsive nanoparticle may have specific benefits for delivering ROS scavengers. Often, sites of acute trauma are associated with oxidative stress (i.e., ROS overproduction) and a drop in pH.¹⁸⁵ This change in pH can be used as a way to ensure targeted delivery of the nitroxide ROS scavengers to sites where oxidative injury is occurring.

In this chapter, the design strategy for pH-responsive silica nanoparticles is discussed. Properties and advantages of using silica are detailed, followed by an overview of current methods for achieving pH-mediated release of small molecules from nanoparticles. The oxazoline is then introduced as a potential linker for achieving controlled release at acidic pH.

3.1 INTRODUCTION

3.1.1 Nanoparticles in Drug Delivery

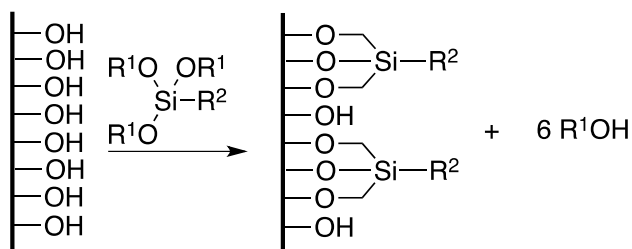
The use of nanoscale materials—materials ranging in size from 1–100 nm—has become an effective strategy for selective drug delivery. Classes of nanoparticles include inorganic (e.g., gold nanoparticles), polymeric nanoparticles, liposomal nanoparticles and nanoparticles based on organic superstructures (e.g., dendrimers).¹⁸⁶ Using nanomaterials for targeted drug delivery has several advantages. The small size of nanoparticles makes cellular uptake via pinocytosis possible, thus providing a means for cellular uptake and subsequent payload release. Moreover, use of nanoparticles allows one to modify the pharmacokinetic properties of a chemical agent without chemically modifying the small molecule adjuvant itself. Because the relative size of the nanoparticles is much larger than the small molecule drugs, the physicochemical properties of the nanoparticle become dominant *in vivo* and thus provide a protective mechanism toward processes that would lead to loss of active material via diffusion, intracellular trafficking, or other mechanisms of degradation. Additionally, nanoparticles can be modified to incorporate functional molecules for diagnostic purposes¹⁸⁷ (e.g., fluorescent labels) or to contain specific targeting sequences.¹⁸⁸ The large surface area of nanoparticles makes it feasible to design a system that will allow for targeted delivery of high doses of active molecules.¹⁸⁶ The use of nanoparticles for drug delivery is a constantly expanding and evolving field. Herein, the focus will be on the controlled release of small molecules from silica nanoparticles.

3.1.1.1 Silica Nanoparticles for Drug Delivery

Among types of nanoparticles, silica nanoparticles are one of the more well-characterized. Silica nanoparticles can be predictably and controllably synthesized to have specific sizes and morphologies using the sol-gel process¹⁸⁹—a method first developed by Stöber in the late 1960's.¹⁹⁰ A typical sol gel synthesis of nanoparticles involves the reaction of tetraethoxysilane (TEOS) with an ammonium catalyst; the size and dispersity of the resulting nanoparticles are controlled by the reagent concentrations, temperature, and degree of aging.¹⁸⁹

Silica nanoparticles are easily modified at the surface by condensation reactions with trialkoxysilanes (Scheme 3-1).

Scheme 3-1. Typical modification of a silica surface by condensation with trialkoxysilanes.



Commonly used silica structures include solid-sphere silica nanoparticles and mesoporous silica nanoparticles (Figure 3-1). Mesoporous silica nanoparticles (MSNs) have porous structures lined with empty channels that can be used to encapsulate small molecules, and organic functionalization of the channels can modify the physical properties of the MSNs. Typically used MSNs include SBA-15 particles (having pore sizes of 6 nm in diameter) and MCM-41 (having pore sizes of 3 nm in diameter).¹⁹¹

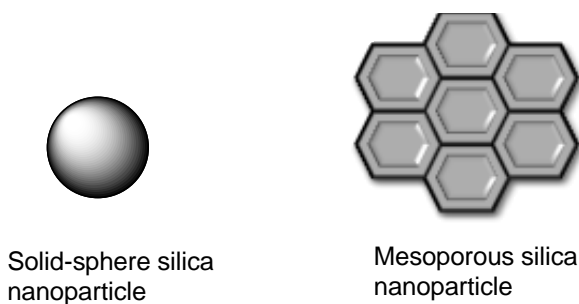


Figure 3-1. Main types of silica nanoparticles.

3.1.1.2 Biocompatibility of Silica Nanoparticles

Biocompatibility is an essential feature for nanoparticle-based therapeutics. The toxicity and inherent biocompatibility of silica nanoparticles depends on size (and corresponding surface area) as well as the degree of surface functionalization—the primary source of silica nanoparticle toxicity is non-functionalized silanol groups on the nanoparticle surface.¹⁸⁴ The effect of silica nanoparticles is also strongly dependent on cell type and method of administration.

Hoet and coworkers investigated the toxicity of mono-dispersed solid-sphere silica nanoparticles on endothelial cells.¹⁹² Smaller nanoparticles generally exhibited higher toxicity. For example, the viability of endothelial cells (EAHY926 cells) exposed to 100 $\mu\text{g/mL}$ concentrations of nanoscale silica particles (14–16 nm) decreased to between 10–23% whereas larger particles (104 and 335 nm) only reduced cell viability to below 50% when high concentrations ($> 1500 \mu\text{g/mL}$) were used.¹⁹² This study of endothelial cells is of particular relevance to biodistribution of nanoparticles if the route of exposure is via injection—nanoparticle entry into circulation would expose nanoparticles to endothelial cells.

Studies comparing the toxicity of solid-sphere silica nanoparticles to mesoporous nanoparticles have been conducted. Generally, mesoporous nanoparticles exhibit lower cellular toxicity, likely due to “caging” of exposed silanol groups within the pores of the “honeycomb” framework of mesoporous particles. Moreover, Tao et al. found that functionalizing the surface of mesoporous silica nanoparticles with amino groups reduced the cellular toxicity toward Jurkat (human T-cell lymphoma) cells; however, various solid-sphere silica nanoparticles exhibited similar toxicities regardless of the extent of surface amination.¹⁹³

Lin and Haynes studied the effect of solid-sphere silica nanoparticles and mesoporous silica nanoparticles on red blood cells (RBCs).¹⁹⁴ As in the case of the endothelial cells, smaller particles (24 nm and 37 nm) showed 50% cell lysis at low concentrations (8.8 $\mu\text{g/mL}$ and 18 $\mu\text{g/mL}$, respectively; 5.5×10^{11} and 3.1×10^{11} nanoparticles/mL, respectively). Larger particles (142 nm and 263 nm) had reduced hemolytic activity (TC_{50} values of 94 and 307 $\mu\text{g/mL}$, respectively, correlating to 2.8×10^{11} and 1.5×10^{10} nanoparticles/mL, respectively). As in the

case of the Jurkat cells, mesoporous silica nanoparticles that were similar in size to the solid-sphere particles had significantly reduced hemolytic activity.

The toxicity of silica nanoparticles is also highly dependent on the cell type studied. For example, Chang et al. showed that normal human fibroblasts, which have a long doubling time, were more susceptible to silica nanoparticle toxicity than tumor cell lines, which have shorter doubling times.¹⁹⁵ Additionally, the toxicity of silica nanoparticles depends strongly on surface modifications. Singh and coworkers developed a bioresponsive mesoporous silica nanoparticle coated with a (PEG)-based polymer shell. The polymer not only attenuated the toxicity of the particles but also served as a stimuli-responsive “shell” that was degraded upon interaction with proteases at tumor sites, thus allowing for a targeted release of therapeutics.¹⁹⁶

Despite the reported cellular toxicity of solid-sphere silica nanoparticles, biocompatibility has been demonstrated. For example, fluorescein isothiocyanate (FITC)-labeled silica nanoparticles of both 30 nm and 100 nm diameters were taken up by endothelial cells, specifically the human umbilical vein endothelial cells (HUVEC) cell line. Cell viability was higher than 91% even at concentrations of 1 mg/mL of nanoparticles.¹⁹⁷ Barandeh et al. also demonstrated that rhodamine functionalized solid-core silica nanoparticles averaging 20 nm in size were incorporated into neuronal tissues of both larval and adult *Drosophila melanogaster*; no deleterious effects on neuronal signaling pathways or premature cell death was observed.¹⁹⁸ Hu et al. report that the toxicity of silica nanoparticles to liver (HepG2) cells is low; as part of the same study, they also demonstrated that FITC-doped silica nanoparticles did not adversely effect the cell cycle in HepG2 cells.¹⁹⁹

The work described above represents only a small fraction of studies evaluating the biocompatibility of silica nanoparticles;¹⁸⁴ it is apparent that the toxicity of silica nanoparticles is dependent on size, surface functionalization, and the cell type being affected. The collective literature data may be used as a predictive tool for designing biocompatible silica nanoparticles, but it is still necessary to evaluate the toxicity of particular nanoparticles on a case-by-case basis.

3.1.1.3 Biodistribution of Silica Nanoparticles

The fate of silica nanoparticles *in vivo* is still an area of active research. The biodistribution of three types of 45-nm RuBPY dye-doped silica nanoparticles (non-functionalized, carboxy-functionalized, and PEG-modified) was studied.²⁰⁰ The particles were administered to mice via iv tail vein injection, and the particles with free hydroxy groups and carboxy groups were cleared from the circulation ($t_{1/2}$ 80 ± 30 min and $t_{1/2}$ 35 ± 10 min, respectively) within 3 h of injection, accumulating mostly in the liver, urinary bladder, and kidney. In contrast, the PEG-terminated particles had longer circulation times ($t_{1/2}$ 180 ± 40 min). The accumulation of particles in organs involved in urine excretion indicates that silica particles may be partially cleared via renal pathways *in vivo*. The authors did detect *intact* nanoparticles in the mouse urine. The phenomenon of accumulation in renal organs and partial excretion in the urine has been corroborated by studies of the biodistribution of mesoporous silica nanoparticles.²⁰¹⁻²⁰³ It should be noted, however, that preferential accumulation in *tumor* cells has also been observed.²⁰³

3.1.1.4 Endocytosis of Silica Nanoparticles

The uptake of nanoparticles into cells can be achieved either by general phagocytosis or receptor-mediated endocytosis (Figure 3-2). In either case, it is generally thought that the inner cellular membrane engulfs the particle, forming an early endosome. From here, fusion with lysosomes containing hydrolytic enzymes will aid in the degradation of particles. Alternatively, particles that are not degraded may undergo exocytosis.^{184,186} Detailed studies performed by Hu and coworkers showed that FITC-doped silica nanoparticles (ranging in size from 60 nm to 600 nm) undergo a clathrin-mediated endocytosis. The hypothesis was supported by the observation that treating cell media with sucrose and amantadine-HCl decreased cellular uptake.¹⁹⁹ It is also documented that the extent of cellular uptake amount is dependent on particle size. In the case of nanoscale particles, surface functionalization and subsequent charge distribution can influence the mechanism of cellular uptake.¹⁸⁴

The overall fate of nanoscale materials after cellular uptake is still an area of ongoing research. In the study by Hu et al.¹⁹⁹ cellular fluorescence decreased over time, indicating

exocytosis did occur. The rate and extent of particle exocytosis is also postulated to be a size-dependent phenomenon, wherein larger particles are less likely to be removed from the cells.¹⁹⁹ The intracellular trafficking of discoidal silicon particles was studied by Serda et al.²⁰⁴ They showed that both 10- and 30-nm chitosan-coated silica particles crossed the endosomal membrane.

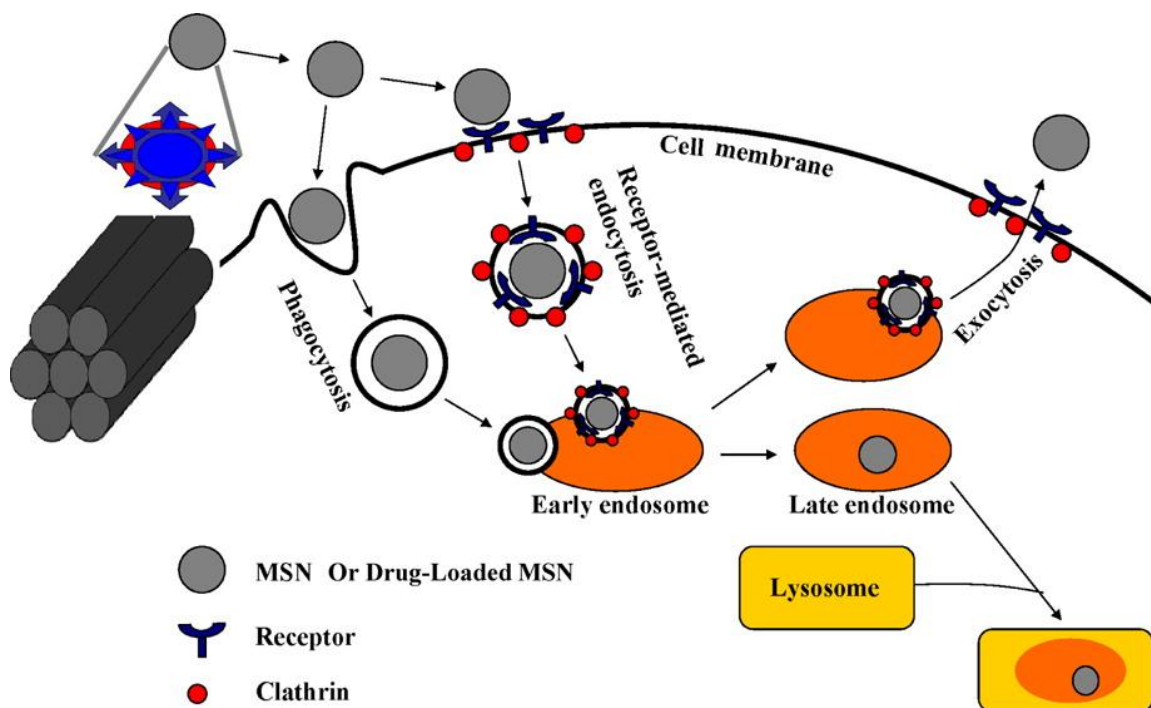


Figure 3-2. General endocytotic pathways for nanoparticles (in this case, MSNs) in mammalian cells.

Reprinted with permission from Asefa, T.; Tao, Z. Biocompatibility of Mesoporous Silica Nanoparticles. *Chem. Res. Toxicol.* **2012**, *25*, 2265-2284. Copyright 2012 American Chemical Society.

3.1.1.5 Use of Nanoparticles to Deliver Antioxidants

The use of nanoparticles to scavenge ROS or RNS is an active area of research.²⁰⁵ Several types of inorganic nanoparticles inherently act as antioxidants, even without surface modification. For example, some ceria and yttria nanoparticles mimic the activity of superoxide dismutase (SOD) and catalase (CAT).^{206,207} These effects are dose-dependent; in fact, some particles that scavenge ROS are also shown to generate ROS.

Conjugation of antioxidants such as Vitamin E to gold nanoparticles has been accomplished by self-assembly of thiol ligands derived from Trolox **3-2**, an analog of α -tocopherol **3-1** (i.e., vitamin E) on gold nanoparticles (Figure 3-3).²⁰⁸ Radical scavenging abilities of the nanoparticle-bound Trolox (**3-3**) were greater than those for Trolox itself. Additionally, nanoparticle encapsulation is often used to improve the pharmacokinetic properties of poorly soluble antioxidants. A curcumin nanoparticle system generated by coprecipitation of curcumin **3-4** and polyvinylpyrrolidone exhibited enhanced antioxidant properties in comparison to curcumin itself.²⁰⁹ A similar strategy was used to improve the pharmacokinetic properties of poorly soluble quercetin **3-5**—encapsulation in poly-D,L-lactide (PLA) nanoparticles improved the physicochemical properties of this compound; however, no difference in antioxidant activity was observed for the PLA-bound quercetin versus nonencapsulated quercetin.²¹⁰

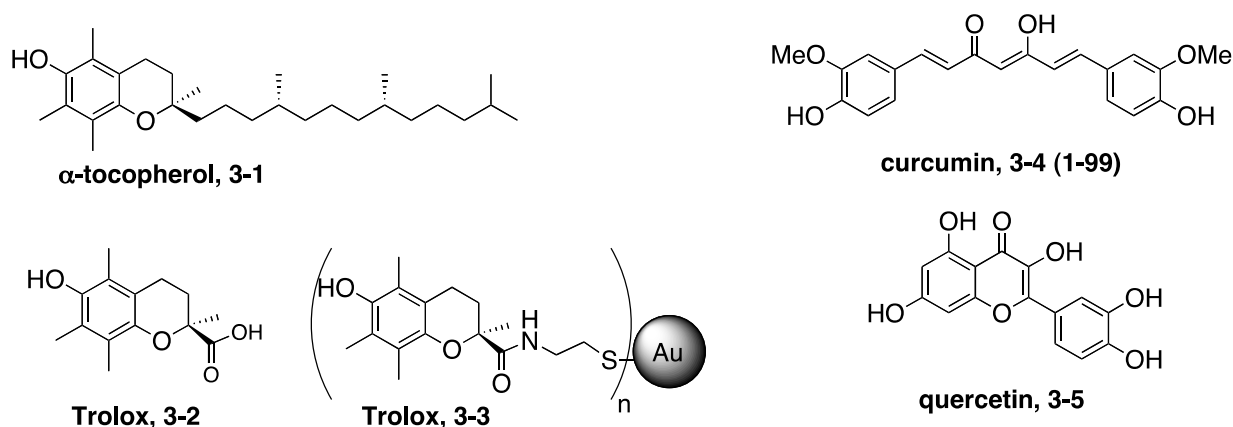


Figure 3-3. Example antioxidant molecules delivered using nanoparticle systems.

3.1.2 Stimuli-Responsive Nanoparticles and Strategies for pH-Mediated Release

The antioxidant 4-hydroxy-TEMPO (TEMPOL) and other small molecule nitroxides are rarely used therapeutically due to their short blood circulation times and rapid, nonspecific bioaccumulation.¹⁸⁵ Incorporation of TEMPO into a nanoparticle would improve the pharmacokinetic properties. Because TEMPO is also a spin label, TEMPO-functionalized nanoparticles may have additional utility for *in vivo* diagnostics. In this next section, strategies for controlled release of therapeutics are discussed, emphasizing pH-mediated release. Specific examples related to TEMPO-functionalized nanoparticles are highlighted.

3.1.2.1 General Strategies for pH-Mediated Release

Strategies for stimuli-responsive release *in vivo* include chemical or physical changes in response to variations in temperature, redox state, or enzymatic reactions. Alternatively, external “triggers” such as photo-irradiation or magnetic force can be used.¹⁹¹

Designing nanoparticles for pH-mediated release of therapeutics is an attractive medicinal strategy. Health aberrations including ischemia, infection, and inflammation are often accompanied by low pH conditions; moreover, oxidative stress injuries related to stroke, myocardial infarction, and acute kidney failure often result in lowering of physiological pH around the site of injury.^{185,211} In these cases, release of therapeutics, particularly antioxidant therapeutics, in response to a low pH environment would lead to tumor or injury-specific targeting.

In terms of *intracellular* targeting, a pH specific release of an organelle-specific therapeutic may be a viable strategy. Often, endosomal capture and disintegration of nanoparticles is a major problem to be overcome when designing nanoparticles for cellular uptake. Yet, one can take advantage of the differential pH in the endosomes and design covalent linkers or self-assembling polymers that specifically degrade under the low pH conditions, thus releasing chemical therapeutics into the cytosol.

3.1.2.2 pH Responsive Polymers

Selective protonation of polymeric materials under acidic conditions is a strategy for stimuli-responsive drug release. For example, Qiu et al. showed that amphiphilic polyphosphazenes containing diisopropylamino (DPA) side chains disrupted endosomal membranes when protonated at pH 6.60–6.82.²¹² The polymers also attenuated P-gp efflux activity, making this drug delivery system particularly attractive for delivery of therapeutics to tumor cells that overexpress P-gp. In a related example, polyplexes from poly(aspartamide) with 1,2-diaminoethane side chains were shown to induce pH-dependent endosomal membrane destabilization (Figure 3-4).²¹³

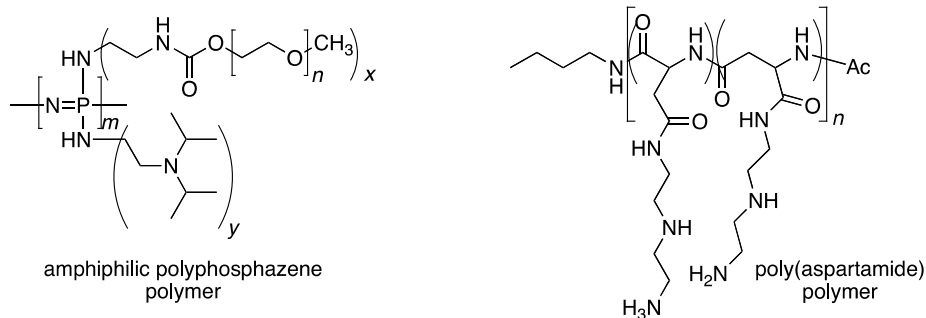


Figure 3-4. Examples of polymers used for construction of pH-responsive nanoparticles.

Another strategy involves coating mesoporous silica nanoparticles with organic micelles that are disrupted at acidic pH. He and coworkers used this approach for selective release of drugs to tumor cells that had an intrinsically lower pH than normal cells.²¹⁴ Other examples of using pH-responsive polymeric nanoparticles include a partially carboxymethylized pullulan nanoparticle, which showed faster release of doxorubicin at pH 5.0 than at pH 7.4 (*in vitro*).²¹⁵ Finally, Sung et al. developed a pH-responsive nanoparticle composed of chitosan and poly(γ -glutamic acid) for release of insulin.²¹⁶ They found that the particles adhere to the mucus layer of the small intestine, where the nanoparticles are then degraded and insulin is released. They hope their research will eventually lead to an orally deliverable form of insulin.

Ke and coworkers developed “smart” poly(D,L-lactic-*co*-glycolic acid) (PLGA) biodegradable hollow microspheres that were incorporated with NaHCO_3 .²¹⁷ When the microspheres enter an acidic environment (e.g., early or late endosomes/lysosomes of pH 6.0 or 5.0, respectively), the NaHCO_3 reacts with acid, which generates CO_2 and disrupts the polymer “shell,” releasing the therapeutic agent.

3.1.2.3 pH-Mediated Release via Cleavage of Covalent Bonds

One example of controlling drug release via pH modification involves covalent cleavage of a boronate ester. Gan et al. “capped” the pores of mesoporous silica nanoparticles by covalent linkage of a boronic acid, which was attached to an iron oxide nanoparticle (Figure 3-5).²¹⁸ Under acidic conditions, the boronate ester bond is cleaved, “uncapping” the pores and allowing for release of the drug (in this case, dexamethasone).²¹⁸ Use of a boronate ester as an acid-cleavable linker was also used to “cap” mesoporous silica nanoparticles with boronic acid-functionalized gold nanoparticles.²¹⁹

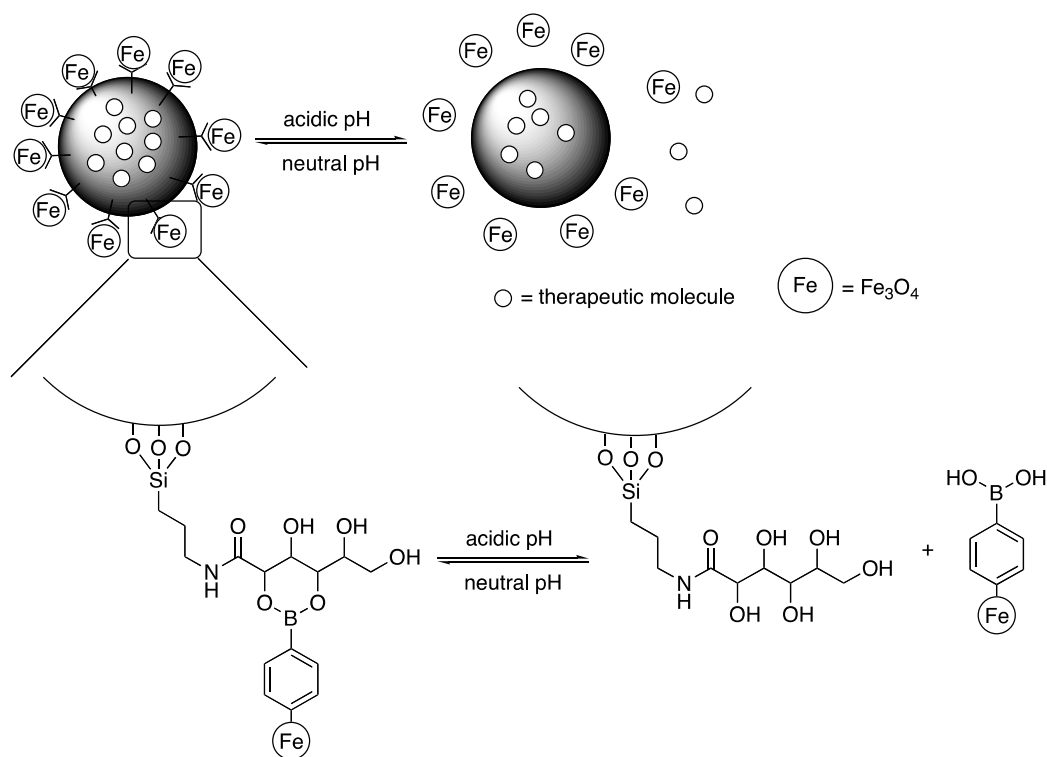


Figure 3-5. pH-Responsive cleavage of boronate esters for release of therapeutics.

3.1.2.4 pH Responsive Nanoparticles for Delivery of Nitroxides

Yoshitomi and coworkers have developed a pH-responsive nanoparticle for delivery of 4-amino-TEMPO.^{185,211,220} They covalently attached TEMPO to the hydrophobic segment of an amphiphilic block copolymer (Figure 3-6). The polymers self-assemble to generate biocompatible nanoparticles (~50 nm in diameter) that show longer blood circulation times (*ca.* 2 h) than free TEMPOL ($t_{1/2}$ *ca.* 15 s) and related derivatives. They hypothesized that protonation of the amine of 4-amino TEMPO at low pH (6.0) results in disintegration of the polymer structure, exposing the nitroxide to the environment and allowing for detection by EPR spectroscopy.¹⁸⁵ Therefore, they postulated that these nanomaterials could be used to probe for low pH conditions (e.g., ischemia) *in vivo*. These functionalized particles could also be used therapeutically to target areas where a decrease in pH is associated with oxidative stress. For example, Yoshitomi and coworkers confirmed that these nanoparticles disintegrated in ischemic brain areas after cerebral ischemia-reperfusion.²²⁰ They also demonstrated the utility of these particles in a renal ischemia-reperfusion acute kidney injury model in mice.²¹¹

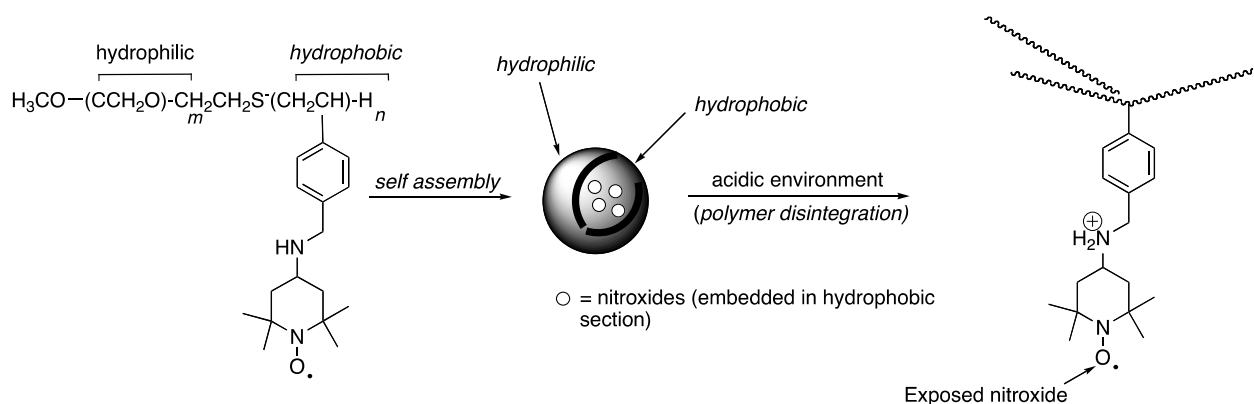


Figure 3-6. pH-Responsive polymeric nanoparticles for selective delivery of nitroxides.

3.1.3 Oxazolines as pH-Controllable Linkers

Oxazolines (4,5-dihydrooxazoles) are planar structures and are weakly basic. Oxazolines are hydrolyzed in acidic, aqueous solutions to afford β -amino alcohols and carboxylic acids (Figure 3-7).¹⁷⁴

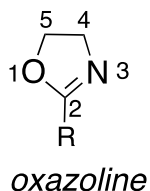


Figure 3-7. General structure of an oxazoline.

Oxazolines are present in several marine natural products including westiellamide^{126,133} and the dimeric versions of westiellamide with improved silver-complexing affinities (Figure 3-8).²²¹ Moreover, oxazolines can serve as precursors to the related thiazolines using thiolysis protocols. For example, Wipf and Venkatraman performed an oxazoline-to-thiazoline transformation in the synthesis of (-)-Thiangazole,²²² and Wipf and Uto applied an oxazoline-to-thiazoline conversion for the synthesis of the marine metabolite Trunkamide A.²²³ The metal-chelating capabilities of oxazolines have also been widely exploited in the context of using dimeric oxazoline ligands (e.g., PyBOX, tBuBOX and PHBOX) for transition metal-mediated reactions.^{224,225}

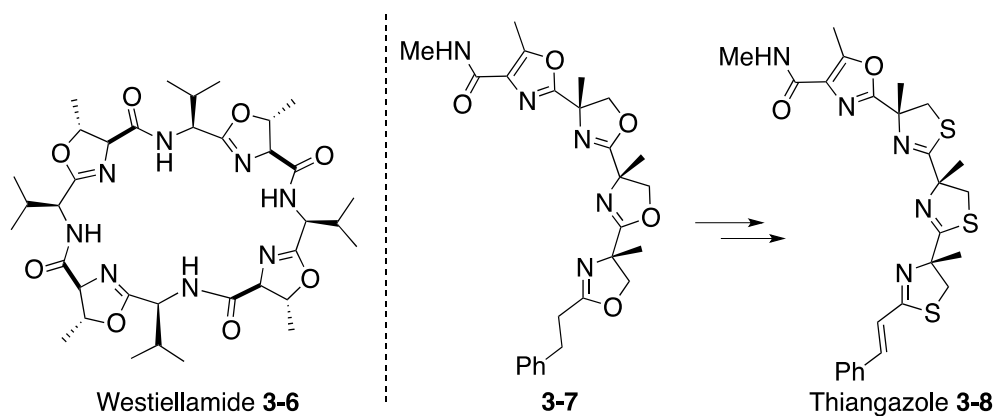


Figure 3-8. Natural products containing oxazolines or prepared by reactions of oxazolines.

3.1.3.1 Oxazolines in Medicinal Chemistry and Use as Prodrugs

Oxazolines can be cleaved under acidic conditions to afford carboxylic acids; therefore, they are often used as masking groups for acids. Despite the predicted metabolic instability of oxazolines in acidic environments, oxazolines are still incorporated into medicinal chemistry discovery initiatives. For example, Mycobactin S (**3-9**) (Figure 3-9) a natural iron chelator, was used as the basis for designing anti-tuberculosis agents derived from both oxazoline and oxazole benzyl esters.²²⁶ Oxazolines had inferior activity than the corresponding oxazoles for inhibition of *M. tuberculosis* H₃₇RV in a fluorometric anti-tuberculosis assay.

Another way to take advantage of oxazoline hydrolysis is to use these heterocycles as pro-drugs and acid-cleavable linkers. Heterocycles related to oxazolines, namely oxazolidinines²²⁷ and oxazolidinones²²⁸ (e.g., **3-10** and **3-11**, Figure 3-9) have been evaluated for use as pro-drugs. A pH profile for the rate of hydrolysis of oxazolidine **3-10** at 37 °C was obtained; it was discovered that the rate of hydrolysis of oxazolidine **3-10** was highest at pH 5.5. The corresponding 4,5-*trans*-fused oxazolidinine was optimally hydrolyzed at pH 4.0.²²⁷ Oxazolidinones such as **3-11** were also investigated as possible pro-drugs. Compound **3-11** was hydrolyzed at pH 7.4 (0.1 M phosphate buffer); the half-life of compound **3-11** was 4.1 min. The rate of hydrolysis of **3-11** in human plasma (pH 7.4, 37 °C) was about 4-fold faster ($t_{1/2} = 1.0$ min). The trend of enhanced hydrolysis in human plasma versus phosphate buffer was observed among a series of oxazolidinones; the authors concluded that enzymes in the plasma facilitated oxazolidinone hydrolysis.²²⁸

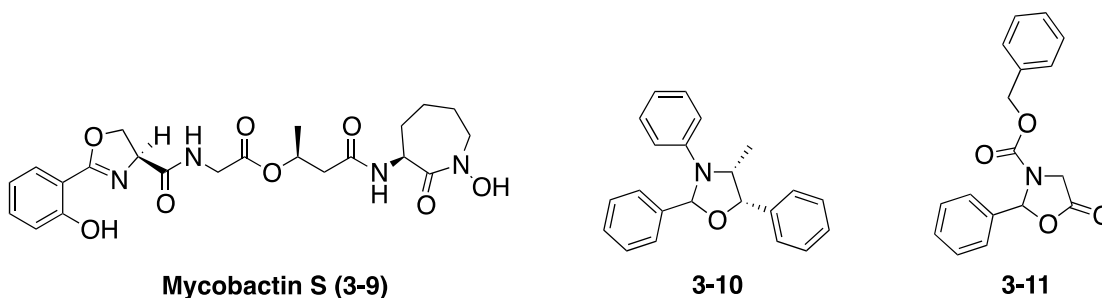
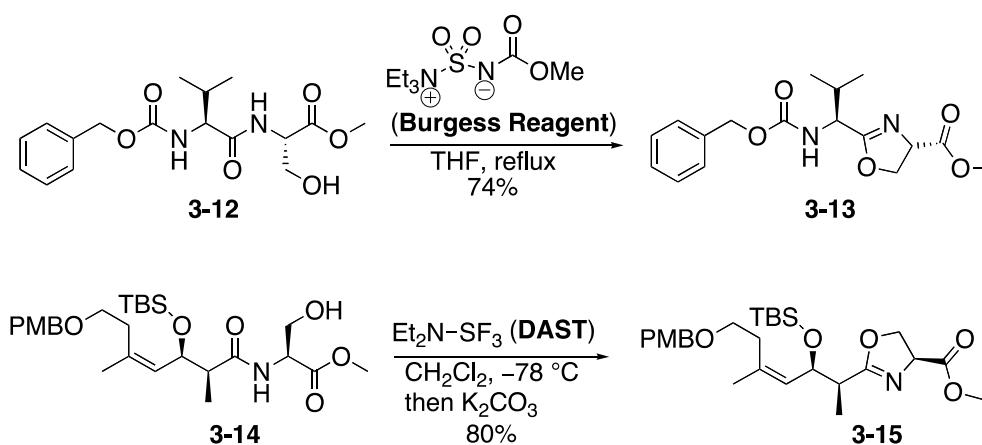


Figure 3-9. Oxazolines, oxazolidines and oxazolidinones studied as potential pro-

3.1.3.2 Methods for Preparation of Oxazolines

Oxazolines can be prepared by reaction of nitriles with amino alcohols.^{229,230} Alternatively, oxazolines are prepared by cyclodehydration of β -hydroxy amides after activation of the alcohol with reagents such as SOCl_2 or TsCl . Methodologies developed in the Wipf group include cyclodehydration reactions using Burgess Reagent^{231,232} or DAST²³³ (Scheme 3-2).

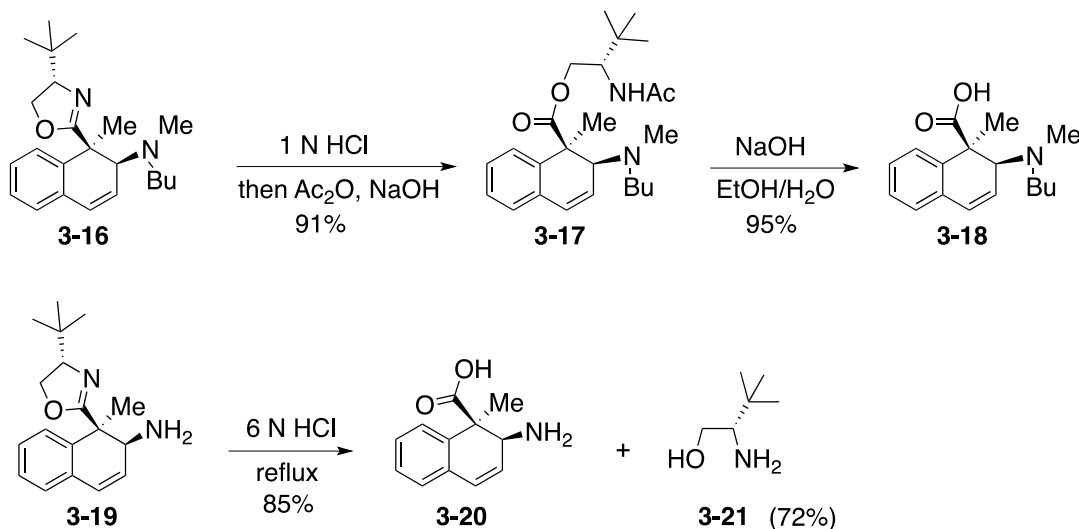
Scheme 3-2. General methods for oxazoline synthesis using cyclodehydration methods.



3.1.3.3 Oxazolines as Acid-Cleavable Protecting Groups and Linkers

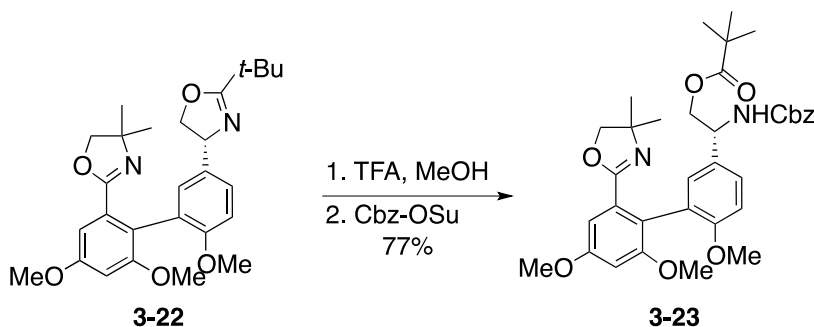
The use of oxazolines as protecting for carboxylic acids is well-precedented. Typical examples illustrating cleavage of oxazolines to carboxylic acids are shown in Scheme 3-3. The oxazoline in **3-16** was hydrolyzed under acidic conditions to the corresponding β -amino ester **3-17**. The resulting ester was then saponified under standard conditions (1 N aqueous NaOH) to afford acid **3-18**. Forcing acidic conditions (e.g., refluxing 6 N aqueous HCl) can be used to generate the carboxylic acid directly—for example, oxazoline **3-19** was converted to acid **3-20** and aminoalcohol **3-21** (Scheme 3-3). The stepwise oxazoline-opening/ester saponification pathway (e.g., conversion of **3-16** to **3-18** via **3-17**) is more commonly used due to a wider substrate and functional group tolerance to the milder conditions.

Scheme 3-3. Acidic cleavage of oxazolines to afford carboxylic acids.



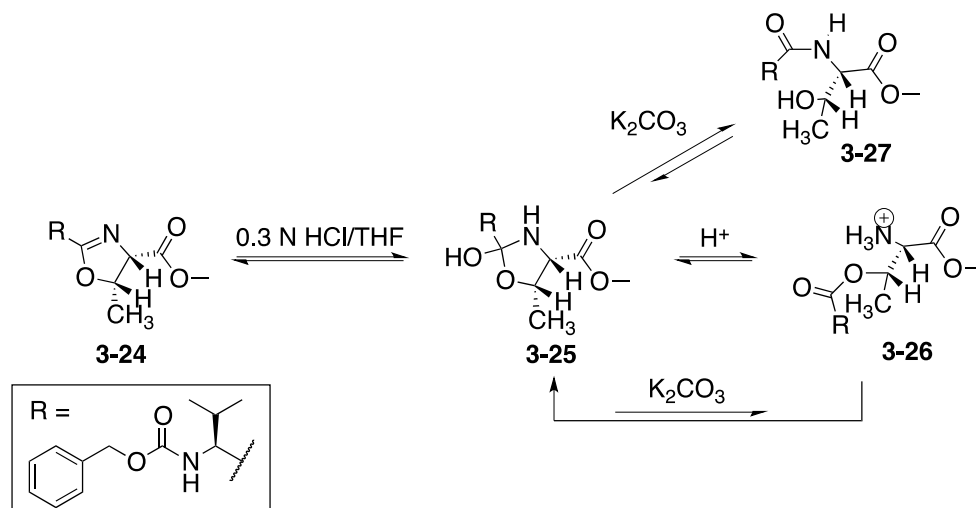
The rate of acid-mediated oxazoline hydrolysis depends on oxazoline substitution, particularly the substitution at the 2-position. Typically, oxazolines with alkyl substituents at the C-2 position are hydrolyzed more quickly than oxazolines with aryl substituents at the C-2 position, and electron density and hydrolytic proclivity are positively correlated. The substitution-dependent hydrolysis of oxazolines was used in the synthesis of actinoidic acid derivatives; the *t*-butyl-substituted oxazoline in **3-22** was preferentially cleaved in the presence of the 3-5-dimethoxy aryl oxazoline in the substrate, affording **3-23**.²³⁴

Scheme 3-4. Selective hydrolysis of a 2-alkyl-substituted oxazoline in the presence of a 2-aryl-substituted oxazoline.



Another example of synthetic utilization of oxazoline hydrolysis was demonstrated by Wipf and Miller; in this case, oxazoline hydrolysis facilitated the interconversion of threonine and *allo*-threonine residues.²³⁵ A general mechanism for the oxazoline hydrolysis is shown in Scheme 3-5. Acid-facilitated addition of water to the oxazoline 2-position of **3-24** generates hydrated intermediate **3-25**. At acidic pH, the intermediate **3-25** opens to the β -amino ester **3-26**. If the pH of the medium is raised by adding base (e.g., K_2CO_3), an $O \rightarrow N$ acyl shift occurs to afford β -amino amides such as **3-27**.

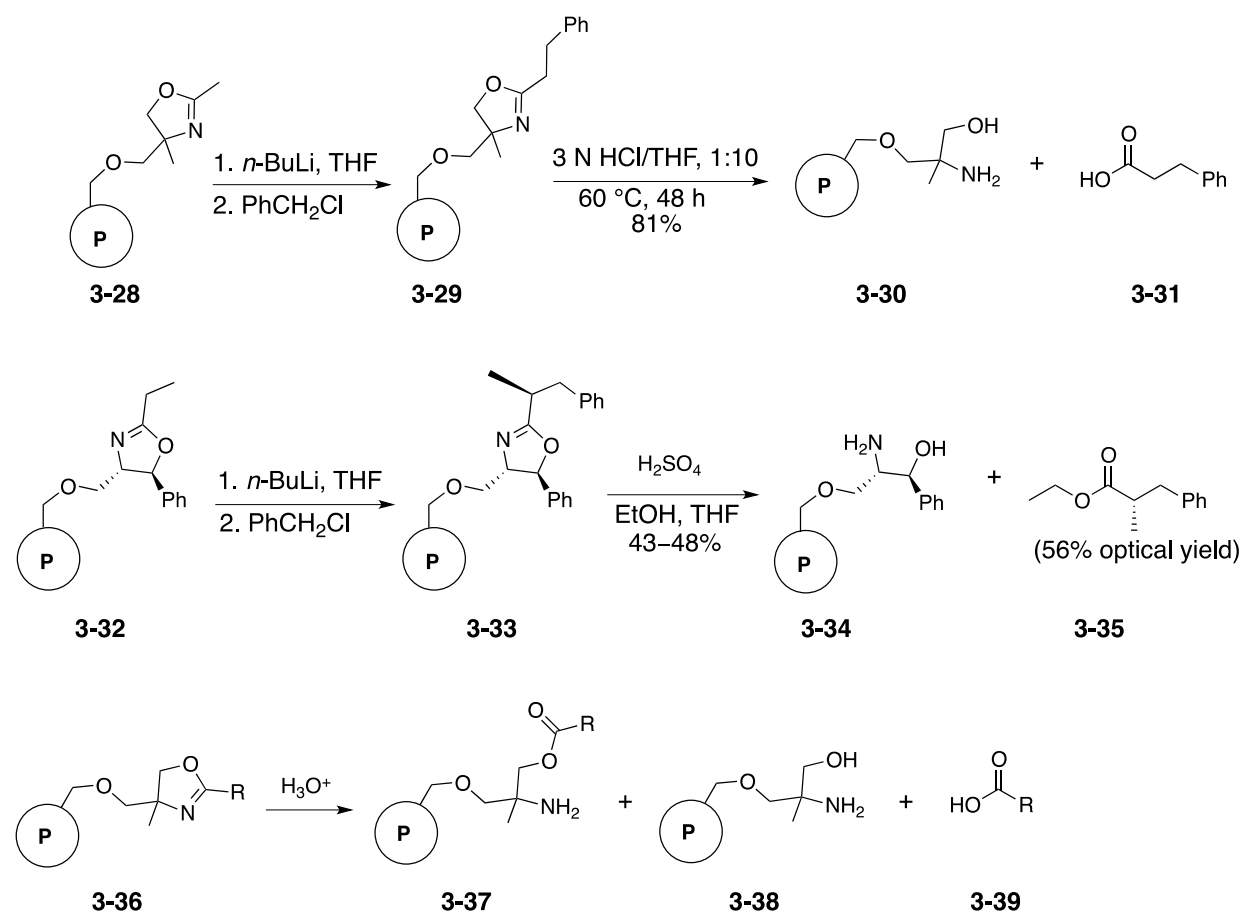
Scheme 3-5. Hydrolysis of oxazolines and subsequent $O \rightarrow N$ acyl shift.



The use of an oxazoline as a linker for solid-phase synthesis of carboxylic acids has been reported.²³⁶ Colwell et al. synthesized polymer-bound oxazolines **3-28** and **3-32** using chloromethylated poly(styrene-*co*-divinylbenzene) (Scheme 3-6). The polymer-bound oxazolines were derivatized by alkylation after deprotonation with *n*-butyllithium. Hydrolysis with either 3 N HCl/THF or H_2SO_4 in EtOH afforded acid **3-31** or ester **3-35** and the corresponding resin-bound amino alcohols **3-30** and **3-34**. The authors found that the resin-bound amino alcohols **3-30** and **3-34** could be recycled to regenerate polystyrene bound oxazolines **3-28** and **3-32**. Moreover, an investigation of the relationship between oxazoline substitution and hydrolytic

proclivity was performed (Scheme 3-6). In general, oxazolines substituted with smaller alkyl chains were hydrolyzed more quickly than those with more sterically hindered alkyl groups, thus indicating that steric encumbrance slows oxazoline hydrolysis.

Scheme 3-6. Oxazolines as polystyrene-supported linkers for synthesis of acids and esters.



Relative Rate of Hydrolysis to 3-38 + 3-39: R = Me \geq Et > PhCH₂CH₂ > PhCH₂C(CH₃)H

Yield 3-37: R = PhCH₂C(CH₃)H > PhCH₂CH₂ > Et \geq Me

Based on the precedents for using oxazolines as acid-cleavable linkers, it was envisioned that an oxazoline could be used for pH-mediated release from a nanoparticle scaffold. These studies are discussed in the next section.

3.2 RESULTS AND DISCUSSION

3.2.1 Nanoparticle Design

The goal of the project is to develop a nanoparticle-based delivery system for reactive oxygen species (ROS) scavengers—namely molecules containing TEMPO. The overall design strategy is depicted in Figure 3-10. Silica nanoparticles were used as the initial nanoparticle system. As discussed in section 3.1.1.1, silica nanoparticles are well-characterized and can be predictably generated to have particular sizes and properties—commercial samples of monodisperse silica nanoparticles averaging 10–15 nm in size were purchased from commercial vendors (Nissan Chemical). More significantly, the ease of surface functionalization by condensation with trialkoxysilanes made it feasible to attach organic molecules in a *covalent* manner.

The silica nanoparticles were elaborated with a spacer, which was further reacted with a molecule containing a hydrolytically labile linker—in this case, an oxazoline. The oxazoline was attached to a payload ROS scavenger—in this case, TEMPO.

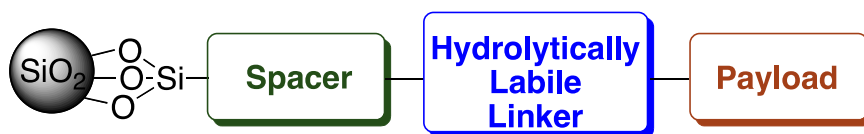
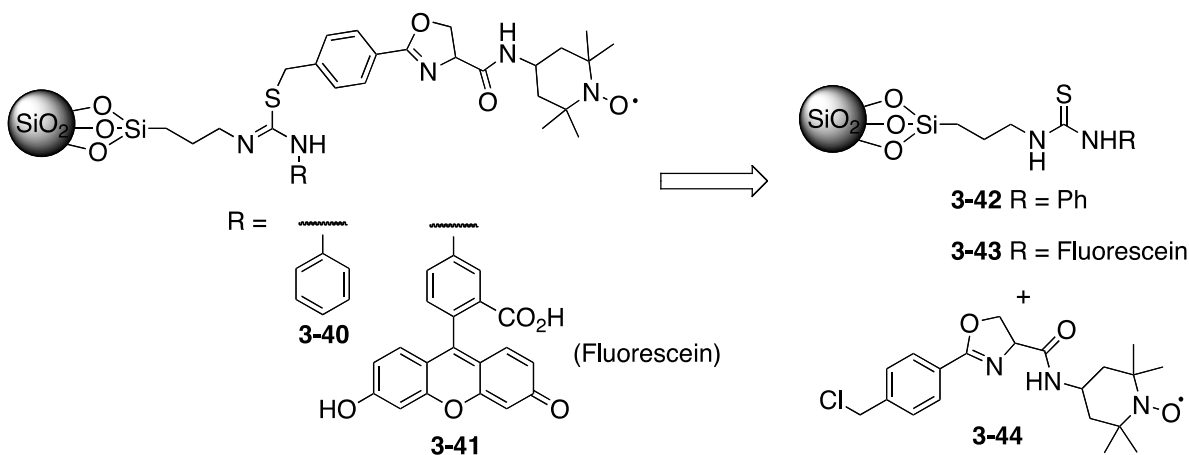


Figure 3-10. General strategy for nanoparticle functionalization.

This strategy was implemented using both phenyl-substituted and fluorescein-substituted imidothiolates **3-40** and **3-41** (Scheme 3-7). The imidothiolates were synthesized by alkylation of the corresponding thioureas **3-42** and **3-43** with benzylic chloride **3-44**. Benzylic chloride **3-44** was chosen as the initial alkylating agent due to ease of synthesis from commercially available materials and the facile incorporation of TEMPO via an amide linkage to the oxazoline. Advantages to this strategy include the convergent nature and the ability to incorporate a

fluorescent or UV-active moiety on the thiourea spacer. In the following sections, the synthesis of alkylating agent **3-44** as well as the methods by which **3-44** was attached to the thiourea-elaborated silica nanoparticles are described.

Scheme 3-7. Thiourea alkylation approach for nanoparticle functionalization.

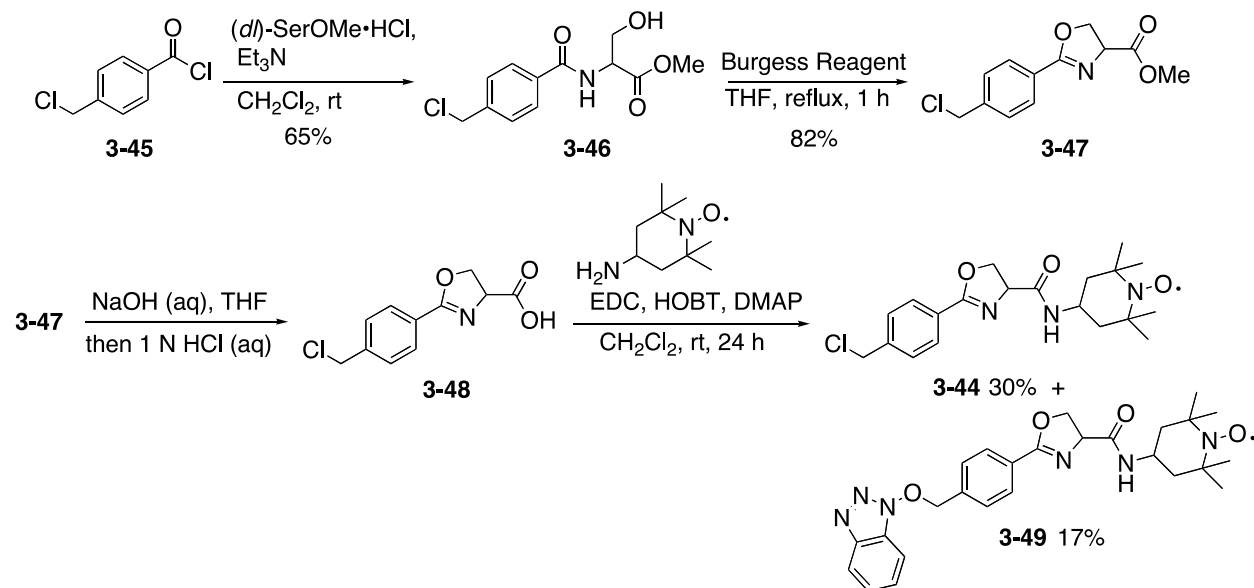


3.2.2 Synthesis of Benzylic Chloride **3-44**

The initial aim was to synthesize the oxazoline-elaborated benzylic chloride via a standard 4-step sequence (Scheme 3-8). Acylation of 4-chloromethylbenzoyl chloride **3-45** with *dl*-serine methyl ester hydrochloride afforded β -hydroxy amide **3-46**. Cyclodehydration using Burgess reagent²³² provided oxazoline methyl ester **3-47** in good yield. Saponification of methyl ester **3-47** to generate the corresponding acid **3-48** was attempted, and the acid would then be coupled with 4-amino TEMPO using a standard procedure (i.e., EDCI, HOBT); however, this protocol resulted in varying yields. One problem was that HOBT displaced the benzylic chloride to generate byproduct **3-49**. The reaction was further complicated by the acid-sensitivity of the

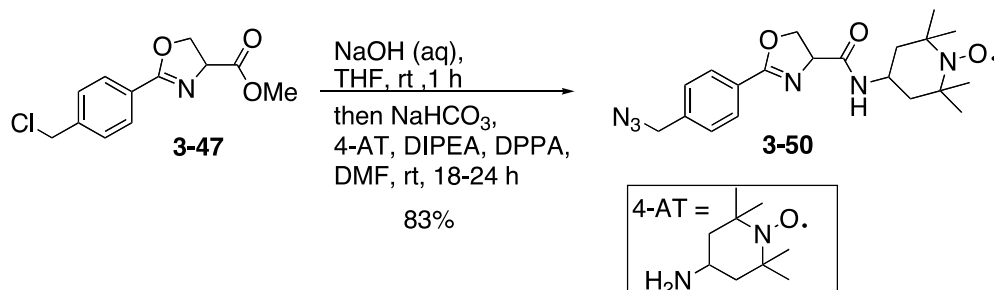
oxazoline moiety—decreasing the pH during acidification often resulted in oxazoline opening and diminished yields.

Scheme 3-8. Synthesis of benzylic chloride **3-44**.



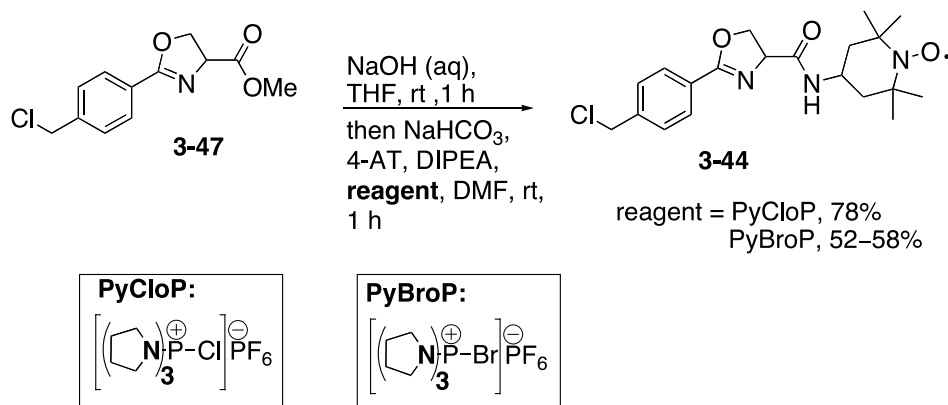
Alternative procedures for amide bond formation were screened. A one-pot saponification-amide bond formation was used to preclude the need for acidification during the conversion of the methyl ester to the acid. Reagents activating the carbonyl via formation of active nucleofuges resulted in displacement of the benzylic chloride—for example, using the Goodman reagent (3-(diethoxyphosphoryloxy)-1,2,3-benzotriazin-4(3*H*)-one, DEPBT) afforded the corresponding benzylic 3-oxy-1,2,3-benzotriazin-4(3*H*)-one. Use of DPPA yielded the corresponding benzyl azide **3-50** in excellent yield—this result proved to be advantageous during the second nanoparticle functionalization approach (section 3.2.5).

Scheme 3-9. Synthesis of TEMPO-coupled benzylic azide **3-50**.



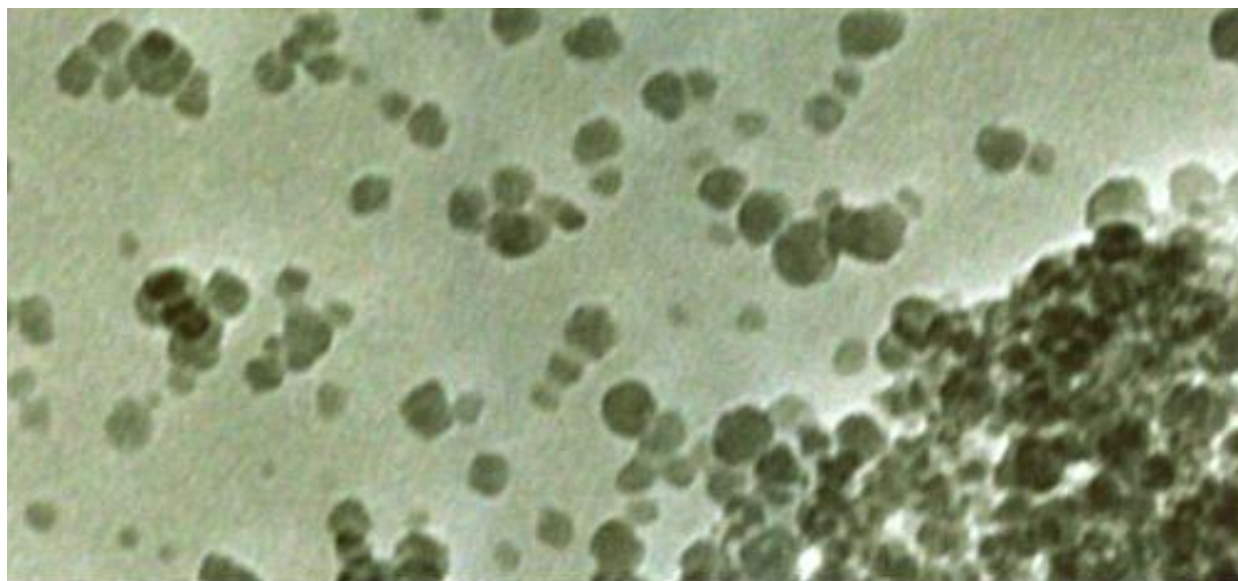
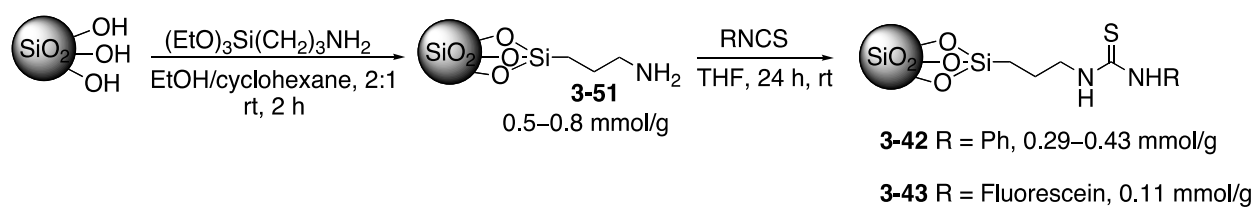
Because the problematic substitution of the benzylic chloride was observed, halotripyrrolidinophosphonium hexafluorophosphates PyBroP and PyCloP were used.²³⁷ In the case of these reagents, the driving force for amide bond formation is expulsion of tripyrrolidinophosphine oxide; it is assumed that the amide bond forms directly from a reaction of an amine (e.g., 4-aminoTEMPO) with the acyloxyphosphonium salt. PyCloP was stable to the buffered conditions (DIPEA and NaHCO_3) and using this reagent reproducibly afforded the desired products in good yields.

Scheme 3-10. Amide bond formation using halotripyrrolidinophosphonium hexafluorophosphates.



To generate the thiourea-functionalized silica nanoparticles, 3-aminopropyl-elaborated silica particles **3-51** were synthesized by stirring a suspension of silica nanoparticles (10–15 nm) with 3-aminopropyltriethoxysilane (Scheme 3-11). A batch of 3-aminopropyl silica nanoparticles **3-51** was analyzed using Transmission-Electron Microscopy (TEM), and the average particle size was 14 ± 4 nm. (Figure 3-11) The loading of the resulting amine was determined to be 0.5–0.8 mmol/g by elemental analysis (N content). The 3-aminopropyl functionalized particles were reacted with either phenyl or fluorescein isothiocyanate to afford the resulting thioureas. Quantitative conversion was not observed, but reasonable loadings of 0.29–0.43 mmol/g were obtained (measured by elemental analysis, S content).

Scheme 3-11. Synthesis of thiourea-functionalized silica nanoparticles.

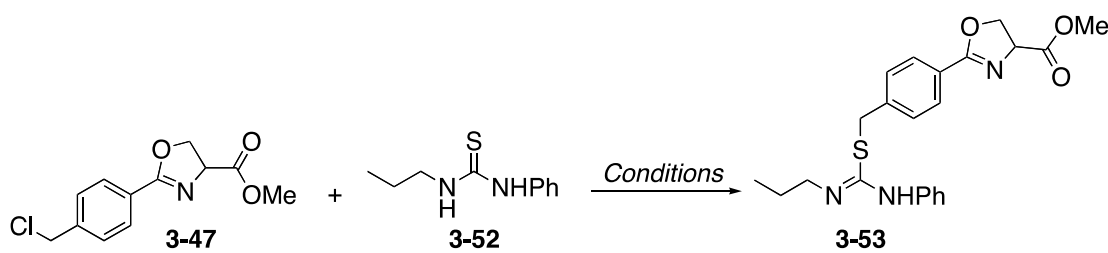


20 nm

Figure 3-11. TEM image of 3-aminopropyl silica nanoparticles.

Because suitable precedents for alkylation of silica-supported thioureas were not documented, solution-phase conditions were screened (Table 3-1). Using DIPEA in 2-MeTHF was an optimal protocol; however, nanoparticles **3-42** and **3-43** did not suspend well in THF (i.e., aggregation was apparent). Therefore DMF was used as the solvent for the alkylation reactions.

Table 3-1. Thiourea alkylation of a model system.



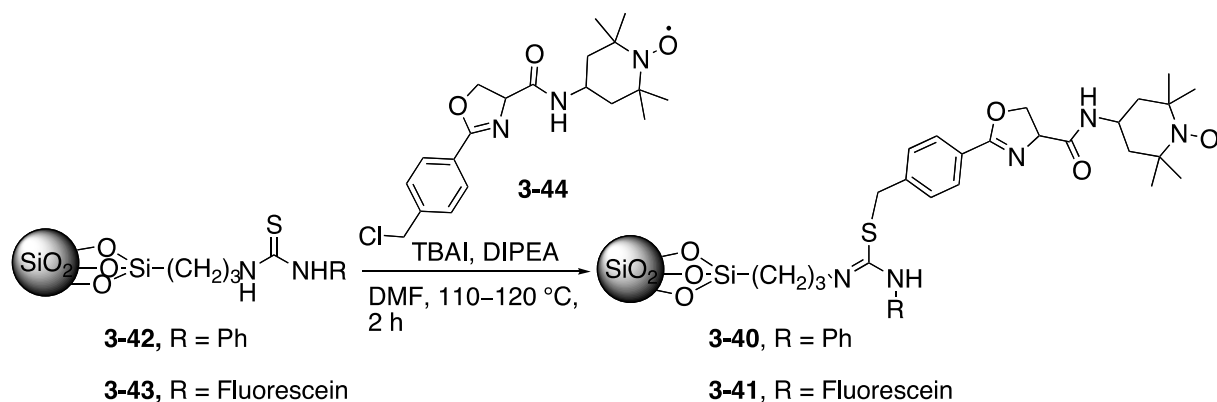
Entry	Conditions	Yield ^a
1	NaHCO ₃ (1.8 equiv), TBAI (20 mol%), DMF, 110 °C, 1 h	58%
2	DIPEA (2 equiv), TBAI (40 mol%), THF, reflux, 2.5 h	58%
3	DIPEA (2 equiv), TBAI (40 mol%), 2-MeTHF, reflux, 2.5 h	75%
4	DIPEA (2 equiv), TBAI (40 mol%), MeCN, reflux, 2.5 h	66%
5	DIPEA (2 equiv), TBAI (40 mol%), DMF, 110 °C, 30 min	65% ^b

^aReported yields were determined by crude ¹H NMR analysis using Ph₃CH as an internal standard. ^bThe reported yield is an isolated yield after purification by chromatography on SiO₂. In a separate trial, the product was isolated in 61% yield.

Once it was established that the thioureas could be alkylated in moderate to good yields, particle-bound thioureas **3-42** and **3-43** were subjected to alkylation conditions in DMF (Scheme 3-12). In general, a large excess of benzylic chloride **3-44** was used in relation to the thiourea particles, and the particles were heated with DIPEA and degassed DMF at 90 °C for 2 h. A major consideration was the detection of adsorbed versus covalently linked material; therefore, the particles were subjected to a rigorous washing procedure. The particles were poured into EtOH/H₂O (9:1), and the solution was centrifuged. The sedimented particles were resuspended in the EtOH/H₂O mixture two additional times, and then the sedimented particles were resuspended in degassed DMF at 90 °C. The particles were then subjected to another three rounds of resuspension and centrifugation in EtOH/H₂O and then finally washed with absolute EtOH and dried. A color change was noted in the particles after alkylation: thiourea particles **3-42** are white in color, whereas imidothiolate particles **3-40** are pale orange in color. Similarly, the fluorescein-substituted thiourea particles **3-43** are yellow, whereas the corresponding imidothiolate particles **3-41** are orange in color.

The mass recoveries of particles after the centrifugation/resuspension procedures were not quantitative. The average particle mass recovery in the case of converting phenyl-substituted thiourea particles **3-42** to imidothiolate **3-40** was 72%; the average mass recovery for conversion of fluorescein-substituted particles **3-43** to **3-41** was higher (87%). Moreover, the unreacted benzylic chloride **3-44** could be recovered from the combined supernatants after aqueous extraction and silica-gel chromatography; the recoveries ranged from 34% to 65% of the original mass of benzylic chloride used in the reactions.

Scheme 3-12. Alkylation of thiourea particles with benzylic chloride 3-44.

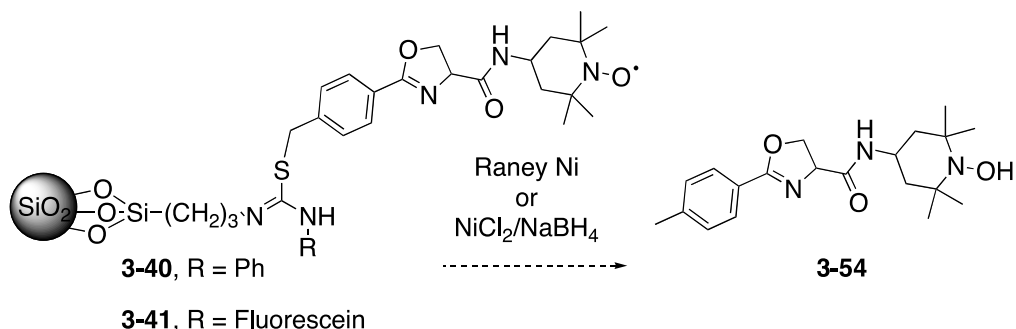


Using elemental analysis alone for loading quantification of imidothiolates **3-40** and **3-41** would be difficult due to the ambiguity of having nitrogen content from the unreacted amines and unreacted thioureas. Moreover, elemental analysis does not allow for confirmation of identity. Therefore, efforts were undertaken to quantify the loading of the imidothiolate particles by cleaving the material from the particles and quantifying the material using either LC-MS analysis.

3.2.3 Assays for Determining the Loading of the Imidothiolate Particles

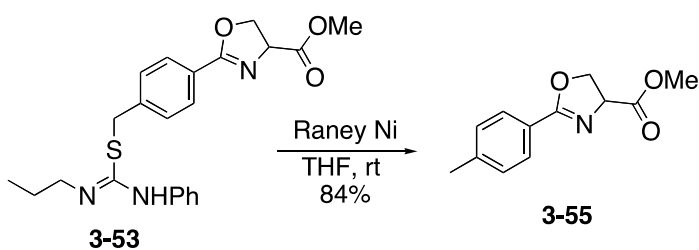
Prior to evaluating the activity of particles **3-40** and **3-41** in cellular assays, I sought to develop an assay to unambiguously determine the loading and identity of the imidothiolate particles. I envisioned treating the functionalized nanoparticles with Raney Ni or nickel boride to cleave the thioether linkage and afford the corresponding toluenic derivative **3-54** (Scheme 3-13).

Scheme 3-13. Proposed thioether cleavage strategy for loading determination.



The possibility of cleaving the imidothiolate was first tested on model system **3-53**; treatment of **3-53** with Raney Ni cleanly afforded the corresponding product **3-55**. Using nickel boride (NiCl₂/NaBH₄) also facilitated clean conversion to the corresponding toluenic derivative **3-55** (Scheme 3-14).

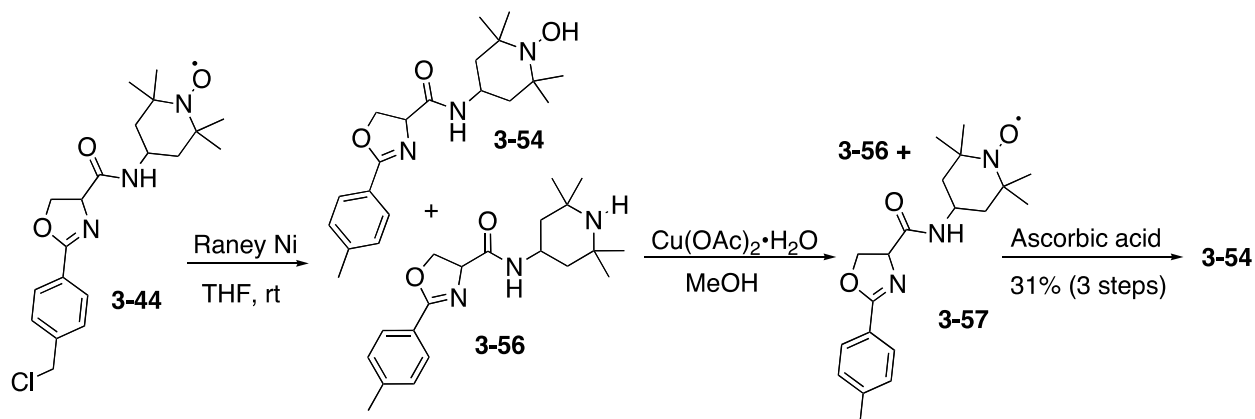
Scheme 3-14. Imidothiolate cleavage using Raney Ni on a solution-phase model system.



Independent synthesis of **3-54** for use as a standard for LC-MS analysis (Scheme 3-15) was carried out. It seemed feasible that standard **3-54** could be synthesized by reduction of benzylic chloride **3-44** with Raney Ni. Subjecting **3-44** to the reduction conditions resulted in a mixture of the hydroxylamine **3-54** and the free amine **3-56**. The free amine **3-56** could be obtained as the exclusive product after extended reaction times with Raney Ni. To obtain a pure sample of the corresponding hydroxylamine, a 3-step sequence was employed. Reduction of **3-44** with Raney Ni afforded a mixture of polar products **3-54** and **3-56**. Treatment of the mixture with

$\text{Cu}(\text{OAc})_2 \cdot \text{H}_2\text{O}$ afforded a mixture of amine **3-56** and nitroxide **3-57**. The nitroxide was easily separated from **3-56** by chromatography on SiO_2 , thus separating the products with an N-H bond from products with an N-O bond. Finally, reduction of purified **3-57** with ascorbic acid in MeOH afforded a pure sample of the hydroxylamine standard **3-54**.

Scheme 3-15. Reduction of benzylic chloride **3-44**; synthesis of standards for LC-MS analysis



3.2.3.1 Reductive Cleavage and Loading Quantification

Imidothiolate particles **3-40** were subjected to a range of reducing conditions using either Raney Ni in THF or $\text{NiCl}_2/\text{NaBH}_4$ in mixtures of EtOH and MeOH. Conventional stirring was used at first, but sonication proved to be a more effective method for executing the solid/solid reaction. In all cases, however, complex LCMS traces were obtained, precluding quantification of products **3-56** or **3-57**.

Part of the difficulty in obtaining useful LC-MS data was the fact that mixtures of N-H and N-O products are obtained after subsection of the nitroxides to reducing conditions. An alternative strategy was employed where 4-amino-TEMPO would be replaced with a UV-active amine; loadings would be quantified using UV/VIS spectroscopy (Figure 3-12). It was assumed that the alkylation yield (i.e., loading) of reacting particles **3-42** with benzylic chloride **3-44** would be comparable that that of reacting particles **3-42** with an analogous UV-labeled benzylic chloride.

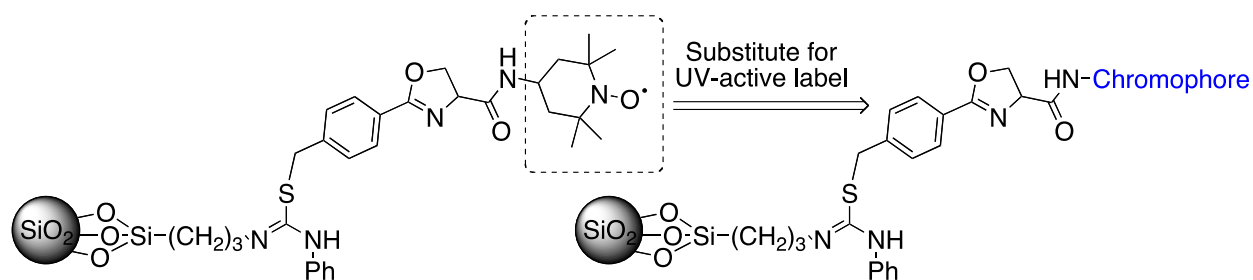
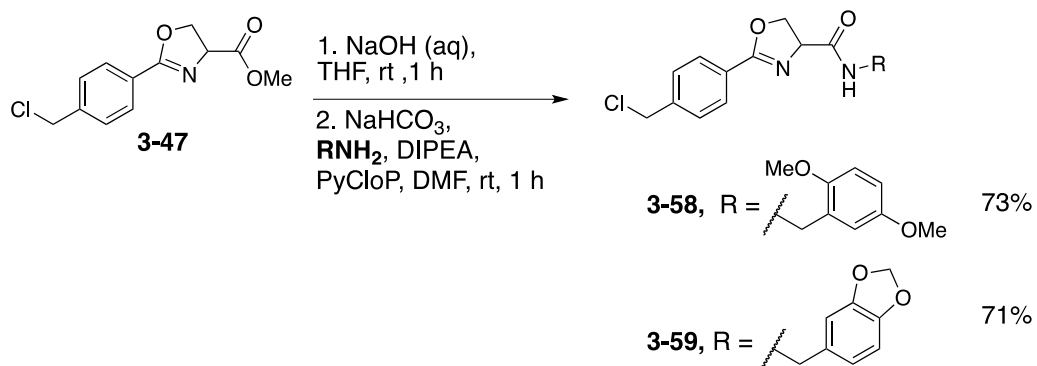


Figure 3-12. General strategy for loading assays using UV/VIS spectroscopy.

A caveat to this approach was that the choice of chromophore could not bear groups that would be reduced under the imidothiolate cleavage conditions. Therefore functional groups common to good chromophores such as nitrile and nitro groups had to be excluded from the design. Compounds analogous to vanillin—i.e., compounds with electron-donating methoxy groups were chosen as a suitable starting point.

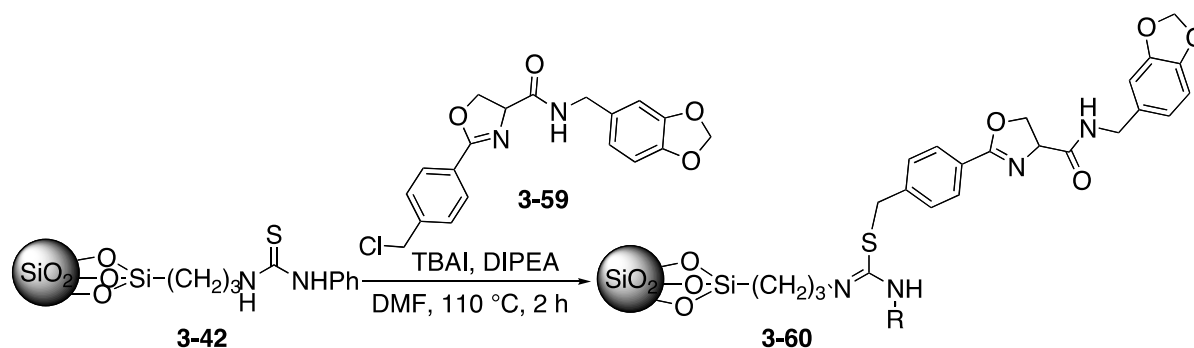
To implement this strategy, methoxy-substituted amides **3-58** and **3-59** were prepared by standard coupling procedures (Scheme 3-16). Although the UV/VIS properties were acceptable for 2,5-dimethoxy derivative **3-58**, the solubility was poor in most organic solvents. The more soluble piperonylamine derivative **3-59** was therefore used; this derivative also had favorable UV properties ($\epsilon_{283} = 14,600 \text{ M}^{-1} \text{ cm}^{-1}$; $\epsilon_{264} = 17,700 \text{ M}^{-1} \text{ cm}^{-1}$ in THF).

Scheme 3-16. Synthesis of benzylic chlorides bearing chromophores.



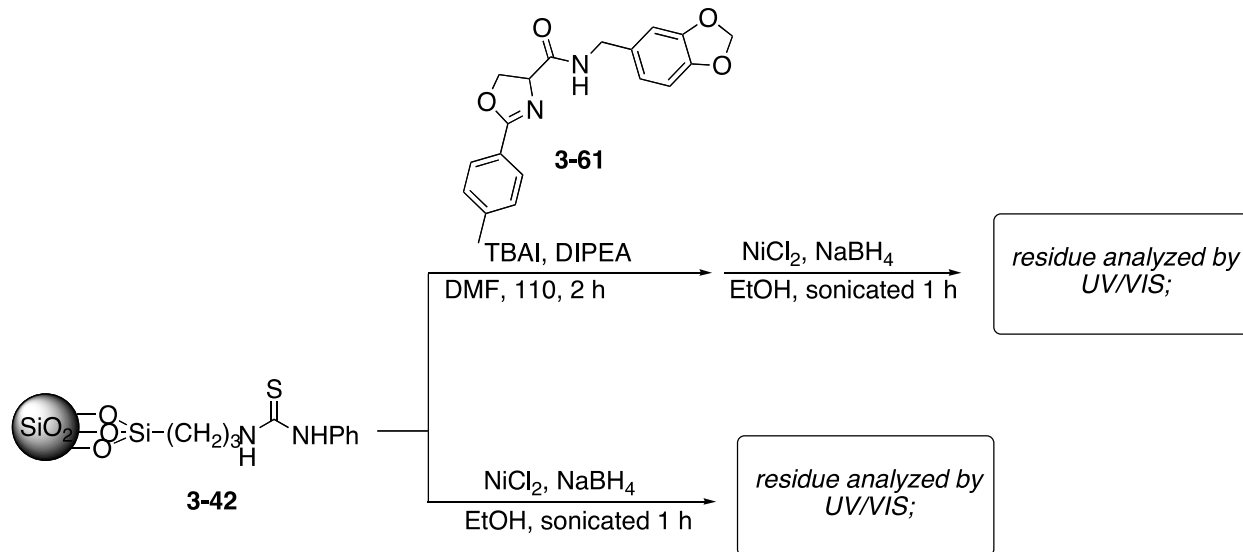
Chromophore-labeled particles **3-60** were synthesized using analogous alkylation and washing protocols to those with alkylation of TEMPO-elaborated substrate **3-44**. Particles **3-60** were suspended in EtOH/MeOH, treated with NiCl₂ and NaBH₄, and sonicated for 1 h. After filtration and concentration *in vacuo*, the residue was taken up in THF and analyzed by UV/VIS spectroscopy. After comparison to a standard curve generated from THF solutions of **3-59**, the loadings were calculated to be *ca.* 0.01 mmol/g.

Scheme 3-17. Synthesis of chromophore-labeled imidothiolate.



It was also a concern that the product particles from the alkylation procedures may contain a mixture of covalently bonded imidothiolate particles as well as adsorbed benzylic chloride (e.g., **3-59**). I designed an experiment wherein toluene derivative **3-61** was reacted with thiourea particles **3-42** using the standard alkylation and washing procedures (Scheme 3-18). The resulting particles were then subjected to the reductive “cleavage” conditions and analyzed by UV/VIS spectroscopy. Surprisingly, the apparent “loading” values calculated were similar to that of particles **3-60**. Thiourea particles **3-42** were also subjected to the reductive cleavage conditions, and, after the standard workup, analyzed the residue by UV/VIS. The absorbance values were again similar to those from performing reductive cleavage of particles **3-60**. Because the loading values calculated for **3-60** did not differ from that of the control experiments, it was concluded that the reductive cleavage assay was not suitable for determining the loading of the imidothiolate particles.

Scheme 3-18. Control reductive cleavage experiments to validate the loading quantification experiments.



Eventually, values obtained from elemental analysis of the imidothiolates were used to determine loading. By calculating the loading based on nitrogen content after each step, the final loading of imidothiolate particles **3-40** was calculated to be 0.051–0.070 mmol/g. The result was corroborated by results from our collaborators.²³⁸ Wei Hong Fang and Valerian Kagan measured the amount of nitroxide in 1 mg/mL of nanoparticles in phosphate buffer; the nitroxide concentration of **3-40** was 12 μ M, and the nitroxide concentration of a suspension of **3-41** in phosphate buffer was 23 μ M. Within experimental error, these concentrations correspond to loadings of 0.012 mmol/g and 0.023 mmol/g, respectively; the calculated loadings based on measuring the nitroxide signal are in agreement with the calculated loadings based on elemental analysis. The loadings were, however, too low for use in the planned ROS scavenging assays.

Although the nitroxide loadings were low, we were interested to ascertain if imiothiolate particles would be viable for use in cellular assays. Both phenyl-substituted and fluorescein-substituted imiothiolate particles **3-40** and **3-41** were analyzed for macrophage uptake.^{231,239} RAW 264.7 macrophages were treated with uncoated nanoparticles, nanoparticles coated with 1,2-dioleoyl-*sn*-glycero-3-phosphocholine (DOPC) or nanoparticles coated with 1,2-dioleoyl-*sn*-

glycero-3-[phospho-L-serine](sodium salt) (DOPS). The uptake of particles was measured by EPR spectroscopy, and the results are depicted in Appendix C. It is apparent that silica nanoparticles coated with phospholipids were more readily taken into cells than uncoated particles; moreover, particles coated with charged phospholipid DOPS were more readily taken up by the macrophages.

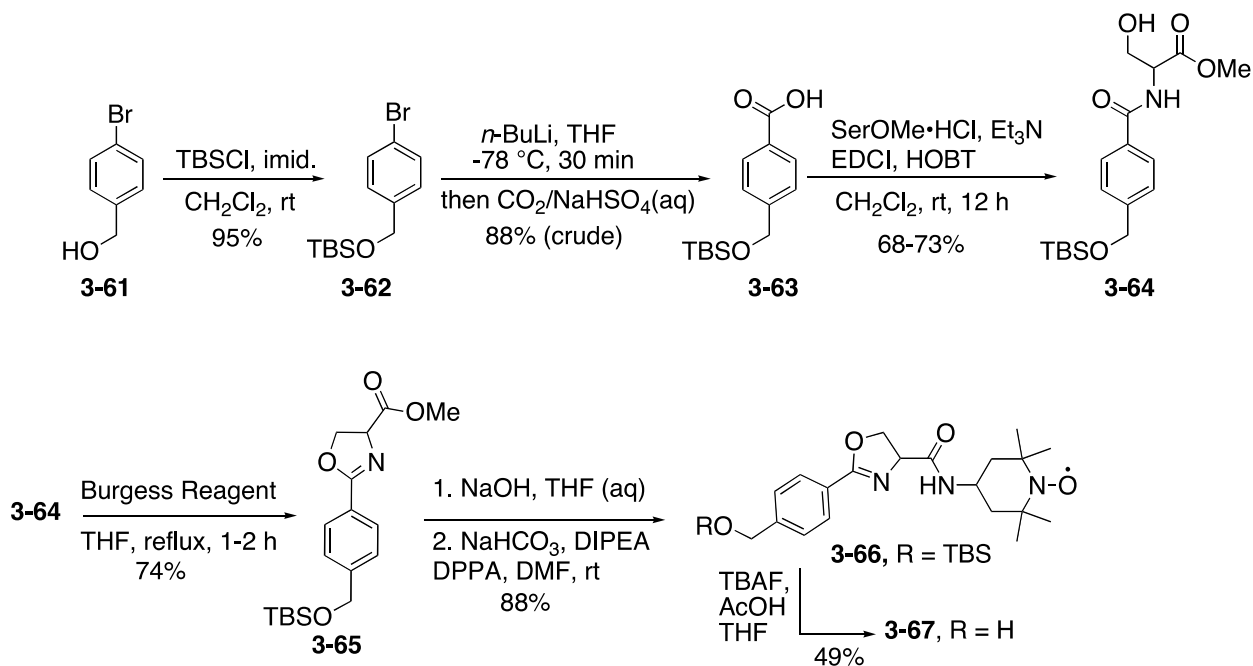
It should be noted that batches of particles **3-40** and **3-41** that were stored for several months showed much weaker EPR signals; moreover, our collaborators noted that these batches were more difficult to suspend in solutions.²³⁹ Based on both the qualitative and quantitative information, it was noted that the functionalized SiO₂ particles degraded and/or aggregated upon prolonged storage. It should also be noted that attempted alkylation of thiourea-functionalized particles **3-42** and **3-43** that were stored for prolonged periods did not yield the desired imidothiolate-functionalized nanoparticles. These observations underscore the importance of using freshly prepared nanoparticles for both synthetic transformations as well as for biological evaluation.

3.2.4 Efforts to Increase Nanoparticle Loading

It was necessary to increase the nanoparticle loading prior to performing ROS scavenging assays. Attempts to improve the yield of the thiourea alkylation step were made by converting the benzylic chloride to alternative leaving groups. In doing so, the imidothiolate alkylation would be carried out at lower temperatures, which may suppress side reactions or decomposition of the imidothiolate thioether bond.

I envisioned using benzylic alcohol **3-67** (Scheme 3-19) as a building block for the convergent screening of different leaving groups. Attempts to convert the benzylic chloride **3-44** directly to the alcohol (e.g., using AgNO₃ and H₂O) did not provide the desired product in acceptable yield. TBS-protected benzylic alcohol **3-66** was accessed through the synthetic sequence shown in Scheme 3-19.

Scheme 3-19. Synthesis of benzylic alcohol for leaving group studies.

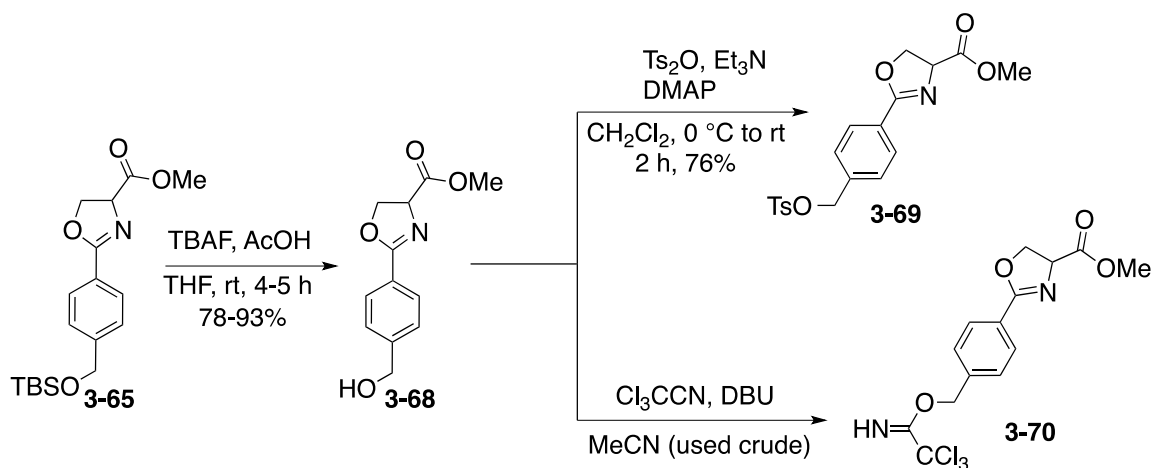


4-Bromobenzyl alcohol **3-61** was converted to the *tert*-butyldimethylsilyl ether **3-62**. Lithiation of the aromatic bromide followed by quenching with CO₂ afforded acid **3-63**. Acid **3-63** was converted to the β-hydroxy amide **3-64** using standard peptide-coupling conditions with dl-serine methyl ester hydrochloride, and cyclodehydration using Burgess reagent provided oxazoline **3-64** in good yield. Because the benzylic position of oxazoline **3-64** is no longer an electrophilic benzylic chloride, amide-bond formation using DPPA can be performed without a concern for side reactions with the azide. Thus, a one-pot procedure involving saponification and azeotroping the sodium salt followed by treatment with DPPA and 4-amino-TEMPO was used to afford amide **3-66**. Removal of the TBS group using buffered TBAF afforded the desired alcohol **3-67**, albeit in moderate yield. Although a successful route to alcohol **3-67** was developed, a leaving group screen was performed on a simpler model system.

The corresponding alcohol of oxazoline **3-65** was chosen as a test system for both incorporation of leaving groups as well as in the thiourea alkylation reaction. Using the methyl

ester **3-68** (Scheme 3-20) would still allow for evaluation of functional group compatibility with the oxazoline as well as use of ^1H NMR analysis for evaluation of reaction mixtures. Deprotection of the silyl protecting group using buffered TBAF afforded alcohol **3-68**. The alcohol was converted to tosylate **3-69** using *p*-toluenesulfonylanhydride; notably, use of *p*-toluenesulfonyl chloride resulted in complex reaction mixtures, likely due to reactions of chloride with the oxazoline ring. Trichloroacetimidate **3-70** was also synthesized using trichloroacetonitrile and DBU—the acetimidate was carried forward without purification.

Scheme 3-20. Synthesis of model substrates for variation of the benzylic leaving group.

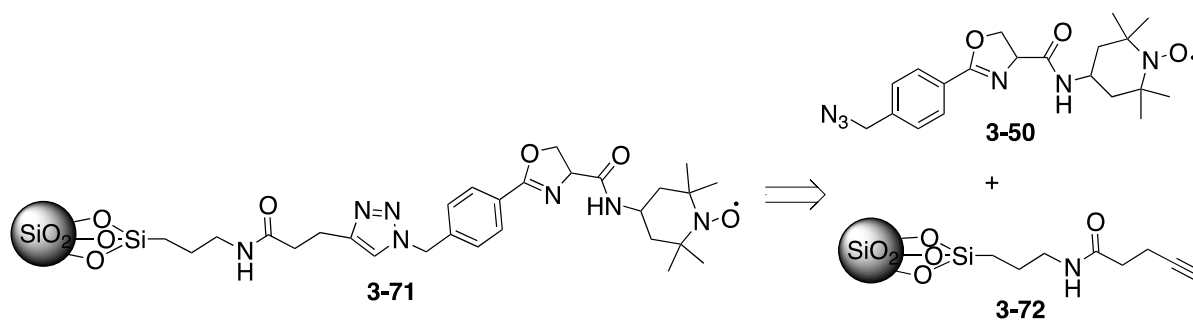


With substrates **3-69** and **3-70** in hand, the model thiourea alkylation was tested. The tosylated substrate **3-69** reacted with thioureas at room temperature, but the reaction was sluggish (times *ca.* 20 h), and the yields were variable (*ca.* 40-65%), likely due to the stability of the tosylate in DMF. Alkylation of a model thiourea with trichloroacetimidate **3-70** using Lewis acids in CH_2Cl_2 was also attempted, but yields were moderate and further optimization would be needed. At this point, the overall strategy was changed to functionalization using a click chemistry approach.

3.2.5 Click Chemistry Approach for Nanoparticle Functionalization

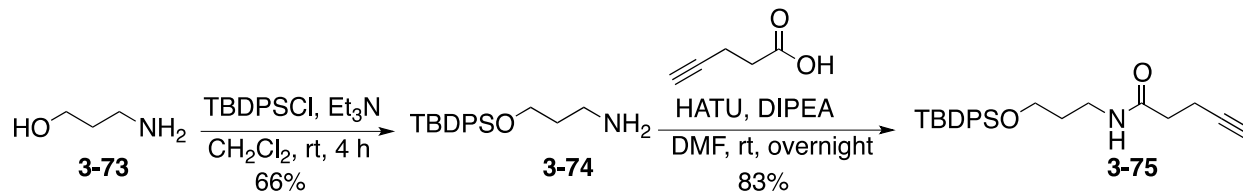
It was postulated that the low loadings from the thiourea alkylation strategy may be from a) the instability of the imidothiolates on the silica nanoparticles or b) the inefficiency of the alkylation reaction on the silica-supported thiourea. The approach was changed to a click chemistry strategy (Scheme 3-21). Click chemistry leads to generation of a stable functional group (i.e., a triazole). Although this approach would not allow for facile incorporation of a fluorescent tag, it was already established (via our collaboration with Wei Hong Feng and Valerian Kagan)²³¹ that the distribution of nanoparticles in the cell could be quantified by EPR spectroscopy. This strategy involved using azide **3-50** in a click reaction with a silica-supported alkyne **3-72**.

Scheme 3-21. General strategy for functionalization using click chemistry.



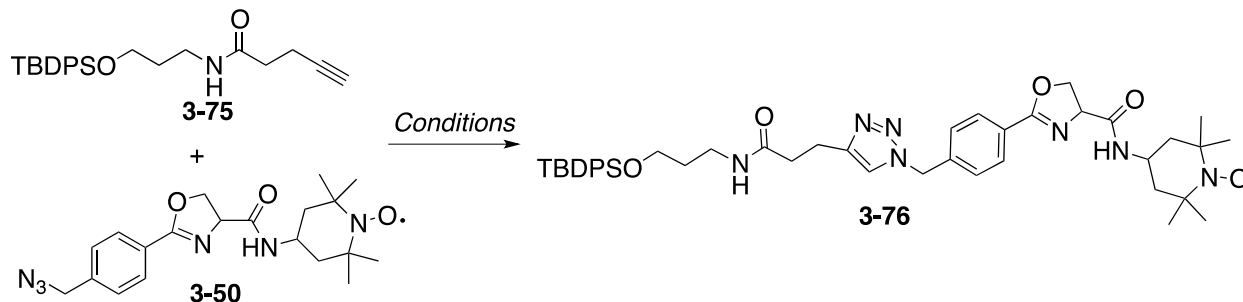
A viable route for the synthesis of azide **3-50** had been discovered in the course of optimizing the coupling of 4-aminoTEMPO to our original benzylic chloride substrate (Scheme 3-9). A model alkyne was used to ensure that azide **3-50** was a viable partner for the 1,3-dipolar cycloaddition (Scheme 3-22). The TBDPS-protected alkyne **3-75** was chosen to limit volatility, and it was synthesized by selective protection of 1-amino-3-propanol to provide requisite amine **3-74** followed by coupling of **3-74** with 5-pentynoic acid using HATU (Scheme 3-22).

Scheme 3-22. Synthesis of model alkyne.



Several conditions for the click chemistry reaction were screened (Table 3-2). Good yields of model triazole **3-76** were obtained when standard conditions were used (e.g., CuI, DIPEA, Table 3-2, entry 1). Because the conditions need to be amenable for use in nanoparticle functionalization, organic-soluble copper reagents (PPh₃)₃CuBr²⁴⁰ and P(OEt)₃•CuI²⁴¹ were screened. Using P(OEt)₃•CuI afforded the model triazole in nearly quantitative yield (Table 3-2, entry 3); however, stoichiometric quantities were necessary for achieving high yields.

Table 3-2. Click chemistry reactions using azide **3-50** and a model alkyne.



Entry	Conditions	Yield ^a
1	CuI (1 equiv), DIPEA (50 equiv) THF, rt, 15 h	75%
2	(PPh ₃) ₃ CuBr (20 mol%), DIPEA (3 equiv) toluene, reflux, overnight	44%
3	P(OEt) ₃ •CuI (1 equiv), DIPEA toluene, 5 h, rt	98%

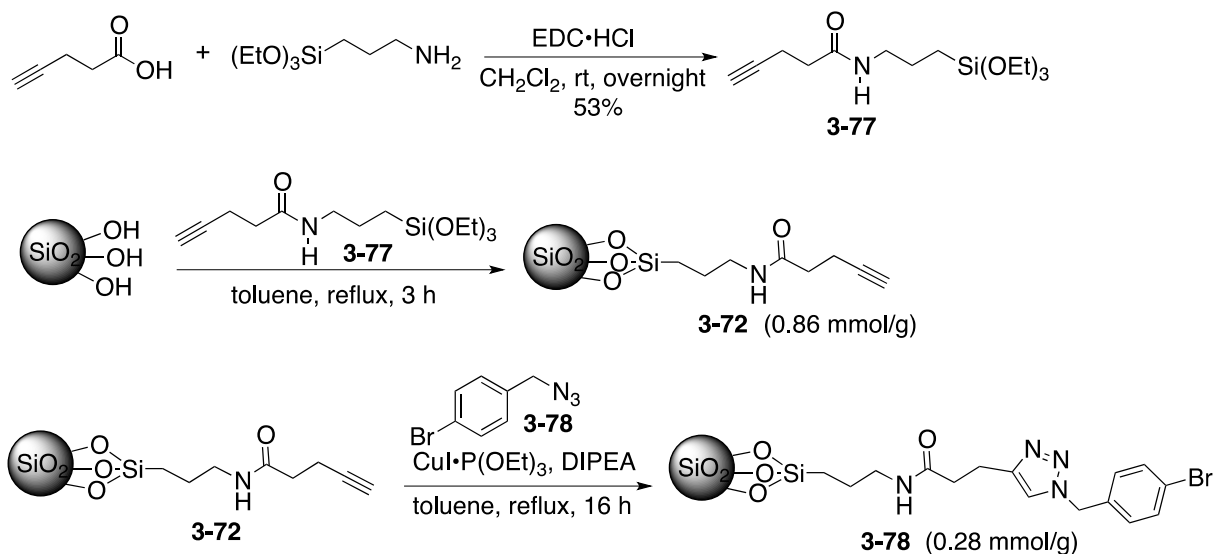
^aThe reported yields reflect the amount of material isolated after silica-gel chromatography.

Silica-supported alkyne **3-72** was synthesized by condensation with alkynyl triethoxysilane **3-77** (Scheme 3-23), which was prepared by coupling of 3-aminopropyltriethoxysilane with 5-pentynoic acid. Heating **3-77** at reflux with silica nanoparticles in toluene afforded alkyne-functionalized particles **3-72**.

The click chemistry reactions were first performed using 4-bromobenzyl azide (Scheme 3-23); combustion analysis could be used to measure the bromine content in the particles. This analysis would unequivocally provide an estimate of the expected loading using azide **3-50**. The loading (0.28 mmol/g, based on %Br content) was sufficiently high for pursuing the click

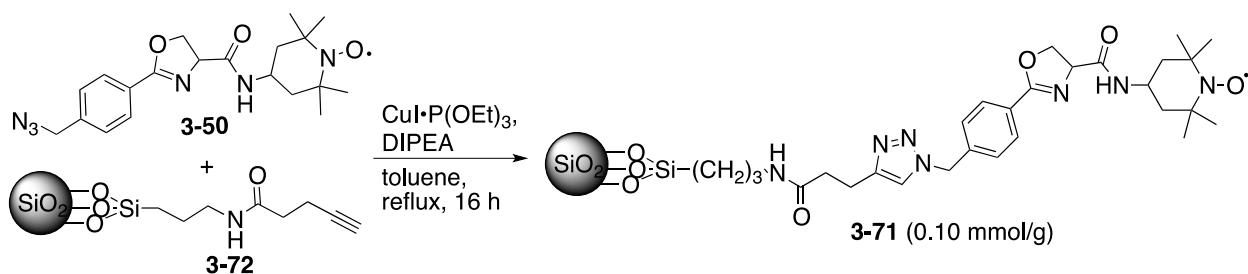
chemistry approach. It should be noted that a similar loading (0.20 mmol/g) was obtained when the same reaction was performed at room temperature rather than reflux.

Scheme 3-23. Synthesis of alkyne-functionalized nanoparticles and click chemistry using 4-bromobenzylazide.



After verifying the viability of the click chemistry approach, azide **3-50** was subjected to the click chemistry conditions (Scheme 3-24). Based on nitrogen content, the loading was estimated to be 0.10 mmol/g. The same reaction was performed at room temperature, and about 2-fold lower loadings (0.05 mmol/g) were obtained.

Scheme 3-24. TEMPO-functionalization of silica nanoparticles using click chemistry.



Two batches of triazole functionalized particles **3-71** submitted to our collaborators for analysis of nitroxide content using EPR spectroscopy.²⁴² The results are shown in Tables 3-3 and 3-4. Batch A refers to particles functionalized using click conditions at room temperature, and Batch B refers to particles functionalized using click conditions at reflux (Scheme 3-24). Particles were suspended in phosphate buffer, vortexed, and gently sonicated; EPR measurements were performed on aliquots of these suspensions. Three experiments were performed on both batches: 1) the EPR signal was measured after sonication of the particles in phosphate buffer (Table 3-3) 2) the sonicated samples were centrifuged, and the EPR signals of the supernatant and the pellet were estimated (Table 3-4), and 3) the samples were not sonicated, and the suspensions in the buffer were centrifuged and the EPR signal of the supernatant and pellet were measured (Table 3-4).

Table 3-3. Nitroxide content of particles suspended in phosphate buffer.

Entry	Batch	Amount of TEMPO measured (pmol/mg particles)	Amount of TEMPO measured (+ K ₃ Fe(CN) ₆) (pmol/mg particles)
1	A	608.7 ± 63.3	660.1 ± 79.1
2	B	1472.8 ± 98.5	1454.5 ± 86.8

Table 3-4. Nitroxide content of particles after both sonication and centrifugation.

Entry	Batch	Procedure	Amount of TEMPO measured in supernatant (pmol/mg particles)	Amount of TEMPO measured in the pellet (pmol/mg particles)
1	A	I	656.8 ± 51.6	374.8 ± 42.2
2	B	I	1348.4 ± 25.8	469.4 ± 49.3
3	A	II	245.3 ± 18.3	235.6 ± 22.8
4	B	II	1332.8 ± 54.8	1150.5 ± 52.5

Procedure I. Samples were vortexed and then sonicated in phosphate buffer and centrifuged (1000 *xg* for 5 min, then 15,000 *xg* for 20 min). Aliquots of the supernatant and pellet (after re-suspension in buffer) were taken for EPR measurements. Procedure II. Samples were vortexed (but not sonicated) in phosphate buffer and centrifuged (15,000 *xg* for 20 min). Aliquots of the supernatant and pellet (after re-suspension in buffer) were taken for EPR measurements.

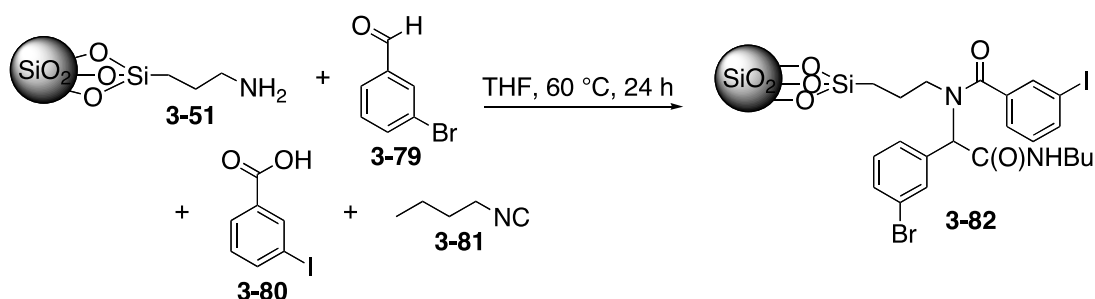
The data indicate that the majority of the nitroxide-containing compound is not immobilized onto the nanoparticles but rather may have been adsorbed and released upon sonication. Our collaborators noted that the EPR spectra recorded was characteristic of an isotropically rotating molecule, also supporting the conclusion that the material was not immobilized.²⁴²

3.2.5.1 Ugi Approach

Attempts to use 3-aminopropyl-functionalized silica particles **3-51** as the amine in an Ugi reaction (Scheme 3-25) were made. An experiment using 3-bromobenzaldehyde **3-79** and 3-iodobenzoic acid **3-80** to generate doubly labeled nanoparticles **3-79** was performed. The presence of adsorbed 3-bromobenzaldehyde **3-79** or 3-iodobenzoic acid **3-80** would be evident by a discrepancy in the ratio of Br : I. Based on elemental analysis, the loading (%Br content)

wa calculated to be 51 $\mu\text{mol/g}$. This strategy was therefore not a viable alternative to the click chemistry approach.

Scheme 3-25. Ugi reaction on a model system.

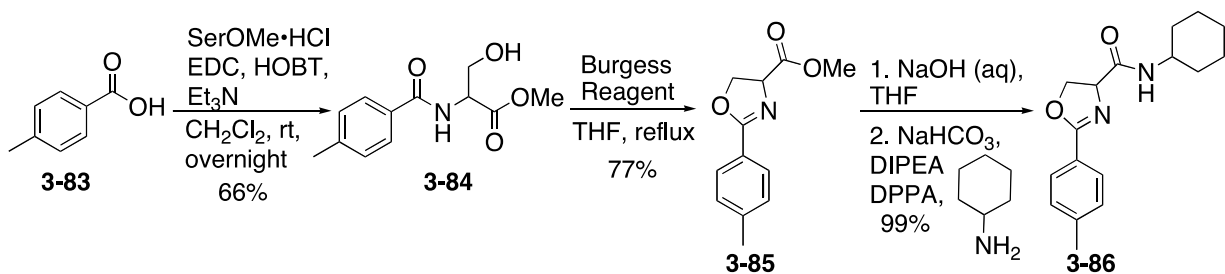


Although the three nanoparticle functionalization strategies did not afford suitable loadings for further biological evaluation, it was still of interest to test the applicability of using an oxazoline linker for controlled release. Therefore, studies of oxazoline hydrolysis were undertaken, and the outcomes are detailed in the following sections.

3.2.6 Oxazoline Hydrolysis of Model Systems

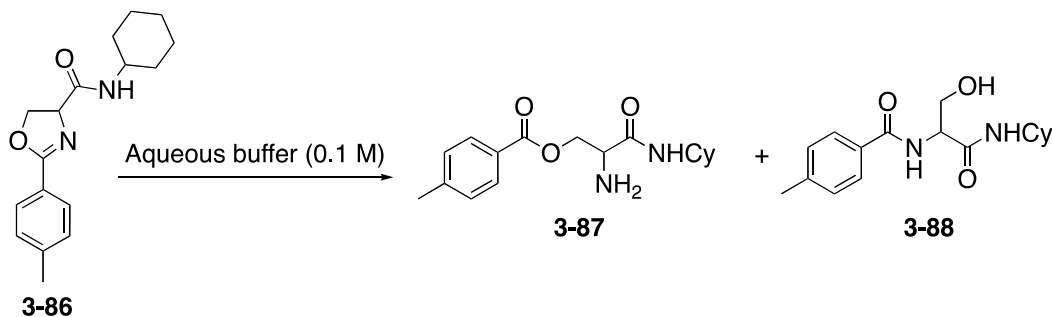
To probe the hydrolytic proclivity of the oxazoline substrates, a model oxazoline was synthesized from *p*-toluic acid **3-83** (Scheme 3-26). The amide-bond coupling reactions were performed with cyclohexylamine instead of 4-amino-TEMPO both to avoid using an expensive amine for model studies and to be able to monitor the reaction progress by ^1H NMR spectroscopy.

Scheme 3-26. Synthesis of model oxazoline **3-86**.



Substrate **3-86** was tested for its proclivity toward hydrolysis at various pH at room temperature. The compound was suspended in aqueous buffers (0.1 M) at pH 1.0 to pH 5.0. Complete hydrolysis was observed at pH 1.0 within 90 min; however, hydrolysis at higher pH-values only occurred at elevated temperatures, and hydrolysis at pH 5.0 occurred only at temperatures greater than or equal to 100 °C. It was hypothesized that increasing the electron density on the aromatic ring or using alkyl substituents on the oxazoline would increase the proclivity toward hydrolysis at higher pH-values.

Scheme 3-27. Hydrolysis of model oxazoline.



A general scheme for synthesis of model oxazolines is shown in Table 3-5. Starting from the requisite carboxylic acid or acid chloride, amide bond formation was accomplished either by standard peptide coupling (e.g., using EDCI, HOBT, Et₃N) in the case of acid starting materials or by acylation in the case of acid chloride starting materials. Cyclodehydration was

accomplished using standard protocols—either by heating with Burgess reagent in THF²³² or by treatment with DAST at -78 °C followed by K₂CO₃.²³³ Finally, cyclohexylamine was coupled to the substrates using the standard protocol of saponification, azeotroping and solvent swapping, and coupling via the acyl azide (i.e., using DPPA).

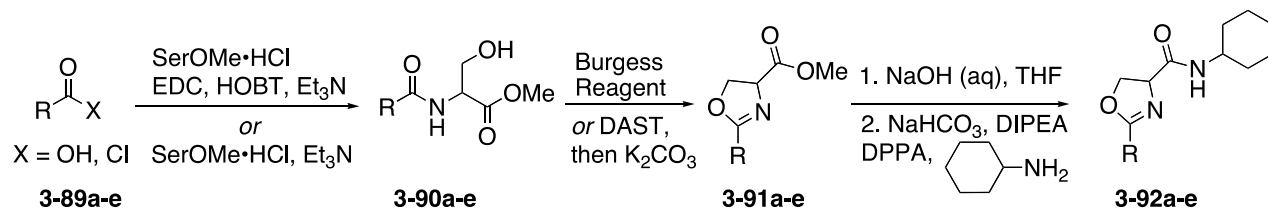
The 2-furanyl-oxazoline **3-92a** as well as the corresponding 2-benzofuranyl oxazoline **3-92b** were synthesized. In the case of 2-furanyl oxazoline **3-92a**, 50% conversion was observed after 1 h at pH 1.0, and complete hydrolysis was observed after stirring for 15 h; in the case of the 2-benzofuranyl oxazoline **3-92b**, only 25% conversion was observed at pH 1.0, even after 15 h.

The 4-methoxyphenyl-substituted oxazoline **3-92c** exhibited similar hydrolytic proclivity to that of the 2-furanyl-substituted oxazoline **3-92a**. Upon moving to the 2,6-dimethoxyoxazoline **3-92d**, a marked drop in hydrolytic proclivity was observed—little to no hydrolysis occurred at pH 1.0 even after 24 h. It is likely that the steric encumbrance from the ortho-substitution superceded the effects from enhanced electron density of the dimethoxy groups.

Benzyl-substituted oxazoline **3-92e** exhibited a marked enhancement in proclivity toward hydrolysis at higher pH-values. At pH 1.0, the substrate was hydrolyzed within 20 min; this same result was observed up to pH 3.0. At pH 4.0, complete hydrolysis was observed after 2.5 h at rt. At pH 5.0, however, ~40% conversion was observed after 15 h at rt.

Based on these studies, it seems reasonable to propose using a more electron-rich aromatic oxazoline or to use the more labile benzyl-substituted oxazoline instead of the simple phenyl-substituted oxazoline. However, the hydrolysis was not tested under physiological conditions (e.g., 37 °C), and it is difficult to predict the consequences of differential oxazoline substitution in a cellular environment. There is likely a delicate balance between having a prohibitively labile substrate and an oxazoline that hydrolyzes at an optimal rate at a specific pH. Currently, we will note the observed trend and use it to guide further design modifications following optimization of our nanoparticle functionalization and assaying strategies.

Table 3-5. Synthesis of model oxazolines.



Entry	Starting material	Conditions/yield for 3-90a-e	Conditions/yield for 3-91a-e	Yield 3-92a-e
1	 3-89a	SerOMe·HCl, Et ₃ N 3-90a , 45%	Burgess Reagent THF, reflux, 3-91a , 66%	3-92a , 79%
2	 3-89b	SerOMe·HCl, EDC, HOBT, Et ₃ N, 3-90b , 77%	Burgess Reagent THF, reflux 3-91b , 45%	3-92b , 68%
3	 3-89c	SerOMe·HCl, Et ₃ N 3-90c , 31%	DAST, then K ₂ CO ₃ CH ₂ Cl ₂ , 3-91c , 73%	3-92c , 45%
4	 3-89d	SerOMe·HCl, Et ₃ N 3-90d , 83%	Burgess Reagent THF, reflux 3-91d , 68%	3-92d , 80%
5	 3-89e	SerOMe·HCl, EDC, HOBT, Et ₃ N, 3-90e , 60%	Burgess Reagent THF, reflux 3-91e , 45%	3-92e , 51%

3.2.7 Functionalization of Controlled-Pore-Glass (CPG)

Because there were difficulties in finding a suitable spacer for the silica-nanoparticles, I decided to use controlled-pore-glass was used both as a model system and, potentially, as an alternative to the nanoscale silica particles. The functionalization of controlled-pore-glass is well precedented²⁴³ and was suitable for rapidly generating models for further evaluation of pH-mediated release of TEMPO via the oxazoline-linker strategy.

3.2.7.1 General Strategy for Functionalization of Porous Glass

Known succinylated-CPG were used as the basis for attaching our TEMPO-derivatives to CPG. Typically, CPG is used for oligonucleotide synthesis, and a leader nucleoside is attached to CPG as a succinate ester (Figure 3-13). I envisioned that an analogous linkage could be formed using a primary alcohol appended to our oxazoline-TEMPO system (Scheme 3-28). Although the ester may be unstable to the oxazoline hydrolysis conditions, it would serve as a suitable starting point and could be modified as needed. Moreover, simple hydrolysis using sodium hydroxide would be a feasible way to quantify the loading of the functionalized glass.

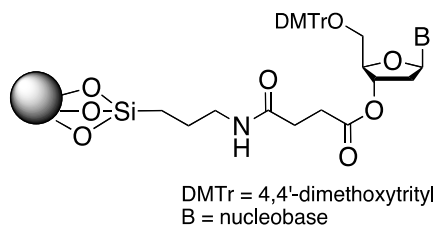
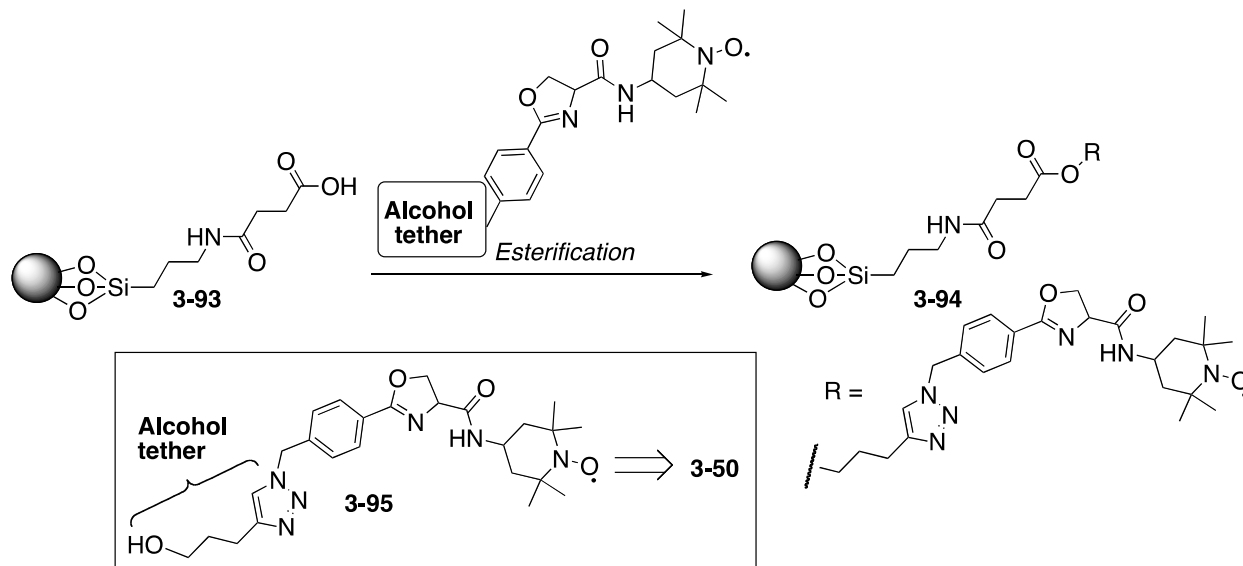


Figure 3-13, Typical design of succinylated CPG for oligonucleotide synthesis.

The requisite alcohols were generated by reaction of azide **3-50** with alkynes. This procedure would be convergent and allow for facile modification of the substrate (e.g., using alkynes with varying numbers of methylene groups). Moreover, high yields were already achieved in solution-phase cycloadditions using azide **3-50**.

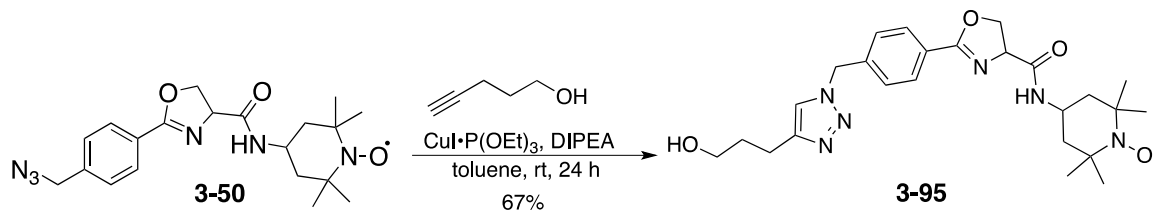
Scheme 3-28. Strategy for functionalization of porous glass.



3.2.7.2 Synthesis of Precursors and Functionalization of CPG

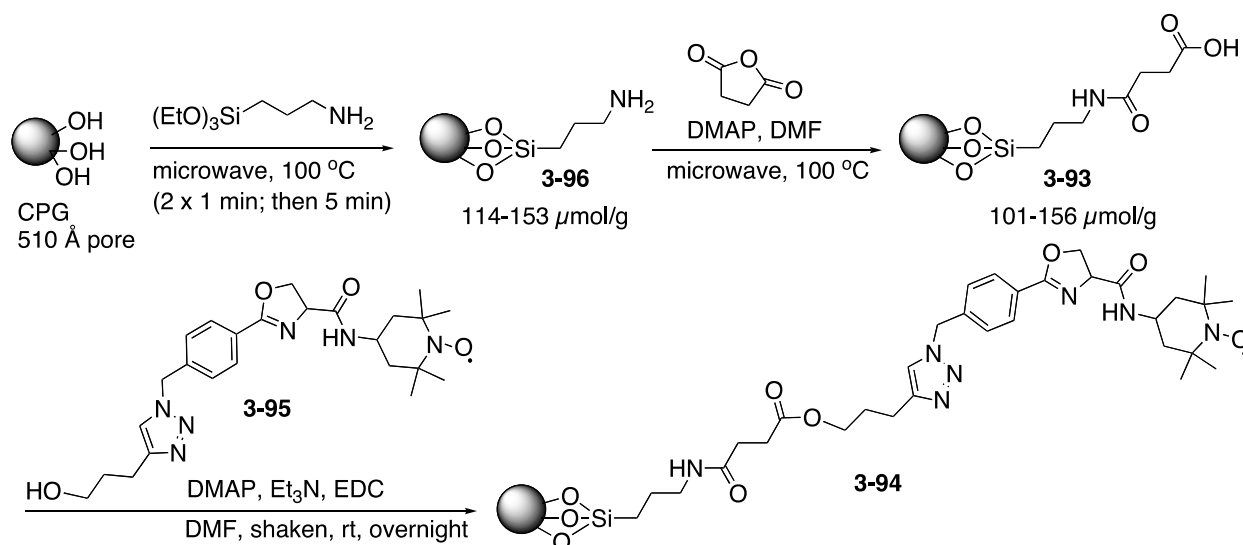
Alcohol **3-95** was synthesized by reaction of azide **3-50** with 4-pentyn-1-ol (Scheme 3-29). It should be noted that the purity of the copper reagent is important; if Cu(II) was present, diminished yields or impure product mixtures containing mixtures of oxazoline and oxazole were obtained.

Scheme 3-29. Synthesis of alcohol **3-95**.



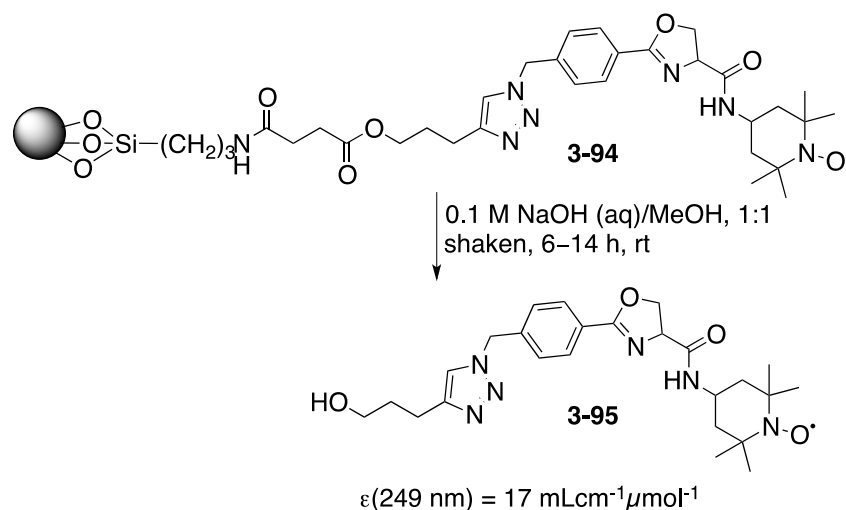
With alcohol **3-95** in hand, the succinylated CPG were elaborated according to established protocols²⁴⁴ (Scheme 3-30). Briefly, treating native CPG (120/200 mesh) with 3-aminopropyltriethoxysilane under microwave conditions afforded 3-aminopropyl-CPG **3-96**. Loadings were calculated using trityl analysis.²⁴⁵ The 3-aminopropyl-CPG was converted to the necessary acid using succinic anhydride and DMAP in DMF (also under microwave conditions). In this case, the acid loading was determined by derivatization with *p*-nitrophenol followed by saponification and UV/VIS quantification of the concentration of phenoxide ion.²⁴³ The particles were esterified with alcohol **3-95** using standard conditions for esterification of succinylated CPG.²⁴⁴

Scheme 3-30. Functionalization of CPG with triazole **3-95**.



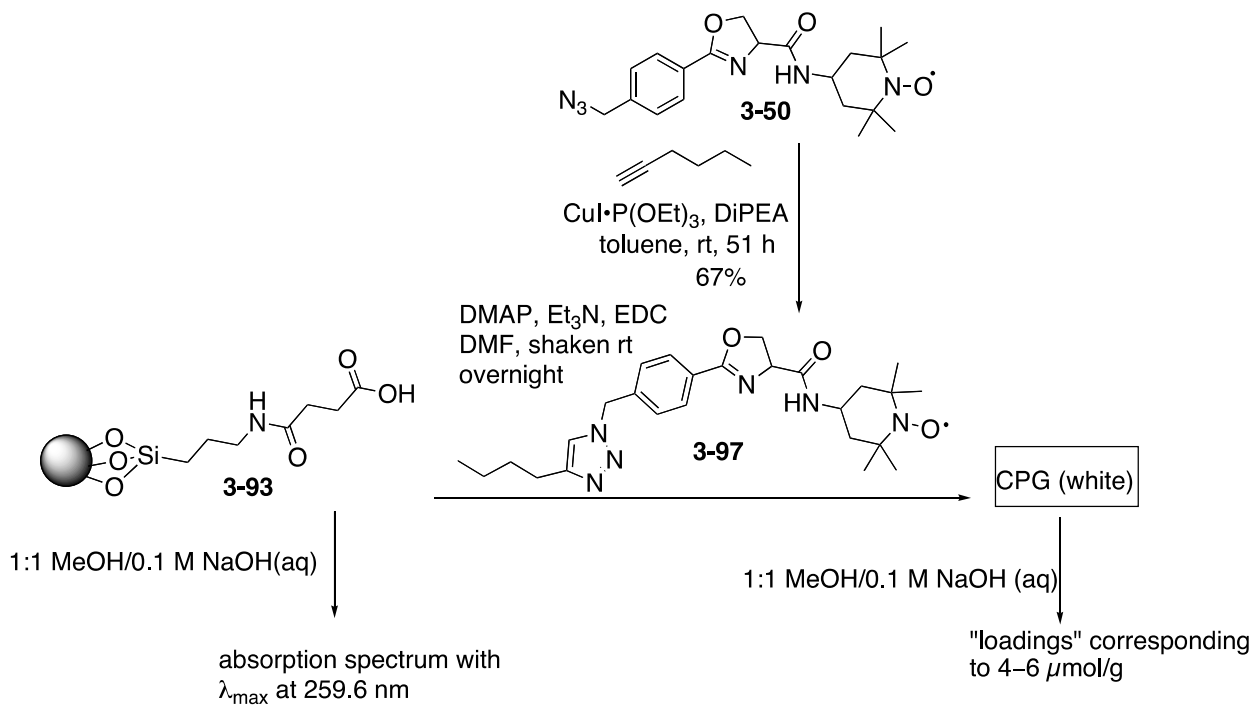
Loadings of triazole **3-94** were quantified by saponifying the ester and measuring the concentration of triazole released from the CPG (Scheme 3-31). A known quantity of beads were shaken in 0.1 N NaOH (aq)/MeOH, 1:1 for at least 6 h. The liquid was transferred to a volumetric flask and diluted with the NaOH/MeOH solution, and the concentration of triazole **3-95** was measured by UV/VIS spectroscopy—absorbance was measured at 247 nm, and an independently generated calibration curve was generated using solutions of **3-95** in 0.1 M aqueous NaOH/MeOH, 1:1. The loading of **3-94** was consistently between 110 and 150 $\mu\text{mol/g}$.

Scheme 3-31. Saponification of CPG-ester for loading determination.



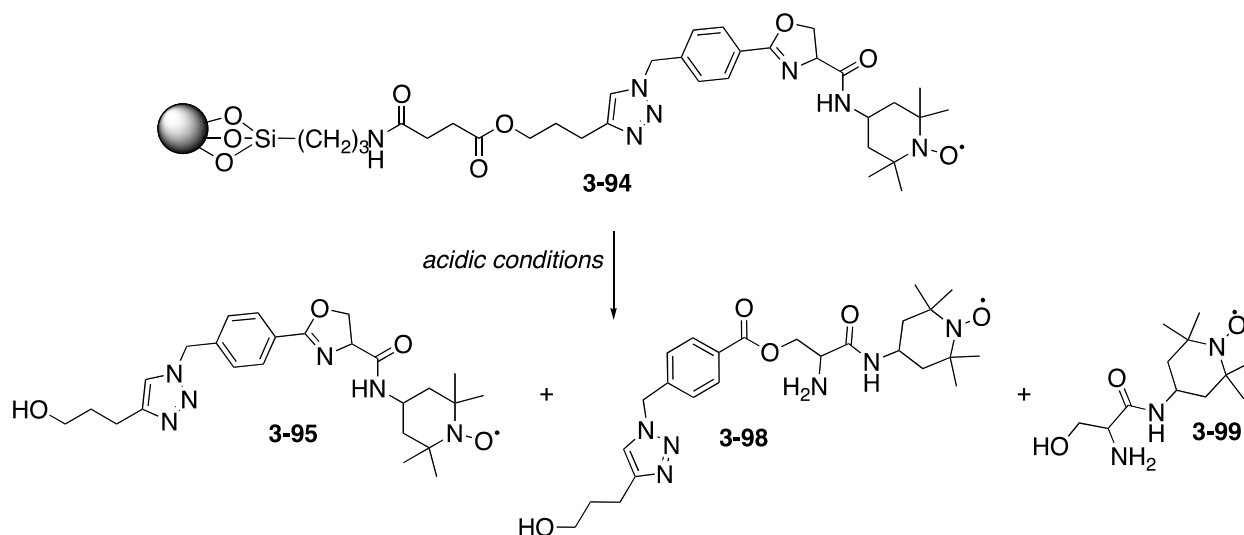
Control experiments were performed to ensure that the measured loadings were from covalently attached material rather than adsorbed material (Scheme 3-32). Triazole **3-97** was prepared from azide **3-50** and 1-hexyne with the click chemistry protocol used for synthesis of triazole **3-95** (i.e., $\text{CuI}\cdot\text{P}(\text{OEt})_3$, DIPEA, toluene, rt). Control triazole was subjected to the esterification conditions, washed using the protocol used for esterification reactions (i.e., formation of **3-94**), and then subjected to the saponification conditions used for loading determination (0.1 M aqueous NaOH/MeOH, 1:1). Minimal UV-absorbance was observed, and the measured concentrations would correspond to loadings of less than 6 $\mu\text{mol/g}$. Succinylated particles **3-93** were also subjected to the saponification conditions, and a significant UV/VIS spectrum with λ_{max} at 259.6 nm was obtained. It was confirmed that this absorption comes from the presence of adsorbed DMAP on the succinylated particles. Yet, because the absorbance values from the control experiment using succinylated particles **3-93** and triazole **3-97** were low, significant carryover of DMAP was not a concern, and the measured loadings were a correct quantification of material that was covalently attached to the CPG.

Scheme 3-32. Validation of the saponification assay for determination of loading on CPG.



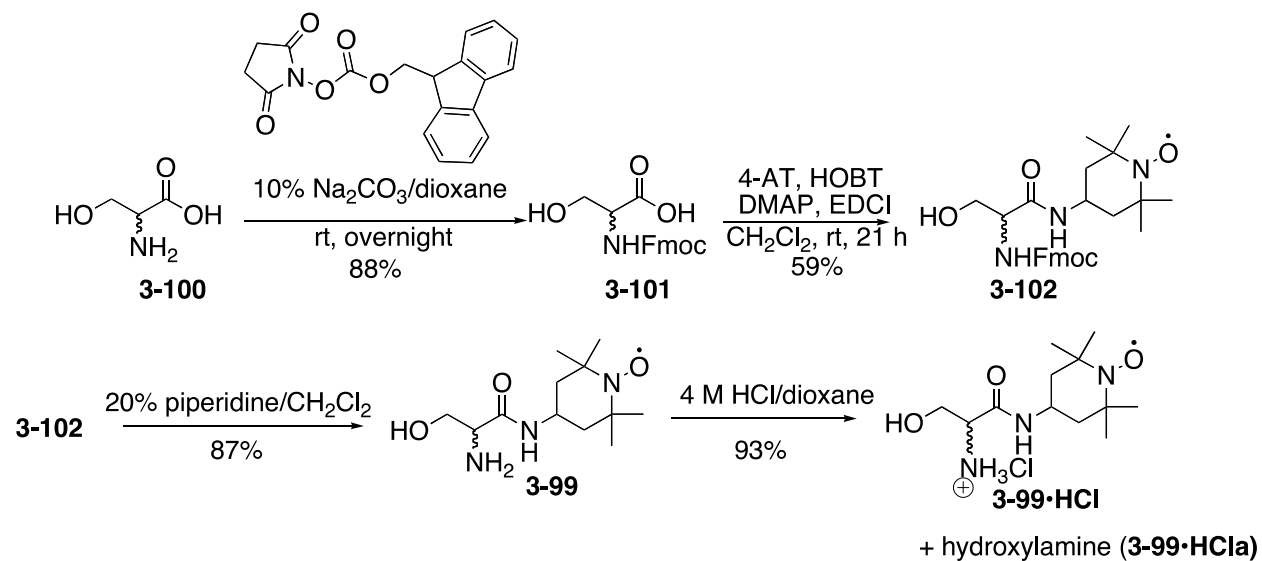
Once a covalently attached substrate with an oxazoline linker was generated, the functionalized porous glass was subjected to acidic media (pH 1.0). Aliquots were filtered and analyzed by LC-MS. Mass values corresponding to saponified **3-95** as well as the oxazoline-opened, saponified product **3-98**, and the serine adduct **3-99** were detected (Scheme 3-33).

Scheme 3-33. Subjection of CPG-ester **3-94** to acidic conditions.



Because the goal was to solely cleave the serine adduct **3-99**, quantification of this product was necessary. A standard (isolated as the hydrochloride salt **3-99•HCl**) was synthesized as shown in Scheme 3-34. *N*-Fmoc *dl*-serine was prepared using a known protocol²⁴⁶ and subsequently coupled with 4-amino-TEMPO to afford **3-102**. The Fmoc group was cleaved using piperidine, and the free amine **3-99** was treated with 4.0 M HCl in 1,4-dioxane and isolated as the hydrochloride salt **399•HCl**. Using LCMS analysis, it was evident that the product existed as a mixture of nitroxide **399•HCl** and the corresponding hydroxylamine **399•HCl_a** (Scheme 3-34).

Scheme 3-34. Synthesis of serine adducts as standards.



3.3 CONCLUSIONS AND FUTURE DIRECTIONS

The functionalization of silica nanoparticles with an oxazoline linker for pH-mediated release of TEMPO was explored. The first approach involved a thiourea alkylation strategy wherein the oxazoline was attached to particles via an imidothiolate linkage. Low loadings of nitroxides were achieved using this approach, and it was suspected that the majority of material on the particles was noncovalent, adsorbed material rather than covalently linked material. The strategy was changed to using a triazole spacer, with the reasoning that this strategy would lead to more stable functionalized products. Although the loadings were promising by elemental analysis, experiments wherein the particles were sonicated and centrifuged indicated that a large amount of material remained in the supernatant, which was indicative of noncovalent attachment of material.

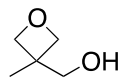
To validate the use of an oxazoline linker, a series of model oxazolines were screened for hydrolytic proclivity. Increasing electron density of oxazolines substituted with aryl groups at the C-2 position led to substrates that had enhanced hydrolytic proclivity. Additionally, using oxazoline substituted with a benzyl group at the C-2 position was readily hydrolyzed at pH values up to 4.0.

Currently, controlled-pore glass is being used as a model system to evaluate our oxazoline linker strategy. These systems are more tractable because the larger particle size facilitates the filtration and washing steps (a medium-sized fritted funnel is sufficient). Moreover, the CPG does not form aggregates in the same manner as observed in the case of the smaller silica nanoparticles. The larger size of functionalized CPG makes it simple to perform assays due to the distinct separation between the solid and liquid phases in the reaction mixtures. Once the substitution of the oxazoline linker is optimized for selective hydrolysis at physiological pH values, the system will be translated to more biologically relevant nanoparticle scaffolds. More specifically, we will incorporate the oxazoline linker strategy into compounds being appended to carbon nanotubes. The use of a pH-responsive system would be of value to achieve site-specific release of nitroxides at desired intracellular sites, particularly the mitochondria.

General Experimental. Moisture-sensitive reactions were performed under an atmosphere of nitrogen. THF, Et₂O, and TBME were distilled from benzophenone ketyl radical anion. CH₂Cl₂ and toluene were dried via percolation through a column packed with neutral Al₂O₃ under a positive pressure of nitrogen. Et₃N and diisopropylethylamine were distilled from CaH₂. *t*-BuOH was distilled from Mg⁰ before use in moisture-sensitive protocols. Oxetane was purchased from Alfa Aesar and filtered through activated neutral Al₂O₃ prior to use. Unless otherwise noted, all solvents used in hydrozirconation studies were purchased from commercial sources, distilled from CaH₂, and subsequently filtered through activated neutral Al₂O₃ prior to each experiment. 1-Hexene and 2-cyclohexen-1-one were distilled before use. Solutions of *n*-BuLi were purchased from Aldrich and titrated using diphenylacetic acid. Solutions of *i*-PrMgCl•LiCl were either purchased from Aldrich or prepared according to a literature protocol.⁵¹ All Grignard reagents were titrated using solutions of menthol in THF with phenanthroline as an indicator. All other commercial reagents were used as received unless otherwise stated. (*R,R*)-salenCo(III)OAc,^{247,248} Burgess Reagent,²⁴⁹ (PPh₃)₃CuBr²³³, and CuI•P(OEt)₃²³⁴ were prepared according to literature protocols.

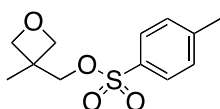
Curcumin (Acros, 95%), naproxen (Acros, 99%), quinine (Acros, 99%), DMSO (Aldrich, 99.9+%), and HPLC-grade water (Aldrich, CHROMASOLV®) were purchased from commercial suppliers and used as received. Carbendazim (Aldrich, 97%) was recrystallized from absolute EtOH, and griseofulvin (Acros, 97%) was recrystallized from toluene. *N*-Methyl-2-pyrrolidone (Acros, 99%) was distilled from CaH₂ under vacuum and stored over 4 Å MS.

Anhydrous DMF (free of molecular sieves for use in nanoparticle functionalization) was purchased from Acros. Suspensions of silica nanoparticles were purchased from Nissan Chemical. Analytical thin-layer chromatography (TLC) was performed on pre-coated silica gel 60 F-254 plates (particle size 0.040–0.050 mm, 230–400 mesh) and visualization was accomplished by staining with KMnO_4 or *p*-anisaldehyde solutions. ^1H NMR spectra (300 MHz, CDCl_3) and ^{13}C NMR spectra (75 MHz, CDCl_3) were referenced to residual chloroform (7.27 ppm, ^1H , 77.00 ppm, ^{13}C). Chemical shifts (δ) are reported in ppm using the following convention: chemical shift, multiplicity (s = singlet, d = doublet, t = triplet, q = quartet, m = multiplet, br = broad), coupling constants, and integration. IR spectra were collected as attenuated-total-reflection infrared (ATR-IR) spectra. Mass spectra were obtained on a Micromass Autospec double focusing instrument. UV/VIS spectra were recorded on a Perkin Elmer Lambda EZ210 spectrophotometer. pH Determinations were made using a 3 mm RossTM glass combination micro pH electrode (model 8220BNWP) after calibration in standard buffer solutions (pH 4.0, 7.0, and 10.0) at rt. Combustion analysis was performed by Atlantic Microlabs.



1-39

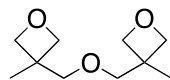
(3-Methyloxetan-3-yl)methanol (1-39). This compound was purchased from commercial sources (Alfa Aesar) or prepared using a modified protocol:^{87,88} A 500-mL round-bottom flask was charged with 1,1,1-tris(hydroxymethyl)ethane (95 g, 0.79 mol), dimethyl carbonate (69 mL, 0.81 mol), KOH (0.75 g, 0.013 mol) and MeOH (1.3 mL, 0.031 mol). The mixture was brought to reflux (bath temperature = 90 °C) and heated at reflux for 15 min. The reflux condenser was switched for a still-head/condenser, and MeOH was removed by distillation. The receiving flask was exchanged, and vacuum was applied to the apparatus (80 Torr). The bath was heated to 140–150 °C, and the pressure was gradually lowered to 30–40 Torr. The pressure was then lowered to *ca.* 15 Torr, and (3-methyloxetan-3-yl)methanol **1-39** was collected in the receiving vessel (27.1 g). The apparatus was allowed to cool (overnight), and distillation under the same conditions (*ca.* 15 Torr) was continued the following day. Additional **1-39** (16.9 g) was collected to afford (3-methyloxetan-3-yl)methanol **1-39** (44 g, 54%) as a colorless liquid: ¹H NMR (300 MHz, CDCl₃) δ 4.53 (d, *J* = 5.9 Hz, 2 H), 4.40 (d, *J* = 5.9 Hz, 2 H), 3.72 (s, 2 H), 1.82 (bs, 1 H), 1.31 (s, 3 H).



1-40

3-Methyl-3-(toluenesulfonyloxymethyl)oxetane (1-40).⁸⁶ To a solution of *p*-toluenesulfonyl chloride (47.8 g, 191 mmol) in anhydrous pyridine (200 mL) was slowly added 3-methyl-3-oxetanemethanol (16.5 mL, 164 mmol). The mixture was stirred for 2 h at rt and poured into a vigorously stirring mixture of ice (570 g) and water (570 mL). The slurry was stirred for 0.5 h, and the precipitate was collected via filtration, washed with cold water, and dried under high vacuum to afford **1-40** (32.4 g, 77%) as a white solid: Mp 56.8–57.5 °C (lit.⁸⁶

59–60 °C); ^1H NMR (300 MHz, CDCl_3) δ 7.82 (d, $J = 8.3$ Hz, 2 H), 7.38 (d, $J = 8.5$ Hz, 2 H), 4.37, 4.35 (AB, $J = 6.3$ Hz, 4 H), 4.12 (s, 2 H), 2.47 (s, 3 H), 1.32 (s, 3 H).



1-37

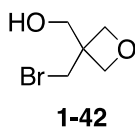
3,3'-Oxybis(methylene)bis(3-methyloxetane) (1-37).⁶² A solution of 3-methyl-3-oxetanemethanol (6.0 mL, 59 mmol) in THF (300 mL) was cooled to 0 °C, and NaH (2.83 g, 70.8 mmol, 60% in mineral oil) was added portion-wise. The solution was warmed to rt and stirred for 4 h. 3-Methyl-3-tosyloxymethyloxetane **1-40** (18.1 g, 63.7 mmol) was added, and the reaction mixture was heated at reflux for 60 h. The mixture was cooled, and the majority of THF was removed *in vacuo*. The concentrate was diluted with Et_2O and filtered, and the filtrate was concentrated *in vacuo*. Residual 3-methyl-3-oxetanemethanol was removed by chromatography on SiO_2 (hexanes/ EtOAc , 4:1). Kugelrohr distillation (120–140 °C at 15 Torr) afforded **1-37** (8.63 g, 76%) as a colorless oil: IR (ATR) 2861, 1107, 1036, 975, 936, 831 cm^{-1} ; ^1H NMR (300 MHz, CDCl_3) δ 4.51 (d, $J = 5.7$ Hz, 4 H), 4.36 (d, $J = 5.7$ Hz, 4 H), 3.54 (s, 4 H), 1.32 (s, 6 H); ^{13}C NMR (75 MHz, CDCl_3) δ 80.0, 76.5, 40.0, 21.3; HRMS (ES) m/z calc for $\text{C}_{10}\text{H}_{18}\text{O}_3$ 209.1154, found 209.1148.



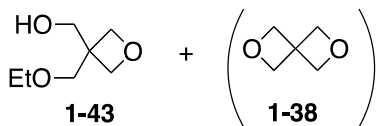
1-38

2,6-Dioxaspiro[3.3]heptane (1-38).⁷³ A 3-necked 500-mL round-bottom flask was outfitted with a reflux condenser and an addition funnel. The flask was charged with KOH (31.0 g, 552 mmol) followed by *t*-BuOH/THF (1:1, 200 mL). The solution was heated to reflux, and a solution of 2,2-bis(bromomethyl)propane-1,3-diol (24.1 g, 91.3 mmol) in *t*-BuOH/THF (1:1, 100 mL) was added dropwise via addition funnel over the course of 3 h. The reflux condenser was exchanged for a distillation head, and *t*-BuOH and THF were distilled from the reaction mixture. The product **1-38** was sublimed from the residue (60 °C at 760 Torr) to afford **1-38** (22.3 g,

22%) as a white solid: Mp 88.2–89.8 °C (lit.⁷³ 89–90 °C); IR (ATR) 2939, 2866, 1223, 964, 917 cm^{-1} ; ^1H NMR (300 MHz, CDCl_3) δ 4.80 (s, 8 H); ^{13}C NMR (75 MHz, CDCl_3) δ 80.3, 43.6; MS (EI) m/z (rel. intensity) 100 (M^+ , 13), 72 (15), 69 (100), 53 (22); HRMS (EI) m/z calc for $\text{C}_5\text{H}_8\text{O}_2$ 100.0524, found 100.0528.

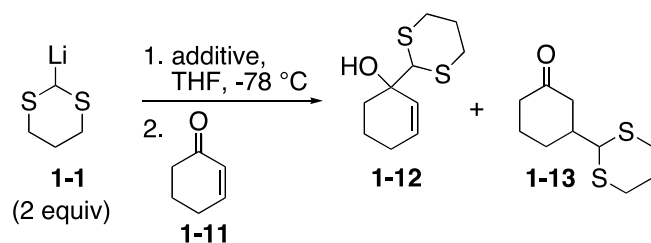


(3-(Bromomethyl)oxetan-3-yl)methanol (1-42). A solution of 2,2-bis(bromomethyl)propane-1,3-diol (1.00 g, 3.82 mmol) in THF (38 mL) was treated (via dropwise addition) with *n*-BuLi (5.20 mL, 7.64 mmol, $c = 1.46$ M in hexanes) at -78 °C. The reaction mixture was maintained at -78 °C for 100 min, warmed to rt, and THF was removed *in vacuo*. The residue was partitioned between Et_2O (30 mL) and water (50 mL), and the aqueous portion was extracted with EtOAc. The combined organic layers were washed with brine, dried (Na_2SO_4) and concentrated. The crude residue was purified by chromatography on SiO_2 (hexanes/EtOAc, 6:4) to afford **1-42** (294 mg, 43%) as a pale yellow oil: IR (neat) 3406, 2954, 2877, 1228, 1039, 974 cm^{-1} ; ^1H NMR (300 MHz, CDCl_3) δ 4.48, 4.45 (AB, $J = 6.5$ Hz, 4 H), 4.00 (s, 2 H), 3.80 (s, 2 H), 1.90–1.82 (bs, 1 H); ^{13}C NMR (75 MHz, CDCl_3) δ 77.0, 64.3, 45.0, 36.1; MS (EI) m/z (rel. intensity) 163 (9), 150 (14), 71 (100).



Confirmation of the intermolecular Williamson ether by synthesis: (3-(ethoxymethyl)oxetan-3-yl)methanol (1-43). A solution of KOH (700 mg, 12.5 mmol) in EtOH (34 mL) was heated at reflux and treated with a solution of **1-42** (1.01 g, 5.52 mmol) dropwise via addition funnel. The mixture was maintained at reflux for 1 h, cooled, and EtOH

was removed *in vacuo*. The residue was dissolved in Et₂O and filtered through neutral Al₂O₃. Et₂O was removed under reduced pressure, and the residue was purified by Kugelrohr distillation (50 °C at 1 Torr) to afford spirocycle **1-38** (27 mg, 5%) as a white solid. Kugelrohr distillation (110 °C at 1 Torr) afforded **1-43** (110 mg, 14%) as a colorless oil: IR (ATR) 3431, 2967, 2868, 1377, 1109, 967 cm⁻¹; ¹H NMR (300 MHz, CDCl₃) δ 4.48, 4.43 (AB, *J* = 6.2 Hz, 4 H), 3.95 (s, 2 H), 3.79 (s, 2 H), 3.55 (q, *J* = 7.0 Hz, 2 H), 2.53 (bs, 1 H), 1.21 (t, *J* = 7.0 Hz, 3 H); ¹³C NMR (75 MHz, CDCl₃) δ 76.6, 75.1, 67.3, 67.1, 43.8, 15.0; MS (EI) *m/z* (rel. intensity) 147 (M⁺, 44), 127 (19), 99 (49), 84 (99), 70 (100), 69 (88), 57 (91); HRMS (EI) *m/z* calc for C₇H₁₅O₃ (M+H) 147.1021, found 147.1021.

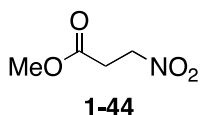


Representative procedure for addition of 2-lithio-1,3-dithiane to 2-cyclohexen-1-one (Table 1-18 entry 4). A solution of 1,3-dithiane (30 mg, 0.25 mmol) in THF (1.8 mL) was degassed (bubbling N₂), cooled to -78 °C, and treated with *n*-BuLi (0.21 mL, 0.27 mmol, *c* = 1.27 M in hexanes). The solution was warmed to -20 °C over 75 min, stirred for an additional 30 min at -20 °C, cooled to -78 °C, and stirred for 70 min prior to addition of a solution of **1-38** (294 mg, 2.94 mmol) in THF (2.0 mL). The mixture was stirred for 1 h at -78 °C, and 2-cyclohexen-1-one (12 mg, 0.13 mmol) in THF (1.0 mL) was added via syringe. The mixture was stirred for 5 min, quenched with saturated aqueous NH₄Cl at -78 °C, warmed to rt, diluted with Et₂O (25 mL) and water (25 mL), and extracted with Et₂O (3 x 20). The combined organic layers were washed with brine, dried (MgSO₄), and concentrated under reduced pressure. The residue was purified by chromatography on SiO₂ (hexanes/EtOAc, 4:1) to afford **1-12** (21 mg, 78%).

The product ratios of **1-12**:**1-13** were determined by crude ^1H NMR analysis using the integration ratio of the singlet at 4.24 ppm in **1-12** and the doublet at 4.10 ppm in **1-13**. When the reaction yielded a mixture of **1-12** and **1-13**, the products were co-eluted, and the isolated yield reflects the mass of the mixture.

1-(1,3-dithian-2-yl)cyclohex-2-enol (1-12). ^1H NMR (300 MHz, CDCl_3) δ 6.00–5.92 (m, 1 H), 5.80–5.70 (m, 1 H), 4.24 (s, 1 H), 3.00–2.80 (m, 4 H), 2.33 (s, 1 H), 2.15–1.90 (m, 4 H), 1.90–1.70 (m, 4 H).

3-(1,3-dithian-2-yl)cyclohexanone (1-13). ^1H NMR (300 MHz, CDCl_3) δ 4.10 (d, $J = 4.9$ Hz, 1 H), 2.95–2.85 (m, 4 H), 2.61–2.32 (m, 4 H), 2.30–2.05 (m, 4 H), 1.95–1.80 (m, 1 H), 1.75–1.60 (m, 2 H).

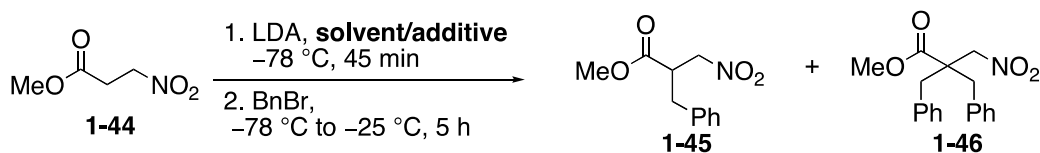


Methyl 3-nitropropanoate (1-44).^{89,90} To a solution of freshly distilled acrolein (10.0 mL, 145 mmol) and NaNO_2 (15.5 g, 225 mmol) in THF (80 mL) at 0 °C was added AcOH (10.7 mL, 186 mmol) by syringe pump over 1 h. The mixture was stirred for an additional 160 min, diluted with water (40 mL) and extracted with CH_2Cl_2 (4 x 30 mL). The combined organic layers were washed with NaHCO_3 (2 x), brine (2 x), and water, dried (MgSO_4), and concentrated *in vacuo* to afford 3-nitropropanal (7.81 g crude) as a yellow oil.

To a solution of crude 3-nitropropanal (7.81 g, 75.8 mmol), $\text{NaH}_2\text{PO}_4 \cdot \text{H}_2\text{O}$ (2.07 g, 15 mmol), and 30% H_2O_2 (6 mL) in MeCN (60 mL) and water (20 mL) was added a solution of NaClO_2 (7.68 g, 66 mmol) in H_2O (80 mL) dropwise via addition funnel at rt. The bright yellow mixture was stirred for 1 h after the addition was complete, Na_2SO_3 was added (3 g), and the mixture was stirred for 20 min. The quenched mixture was acidified with 10% aqueous HCl, diluted with water, and extracted with EtOAc (3 x 40 mL). NaCl was added to the aqueous

layer, and the aqueous layer was extracted with EtOAc (3 x 40 mL). The combined organic layers were dried (Na₂SO₄) and concentrated to afford 3-nitropropanoic acid as a white solid.

Crude 3-nitropropanoic acid was dissolved in MeOH (100 mL) and H₂SO₄ (1.8 mL). The mixture was heated at reflux overnight, cooled, and concentrated to ~1/4 volume. The mixture was dissolved in Et₂O, washed with water, dried (MgSO₄) and concentrated *in vacuo*. The residue was distilled (95 °C at 6 Torr) to afford **1-44** (2.19 g, 11%) as a colorless oil: ¹H NMR (300 MHz, CDCl₃) δ 4.67 (t, *J* = 6.0 Hz, 2 H), 3.76 (s, 3 H), 3.01 (t, *J* = 6.0 Hz, 2 H); HRMS (EI) *m/z* calc for C₄H₇NO₄ 133.0375, found 133.0376.



Representative Procedure for Dianion Solubility Studies (Table 1-19, entry 2): A flame-dried 3-necked 250-mL round-bottom flask equipped with thermometer was charged with distilled THF (3.0 mL), which was degassed by sparging with nitrogen. *i*-Pr₂NH (0.22 mL, 1.54 mmol) was added, and the solution was cooled to -72 °C (T_{int}). To this solution was added *n*-BuLi (0.670 mL, 1.54 mmol *c* = 2.23 M in hexanes), and the pale yellow solution was transferred to an ice-water bath, stirred for 20 min, and cooled back to -76 °C (T_{int}). DMPU (0.920 mL, 7.51 mmol) was added via syringe (neat), and the resulting bright yellow solution was stirred for 20 min. A solution of methyl 3-nitropropanoate (100 mg, 0.751 mmol) in THF (1.0 mL) was added dropwise via syringe. The solution was stirred between -76 °C and -70 °C for 1 h, and freshly distilled BnBr (0.12 mL, 1.0 mmol) was added slowly *via* syringe. The reaction mixture was stirred between -76 °C and -60 °C for 1 h, then gradually warmed to -25 °C over an additional hour. The reaction mixture was quenched at -25 °C with glacial AcOH (0.3 mL), followed 5 min later by water (0.5 mL). The quenched mixture was warmed to rt and diluted with Et₂O and water (30 mL each). The aqueous layer was extracted with Et₂O (3 x 20

mL), and the combined organic layers were washed with water, saturated aqueous NaHCO₃, and water, dried (MgSO₄) and concentrated. The crude residue was purified by chromatography on SiO₂ (hexanes/EtOAc, 9:1) to afford methyl 2-benzyl-3-nitropropanoate **1-45** (106 mg, 63%) as a colorless oil and methyl 2,2-dibenzyl-3-nitropropanoate **1-46** (9 mg, 4%) as a colorless oil:

Methyl 2-benzyl-3-nitropropanoate (1-45).²⁵² R_f 0.1 (hexanes/EtOAc, 9:1); ¹H NMR (300 MHz, CDCl₃) δ 7.40–7.26 (m, 2 H), 7.18–7.15 (m, 3 H), 4.68 (dd, *J* = 14.7, 9.0 Hz, 1 H), 4.37 (dd, *J* = 14.7, 4.5 Hz, 1 H), 3.75 (s, 3 H), 3.55–3.44 (m, 1 H), 3.16 (dd, *J* = 14.1, 6.0 Hz, 1 H), 2.84 (dd, *J* = 14.0, 9.0 Hz, 1 H); MS (EI) *m/z* (rel. intensity) 224 ([M+H]⁺, 8), 163 (48), 133 (41), 91 (99), 77 (58), 59 (63); HRMS (EI) *m/z* calc for C₁₁H₁₃NO₄ (M+H) 224.0923, found 224.0921.

Methyl 2,2-dibenzyl-3-nitropropanoate (1-46). R_f 0.2 (hexanes/EtOAc, 9:1); IR (ATR) 3060, 2883, 1729, 1549, 1448, 1374, 1215 cm⁻¹; ¹H NMR (300 MHz, CDCl₃) δ 7.38–7.25 (m, 6 H), 7.11–7.08 (m, 4 H), 4.39 (s, 2 H), 3.62 (s, 3 H), 3.30, 3.12 (AB, *J* = 14.0 Hz, 4 H); ¹³C NMR (75 MHz, CDCl₃) δ 172.7, 135.3, 130.0, 128.7, 127.5, 74.6, 52.1, 51.9, 40.7; MS (EI) *m/z* (rel. intensity) 313 (M⁺, 21), 282 (12), 91 (99); HRMS (EI) *m/z* calc for C₁₈H₁₉NO₄ 313.1314, found 313.1305.

Table 1-19, entry 3: Following the representative procedure, HMPA (0.670 mL, 3.79 mmol) was substituted for DMPU. After purification, **1-45** (98 mg, 58%) was isolated as a colorless oil and **1-46** (21 mg, 9%) was isolated as a colorless oil.

Table 1-19, entry 4: Following the representative procedure, dimer **1-37** (700 mg, 3.76 mmol) was substituted for DMPU. After purification, **1-45** (70 mg, 42%) was isolated as a colorless oil, and **1-46** (5 mg, 2%) was isolated as a colorless oil.

Preparation of Schwartz reagent (Cp₂Zr(H)Cl).²⁵³ To a flame-dried 2-necked 100-mL round-bottom flask was added zirconocene dichloride (5.0 g, 17 mmol) and THF (45 mL) at rt. LiAlH₄ (4.27 mL, 4.27 mmol, c = 1.0 M in Et₂O) was added dropwise via syringe pump (0.1 mL/min). The reaction mixture was stirred at rt for an additional 30 min, filtered under N₂

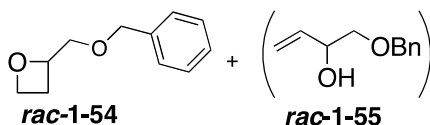
(Schlenk filtration), and washed with THF (4 x 10 mL), CH₂Cl₂ (10 mL), THF (10 mL) and Et₂O (5 mL). The product was dried in the Schlenk filter under high vacuum overnight. Schwartz reagent (3.14 g, 71%) was isolated as beige solid. The reagent was titrated by reacting 1 equiv of Schwartz reagent with 1 equiv of 1-hexyne in CH₂Cl₂ at rt and analyzing the conversion by GC analysis using the GC method described below.

General procedure for hydrozirconation kinetics experiments. Gas chromatography data were obtained on an Agilent Technologies Network GC system (6890N). Components were separated using an HP-5 5% phenyl methyl siloxane column (30.0 m length x 0.05 mm i.d.). Helium (1.0 mL/min) was used as the carrier gas. The flame ionization detector was heated to 250 °C and ignited using a mixture of compressed air (450 mL/min) and hydrogen (40 mL/min). All injections (1 µL) were performed via autosampler as split injections (split ratio 50.0:1.0). The GC oven temperature was held constant at 40 °C for 10 min.

To an oven-dried round-bottom flask under a nitrogen atmosphere was added solvent (1.0 mL) and Schwartz reagent (155 mg, 0.605 mmol, 1 equiv). The solution was stirred at rt for 1 min, cooled to 0 °C, and stirred for 4 min. 1-Hexene (0.075 mL, 0.605 mmol, 0.605M) was added. Aliquots of the reaction mixture were taken at 15–30 min intervals over 2.5 h. Each aliquot (50–100 µL) was transferred into a test tube containing water (1 mL) and Et₂O (0.5 mL). The ethereal layer was filtered through a plug of silica and analyzed by GC, employing the method described above. For each time-point, the concentration of 1-hexene was calculated based on the ratio of *n*-hexane:1-hexene in the GC trace (a calibration correlating the mole ratio of *n*-hexane:1-hexene with the area ratio of *n*-hexane:1-hexene was used). Estimated half-lives were calculated assuming a rate expression whereby the reaction is first order in 1-hexene and zeroth order in Schwartz reagent ($c = Ae^{-kt}$), and the measured half-lives are calculated by the expression $t_{1/2} = \ln(2)/k$.

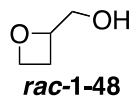


2-(Benzyloxymethyl)oxirane (rac-1-53).²⁵⁴ A solution of benzyl alcohol (25.0 mL, 242 mmol) in THF (800 mL) was cooled to 0 °C and treated with NaH (12.6 g, 314 mmol, 60% dispersion in mineral oil). The mixture was stirred for 0.5 h, and epichlorohydrin (58.0 mL, 732 mmol) was added. The solution was heated at reflux for 14 h, cooled, quenched with water, dried (MgSO₄), and filtered. The filtrate was concentrated *in vacuo*. Excess epichlorohydrin was removed by Kugelrohr distillation (60 °C at 15 Torr) and further Kugelrohr distillation (95 °C at 2.5 Torr) afforded **rac-1-53** (19.0 g, 48%) as a colorless oil: ¹H NMR (300 MHz, CDCl₃) δ 7.37–7.28 (m, 5 H), 4.62, 4.57 (AB, *J* = 11.9 Hz, 2 H), 3.78 (dd, *J* = 11.4, 3.0 Hz, 1 H), 3.45 (dd, *J* = 11.3, 5.8 Hz, 1 H), 3.23–3.18 (m, 1 H), 2.81 (app t, *J* = 4.5 Hz, 1 H), 2.63 (dd, *J* = 5.0, 2.7 Hz, 1 H); MS (EI) *m/z* (rel. intensity) 164 (M⁺, 44), 107 (86), 91 (100), 77 (262); HRMS (EI) *m/z* calc for C₁₀H₁₂O₂ 164.0837, found 164.0836.



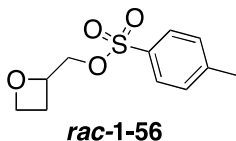
2-(Benzyloxymethyl)oxetane (rac-1-54).⁹³ A solution of *t*-BuOK (28.2 g, 244 mmol) and Me₃SOI (54.8 g, 224 mmol) in dry *t*-BuOH (350 mL) was heated at 50 °C for 1 h. A solution of 2-(benzyloxymethyl)oxirane (**rac-1-53**) (20.0 g, 122 mmol) in *t*-BuOH (150 mL) was added slowly via syringe. The reaction mixture was stirred at 50 °C for 3 d, cooled, filtered, and the solids were washed with Et₂O. *t*-BuOH was removed *in vacuo*, and the residue was dissolved in water (100 mL) and Et₂O (150 mL). The aqueous layer was extracted with Et₂O (3 x 75 mL) and the combined organic layers were washed with brine, dried (MgSO₄) and concentrated *in vacuo*. The residue was purified by chromatography on SiO₂ (pentane/Et₂O, 3:1) to afford crude **rac-1-54** (10.5 g, 48%) as a colorless oil: ¹H NMR (300 MHz, C₆D₆) δ 7.40 (d, *J* = 7.40 Hz, 2 H), 7.29–7.25 (m, 2 H), 7.25–7.16 (m, 1 H), 4.84 (ddt, *J* = 7.7, 6.7, 4.1 Hz, 1 H), 4.55, 4.50 (AB, *J* = 12.2 Hz, 2 H), 4.42 (app t, *J* = 6.8 Hz, 2 H), 3.47 (d, *J* = 4.1 Hz, 2 H), 2.34 (ddt, *J* = 14.7, 10.1,

8.0 Hz, 1 H), 2.20 (ddt, $J = 14.7, 10.8, 7.9$ Hz, 1 H); MS (EI) m/z 178 (M^+ , 41), 107 (100), 92 (70), 91 (51), 77 (60), 57 (88); HRMS (EI) m/z calc for $C_{11}H_{14}O_2$ 178.0994, found 178.0992.



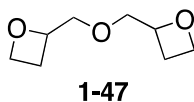
2-Oxetanemethanol (rac-1-48).⁸⁰ A solution of crude 2-(benzyloxymethyloxetane **rac-1-54** (3.79 g, 20.2 mmol) in EtOAc (200 mL) was treated with 10% Pd/C (10.8 g, 10.2 mmol).^a The solution was purged with H_2 gas (balloon), and the mixture was maintained under H_2 atmosphere. The reaction mixture was stirred for 11 h at rt, filtered through Celite, and concentrated *in vacuo*. The residue was purified by chromatography on SiO_2 (MeOH/ CH_2Cl_2 , 5:95) to afford **rac-1-48** (1.20 g, 67%) as a colorless oil: IR (ATR) 3390, 2881, 962 cm^{-1} ; 1H NMR (300 MHz, $CDCl_3$) δ 4.97–4.90 (m, 1 H), 4.74–4.66 (m, 1 H), 4.57–4.50 (m, 1 H), 3.76 (ddd, $J = 12.6, 4.9, 2.9$ Hz, 1 H), 3.61 (ddd, $J = 12.4, 8.1, 4.0$ Hz, 1 H), 2.73–2.54 (m, 2 H), 2.43 (bs, 1 H); ^{13}C NMR (75 MHz, $CDCl_3$) δ 82.8, 68.9, 65.3, 22.5; MS (EI+) m/z (rel. intensity) 88 (M^+ , 10), 57 (99); HRMS (EI) m/z calc for $C_4H_8O_2$ 88.0524, found 88.0522.

^aThe amount of Pd/C was inadvertently high (1 equiv Pd). The reaction was repeated with lower loadings of Pd/C (1–10 mol%), but the yield was consistent with that reported above (62%).

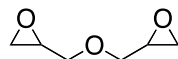


Oxetan-2-ylmethyl 4-methylbenzenesulfonate (rac-1-56).⁸⁰ A solution of TsCl (2.81 g, 14.8 mmol) in anhydrous pyridine (5.7 mL) at 0 °C was treated with 2-hydroxymethyloxetane **rac-1-48** (0.930 mL, 11.4 mmol) via syringe. The solution was stirred for 7 h at 0 °C, diluted with ice-water (15 mL), and extracted with Et_2O . The ethereal layer was washed with water (3 x) and brine, dried ($MgSO_4$) and concentrated *in vacuo*. Residual pyridine was removed from the

concentrate by addition of benzene and concentration under reduced pressure (2 x). The residue was taken up in Et₂O, filtered through neutral Al₂O₃, and concentrated under reduced pressure to afford **rac-1-56** (2.18 g, 79%) as a white solid: Mp 57.1–59.6 °C (lit.⁸⁰ 58–59 °C); IR (ATR) 2974, 1593, 1355, 1174, 941; ¹H NMR (300 MHz, CDCl₃) δ 7.83 (d, *J* = 8.2 Hz, 2 H), 7.36 (d, *J* = 8.1 Hz, 2 H), 4.97–4.89 (m, 1 H), 4.65–4.57 (m, 1 H), 4.55–4.48 (m, 1 H), 4.16 (d, *J* = 3.8 Hz, 2 H), 2.77–2.66 (m, 1 H), 2.63–2.52 (m, 1 H), 2.46 (s, 3 H); ¹³C NMR (75 MHz, CDCl₃) δ 144.9, 132.8, 129.9, 128.0, 78.6, 71.9, 69.0, 23.4, 21.7; MS (EI) *m/z* (rel. intensity) 243 (M⁺, 52), 173 (82), 155 (50), 119 (100), 63 (92); HRMS (EI+) *m/z* calc for C₁₁H₁₅O₄S (M+H) 243.0691, found 243.0690.



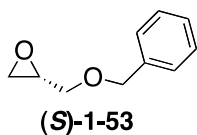
2,2'-Oxybis(methylene)dioxetane (1-47). A solution of alcohol **rac-1-48** (0.65 mL, 7.9 mmol) in THF (30 mL) was treated with NaH (260 mg, 10.3 mmol, 95%) at 0 °C. The mixture was stirred for 0.5 h at 0 °C, and a solution of tosylate **rac-1-56** (2.3 g, 9.5 mmol) in THF (15 mL) was added slowly via syringe. The reaction mixture was stirred at 50 °C for 10 h and heated at reflux for an additional 4 h. The solution was filtered and concentrated *in vacuo*, and the residue was purified by chromatography on SiO₂ (hexanes/EtOAc, 1:1 to 100% EtOAc). Fractions containing the desired product were further purified by Kugelrohr distillation (80 °C < T < 100 °C at 2.5 Torr) to afford **1-47** (618 mg, 49%) (mixture of *dl*- and meso- diastereomers) as a colorless oil: IR (ATR) 2993, 2877, 1448, 1110, 971, 949, 855 cm⁻¹; ¹H NMR (300 MHz, CDCl₃) δ 4.89–4.89 (m, 2 H), 4.66–4.59 (m, 2 H), 4.57–4.49 (m, 2 H), 3.77–3.62 (m, 4 H), 2.69–2.47 (m, 4 H); ¹³C NMR (125 MHz, CDCl₃) δ 81.3, 75.0, 74.8, 68.9, 23.6; MS (EI) *m/z* (rel. intensity) 159 (M⁺, 22), 128 (68), 88 (100), 71 (91), 57 (90); HRMS (EI) *m/z* calc for C₈H₁₅O₃ 159.1021, found 159.1020.



1-58

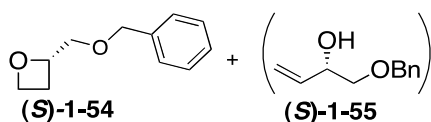
2,2' Oxybis(methylene)dioxirane (1-58). A solution of allyl glycidyl ether (7.1 g, 62 mmol) in CH₂Cl₂ (20 mL) was treated with a solution of *m*-CPBA (23.0 g, 93.3 mmol) in CH₂Cl₂ (120 mL), which was added dropwise via addition funnel. The white slurry was stirred for 23 h and quenched with 1 M aqueous Na₂S₂O₃ (100 mL). The aqueous layer was extracted with CH₂Cl₂ (2 x), and the combined organic layers were washed with 0.5 M aqueous NaOH, dried, and concentrated under reduced pressure. Residual allyl glycidyl ether (1.2 g) was removed via Kugelrohr distillation to afford **1-58** (4.9 g, 60%; 75% BRSM) as a colorless oil: ¹H NMR 3.85 (ddd, *J* = 16.0, 11.6, 2.8 Hz, 2 H), 3.45 (ddd, *J* = 21.0, 11.6, 6.0 Hz, 2 H), 3.22–3.15 (m, 2 H), 2.83–2.80 (m, 2 H), 2.66–2.61 (m, 2 H). HRMS (EI+) *m/z* calc for C₆H₁₀O₃ 130.0630, found 130.0631.

Attempted formation of 1-47 via double methylene transfer to 1-58. A solution of Me₃SOI (13.8 g, 61.5 mmol) and *t*-BuOK (7.11 g, 61.5 mmol) in *t*-BuOH (75 mL) was heated at 50 °C for 1 h. A solution of diglycidyl ether **1-58** (2.0 g, 15 mmol) in 25 mL *t*-BuOH was added via syringe. The reaction mixture was stirred at 50 °C for 20 h (an aliquot was taken to ascertain starting material consumption by ¹H NMR analysis). The mixture was cooled to rt and *t*-BuOH was removed *in vacuo*. The concentrate was diluted with water (200 mL) and CH₂Cl₂ (200 mL), and the aqueous layer was extracted with CH₂Cl₂ (3 x 100 mL). The combined organic layers were washed with brine (twice), dried (MgSO₄) and concentrated *in vacuo*. The crude mixture (1.5 g) was subjected to Kugelrohr distillation at 3 Torr to afford several fractions of colorless oil (at 20 °C increments starting at 60 °C to 100 °C). Each fraction contained a mixture of olefinic and oxetane peaks (¹H NMR analysis), and the distillate fractions were combined and subjected to chromatography on SiO₂ (hexanes/EtOAc, 4:1). No pure dimer **1-47** could be obtained from these mixtures.

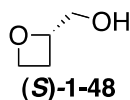


(S)-Benzyl glycidyl ether ((S)-1-53).²⁵⁵ A solution of (*R,R*)-salenCo(III)OAc (605 mg, 0.910 mmol) in neat benzyl glycidyl ether (30.1 g, 183 mmol) was cooled to 0 °C. Water (1.8 mL, 100 mmol) was added dropwise over 20 min. The reaction mixture was warmed to rt and stirred for 4.5 h. The mixture was diluted with EtOAc (250 mL) and dried (Na₂SO₄) overnight. The drying agent was filtered, and the solvent was concentrated to afford a brown liquid that was purified by chromatography on SiO₂ (hexanes/EtOAc, 9:1 to 100% EtOAc) to afford partially purified (*S*)-benzyl glycidyl ether (eluted in 9:1), which was subsequently purified by Kugelrohr distillation (75 °C < T < 85 °C at 10–11 Torr) to afford (*S*)-benzyl glycidyl ether (13.40 g, 45%) as a colorless oil. The enantiomeric excess was determined to be 99% by chiral HPLC analysis (Chiralcel OD, 2% isopropanol/hexanes, 1.0 mL/min, 220 nm) *t*_r(major) = 12.0 min, *t*_r(minor) = 14.7 min: [α]_D 15.0 (neat); ¹H NMR (300 MHz, CDCl₃) δ 7.37–7.27 (m, 5 H), 4.63, 4.58 (AB, *J* = 12.0 Hz, 2 H), 3.79 (dd, *J* = 11.4, 3.0 Hz, 1 H), 3.45 (dd, *J* = 11.4, 5.9 Hz, 1 H), 3.23–3.18 (m, 1 H), 2.82 (t, *J* = 4.5 Hz, 1 H), 2.64 (dd, *J* = 5.0, 2.7 Hz, 1 H).

Alternative Preparation of (S)-Benzyl glycidyl ether ((S)-1-53). A slurry of NaH (3.12 g, 78. mmol, 60% in mineral oil) and BnBr (19.0 mL, 159 mmol) in anhydrous DMF (120 mL) was cooled to 0 °C and stirred for 30 min. To this solution was added (*R*)-glycidol (4.0 mL, 58 mmol) dropwise via syringe. The reaction mixture was stirred for 5 h at rt, and the mixture was poured into a separatory funnel containing saturated aqueous NH₄Cl (10 mL) and EtOAc (30 mL). The organic layer was washed with 5% aqueous NaHCO₃ and water, and the combined aqueous layers were extracted with EtOAc (4 x 10 mL). The combined organic layers were dried (Na₂SO₄) and concentrated. The residue was purified by chromatography on SiO₂ hexanes/EtOAc, 9:1) to afford (*S*)-benzyl glycidyl ether (6.98 g, 73%) as a colorless oil.

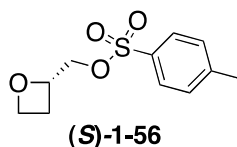


(S)-2-(Benzyloxymethyl)oxetane ((S)-1-54). A solution of *t*-BuOK (17.7 g, 158 mmol) and Me₃SOI (34.9 g, 158 mmol) in *t*-BuOH (250 mL) was heated to 50 °C (T_{int}). The solution was stirred for 1 h at 50 °C. A solution of (*S*)-(+)-benzyl glycidyl ether (13.0 g, 79.2 mmol) in *t*-BuOH (100 mL) was added via addition funnel over a period of 90 min. The foamy white reaction mixture was stirred at 50 °C for 90 h, cooled to rt, and diluted with water (350 mL) and Et₂O (300 mL). The aqueous layer was extracted with Et₂O (3 x 200 mL), and the combined organic layers were washed with brine, dried (Na₂SO₄), and concentrated *in vacuo*. The crude residue was purified by chromatography on SiO₂ (hexanes/EtOAc, 4:1) to afford crude (*S*)-2-(benzyloxymethyl)oxetane **(S)-1-54** (7.79 g, 55%) as a pale yellow oil: ¹H NMR (300 MHz, CDCl₃) δ 7.40–7.28 (m, 5 H), 5.03–4.95 (m, 1 H), 4.72–4.56 (m, 4 H), 3.65 (dddd, *J* = 15.7, 11.0, 11.0, 4.8 Hz, 2 H), 2.73–2.53 (m, 2 H).

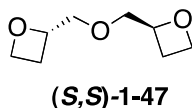


(S)-Oxetan-2-ylmethanol ((S)-1-48). A solution of crude **(S)-1-54** (7.00 g, 39.3 mmol) in EtOAc (350 mL) was treated with 10% Pd/C (2.09 g, 1.96 mmol) and exposed to H₂ at 1 atm (balloon). The mixture was stirred for 5 h at rt, and the mixture was filtered through a plug of Celite and washed with EtOAc and MeOH. The solvent was removed *in vacuo*, and the residue was purified by chromatography on SiO₂ (MeOH/CH₂Cl₂, 5:95) to afford (*S*)-oxetan-2-ylmethanol (1.98 g, 57%) as a colorless oil: [α]_D + 7.1 (*c* = 5.0, CDCl₃)^a; ¹H NMR (300 MHz, CDCl₃) δ 4.97–4.90 (m, 1 H), 4.70 (ddd, *J* = 8.4, 7.6, 5.9 Hz, 1 H), 4.53 (ddd, *J* = 9.0, 6.0, 6.0 Hz, 1 H), 3.76 (ddd, *J* = 12.5, 4.6, 2.9 Hz, 1 H), 3.64 (ddd, *J* = 12.1, 7.8, 3.9 Hz, 1 H), 2.73–2.54 (m, 2 H), 2.45 (bs, 1 H).

^aThe optical rotation of a separate sample of **(S)-1-48** was measured: [α]_D + 8.6 (*c* = 5.8, CH₂Cl₂).

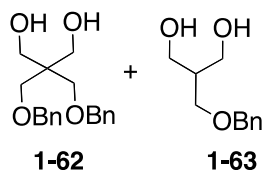


(S)-Oxetan-2-ylmethyl 4-methylbenzenesulfonate (S-1-56). A solution of TsCl (2.81 g, 14.7 mmol) in anhydrous pyridine (5.7 mL) was cooled to 0 °C. (S)-Oxetan-2-ylmethanol (**(S)-1-48**) (0.93 mL, 11. mmol) was added (neat) dropwise via syringe. The mixture was stirred for 5 h, gradually warming to rt, and poured into a flask containing ice-water. The aqueous mixture was extracted with Et₂O, and the ethereal portion was washed with water and brine, dried, and concentrated *in vacuo*. To the residue was added benzene, and the residue/benzene was concentrated (twice). The residue was filtered through neutral Al₂O₃ and used without further purification. (S)-oxetan-2-ylmethyl 4-methylbenzenesulfonate (**(S)-1-56**) (1.97 g, 72%) was isolated as a colorless oil which solidified upon standing: ¹H NMR (300 MHz, CDCl₃) δ 7.83 (d, *J* = 8.4 Hz, 2 H), 7.36 (d, *J* = 8.0 Hz, 2 H), 4.97–4.89 (m, 1 H), 4.61 (ddd, *J* = 8.6, 7.1, 5.8 Hz, 1 H), 4.51 (ddd, *J* = 12.2, 9.0, 9.0 Hz, 1 H), 4.16 (d, *J* = 3.9 Hz, 2 H), 2.78–2.66 (m, 1 H), 2.63–2.52 (m, 1 H), 2.46 (s, 3 H); MS (EI) *m/z* (rel. intensity) 242 (M⁺, 17), 172 (16), 156 (72), 155 (56), 91 (89); HRMS (EI) *m/z* calc for C₁₁H₁₄O₄S 242.0613, found 242.0620.



(2S,2'S)-2,2'-oxybis(methylene)dioxetane ((S,S)-1-47). A slurry of NaH (156 mg, 6.18 mmol, 95%) and (**(S)-1-56**) (1.28 g, 5.27 mmol) in anhydrous MeCN (43 mL) was treated with (**(S)-1-48**) (0.350 mL, 4.29 mmol) at 0 °C (dropwise). The solution was warmed to rt over a period of 30 min and subsequently heated at reflux for 27 h. The solution was cooled to 0 °C and quenched by dropwise addition of water. The mixture was dried (MgSO₄), filtered, and the solvent was removed *in vacuo*. The residue was purified by chromatography on SiO₂ (100%

EtOAc), and the isolated residue was further purified by Kugelrohr distillation (75 °C < T < 95 °C at 15 Torr) to afford (2*S*, 2'*S*)-2,2'-oxybis(methylene)dioxetane (**(*S,S*)-1-47**) (390 mg, 57%) as a colorless oil: $[\alpha]_D -5.8$ ($c = 5.1$, CDCl_3); IR (ATR) 2876, 1109, 973, 949 cm^{-1} ; $^1\text{H NMR}$ (500 MHz, CDCl_3) δ 4.99–4.95 (m, 2 H), 4.69–4.64 (m, 2 H), 4.60–4.54 (m, 2 H), 3.84–3.76 (m, 2 H), 3.70–3.62 (m, 2 H), 2.70–2.56 (m, 4 H); $^{13}\text{C NMR}$ (125 MHz, CDCl_3) δ 81.3, 74.9, 68.9, 23.7; HRMS (EI) m/z calc for $\text{C}_8\text{H}_{14}\text{O}_3$ (M+H) 159.1021, found 159.1020.



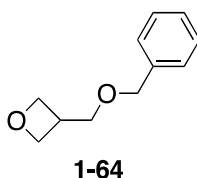
2-(Benzyloxymethyl)propane-1,3-diol (1-63) and 2,2-bis(benzyloxymethyl)propane-1,3-diol (1-62).^{73,256} To a solution of diethyl malonate (18.5 mL, 121 mmol) in THF (200 mL) at 0 °C was added NaH (4.83 g, 120.8 mmol, 60% dispersion in mineral oil). The solution was stirred at 0 °C for 20 min, warmed to rt, and stirred for an additional 30 min. Benzyl chloromethyl ether (10.0 mL, 50.3 mmol, ~70%) was added via syringe pump (0.1 mL/min). After the addition was complete, the reaction mixture was stirred for an additional 10 h at rt, quenched at 0 °C by dropwise addition of H_2O , dried (MgSO_4), and filtered. Most of the solvent was removed *in vacuo*. The concentrate was diluted with EtOAc (150 mL) and water (100 mL), and the aqueous portion was extracted with EtOAc (3 x 50 mL). The combined organic layers were washed with water and brine, dried (MgSO_4) and concentrated *in vacuo*. Excess diethyl malonate was removed via Kugelrohr distillation (90 °C < T < 110 °C at 3 Torr).

The crude mixture was dissolved in Et_2O (60 mL) and added to a solution of LAH (27.7 mL, 111 mmol, $c = 4.0$ M in Et_2O) in Et_2O (200 mL) via syringe pump at 0 °C (0.10 mL/min). The reaction mixture was warmed to rt, stirred for 12 h, and quenched at 0 °C by sequential addition of water (4.2 mL), 15% aqueous NaOH (4.2 mL), and water (12.6 mL). The slurry was stirred for 0.5 h, and the resultant solid was filtered and washed with Et_2O and EtOAc. The

filtrate was concentrated *in vacuo*, and the residue was purified by chromatography on SiO₂ (hexanes/EtOAc, 1:1 to EtOAc, 100%) to afford **1-63** (2.33 g, 24%) and **1-62** (353 mg, 2%).

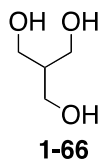
1-63. Obtained as a white solid: R_f 0.3 (100% EtOAc); Mp 41.2–43.1 °C (hexanes/EtOAc); IR (ATR) 3321, 3252, 2855, 1726, 1452, 1366, 1092, 1028 cm⁻¹; ¹H NMR (300 MHz, CDCl₃) δ 7.37–7.32 (m, 5 H), 4.54 (s, 2 H), 3.84 (t, *J* = 5.0 Hz, 4H), 3.66 (d, *J* = 5.5 Hz, 2 H), 2.16 (t, *J* = 5.2 Hz, 2 H), 2.07 (sept, *J* = 5.5 Hz, 1 H); ¹³C NMR (75 MHz, CDCl₃) δ 137.8, 128.5, 127.8, 127.6, 73.5, 70.5, 63.3, 42.7; MS (EI) *m/z* (rel. intensity) 197 (M⁺, 8), 196 (M⁺, 14), 178 (13), 177 (18), 120 (38), 108 (66), 92 (100), 79 (83), 65 (83), 57 (79); HRMS (EI) *m/z* calc for C₁₁H₁₆O₃ 196.1099, found 196.1103.

1-62. Obtained as a white solid: R_f 0.6 (100% EtOAc); Mp 69.1–70.8 °C (hexanes/EtOAc) (lit.²⁵⁶ 72–73 °C); IR (ATR) 3284, 2982, 1452, 1116, 1028, 731 cm⁻¹; ¹H NMR (300 MHz, CDCl₃) δ 7.39–7.31 (m, 10 H), 4.51 (s, 4 H), 3.70 (d, *J* = 6.0 Hz, 4 H), 3.58 (s, 4 H), 2.55 (t, *J* = 6.3 Hz, 2 H); ¹³C NMR (75 MHz, CDCl₃) δ 137.8, 128.5, 127.8, 127.6, 73.7, 72.1, 65.1, 44.9; MS (API-ES) *m/z* (rel. intensity) 339 (100).

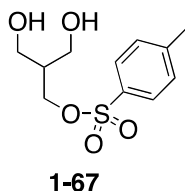


3-(Benzyloxymethyl)oxetane (1-64). A solution of diol **1-63** (1.31 g, 6.67 mmol) in dry THF (16.5 mL) was treated with *n*-BuLi (4.87 mL, 6.68 mmol, *c* = 1.37 M in hexanes). The solution was stirred for 0.5 h at 0 °C, and a solution of TsCl (1.30 g, 6.67 mmol) in dry THF (2.5 mL) was added slowly via syringe. The reaction mixture was stirred for 1 h and subsequently treated with *n*-BuLi (4.87 mL, 6.68 mmol, *c* = 1.37 M in hexanes), stirred at rt for 1 h, and heated at reflux for 15 h. The mixture was cooled, and the majority of the THF was removed *in vacuo*. The concentrate was diluted with water and Et₂O, and the aqueous portion was extracted with

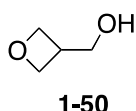
Et₂O (3 x 30 mL). The combined organic layers were washed with water and brine, dried (MgSO₄) and concentrated *in vacuo*. The residue was purified by chromatography on SiO₂ (hexanes/EtOAc, 3:1) to afford **1-64** (542 mg, 45%) as a colorless oil: R_f 0.2 (hexanes/EtOAc, 3:1); IR (ATR) 2954, 2861, 1448, 1377, 1107, 975, 936 cm⁻¹; ¹H NMR (300 MHz, CDCl₃) δ 7.40–7.28 (m, 5 H), 4.81 (dd, *J* = 7.8, 6.2 Hz), 4.56 (s, 2 H), 4.46 (t, *J* = 6.0 Hz, 2 H), 3.72 (d, *J* = 6.9 Hz, 2 H), 3.33–3.19 (m, 1 H); ¹³C NMR (300 MHz, CDCl₃) δ 138.0, 128.4, 127.7, 127.6, 74.7, 73.3, 71.8, 34.9; MS (EI) *m/z* (rel. intensity) 178 (M⁺, 12), 120 (100), 107 (66), 91 (86); HRMS (EI) *m/z* calc for C₁₁H₁₄O₂ 178.0994, found 178.0991.



2-(Hydroxymethyl)propane-1,3-diol (1-66).⁹⁵ To a solution of triethyl methanetricarboxylate (27.0 mL, 125 mmol) in degassed THF (200 mL) was added BH₃•Me₂S (40.3 mL, 399 mmol). The reaction mixture was heated at reflux for 8 h, cooled, and MeOH (170 mL) was added dropwise by addition funnel. After gas evolution had ceased, the solvent was removed *in vacuo*, and the crude residue was dissolved in MeOH (500 mL) and stirred for 12 h at rt. MeOH was removed under reduced pressure and the concentrate was purified by chromatography on SiO₂ (CHCl₃/MeOH, 5:1 to 3:1) to afford a yellow oil which was subsequently recrystallized from THF to afford **1-66** (8.61 g, 65%) as a white solid: ¹H NMR (300 MHz, DMSO-d₆) δ 4.28 (t, *J* = 5.2 Hz, 3 H), 3.39 (t, *J* = 5.6, 6H), 1.59 (sept, *J* = 5.9 Hz, 1 H); MS (EI) *m/z* (rel. intensity) 107 (M⁺, 23), 70 (47), 58 (97); HRMS (EI+) calc for C₄H₁₁O₃ 107.0708, found 107.0709.

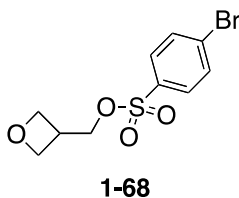


3-Hydroxy-2-(hydroxymethyl)propyl 4-methylbenzenesulfonate (1-67). A solution of **1-66** (8.01 g, 75.5 mmol) in THF (440 mL) was treated with NaH (2.00 g, 79.3 mmol, 95%) at 0 °C and stirred for 0.5 h. A solution of TsCl (14.4 g, 75.5 mmol) in THF (60 mL) was added via syringe pump (0.25 mL/min). After the addition was complete, the mixture was quenched by dropwise addition of water, dried (MgSO₄), filtered and concentrated *in vacuo*. The crude residue was purified by chromatography on SiO₂ (CH₂Cl₂/acetone, 9:1) to afford **1-67** (7.43 g, 38%) as a pale brown oil: IR (ATR) 3563, 3496, 2950, 1705, 1351, 1170, 960, 811 cm⁻¹; ¹H NMR (300 MHz, CDCl₃) δ 7.80 (d, *J* = 8.3 Hz, 2 H), 7.37 d, *J* = 8.1 Hz, 2 H), 4.19 (d, *J* = 6.2 Hz, 2 H), 3.78 (d, *J* = 4.8 Hz, 4 H), 2.46 (s, 3 H), 2.25–2.02 (m, 3 H); ¹³C NMR (75 MHz, CDCl₃) δ 145.1, 132.6, 130.0, 127.9, 68.4, 61.6, 42.2, 21.6; MS (EI) *m/z* (rel. intensity) 260 (M⁺, 22), 173 (84), 155 (40), 91 (100) 65 (70), 58 (96); HRMS (EI) *m/z* calc for C₁₁H₁₆O₅S 260.0718, found 260.0718.

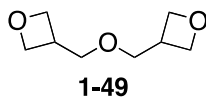


Oxetane-3-ylmethanol (1-50). Via cyclization of 1-67: A solution of monotosylate **1-67** (6.0 g, 23 mmol) in THF (30 mL) was added dropwise to a solution of *t*-BuOK (3.92 g, 34.9 mmol) in THF (430 mL) over 1 h. The mixture was stirred for an additional 10 min and quenched with water, dried (MgSO₄), filtered, and concentrated *in vacuo*. The residue was purified via Kugelrohr distillation (80 °C < T < 90 °C) to afford **1-50** (860 mg, 42%).

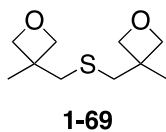
Via deprotection of 1-64: A solution of **1-64** (498 mg, 2.79 mmol) in EtOAc (28 mL) was treated with 10% Pd/C (1.5 g, 0.14 mmol). H₂ (balloon) was drawn into solution via vacuum, and the mixture was maintained under a H₂ atmosphere for 10 h at rt. The solution was filtered through a short pad of neutral Al₂O₃, and EtOAc was evaporated under reduced pressure. The residue was purified by chromatography on SiO₂ (10% MeOH/CH₂Cl₂) to afford crude **1-64** (158 mg, 64%): ¹H NMR (300 MHz, CDCl₃) δ 4.83 (dd, *J* = 7.7, 6.2 Hz, 2 H), 4.49 (t, *J* = 5.9 Hz, 2 H), 3.91 (d, *J* = 6.6 Hz, 2 H), 3.24–3.10 (m, 1 H), 1.66 (bs, 1 H); MS (EI) *m/z* (rel. intensity) 88 (M⁺, 17), 71 (5), 58 (90), 57 (100); HRMS (EI) *m/z* calc for C₄H₈O₂ 88.0524, found 88.0521.



Oxetane-3-ylmethyl-4-bromobenzenesulfonate (1-68). A solution of BsCl (2.22 g, 8.50 mmol) in anhydrous pyridine (3.0 mL) at 0 °C was treated with alcohol **1-50** (515 mg, 5.80 mmol) (the alcohol was massed in a pre-weighed syringe). The mixture was stirred for 2 h at 0 °C and subsequently poured into ice-water (15 mL) and extracted with Et₂O (3 x). The combined organic layers were washed with water (3 x), brine, dried (MgSO₄), and concentrated *in vacuo*. Residual pyridine was removed by coevaporation with benzene (2 x). The residue was dissolved in EtOAc, filtered through neutral Al₂O₃, and concentrated to afford **1-68** (930 mg, 52%) as a white solid: Mp 76.8–78.6 °C; IR (ATR) 2943, 2877, 1573, 1357, 1185, 1174, 958, 928 cm⁻¹; ¹H NMR (300 MHz, CDCl₃) δ 7.82–7.71 (m, 4 H), 4.78 (dd, *J* = 7.7, 6.6 Hz, 2 H), 4.36 (t, *J* = 5.9 Hz, 2 H), 4.31 (d, *J* = 7.0 Hz, 2 H), 3.39–3.25 (m, 1 H); ¹³C NMR (75 MHz, CDCl₃) δ 134.7, 132.7, 129.3, 73.2, 71.1, 34.0; MS (EI) *m/z* (rel. intensity) 307 (M⁺, 65), 219 (185), 157 (98), 76 (91), 70 (96), 57 (77); HRMS (EI) *m/z* calc for C₁₀H₁₂O₄SBr 306.9640, found 306.9636.



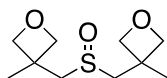
3,3'-Oxybis(methylene)dioxetane (1-49). A solution of alcohol **1-50** (150 mg, 1.70 mmol) in THF (15 mL) at 0 °C was treated with NaH (47 mg, 1.9 mmol, 95%) followed by a solution of brosylate **1-68** (627 mg, 2.04 mmol) in THF (2 mL). The mixture was heated at reflux for 20 h, cooled to rt, quenched by dropwise addition of water, dried (MgSO₄), filtered, and concentrated *in vacuo*. The residue was purified by chromatography on SiO₂ (CH₂Cl₂/acetone, 9:1) to afford **1-49** (77 mg, 28%) as a yellow oil: IR (ATR) 2932, 2866, 947, 973, cm⁻¹; ¹H NMR (300 MHz, CDCl₃) δ 4.77 (dd, *J* = 7.7, 6.2 Hz, 2 H), 4.41 (t, *J* = 5.9 Hz, 2 H), 3.68 (d, *J* = 6.9 Hz, 2 H), 3.26–3.13 (m, 1 H); ¹³C NMR (75 MHz, CDCl₃) δ 74.4, 72.7, 34.7; MS (EI) *m/z* (rel. intensity) 159 (M⁺, 13), 131 (49), 88 (49), 71 (85), 57 (99); HRMS (EI) *m/z* calc for C₈H₁₅O₃ (M+H) 159.1021, found 159.1028.



Optimized procedure for scale-up of bis((3-methyloxetan-3-yl)methyl)sulfane (1-69). A 2-necked 1-L round-bottom flask equipped with internal thermometer and maintained under Ar atmosphere was charged with acetonitrile (1 L, degassed by sparging with Ar) and 3-tosyloxymethyl-3-methyl-oxetane **1-40** (108 g, 421 mmol) (added portion-wise). A solution of Na₂S•9H₂O (59.0 g, 240 mmol) in degassed water (100 mL) was added slowly via addition funnel (over ~10 min). The mixture was heated to 70 °C over a period of 45 min and then maintained at 70 °C for 75 min.

The mixture was cooled to rt and concentrated *in vacuo* to ~1/4 volume. Water (500 mL) and EtOAc (700 mL) were added, the layers were separated, and the aqueous layer was extracted

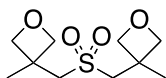
with EtOAc (3 x 500 mL). The combined organic layers were washed with brine, dried (Na₂SO₄), and concentrated *in vacuo*. The residue was taken up in EtOAc (200 mL) and washed with water (2 x 50 mL) and brine (2 x 50 mL), diluted with more EtOAc (200 mL) and dried (Na₂SO₄). The solution was filtered and concentrated *in vacuo*, and the crude mixture was purified by Kugelrohr distillation (100-mL bulbs). The fraction distilling at 8 Torr and T < 100 °C was discarded; the product was collected at 1–2 Torr and 120 °C to afford **3** (33.2 g, 78%) as a yellow-green oil: IR (ATR) 2925, 2860, 973, 830 cm⁻¹; ¹H NMR (300 MHz, CDCl₃) δ 4.48 (d, *J* = 5.9 Hz, 4 H), 4.39 (d, *J* = 5.9 Hz, 4 H), 2.93 (s, 4 H), 1.39 (s, 6 H); ¹³C NMR (100 MHz, CDCl₃) δ 81.7, 43.6, 40.2, 22.9; HRMS (ESI) *m/z* calc for C₁₀H₁₉O₂S (M+H) 203.1106, found 203.1109.



1-70 (MMS350)

MMS350: 3,3'-sulfinylbis(methylene)bis(3-methyloxetane) (1-70). A 2-L 3-necked round-bottom flask outfitted with a mechanical stirrer was charged with a solution of **1-69** (29.7 g, 147 mmol) in MeOH (700 mL). The solution was cooled to 0 °C, and a solution of NaIO₄ (31.4 g, 147 mmol) in water (360 mL) was added via addition funnel over 1 h. The mixture was warmed to rt and stirred for 18 h. The mixture was filtered through a coarse fritted filter, and the white precipitate was washed with MeOH (~200 mL). The combined filtrate and washings were concentrated *in vacuo*. Toluene (~500 mL, added in two portions) was added to remove residual water. CH₂Cl₂ (800 mL) was added to the residue, followed by MgSO₄. The mixture was filtered, and the filtrate was concentrated *in vacuo* to afford crude **MMS350** (30.6 g) as a yellow-tinted solid. To the flask containing the crude solid was added toluene (480 mL), and the slurry was heated to 60 °C to affect complete dissolution. Decolorizing carbon was added, and the mixture was filtered (gravity, Whatman #1 filter paper) into a 1-L Erlenmeyer flask. Distilled hexanes (120 mL) was added (until slight cloudiness was observed), and the suspension was allowed to stand overnight. The crystals were filtered (Buchner funnel, aspirator, Whatman #1

filter paper) to afford MMS350 (crop 1, 14.7 g) as white needles. The mother liquor was concentrated *in vacuo*, and the residue was recrystallized from toluene/hexanes to afford additional **MMS350** (9.2 g) for a combined yield of **MMS350** (23.9 g, 75%) as white needles: Mp 94.5–96.5 °C (toluene/hexanes); IR (ATR) 2938, 2861, 1456, 1381, 1025, 969 cm⁻¹; ¹H NMR (400 MHz, CDCl₃) δ 4.78 (d, *J* = 6.4 Hz, 2 H), 4.59 (d, *J* = 6.0 Hz, 2 H), 4.47 (d, *J* = 6.0 Hz, 2 H), 4.42 (d, *J* = 6.4 Hz, 2 H), 3.36 (d, *J* = 12.9 Hz, 2 H), 2.72 (d, *J* = 12.9 Hz, 2 H), 1.59 (s, 6 H); ¹³C NMR (100 MHz, CDCl₃) δ 82.3, 81.9, 61.7, 38.3, 23.4; HRMS (ESI) *m/z* calc for C₁₀H₁₉O₃S (M+H) 219.1055, found 219.1043.

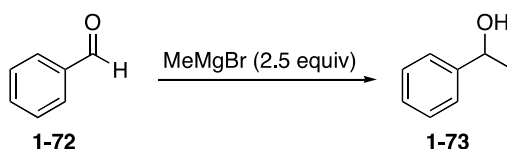


1-71

3,3'-Sulfonylbis(methylene)bis(3-methyloxetane) (1-71). A suspension of oxone (650 mg, 1.06 mmol) in water (2.0 mL) was cooled to 10 °C and treated (dropwise) with a solution of **1-69** (108 mg, 0.533 mmol) in MeOH (2.0 mL). The solution was warmed to rt and stirred for 1 h. MeOH was removed *in vacuo*, and the aqueous layer was diluted with water (5 mL) and extracted with CH₂Cl₂ (4 x 10 mL). The combined organic layers were washed with brine (5 mL), dried (MgSO₄), and concentrated *in vacuo* to afford **1-71** (120 mg, 96%) as a white solid: Mp 93.4–95.1 °C; IR (ATR) 2949, 2867, 1456, 1301, 1277, 967 cm⁻¹; ¹H NMR (400 MHz, CDCl₃) δ 4.68 (d, *J* = 6.4 Hz, 4 H), 4.46 (d, *J* = 6.4 Hz, 4 H), 3.43 (s, 4 H), 1.69 (s, 6 H); ¹³C NMR (100 MHz, CDCl₃) δ 82.2, 62.6, 37.9, 23.3; HRMS (APCI) *m/z* calc for C₁₀H₁₉O₄S (M+H) 235.1004, found 235.1032.

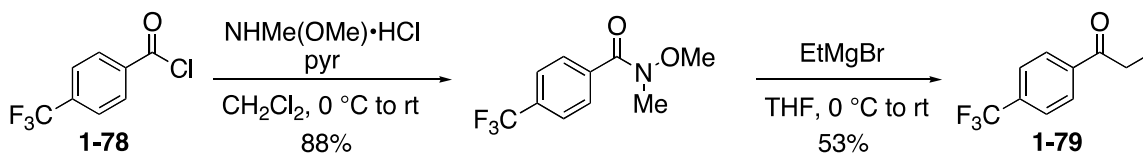
Alternatively, sulfone **1-71** can be prepared by oxidation of sulfoxide **1-70** (MMS350). A suspension of oxone (3.10 g, 5.04 mmol) in deionized water (20 mL) was cooled to *ca.* 10 °C and treated (dropwise) with a solution of MMS350 (1.10 g, 5.04 mmol) in MeOH (20 mL). The solution was warmed to rt and stirred for 2 h. MeOH was removed *in vacuo*, and the remaining suspension was diluted with water (30 mL) and CH₂Cl₂ (80 mL), and the aqueous layer was

extracted with CH₂Cl₂ (4 x 40 mL). The combined organic layers were washed with water (20 mL) and brine (20 mL), dried (MgSO₄), and concentrated *in vacuo* to afford **1-71** (1.08 g); the material was taken up in CH₂Cl₂ and filtered through a short plug of SiO₂, flushing with CH₂Cl₂ and 5% MeOH/CH₂Cl₂ to afford the **1-71** (1.05 g, 89%) as a white solid.



Representative procedure for additions of MeMgBr to benzaldehyde (Table 1-23 entry 6). A flame-dried Schlenk tube equipped with an internal thermometer was charged with a 4:1 solution of sulfide **1-69** and heptane (1.00 mL). To the solution was added freshly distilled PhCHO (10.0 μ L, 0.0985 mmol), and the solution was placed in an ice-water bath and cooled to 0 °C. MeMgBr (0.11 mL, 0.25 mmol, c = 2.30 M in Et₂O) was added slowly *via* syringe. The mixture was stirred for 25 min at 0 °C and warmed gradually to rt. The turbid reaction mixture was stirred for 90 min at rt, quenched with saturated aqueous NH₄Cl (1 mL) and water (1 mL), and diluted with water (2 mL) and Et₂O (10 mL). The layers were separated, and the aqueous layer was extracted with Et₂O (3 x 5 mL), washed with water and brine, dried (MgSO₄) and concentrated *in vacuo*. The concentrate was diluted with 5.0 mL ether, and an aliquot (~200 μ L) was analyzed by GC. The ratio of benzaldehyde to 1-phenylethanol refers to the relative areas of benzaldehyde and 1-phenylethanol. Gas chromatography data were obtained on an Agilent Technologies Network GC system (6890N). Components were separated using an Alltech Econo-CapTM ECTM-1 column (30 in length x 0.32 mm i.d.), t(benzaldehyde) = 4.57 min and t(1-phenylethanol) = 5.49 min. Helium (1.0 mL/min) was used as the carrier gas. The flame ionization detector was heated to 250 °C and ignited using a mixture of compressed air (450 mL/min) and hydrogen (40 mL/min) with a makeup gas of helium (50 mL/min). All injections (1 μ L) were performed *via* autosampler as split injections (split ratio 50.0:1.0). The GC oven temperature was started at 90 °C and ramped at 10 °C/min to 220 °C and held at 220 °C for 5

min. For runs containing high boiling materials such as 15-crown-5, the run was held at 220 °C for 20 min.



Synthesis of 1-(4-(trifluoromethyl)phenyl)propan-1-one (1-79) as a GC standard:

***N*-methoxy-*N*-methyl-4-(trifluoromethyl)benzamide.** A slurry of *p*-trifluorobenzoyl chloride (0.180 mL, 252 mg, 1.21 mmol) and Weinreb amine-HCl (118 mg, 1.21 mmol) in CH_2Cl_2 (8 mL) was cooled to 0 °C and treated with pyridine (0.220 mL, 2.72 mmol). The mixture was stirred for 30 min at 0 °C and then for 1 h at rt. To the mixture was added 1 M aqueous HCl (3 mL), and water (15 mL), and the aqueous layer was separated and extracted with Et_2O (2 x 10 mL). The combined organic layers were washed twice with saturated aqueous NaHCO_3 , once with brine, dried (MgSO_4), and concentrated *in vacuo* to afford *N*-methoxy-*N*-methyl-4-(trifluoromethyl)benzamide (249 mg, 88%) as a colorless oil. Spectral data matched those previously reported:²⁵⁷ ^1H NMR (400 MHz, CDCl_3) δ 7.80 (d, J = 8.2 Hz, 2 H), 7.68 (d, J = 8.2 Hz, 2 H), 3.54 (s, 3 H), 3.39 (s, 3 H).

1-(4-(Trifluoromethyl)phenyl)propan-1-one (1-79). A solution of *N*-methoxy-*N*-methyl-4-(trifluoromethyl)benzamide (237 mg, 1.02 mmol) in THF (20 mL) was treated at 0 °C with EtMgBr (0.75 mL, 1.1 mmol, c = 1.5 M in THF). The solution was warmed gradually to rt over 2 h. Additional EtMgBr (0.10 mL) was added at 0 °C, and the solution was warmed to rt and stirred for 30 min. The reaction mixture was cooled to 0 °C, quenched with saturated aqueous NH_4Cl (5 mL), and diluted with water (10 mL) and Et_2O (30 mL). The aqueous layer was extracted with Et_2O (2 x 20 mL), and the combined organic layers were washed with brine, dried (MgSO_4), and concentrated *in vacuo*. Purification by chromatography on SiO_2 (pentane/ether 4:1, then 100% EtOAc) afforded 1-79 (108 mg, 53%) as a white solid. Spectral

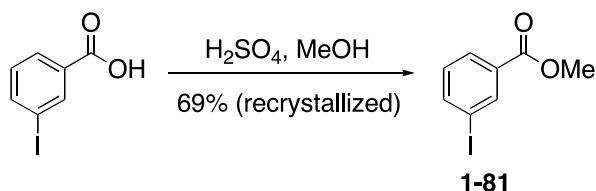
data corresponded to those previously reported^{258,259}: ¹H NMR (300 MHz, CDCl₃) δ 8.08 (d, *J* = 8.1 Hz, 2 H), 7.74 (d, *J* = 8.2 Hz, 2 H), 3.05 (q, *J* = 7.2 Hz, 2 H), 1.26 (t, *J* = 7.2 Hz, 3 H).

Representative procedure for addition of EtMgBr to *p*-trifluoromethylbenzoyl chloride (Table 1-23, entry 2). A solution of **1-69** (0.14 mL, 0.76 mmol) in THF (2.5 mL) was cooled to 0 °C, stirred for 15 min, and treated dropwise with EtMgBr (0.43 mL, 0.76 mmol). The solution was added using a syringe pump (0.24 mL/min) to a solution of *p*-trifluoromethylbenzoyl chloride **1-78** (120 mg, 0.59 mmol) in THF (1.2 mL) (Note: the solution was prepared in a flame-dried Schlenk tube equipped with an internal thermometer and was cooled to an internal temperature of -60 °C.) The solution temperature stayed between -55 °C and -60 °C throughout the addition, and the solution remained white/clear in color. The solution was stirred for an additional 10 min following completion of the Grignard addition, and the solution was quenched at -60 °C with saturated aqueous NH₄Cl (1.0 mL) and diluted with water (2 mL) and Et₂O (3 mL). The layers were separated, and the aqueous layer was extracted with Et₂O (2 mL), and the combined organic layers were washed with brine and then transferred to a 10 mL volumetric flask, which was filled to the mark with Et₂O. A 1.00 mL aliquot was filtered into a GC autosampler vial and spiked with dodecane (10 μL) and analyzed by GC. This analysis was performed in triplicate (i.e, 3 1.00 mL aliquots were spiked and analyzed). GC yields are based on a response curve of mmol ratio 1-(4-(trifluoromethyl)phenyl)propan-1-one:dodecane versus respective area ratios.

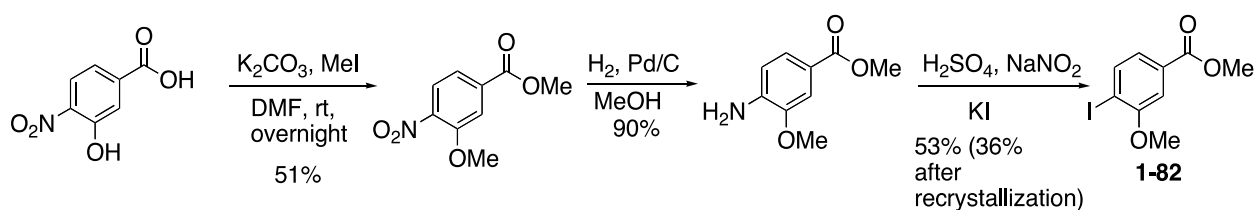
Gas chromatography data were obtained on an Agilent Technologies Network GC system (6890N). Components were separated using an Alltech Econo-CapTM ECTM-1 column (30 in length x 0.32 mm i.d.), *t*(1-(4-(trifluoromethyl)phenyl)propan-1-one) = 5.94 min and *t*(dodecane) = 6.44 min. Helium (1.0 mL/min) was used as the carrier gas. The flame ionization detector was heated to 250 °C and ignited using a mixture of compressed air (450 mL/min) and hydrogen (40 mL/min) with a makeup gas of helium (50 mL/min). All injections (1 μL) were performed *via* autosampler as split injections (split ratio 50.0: 1.0). The GC oven temperature was started at 90 °C and ramped at 10 °C/min to 220 °C and held at 220 °C for 5 min.

Preparation of substrates for Mg/I exchange reactions (Figure 1-10).

Methyl 4-iodobenzoate **1-80** was purchased from a commercial vendor and used as received. Methyl 3-iodobenzoate **1-81** and Methyl 4-iodo-3-methoxybenzoate **1-82** were synthesized as described below:



Methyl 3-iodobenzoate (1-81). A solution of 3-iodobenzoic acid (5.00 g, 20 mmol) in absolute MeOH (100 mL) was treated with concentrated H₂SO₄ (2.5 mL) and heated at reflux for 18 h. MeOH was removed by distillation until the pot contained ~1/4 volume of the reaction mixture. Upon cooling, the concentrated mixture was dissolved in ether (200 mL) and washed with water (150 mL), saturated aqueous NaHCO₃ (50 mL) and brine (50 mL), dried (MgSO₄), filtered, and concentrated *in vacuo* to afford 4.90 g white/yellow solid. The residue was dissolved in MeOH (~10 mL), heated to boiling, cooled to rt, then to 0 °C. Upon cooling to 0 °C a white solid precipitated. The solid was collected by filtration and washed with cold MeOH (~10 mL) to afford methyl-3-iodobenzoate (3.67 g, 69%) as a white solid: Mp 47.3–49.0 °C (MeOH) (lit.²⁶⁰ 50–52 °C); ¹H NMR (400 MHz, CDCl₃) δ 8.39 (t, *J* = 1.6 Hz, 1 H), 8.01 (d, *J* = 7.8 Hz, 1 H), 7.90 (d, *J* = 7.9 Hz, 1 H), 7.20 (t, *J* = 7.8 Hz, 1 H), 3.93 (s, 3 H).



Methyl 3-methoxy-4-nitrobenzoate.²⁶¹ A flame-dried 50-mL round-bottom flask was charged with 3-hydroxy-4-nitrobenzoic acid (3.00 g, 16 mmol), dry DMF (17 mL) and powdered K₂CO₃ (6.79 g, 49 mmol). The solution was cooled to 0 °C and MeI (2.2 mL, 36 mmol) was

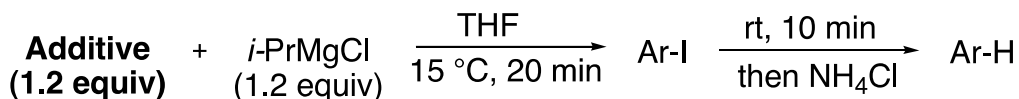
added via syringe. The reaction mixture was warmed to rt and stirred overnight (18 h). The mixture was poured into water (80 mL), and the flask was rinsed with water and toluene. The aqueous layer was extracted with toluene (2 x 75 mL). The combined organic layers were washed with 0.1 M aqueous NaOH (50 mL), water (50 mL), and brine (50 mL), dried (Na₂SO₄) and concentrated *in vacuo* to afford methyl 3-methoxy-4-nitrobenzoate (1.77 g, 51%) as an orange, crystalline solid: ¹H NMR (400 MHz, CDCl₃) δ 7.85 (d, *J* = 8.3 Hz, 1 H), 7.77 (d, *J* = 1.4 Hz, 1 H), 7.70 (dd, *J* = 8.3, 1.6 Hz, 1 H), 4.03 (s, 3 H), 3.98 (s, 3 H).

Methyl 4-amino-3-methoxybenzoate.²⁶¹ A solution of methyl 3-methoxy-4-nitrobenzoate (1.77 g, 8.38 mmol) in MeOH (250 mL) was treated with 10% Pd/C (360 mg) and stirred under an H₂ atmosphere for 15 h. The reaction mixture was filtered through a pad of Celite, (washing with MeOH) and concentrated *in vacuo* to afford methyl 4-amino-3-methoxybenzoate (1.37 g, 90% crude) as a tan solid: Mp 126.8–128.8 °C (lit.²⁶¹ 128 °C); ¹H NMR (400 MHz, CDCl₃) δ 7.55 (dd, *J* = 8.2, 1.6 Hz, 1 H), 7.46 (d, *J* = 1.6 Hz, 1 H), 6.67 (d, *J* = 8.2 Hz, 1 H), 4.21 (bs, 2 H), 3.91 (s, 3 H), 3.87 (s, 3 H).

Methyl 4-iodo-3-methoxybenzoate (1-82).²⁶¹ A 100-mL round-bottom flask with a 24/40 jointed neck was charged with 4-amino-3-methoxybenzoate (1.20 g, 6.62 mmol), deionized water (16 ml) and 20% H₂SO₄ (3.6 mL). The suspension was cooled to 0 °C and capped with a septum and an empty balloon. A solution of NaNO₂ (503 mg, 7.29 mmol) in water (3.0 mL) was added slowly, and the suspension became bright yellow in color. The solution was stirred for 15 min, and urea (120 mg) was added, followed almost immediately by dropwise addition of a solution of KI (1.15 g, 6.95 mmol) in water (3.0 mL). The solution (deep brown) was stirred at 0 °C to rt for 20 min, and then moved to a pre-heated oil bath (50 °C) and stirred at 50 °C for 2 h. To the reaction mixture was added a solution of saturated aqueous Na₂S₂O₅ (~15 mL), and the mixture was extracted with Et₂O (3 x 20 mL). The aqueous layer was neutralized with 1 N aqueous NaOH and extracted with Et₂O (once). The combined organic layers (deep orange/red) were washed with 1 N NaOH and brine (2x), dried (Na₂SO₄) and concentrated *in vacuo* to afford a crude brown residue (1.63 g). Purification by chromatography on neutral Al-

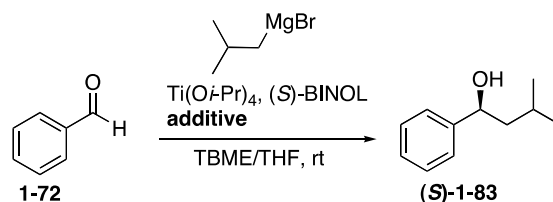
O_3 (pentane/ Et_2O , 95:5 to 90:10) afforded **1-82** (1.03 g, 53%) as a slightly yellow oil. The product was further purified by recrystallization from MeOH as follows:

The oil was dissolved in MeOH (5 mL), heated to boiling, and cooled to $-20\text{ }^\circ\text{C}$. The crystals were collected by filtration and washing with cold MeOH. The mother liquor was concentrated, and trituration of the resulting solid with MeOH afforded additional **1-82** (100 mg) for a total yield of **1-82** (700 mg, 36%) as a white solid: Mp $53.5\text{--}55.2\text{ }^\circ\text{C}$ (MeOH) (lit.²⁶¹ $50\text{--}52\text{ }^\circ\text{C}$); ^1H NMR (300 MHz, CDCl_3) δ 7.87 (d, $J = 8.1$ Hz, 1 H), 7.46 (d, $J = 1.8$ Hz, 1 H), 7.38 (dd, $J = 8.1$, 1.8 Hz, 1 H), 3.95 (s, 3 H), 3.93 (s, 3 H).



General procedure for the Mg/I exchange reaction using *i*-PrMgCl in different media (Table 1-24, entry 6).¹⁰¹ A flame-dried 25-mL round-bottom flask was charged with freshly distilled THF (4.9 mL) and sulfide **1=69** (243 mg, 1.20 mmol) and cooled in an ice-water bath maintained at $15\text{ }^\circ\text{C}$. *i*-PrMgCl (0.690 mL, 1.20 mmol, $c = 1.75$ M in THF) was added slowly *via* syringe. (Note: the solution became cloudy and white). The solution was stirred at $15\text{ }^\circ\text{C}$ for 20 min and then methyl 3-iodobenzoate (262 mg, 1.00 mmol) in THF (0.71 mL) was added slowly *via* syringe. The ice-water bath was removed, and the reaction mixture was stirred at ambient temperature for 10 min. The reaction mixture was quenched with saturated aqueous NH_4Cl (1 mL) and poured into a separatory funnel. EtOAc (10 mL) and water (5 mL) were added. The layers were separated, and the organic layer was washed with brine (5 mL). The organic layer was spiked with dodecane (100 μL). An aliquot (0.1 mL) was transferred to a GC autosampler vial and diluted with additional EtOAc (0.4 mL). GC yields were determined using based on the area ratio of methyl benzoate and dodecane; an area ratio to mmol ratio relationship was determined by generating a calibration curve with known mmol ratios of methyl benzoate and dodecane. Note: In the case of reactions with substrate **1-82**, the GC yields are estimated assuming that the response of methyl 3-methoxybenzoate is similar to that of methyl benzoate.

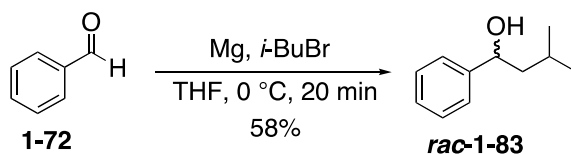
Gas chromatography data were obtained on an Agilent Technologies Network GC system (6890N). Components were separated using an Agilent HP-5 column (30.0 m x 320 μ m x 0.25 μ m (nominal)), t(methyl benzoate) = 5.43 min, t(dodecane) = 6.43 min and t(methyl 3-iodobenzoate) = 9.79 min. Helium (1.0 mL/min, 6.33 psi) was used as the carrier gas. The flame ionization detector was heated to 250 °C and ignited using a mixture of compressed air (450 mL/min) and hydrogen (40 mL/min) with a makeup gas of helium (45 mL/min). All injections (1 μ L) were performed *via* autosampler as split injections (split ratio 50.0:1.0). The GC oven temperature was started at 90 °C and ramped at 10 °C/min to 250 °C and held at 250 °C for 5 min.



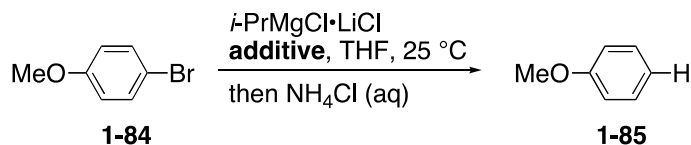
Representative procedure for asymmetric Grignard additions to benzaldehyde (Table 1-25, entry 2).¹⁰² A flame-dried 10-mL round-bottom flask was flushed with Ar and charged with (S)-BINOL (24.2 mg, 0.0848 mmol) and distilled MTBE (2.2 mL). $\text{Ti(O}i\text{-Pr)}_4$ was added dropwise *via* syringe, and the resulting bright orange/yellow solution was stirred for 30 min at rt. A second flame-dried 10-mL round-bottom flask was flushed with Ar and charged with sulfide **1-69** (229 mg, 1.13 mmol) and dry MTBE (2.2 mL) and cooled to 0 °C. *i*-BuMgBr (1.3 mL, 1.1 mmol, c = 0.90 M in THF) was added slowly *via* syringe over the course of 6 min. The cloudy white solution was stirred for 30 min at 0 °C. The $\text{Ti(O}i\text{-Pr)}_2$ -BINOL solution was slowly added to the Grignard solution at 0 °C, and the mixture was allowed to warm to ambient temperature. The mixture was stirred for a total time of 1 h at rt. The reaction mixture was cooled to -5 °C (ice/salt bath), and freshly distilled PhCHO (60.0 μ L, 0.565 mmol) was added dropwise *via* syringe. The ice bath was removed, and the mixture was allowed to warm to rt. The mixture was stirred under Ar at rt for 20 h and quenched with 5% aqueous HCl (3 mL) and extracted with Et_2O (3 x 10 mL). The combined organic layers were washed with saturated aqueous NaHCO_3 and brine, dried (Na_2SO_4) and concentrated *in vacuo*. Purification by

chromatography on SiO₂ (pentane/Et₂O, 4:1) afforded an analytically clean sample (3 mg) as well as other product containing impurities (11 mg). The enantiomeric excess was determined to be 95% by chiral HPLC analysis (Chiralcel OD, 5% isopropanol/hexanes, 1.0 mL/min, 220 nm) $t_r(\text{major}) = 7.1 \text{ min}$, $t_r(\text{minor}) = 8.0 \text{ min}$.

Synthesis of *rac*-1-83 for us as an HPLC standard.

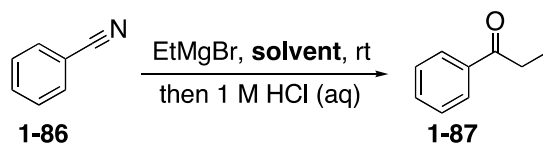


3-Methyl-1-phenylbutan-1-ol (*rac*-1-83).^{262,263} A flame-dried Schlenk flask was charged with activated Mg turnings (53 mg, 2.2 mmol), distilled THF (5 mL) and 1-bromo-2-methylpropane (0.100 mL) and an iodine crystal. The vessel was gently warmed with a heating mantle until dissipation of the iodine color was observed. Additional 1-bromo-2-methylpropane (0.14 mL) in THF (5 mL) was added slowly via syringe. The now cloudy solution was stirred an additional 2 h at rt. The mixture was cooled to 0 °C, and freshly distilled benzaldehyde (100 μL , 0.985 mmol) was added dropwise. The reaction mixture was stirred at 0 °C for 20 min and then quenched with saturated aqueous NH₄Cl. The mixture was diluted with Et₂O (20 mL) and water (10 mL), and the aqueous layer was extracted with Et₂O (2 x 10 mL). The combined organic layers were washed with water and brine, dried (MgSO₄) and concentrated *in vacuo*. The crude material was purified by chromatography on SiO₂ (pentane/Et₂O, 85:15) to afford *rac*-1-83 (94 mg, 58%) as a colorless oil: ¹H NMR (300 MHz, CDCl₃) δ 7.36 (d, $J = 4.3 \text{ Hz}$, 4 H), 7.33–7.28 (m, 1 H), 4.79–4.73 (m, 1 H), 1.80–1.63 (m, 2 H), 1.57–1.43 (m, 1 H), 0.96 (dd, $J = 6.4, 1.1 \text{ Hz}$, 6 H).



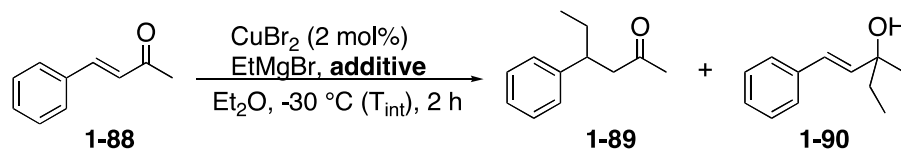
Representative procedure for Mg/Br exchange reactions of 4-bromoanisole (Table 1-26, entry 4). An oven-dried microwave vial equipped with stir bar was cooled under Ar atmosphere and back-filled with Ar 3 times. To the flask was added a solution of *i*-PrMgCl-LiCl in THF (0.840 mL, 1.05 mmol, *c* = 1.25 M in THF), followed by distilled THF (0.16 mL). 4-Bromoanisole (125 μ L, 1.00 mmol) was added at rt. Sulfide **1-69** (201 mg 1.00 mmol) was added in one portion. (Note: sulfide **1-69** was dried by neat filtration through activated basic Al₂O₃). The reaction mixture was stirred at rt for 24 h. The mixture was quenched with saturated aqueous NH₄Cl (3 mL), and diluted with water (3 mL) and Et₂O (10 mL). The layers were separated, and the organic layer was spiked with dodecane (100 μ L). An aliquot of the organic layer was filtered through a short cotton plug and analyzed by GC. Conversion/yields are based on calibrations of the relative concentration to area response of 4-bromoanisole, anisole and dodecane.

Gas chromatography data were obtained on an Agilent Technologies Network GC system (6890N). Components were separated using an Alltech Econo-CapTM ECTM-1 column (30 in length x 0.32 mm i.d.), *t*(anisole) = 3.90 min and *t*(dodecane) = 6.44 min, and *t*(4-bromoanisole) = 6.56 min. Helium (1.0 mL/min) was used as the carrier gas. The flame ionization detector was heated to 250 °C and ignited using a mixture of compressed air (450 mL/min) and hydrogen (40 mL/min) with a makeup gas of helium (50 mL/min). All injections (1 μ L) were performed *via* autosampler as split injections (split ratio 50.0: 1.0). The GC oven temperature was started at 90 °C and ramped at 10 °C/min to 220 °C and held at 220 °C for 5 min. For experiments using high boiling materials such as 15-crown-5, the run was held at 220 °C for 20 min.



Representative procedure for addition of EtMgBr to benzonitrile (Table 1-27, entry 2). A flame-dried thick-walled vial was flushed with N₂ and charged with distilled Et₂O (1.10 ml) and 0 sulfide **1-69** (0.13 mL, 140 mg, 0.68 mmol). To the solution was added freshly distilled benzonitrile (20 μL, 0.19 mmol) and EtMgBr (0.12 mL, 0.29 mmol, c = 2.4 M in Et₂O). The reaction mixture was stirred under N₂ atmosphere for 3 h at rt. An aliquot (100 μL) was removed, quenched with 1 N aqueous HCl, and partitioned into EtOAc for GC analysis. The reaction mixture was flushed with Ar, sealed, and stirred at rt for an additional 12 h. The reaction mixture was cooled to 0 °C, and 1 N aqueous HCl (0.50 mL) was slowly added. The solution was warmed to rt and stirred for 20 min. The solution was extracted with Et₂O (1 mL), and the ethereal layer was washed with saturated aqueous NaHCO₃ and filtered for GC analysis. The reported ratios of benzonitrile to propiophenone are based on an area ratio to mmol ratio response curve of known ratios of benzonitrile and propiophenone.

Gas chromatography data were obtained on an Agilent Technologies Network GC system (6890N). Components were separated using an Alltech Econo-CapTM ECTM-1 column (30 in length x 0.32 mm i.d.), t(benzonitrile) 4.23 min and t(propiofenone) = 6.20 min. Helium (1.0 mL/min) was used as the carrier gas. The flame ionization detector was heated to 250 °C and ignited using a mixture of compressed air (450 mL/min) and hydrogen (40 mL/min) with a makeup gas of helium (50 mL/min). All injections (1 μL) were performed *via* autosampler as split injections (split ratio 50.0: 1.0). The GC oven temperature was started at 90 °C and ramped at 10 °C/min to 220 °C and held at 220 °C for 5 min.



Representative procedure for addition of EtMgBr to enone 1-88 (Table 1-28, entry 3). A flame-dried Schlenk tube cooled under N₂ was charged with CuBr₂ (2.2 mg, 0.010 mmol) and then equipped with an internal thermometer. The tube was charged with Et₂O (1.0 mL), followed by sulfide **1** (20 mg, ~0.02 mL, 0.010 mmol). A solution of **14** (75.0 mg, 0.513 mmol) in Et₂O (1.0 mL) was added at rt. The solution was cooled to -30 °C (T_{int}), and the temperature was maintained using a cryocool. A solution of EtMgBr (0.43 mL, 1.0 mmol, c = 2.4 M in Et₂O) further diluted Et₂O (1.5 mL) was added *via* syringe pump over 40 min. The reaction mixture was maintained at -30 °C for 2 h after the addition was complete. The reaction mixture was quenched with saturated aqueous NH₄Cl and extracted into Et₂O (3 x). The ethereal layers were washed with brine, dried (MgSO₄) and concentrated *in vacuo*. The crude concentrate was purified by chromatography on SiO₂ (pentane/Et₂O, 4:1 deactivated with 0.1% Et₃N) to afford **1-89** (27 mg, 30%) as a yellow oil and 1,2-product **1-90** (23 mg, 20%, ~80% purity) as yellow oil.

1-89.²⁶⁴ ¹H NMR (400 MHz, CDCl₃) δ 7.33–7.28 (m, 2 H), 7.23–7.18 (m, 3 H), 3.09–3.02 (m, 1 H), 2.75 (d, *J* = 7.2 Hz, 2 H), 2.04 (s, 3 H), 1.76–1.65 (m, 1 H), 1.63–1.53 (m, 1 H), 0.80 (t, *J* = 7.4 Hz, 3 H).

1-90. ¹H NMR (400 MHz, CDCl₃) δ 7.23 (d, *J* = 7.2 Hz, 1 H), 7.34 (t, *J* = 7.6 Hz, 2 H), 7.28–7.18 (m, 2 H), 6.62 (d, *J* = 16.4 Hz, 1 H), 6.30 (d, *J* = 16.4 Hz, 1 H), 1.69 (q, *J* = 7.2 Hz, 2 H), 1.50 (b, 1 H), 1.40 (s, 3 H), 0.96 (t, *J* = 7.2 Hz, 3 H).

Determination of LogP value of MMS350 (1-70). The logP (octanol-water partition coefficient) was determined using the shake-flask method. Three determinations were made. A representative procedure is as follows: a 250-mL separatory funnel was charged with a solution of MMS350 (50.0 mg) in water (50.0 mL) and *n*-octanol (50.0 mL). The funnel was capped and inverted 100 times. The funnel and contents were left to stand at rt (23.5 °C) for 40 h. Aliquots

of both phases were analyzed by UV/VIS (214 nm for the aqueous layer and 218 nm for the octanol layer), and the concentration in each layer was determined using previously generated calibration curves. In the case of the aqueous layer, a 10-fold dilution was necessary prior to measurement. All measurements were run in triplicate. The logP was determined as $\log\left(\frac{[\text{MMS350}]_{\text{octanol}}}{[\text{MMS350}]_{\text{aqueous}}}\right)$, and the average logP value from the 3 trials was -0.87.

General procedure for determination of solubility in solutions of MMS350 and HPLC-grade water.

Preparation of sulfoxide/water solutions. Solutions of **MMS350** and HPLC-grade water were prepared in 1 dram vials by dissolving the appropriate amount of **MMS350** in HPLC-grade water (2.00 mL). In the case of the 25% solution of **MMS350** in H₂O (w/w), **MMS350** (500 mg) was dissolved in water (1.50 mL). Each vial was placed on a platform shaker and shaken at 200 rpm for 30 min.

Solubility measurements. Eppendorf vials (1.5 mL size) were charged with model compounds in excess. Vials were charged with HPLC-grade water (0.500 mL) or the appropriate **3**/water solution (0.500 mL). The vials were briefly vortexed and equilibrated in an end-over-end rotator at 30.0 °C for 20 h. The vials were centrifuged (4000 rpm, 1300 xg, 15 min, rt) directly after removal from the rotator, and aliquots of the supernatant (0.400 mL) were filtered through 0.45 μm syringe filters. The pH of each solution was measured using a ThermoScientific electrode (3 mm tip). Each solution was diluted with an appropriate volume of either absolute ethanol (quinine, naproxen, griseofulvin) or methanol (carbendazim). Concentrations were calculated by using previously generated calibration curves. Appropriate blanks were prepared by diluting aliquots (0.400 mL) of the **MMS350**/water solutions (or HPLC-grade water in the case of the control) in an analogous fashion to the sample being measured.

General procedure for determination of solubility in solutions of DMSO and HPLC-grade water.

Preparation of DMSO/water solutions. Solutions of DMSO and HPLC-grade water were prepared in 1 dram vials by dissolving the appropriate amount of DMSO in HPLC-grade water (2.00 mL). Each vial was placed on a platform shaker and shaken at 200 rpm for 30 min.

Solubility measurements. Eppendorf vials (1.5 mL size) were charged with model compounds in excess. Vials were charged with either HPLC-grade water (1.00 mL) or the appropriate DMSO/water solution (1.00 mL). The vials were briefly vortexed and equilibrated in an end-over-end rotator at 30.0 °C for 20 h. The vials were centrifuged directly after removal from the rotator (4000 rpm, 1300 *xg*, 15 min, rt), and aliquots of the supernatant (0.800 mL) were filtered through 0.45 µm syringe filters. The pH of each solution was measured using a ThermoScientific electrode (3 mm tip). Each solution was diluted with an appropriate volume of either absolute ethanol (quinine, naproxen, griseofulvin) or methanol (carbendazim). Concentrations were calculated by using previously generated calibration curves. Appropriate blanks were prepared by diluting aliquots (0.800 mL) of the DMSO/water solutions (or HPLC-grade water in the case of the control) in analogous fashion to the sample being measured.

General procedure for determination of estrone solubility in solutions of MMS350 and pH 9.0 buffer.

Preparation of sulfoxide/buffer solutions. A 25% w/w solution of **MMS350** in pH 9.0 buffer was prepared by dissolving **MMS350** (565 mg) in pH 9.0 buffer (1.70 mL). A 3:1 buffer/NMP solution was prepared from pH 9.0 buffer (3.00 mL) and NMP (1.00 mL). A 3:1:1 buffer/NMP/**MMS350** solution was prepared from pH 9.0 buffer (1.50 mL), NMP (0.500 mL), and **MMS350** (515 mg).

A 25% DMSO/buffer w/w solution was prepared by mixing anhydrous DMSO (1.54 mL) with pH 9.0 buffer (5.10 mL). A 3:1:1 pH 9.0 buffer:NMP:DMSO solution was prepared by

mixing NMP (1.50 mL), DMSO 1.40 mL, and pH 9.0 buffer (4.50 mL). Each vial was placed on a platform shaker and shaken at 200 rpm for 30 min.

Solubility measurements. Eppendorf vials (1.5 mL size) were charged with estrone in excess. Vials were charged with 0.500 mL of either pH 9.0 buffer (control) or the appropriate solution described above. The vials were briefly vortexed and equilibrated in an end-over-end rotator at 30.0 °C for 20 h. Aliquots (0.40 mL) were filtered through 0.45 µm syringe filters. The pH of each solution was measured using a ThermoScientific electrode (3 mm tip). Each solution was diluted with an appropriate volume of either absolute ethanol and analyzed by UV/VIS. Concentrations were verified by preparing standards of estrone in the appropriate ethanol/sulfoxide/buffer solutions. Appropriate blanks were prepared by diluting 0.400 mL aliquots of the buffer solutions (or 0.400 mL buffer in the case of the control) in analogous fashion to the sample being measured.

General procedure for solubility determination in mixtures of sulfoxide MMS350 in pH 7.0 buffer.

Preparation of sulfoxide/buffer solutions. In the case of a 10% w/w solution of sulfoxide **MMS350** in 0.01 M pH 7.0 phosphate buffer, **MMS350** (700 mg) was dissolved in 0.01 M Na₂HPO₄/NaH₂PO₄ buffer (6.30 mL) and equilibrated on a platform shaker at 200 rpm for 30 min. at rt. In the case of a 25% w/w solution of sulfoxide **MMS350** in 0.01 M pH 7.0 phosphate buffer, **MMS350** (1.50 g) was dissolved in 0.01 M Na₂HPO₄/NaH₂PO₄ buffer (4.50 mL) and equilibrated on a platform shaker at 200 rpm for 30 min. at rt.

Solubility measurements. Eppendorf vials (1.5 mL size) were charged with model compounds in excess. Vials were charged with either pH 7.0 phosphate buffer (1.00 mL) or the appropriate **MMS350**/buffer solution. The vials were briefly vortexed and equilibrated in an end-over-end rotator at 30.0 °C for 20 h. The vials were centrifuged directly after removal from the rotator (4000 rpm, 1300 xg, 15 min, rt), and aliquots of the supernatant (0.800 mL) were filtered through 0.45 µm syringe filters. The pH of each solution was measured using a

ThermoScientific electrode (3 mm tip) after calibration. Each solution was diluted with an appropriate volume of either absolute ethanol (quinine, naproxen) or methanol (carbendazim). Concentrations were determined using standard additions of a stock solution of the compound in either absolute ethanol (quinine, naproxen) or methanol (carbendazim) to aliquots of the diluted filtrates.

General procedure for kinetic solubility measurements. A polypropylene tube was charged with PBS solution (490 μL). To the buffer was added a 10 mM stock solution of compound (10 μL). The tube was vortexed and equilibrated on an end-over-end rotator for 15 min at rt. Aliquots (400 μL) were filtered through 0.45 μm syringe filters and diluted to 5.0 mL with absolute MeOH. Concentrations were determined by UV/VIS analysis.

General procedure for calculation of water absorption. Oven-dried flasks capped with septa were cooled under a N_2 atmosphere and charged with a volume of the appropriate solutions (DMSO, 3.0 mL; NMP, 600 μL ; 25% **MMS350**/NMP, 600 μL). The water content was determined by Karl Fischer titration using ~ 100 μL aliquots ($t = 0$ measurement). Each septum was pierced with a 1.5 inch 18 gauge needle and left to stand at rt for 7 d. The water content was measured at the end of this period ($t = 7$ d measurement) by Karl Fischer titration. All measurements were made in duplicate.

General procedure for brine shrimp toxicity assays.²⁶⁵

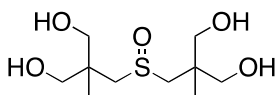
Sample preparation. Stock solutions of **MMS350** were prepared by dissolving **MMS350** (50.0 mg) in 5.0 HPLC grade water (5.0 mL), (solution A) and **MMS350** (2.50 g) in HPLC grade water (10.0 mL) (solution B). Stock solutions of DMSO were prepared by diluting DMSO (45 μL) with HPLC grade water (5.0 mL) (solution C) and DMSO (2.27 mL) with HPLC grade water (10.0 mL) (solution D).

In each case, 5 replicates were performed. Each replicate was performed in a 2 dram vial marked at the 4 and 5 mL volume points. To each vial was added artificial sea water (3 mL) followed by the appropriate volume of stock solution. For set 1 (1.0 mg/mL), solution A (0.500

mL) or solution C (0.500 mL) was added. For set 2 (5.0 mg/mL), solution B (0.100 mL) or solution D (0.100 mL) was added to each vial. For set 3 (20.0 mg/mL), solution B (0.400 mL) or solution D (0.400 mL) was added to each vial. For set 4 (50.0 mg/mL), solution B (1.00 mL) or solution D (1.00 mL) was added to each vial. Controls containing HPLC grade water (0.100 mL, 0.400 mL, and 1.00 mL) were prepared in the same manner, and five replicates of each control were prepared.

Brine shrimp hatching. Brine shrimp eggs (San Francisco Bay Brand) were hatched in a commercial salt mixture (Instant Ocean). Constant aeration was provided using a pump and airstone, and illumination was maintained using a desk lamp. The shrimp were collected in a separate tank after 48 h and used within 3-4 h of collection.

Assay. Brine shrimp (10) were added to each vial using a plastic transfer pipet. After the shrimp were transferred, artificial sea-water was added until the volume reached the 5-mL mark. One drop of a yeast suspension prepared by suspending 11 mg yeast in sea-water (20 mL) was added to each vial. The shrimp were counted at $t = 24$ h. Another drop of freshly prepared yeast solution (6 mg in 10 mL sea water) was added, the vials were maintained under illumination, and shrimp were counted at $t = 48$ h.

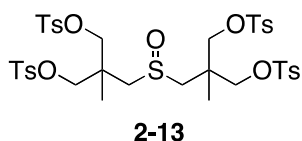


2-6 (MMS399)

2,2'-Sulfinylbis(methylene)bis(2-methylpropane-1,3-diol) (MMS399). A solution of MMS350 (200 mg, 0.916 mmol) in 0.5 M aqueous H_2SO_4 (6 mL) was heated at 65°C for 10 h. The solution was neutralized with solid NaHCO_3 , and water was removed *in vacuo*. The concentrated solids were suspended in EtOH and filtered through a short plug of Celite, and the filtrate was concentrated *in vacuo*. The residue was dissolved in water, and insoluble materials were removed by filtration through a $0.65\ \mu\text{m}$ PVDF filter. The filtrate was concentrated *in*

vacuo, and the residue was dissolved in water, transferred to a scintillation vial, and water was removed using the Genevac (EZ-2, 45 °C) to afford **MMS399** (226 mg, 97%) as a viscous pale yellow oil: IR (ATR) 3314, 3294, 2929, 1463, 1035 cm⁻¹; ¹H NMR (400 MHz, D₂O)^a δ 3.60–3.52 (m, 8 H), 2.96, 2.93 (AB, *J* = 14.0 Hz, 4 H), 1.07 (s, 6 H); ¹³C NMR (100 MHz, D₂O) δ 66.4, 66.3, 59.3, 41.2, 18.9; HRMS (HESI) *m/z* calc for C₁₀H₂₃O₅S (M+H) 255.1261, found 255.1266.

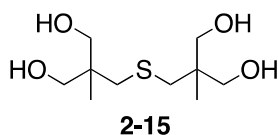
^a NMR samples were spiked with acetone, and chemical shifts (δ) are recorded in ppm and referenced to acetone (¹H NMR, 2.22; ¹³C NMR, 30.89).



2,2'-Sulfinylbis(methylene)bis(2-methylpropane-3,2,1-triyl)tetrakis(4-methylbenzenesulfonate) (2-13). A solution of **MMS399 (2-6)** was prepared by adding DMF (8 mL, 4 mL per vial) between 2 20-mL scintillation vials of pre-weighed **MMS399** samples and sonicating under an Ar atmosphere. THF (16 mL) was divided between the vials, followed by TsCl (3.64 g, 19.1 mmol), also divided between the vials.

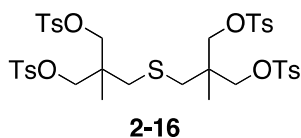
The solution of **MMS399** and TsCl was added to a suspension of powdered KOH (2.86 g, 50.9 mmol) in THF (16 mL) at 0 °C via syringe pump (0.6 mL/min). The mixture was stirred at 0 °C for 1 h and at rt overnight. The mixture was concentrated *in vacuo*, and the residue was partitioned between water (80 mL) and CH₂Cl₂ (200 mL). The aqueous layer was extracted with CH₂Cl₂ (1 x 100 mL). The combined organic layers were washed with water and brine, dried (MgSO₄), and concentrated *in vacuo*. Purification by chromatography (ISCO 40 g silica cartridge; 100% hexanes over 15 min; 0%–100% EtOAc to 12 min; 100% EtOAc) afforded **2-13** (928 mg) as a viscous oil that was contaminated with DMF. The oil was taken up in EtOAc (50 mL) and washed with water (3 x 20 mL) and brine, dried (MgSO₄), and concentrated *in vacuo* to afford **2-13** (780 mg, 26%) as a white foam: IR (ATR) 2960, 1596, 1355, 1171, 956 cm⁻¹; ¹H

NMR (400 MHz, CDCl₃) δ 7.77–7.73 (m, 8 H), 7.37 (t, J = 7.9 Hz, 8 H), 3.96, 3.90 (AB, J = 10.0 Hz, 4 H), 3.92, 3.90 (AB, J = 10.0 Hz, 4 H), 2.70 (d, J = 13.7 Hz, 2 H), 2.51 (d, J = 13.6 Hz, 2 H), 2.47 (s, 6 H), 2.46 (s, 6 H), 1.12 (s, 6 H); ¹³C NMR (100 MHz, CDCl₃) δ 145.5, 145.3, 132.1, 132.0, 130.1, 130.1, 128.0, 128.0, 71.8, 71.6, 57.9, 39.1, 21.7, 18.4; HRMS (ESI) m/z calc for C₃₈H₄₆O₁₃NaS₅ (M+Na) 893.1440, found 893.1433.

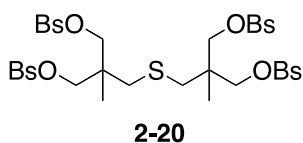


2,2'-Thiobis(methylene)bis(2-methylpropane-1,3-diol) (2-15). A suspension of sulfide **1-69** (1.50 g, 7.41 mmol) in 0.5 M aqueous H₂SO₄ (45 mL) was heated at 65 °C overnight. Upon cooling, the solution was neutralized with solid NaHCO₃, and water was removed *in vacuo*. The partially concentrated sample was coevaporated with EtOH. The resulting solids were taken up in EtOH, and the mixture was filtered through Celite. The filtrate was concentrated *in vacuo*. The concentrated material was dissolved in water (40 mL) and divided between four 20-mL scintillation vials, and water was removed using the Genevac (EZ-2) to afford crude tetrol **2-15** (1.98 g, 112%) as a white solid: ¹H NMR (500 MHz, D₂O)^a δ 3.48 (s, 8 H), 2.62 (s, 4 H), 0.92 (s, 6 H); HRMS (HESI) m/z calc for C₁₀H₂₃O₄S (M+H) 239.1312, found 239.1305.

^a NMR samples were spiked with acetone, and chemical shifts (δ) are recorded in ppm and referenced to acetone (¹H NMR, 2.22).

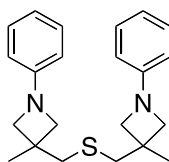


2,2'-Thiobis(methylene)bis(2-methylpropane-3,2,1-triyl)tetrakis(4-methylbenzenesulfonate) (2-16). A solution of **2-6** (MMS399) (1.2 g, 5.0 mmol) and TsCl (6.2 g, 33 mmol) in DMF (12 mL) and THF (24 mL) was added via syringe pump (0.6 mL/min) to a suspension of powdered KOH (4.9 g, 87 mmol) in THF (24 mL) at 0 °C. The reaction mixture was warmed to rt and stirred for 12 h. THF was removed *in vacuo*, and the concentrate was partitioned between EtOAc (200 mL) and water (100 mL). The aqueous layer was extracted with EtOAc (3 x 100 mL), and the combined organic layers were washed with water (3 x 100 mL) and brine (100 mL), dried (MgSO₄), and concentrated *in vacuo*. The crude residue was purified by chromatography (ISCO, 80 g silica cartridge, linear gradient of 0-100% EtOAc/hexanes over 30 min; product elutes at 50%–60% EtOAc/hexanes) to afford **2-16** (1.69 g, 40%) as a yellow foam: ¹H NMR (500 MHz, CDCl₃) δ 7.74 (d, *J* = 8.3 Hz, 8 H), 7.37 (d, *J* = 8.1 Hz, 8 H), 3.80, 3.75 (AB, *J* = 9.6 Hz, 8 H), 2.50 (s, 12 H), 2.38 (s, 4 H), 0.86 (s, 6 H); ¹³C NMR (125 MHz, CDCl₃) δ 145.1, 132.0, 129.9, 127.7, 71.2, 39.7, 38.6, 21.5, 17.9.



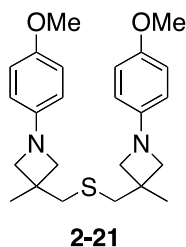
2,2'-Thiobis(methylene)bis(2-methylpropane-3,2,1-triyl)tetrakis(4-bromobenzenesulfonate) (2-20). A 100-mL round-bottom flask was charged with crude **2-15** (548 mg, 2.30 mmol). The tetrol **2-15** was dissolved in a minimal amount of water (5 mL), and 50% aqueous NaOH (15 mL) was added, followed immediately by Bu₄NHSO₄ (312 mg, 0.920 mmol). A solution of 4-bromobenzenesulfonyl chloride (9.40 g, 36.8 mmol) in 1,2-dichloroethane was slowly added (CAUTION: slight exotherm). The slurry was stirred vigorously for 30 min at rt and subsequently heated at reflux for 3.5 h. The mixture was cooled and diluted with CH₂Cl₂ (250 mL) and water (100 mL). The aqueous layer was extracted with

CH₂Cl₂ (100 mL), and the combined organic layers were washed with water and brine, dried (MgSO₄), and concentrated *in vacuo* to afford crude yellow oil. The crude residue was purified by chromatography on SiO₂ (deactivated with 0.1% Et₃N; hexanes/EtOAc 9:1 to 7:3) to afford **2-20** (0.93 g, 36%) as a white foam: IR (ATR) 1573, 1359, 1184, 1172 cm⁻¹; ¹H NMR (500 MHz, CDCl₃) δ 7.73 (s, 16 H), 3.87, 3.81 (AB, *J* = 9.6 Hz, 8 H), 2.44 (s, 4 H), 0.91 (s, 6 H); ¹³C NMR (125 MHz, CDCl₃) δ 134.2, 132.8, 129.4, 129.3, 71.5, 39.9, 38.7, 18.1; HRMS (ESI) *m/z* calc for C₃₄H₃₄O₁₂NaS₅Br₄ (M+Na) 1132.7285, found 1132.7296.

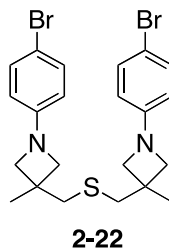


2-17

Bis((3-methyl-1-phenylazetididin-3-yl)methyl)sulfane (2-17). An oven-dried microwave vial was charged with **2-20** (137 mg, 0.123 mmol), MeCN (0.50 mL), aniline (45 μL, 0.49 mmol) and K₂CO₃ (170 mg, 1.23 mmol). Argon was bubbled through the solution for 5 min. The vial was flushed with Ar and placed in a pre-heated oil bath (90 °C) and heated at 90 °C for 12 h. Upon cooling, the mixture was diluted with CH₂Cl₂ (10 mL) and water (3 mL). The aqueous layer was extracted with CH₂Cl₂ (2 x 5 mL), and the combined organic layers were washed with 1 M aqueous NaOH (3 mL), and brine (5 mL), dried (MgSO₄), filtered, and concentrated *in vacuo*. The crude residue was purified by chromatography on SiO₂ (deactivated with 0.1% Et₃N, hexanes/EtOAc, 9:1) to afford **2-17** (26.5 mg, 61%) as a yellow solid: Mp 90–92 °C; IR (ATR) 2954, 2836, 1599, 1500, 1474, 1353, 1174 cm⁻¹; ¹H NMR (500 MHz, CDCl₃) δ 7.22 (t, *J* = 7.9 Hz, 4 H), 6.74 (t, *J* = 7.4 Hz, 2 H), 6.46 (d, *J* = 7.7 Hz, 4 H), 3.71 (d, *J* = 6.9 Hz, 4 H), 3.58 (d, *J* = 6.9 Hz, 4 H), 2.94 (s, 4 H), 1.41 (s, 6 H); ¹³C NMR (125 MHz, CDCl₃) δ 151.6, 128.9, 117.3, 111.3, 62.4, 45.1, 36.1, 24.3; HRMS (ESI) *m/z* calc for C₂₂H₂₉N₂S (M+H) 353.2051, found 353.2039.

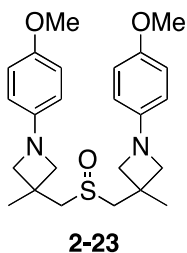


Bis((1-(4-methoxyphenyl)-3-methylazetididin-3-yl)methyl)sulfane (2-21). An oven-dried microwave vial maintained under Ar atmosphere was charged with **2-20** (173 mg, 0.155 mmol), dry MeCN (0.90 mL), *p*-anisidine (88 mg, 0.71 mmol), and K₂CO₃ (248 mg, 1.79 mmol). Argon was bubbled through the solution for 10 min. The vial was flushed with Ar, sealed, and placed in a pre-heated oil bath (90 °C) and heated at 90 °C for 12 h. Upon cooling, the mixture was diluted with CH₂Cl₂ (20 mL) and water (5 mL). The aqueous layer was extracted with CH₂Cl₂ (10 mL), and the combined organic layers were washed with 1 M aqueous NaOH (5 mL) and brine (10 mL), dried (MgSO₄), and concentrated *in vacuo*. The crude residue was purified by chromatography on SiO₂ (deactivated with 0.1% Et₃N, hexanes/EtOAc, 9:1) to afford **2-21** (45.2 mg, 71%) as a yellow solid: R_f 0.3 (hexanes/EtOAc, 8:2); Mp 76.0–77.2 °C; IR (ATR) 2949, 2828, 1508, 1478, 1232, 1036 cm⁻¹; ¹H NMR (400 MHz, CDCl₃) δ 6.84–6.80 (m, 4 H), 6.44–6.40 (m, 4 H), 3.76 (s, 6 H), 3.66 (d, *J* = 6.8 Hz, 4 H), 3.53 (d, *J* = 6.8 Hz, 4 H), 2.93 (s, 4 H), 1.40 (s, 6 H); ¹³C NMR (100 MHz, CDCl₃) δ 152.1, 146.5, 114.7, 112.6, 63.1, 55.8, 45.1, 36.1, 24.3; HRMS (ESI) *m/z* calc for C₂₄H₃₃N₂O₂S (M+H) 413.2263, found 413.2253.



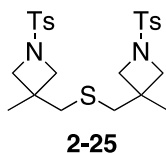
Bis((1-(4-bromophenyl)-3-methylazetididin-3-yl)methyl)sulfane (2-22). An oven-dried conical microwave vial equipped with stir bar was charged with **2-20** (200 mg, 0.179 mmol), dry MeCN (0.50 mL), *p*-bromoaniline (123 mg, 0.718 mmol), and K₂CO₃ (248 mg, 1.79 mmol).

Argon was bubbled through the solution for 5 min. The vial was flushed with Ar, sealed, and placed in a pre-heated oil bath (90 °C) and heated at 90 °C for 12 h. Upon cooling, the mixture was diluted with CH₂Cl₂ (10 mL) and water (5 mL), and the aqueous layer was extracted with CH₂Cl₂ (10 mL). The combined organic layers were washed with 1 N aqueous NaOH (5 mL) and brine (5 mL), dried (MgSO₄), and concentrated *in vacuo*. Purification by chromatography on SiO₂ (deactivated with 0.1% Et₃N, hexanes/EtOAc, 9:1) afforded **2-22** (48.1 mg, 53%) as a yellow solid: Mp 139–141 °C; IR (ATR) 2952, 2842, 1588, 1489, 1353, 807 cm⁻¹; ¹H NMR (500 MHz, CDCl₃) δ 7.29 (d, *J* = 8.5 Hz, 4 H), 6.31 (d, *J* = 8.5 Hz, 4 H), 3.68 (d, *J* = 6.9 Hz, 4 H), 3.54 (d, *J* = 6.9 Hz, 4 H), 2.91 (s, 4 H), 1.41 (s, 6 H); ¹³C NMR (125 MHz, CDCl₃) δ 150.4, 131.6, 113.0, 109.3, 62.4, 44.9, 36.1, 24.4.

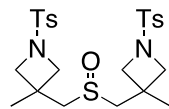


3,3'-Sulfinylbis(methylene)bis(1-(4-methoxyphenyl)-3-methylazetidinium) (2-23). A solution of **2-21** (40 mg, 0.097 mmol) in glacial AcOH (1.2 mL) was treated with H₂O₂ (*ca.* 30%, 11 μL, *ca.* 0.11 mmol). The mixture (which became purple in color almost immediately) was stirred at rt for 15 h. The mixture was concentrated *in vacuo* to ~1/5 volume and diluted with CH₂Cl₂ (25 mL) and saturated aqueous NaHCO₃ (10 mL). The aqueous layer was extracted with CH₂Cl₂ (10 mL), and the combined organic layers were dried (Na₂SO₄), filtered, and concentrated *in vacuo* to afford a crude brown residue (53 mg). Purification by chromatography on SiO₂ (deactivated with 0.1% Et₃N, hexanes/EtOAc, 1:2) afforded recovered **2-21** (9.0 mg) as well as **2-23** (24.5 mg, 59%) as a pink solid: IR (ATR) 2950, 2844, 1588, 1508, 1234, 813 cm⁻¹; ¹H NMR (500 MHz, CDCl₃) δ 6.82 (d, *J* = 8.8 Hz, 4 H), 6.42 (d, *J* = 8.9 Hz, 4 H), 3.95 (d, *J* = 7.1 Hz, 2 H), 3.78–3.76 (m, 2 H), 3.76 (s, 6 H), 3.67

(d, $J = 6.8$ Hz, 2 H), 3.62 (d, $J = 7.1$ Hz, 2 H), 3.29 (d, $J = 13.1$ Hz, 2 H), 2.83 (d, $J = 13.0$ Hz, 2 H), 1.60 (s, 6 H); ^{13}C NMR (125 MHz, CDCl_3) δ 152.4, 146.2, 114.7, 112.8, 63.9, 63.5, 63.3, 55.8, 34.0, 24.6; HRMS (ESI) m/z calc for $\text{C}_{24}\text{H}_{32}\text{N}_2\text{O}_3\text{S}$ 429.2212, found 429.2227.

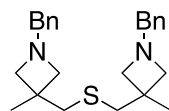


Bis((3-methyl-1-tosylazetididin-3-yl)methyl)sulfane (2-25). An oven-dried thick-walled glass tube was charged with **2-20** (200 mg, 0.179 mmol), dry MeCN (0.9 mL), *p*-toluenesulfonamide (123 mg, 0.718 mmol) and K_2CO_3 (248 mg, 1.79 mmol). Ar was bubbled through the mixture for 10 min, and the vial was sealed and heated at 90 °C overnight (15 h). Upon cooling, the mixture was diluted with CH_2Cl_2 (15 mL) and water (10 mL), and the aqueous layer was extracted with CH_2Cl_2 (10 mL). The combined organic layers were washed with 1 M aqueous NaOH and brine, dried (MgSO_4), and concentrated *in vacuo*. Chromatography on SiO_2 (hexanes/EtOAc, 2:1 with ~1% Et_3N) afforded **2-25** and mixed fractions, The collected fractions were combined and repurified by chromatography on SiO_2 (hexanes/EtOAc, 9:1 to 2:1 to 1:1) to afford **2-25** (48.5 mg, 53%) as a viscous yellow oil: IR (ATR) 2960, 1596, 1448, 1339, 1154 cm^{-1} ; ^1H NMR (300 MHz, CDCl_3) δ 7.56 (d, $J = 8.2$ Hz, 4 H), 7.39 (d, $J = 8.0$ Hz, 4 H), 3.54 (d, $J = 8.0$ Hz, 4 H), 3.40 (d, $J = 8.0$ Hz, 4 H), 2.49 (s, 4 H), 2.47 (s, 6 H), 1.07 (s, 6 H); ^{13}C NMR (100 MHz, CDCl_3) δ 144.1, 131.4, 129.7, 128.3, 60.5, 43.9, 34.5, 23.7, 21.6; HRMS (HESI) m/z calc for $\text{C}_{24}\text{H}_{33}\text{N}_2\text{O}_4\text{S}_3$ (M + H) 509.1597, found 509.1585.



2-26

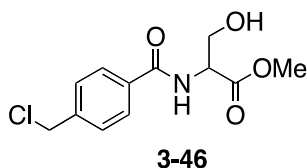
3,3'-(sulfinylbis(methylene))bis(3-methyl-1-tosylazetidines (2-26). A solution of **2-25** (45 mg, 0.088 mmol) in glacial AcOH (1 mL) was treated with H₂O₂ (ca. 3% aqueous, 0.11 mL, ca. 0.11 mmol) and stirred at rt for 12 h. The solution (which was colorless) was concentrated *in vacuo* to ~1/5 volume and diluted with saturated aqueous NaHCO₃ (5 mL) and CH₂Cl₂ (20 mL). The aqueous layer was extracted with CH₂Cl₂ (10 mL), and the combined organic layers were dried (Na₂SO₄), and concentrated *in vacuo* to afford **2-26** (crude, 43 mg, 93%) as a viscous colorless oil that solidifies upon standing: ¹H NMR (300 MHz, CDCl₃) δ 7.73 (d, *J* = 8.2 Hz, 4 H), 7.39 (d, *J* = 8.1 Hz, 4 H), 3.86 (d, *J* = 8.3 Hz, 2 H), 3.67 (d, *J* = 8.0 Hz, 2 H), 3.57 (d, *J* = 8.0 Hz, 2 H), 3.49 (d, *J* = 8.3 Hz, 2 H), 2.90 (d, *J* = 13.0 Hz, 2 H), 2.49 (d, *J* = 12.8 Hz, 2 H), 2.48 (s, 6 H), 1.33 (s, 6 H); HRMS (HESI) *m/z* calc for C₂₄H₃₃N₂O₅S₃ (M+H) 525.1546, found 525.1536.



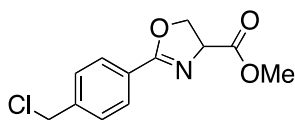
2-27

An oven-dried thick-walled vial was charged with **2-27** (700 mg, 0.628 mmol), dry MeCN (3.1 mL), benzylamine (0.27 mL, 2.5 mmol), and K₂CO₃ (868 mg, 6.28 mmol). Ar was bubbled through the solution for 10 min. The vial was sealed and heated at 90 °C overnight (15 h). Upon cooling, the mixture was diluted with CH₂Cl₂ (40 mL) and water (10 mL), and the aqueous layer was extracted with CH₂Cl₂ (20 mL). The combined organic layers were washed with 1 M aqueous NaOH and brine, dried (MgSO₄), and concentrated *in vacuo*. The crude residue was purified by chromatography on SiO₂ (hexanes/EtOAc, 1:2 with 1% Et₃N to 100% EtOAc to 5% MeOH/EtOAc) to afford **2-27** (150 mg, ~63% crude). Reported characterization data represent data obtained from an analytical sample from a separate batch of material: IR

(ATR) 2947, 2902, 1644, 1493, 1450 cm^{-1} ; ^1H NMR (500 MHz, CDCl_3) δ 7.34–7.24 (m, 10 H), 3.65 (s, 4 H), 3.13 (d, $J = 7.2$ Hz, 4 H), 3.00 (d, $J = 7.2$ Hz, 4 H), 2.84 (s, 4 H), 1.3 (s, 6 H); ^{13}C NMR (125 MHz, CDCl_3) δ 138.4, 128.3, 128.2, 126.8, 64.9, 63.4, 45.2, 35.9, 24.6; HRMS (HESI) m/z calc for $\text{C}_{24}\text{H}_{33}\text{N}_2\text{S}$ (M+H) 381.2359, found 381.2352.

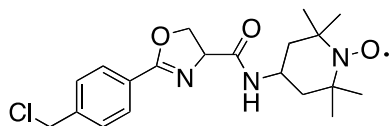


Methyl 2-(4-(chloromethyl)benzamido)-3-hydroxypropanoate (3-46). A flame-dried 250-mL round-bottom flask was charged with *dl*-serine methyl ester hydrochloride (6.59 g, 41.9 mmol), dry CH_2Cl_2 (60 mL), and Et_3N (5.9 mL, 42 mmol). To this cloudy solution was added a solution of 4-(chloromethyl)benzoyl chloride (5.09 g, 26.1 mmol) in dry CH_2Cl_2 (60 mL) slowly via syringe in 3 portions. The cloudy solution was stirred at rt for 15 h and subsequently diluted with CH_2Cl_2 (100 mL), washed with water and brine, dried (MgSO_4) and concentrated *in vacuo*. The crude residue was purified by chromatography on SiO_2 (hexanes/ EtOAc , 1:1) to elute bis-a2-(4-(chloromethyl)-*N*-(4-(chloromethyl)benzoyl)benzamido)-3-hydroxypropanoate (R_f 0.47 hexanes/ EtOAc , 1:1). Subsequent elution with 100% EtOAc afforded **3-46** (4.64 g, 65%) as a white solid: Mp 83.4–85.1 $^\circ\text{C}$ (CH_2Cl_2); IR (ATR) 3360, 1728, 1620, 1258, 1053 cm^{-1} ; ^1H NMR (300 MHz, CDCl_3) δ 7.81 (d, $J = 8.3$ Hz, 2 H), 7.45 (d, $J = 8.3$ Hz, 2 H), 7.19 (d, $J = 6.8$ Hz, 1 H), 4.86 (dt, $J = 7.3, 3.6$ Hz, 1 H), 4.60 (s, 2 H), 4.12–4.01 (m, 2 H), 3.81 (s, 3 H), 2.93 (bs, 1 H); ^{13}C NMR δ 171.0, 167.0, 141.3, 133.3, 128.7, 127.6, 63.3, 55.1, 52.9, 45.3.



3-47

Methyl 2-(4-(chloromethyl)phenyl)-4,5-dihydrooxazole-4-carboxylate (3-47). A solution of methyl 2-(4-(chloromethyl)benzamido)-3-hydroxypropanoate **3-46** (984 mg, 3.65 mmol) in distilled THF (20 mL) was treated with Burgess Reagent (1.15 g, 4.83 mmol). The solution was heated at reflux for 1 h, cooled to rt, and the resulting white precipitate was removed *via* Buchner filtration. The filtrate was concentrated *in vacuo*, and the residue was dissolved in CH₂Cl₂ and concentrated onto SiO₂. Purification via chromatography on SiO₂ (hexanes/EtOAc, 2:1) afforded **3-47** (754 mg, 82%) as a white solid; Mp 70.0–71.8 °C (CH₂Cl₂); IR (ATR) 2959, 1735, 1636, 1213, 1084 cm⁻¹; ¹H NMR (300 MHz, CDCl₃) δ 7.99 (d, *J* = 8.3 Hz, 2 H), 7.45 (d, *J* = 8.3 Hz, 2 H), 4.97 (dd, *J* = 10.6, 8.0 Hz, 1 H), 4.72 (t, *J* = 8.3 Hz, 1 H), 4.65–4.58 (m, 1 H), 4.61 (s, 2 H), 3.83 (s, 3 H); ¹³C NMR (75 MHz, CDCl₃) δ 171.5, 165.8, 141.1, 129.0, 128.5, 126.9, 69.6, 68.6, 52.7, 45.4; HRMS (EI) *m/z* calc for C₁₂H₁₂ClNO₃ 253.0506, found 253.0512.

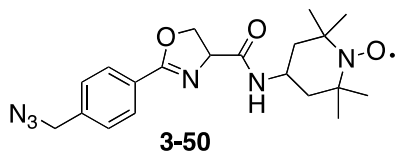


3-44

2-(4-(chloromethyl)phenyl)-N-(1-oxyl-2,2,6,6-tetramethylpiperidin-4-yl)-4,5-dihydrooxazole-4-carboxamide (3-44). A solution of **3-47** (305 mg, 1.20 mmol) in THF (15 mL) was treated with 1 N aqueous NaOH (1.80 mL, 1.80 mmol) and stirred at rt for 1 h. NaHCO₃ (500 mg, 5.95 mmol) was added, and the solvent was removed *in vacuo*. Residual water was removed coevaporation with benzene (3 x). To the residue was added a solution of 4-amino TEMPO (415 mg, 2.35 mmol) in anhydrous DMF, and additional DMF was added to

bring the total volume to 30 mL. The solution was cooled to 0 °C, and DIPEA (0.10 mL, 6.0 mmol) and PyCloP (602 mg, 1.43 mmol) were added. The ice bath was removed, and the solution was stirred for 1 h at rt. The reaction mixture was poured into EtOAc (500 mL), and the resulting solution was washed successively with 5% NaHSO₄ (100 mL), 5% NaHCO₃ (100 mL), water, and brine, dried (Na₂SO₄), and concentrated. The residue was purified by chromatography on SiO₂ (hexanes/EtOAc, 1:2) to afford **3-44** (367 mg, 78%) as a peach-colored foam. IR (ATR) 3392, 2971, 1640, 1510, 1359, 1239, 1081 cm⁻¹; HRMS (EI) *m/z* calc for C₂₀H₂₇ClN₃O₃ 392.1741, found 392.1737.

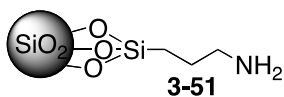
NMR characterization was carried out on the corresponding hydroxylamine (**3-44a**), which was obtained as follows: the analyte was dissolved in MeOH and treated with excess ascorbic acid. Once the color turned from orange to clear, the solution was diluted with ether and washed with sat. NaHCO₃(aq), water, and brine, dried (MgSO₄) and concentrated: ¹H NMR (300 MHz, CDCl₃) δ 7.97 (d, *J* = 8.0 Hz, 2 H), 7.48 (d, *J* = 8.0 Hz, 2 H), 6.44 (d, *J* = 8.0 Hz, 1 H), 4.83 (app t, *J* = 9.6 Hz, 1 H), 4.71 (app t, *J* = 9.6 Hz, 1 H), 4.64–4.58 (m, 3 H), 4.63 (s, 2 H), 4.24–4.11 (m, 1 H), 1.93 (dt, *J* = 12.5, 3.3 Hz, 1 H), 1.80 (dt, *J* = 12.5, 3.2 Hz, 1 H), 1.46–1.31 (m, 2 H), 1.22 (s, 3 H), 1.20 (s, 3 H), 1.19 (s, 3 H), 1.15 (s, 3 H); ¹³C NMR (75 MHz, CDCl₃) δ 170.6, 165.4, 141.1, 128.6, 128.4, 126.7, 70.3, 68.7, 58.7, 45.2, 45.0, 40.6, 32.1, 19.4.



2-(4-(Azidomethyl)phenyl)-N-(1-oxyl-2,2,6,6-tetramethylpiperidin-4-yl)-4,5-dihydrooxazole-4-carboxamide (3-50). A solution of **3-47** (499 mg, 1.97 mmol) in absolute MeOH (20.0 mL) was treated with 1 N aqueous NaOH (2.4 mL, 2.4 mmol) at rt. The solution was stirred for 2 h at rt, NaHCO₃ (830 mg, 9.85 mmol) was added, and the solvent was removed *in vacuo*. Residual water was removed via coevaporation with benzene (2 x). To the dried

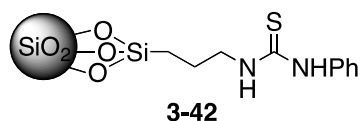
mixture was added a solution of 4-amino TEMPO (700 mg, 3.94 mmol) in dry DMF, followed by additional DMF to bring the total volume to 40 mL. The solution was cooled to 0 °C, and DIPEA (1.64 mL, 9.85 mmol) and DPPA (1.32 mL, 5.91 mmol) were added. The reaction mixture was stirred for 33 h, gradually warming to rt. The mixture was quenched with saturated aqueous NaHCO₃ (16 mL) and stirred an additional 1 h. The mixture was partitioned between water (100 mL) and Et₂O (100 mL), and the aqueous layer was extracted with Et₂O until the ethereal layer showed no orange color. The combined organic layers were washed with water (6 x), brine, dried (Na₂SO₄) and concentrated *in vacuo*. Purification by chromatography on SiO₂ (hexanes/EtOAc,1:2) afforded **3-50** (658 mg, 83%) as an orange foam: IR (ATR) 3388, 3343, 2971, 2095, 1640, 1239, 1081 cm⁻¹; EI-MS *m/z* 400 ([M+H]⁺, 20), 399 (M⁺, 13), 372 (8), 341 (6), 201 (26), 124 (99), 84 (73). HRMS (EI) *m/z* calc for C₂₀H₂₈N₆O₃ (M+H) 400.2223, found 400.2214.

NMR analysis was performed after reducing **3-50** to the corresponding hydroxylamine (**3-50a**) by dissolving **3-50** in MeOH and treating with ascorbic acid. After the solution turned from orange to colorless, the solution was diluted with Et₂O and washed with saturated aqueous NaHCO₃, water, and brine, dried and concentrated *in vacuo*: ¹H NMR (500 MHz, CDCl₃) δ 8.00 (d, *J* = 8.2 Hz, 2 H), 7.41 (d, *J* = 8.1 Hz, 2 H), 6.42 (d, *J* = 7.9 Hz, 1 H), 4.83 (dd, *J* = 11.0, 8.4 Hz, 1 H), 4.71 (dd, *J* = 11.0, 8.8 Hz, 1 H), 4.61 (t, *J* = 8.6 Hz, 1 H), 4.43 (s, 2 H), 4.27 (b, 1 H), 4.22–4.14 (m, 1 H), 1.93 (dt, *J* = 12.6, 3.4 Hz, 1 H), 1.81 (dt, *J* = 12.5, 3.4 Hz, 1 H), 1.45–1.33 (m, 2 H), 1.22 (s, 3 H), 1.20 (s, 3 H), 1.19 (s, 3 H), 1.16 (s, 3 H); ¹³C NMR (125 MHz, CDCl₃) δ 170.7, 165.5, 139.3, 128.8, 127.9, 126.8, 70.4, 68.8, 58.8, 54.1, 45.1, 40.7, 32.2, 19.5.



Representative procedure for synthesis of 3-aminopropyl functionalized nanoparticles (3-51). To a solution of cyclohexane (10 mL) and absolute EtOH (20 mL) in a 250-mL round-bottom flask was added commercial IPAST solution (6.17 g, 1.85 g SiO₂, 30 wt% in *i*-PrOH).

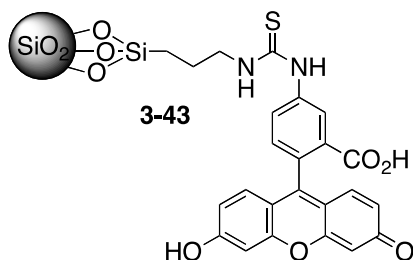
The suspension was stirred vigorously using a pearl-shaped stir bar, and 3-aminopropyltriethoxysilane (1.85 mL, 7.79 mmol) was added dropwise via syringe. The solution, which became cloudy within minutes of the addition, was stirred vigorously at rt for 2 h. The reaction mixture was poured into a 50 mL Falcon tube and water (~5 mL) was added. The tube was centrifuged (4400 rpm, 3000 xg, 15 min). The supernatant was decanted, and the sediment was suspended in EtOH (30 mL) and sonicated (ultrasonic bath) for 30 min. This washing procedure was repeated, and at this point, it was clear some aggregates that were not suspending were present. The suspension was decanted away from the aggregates into a clean 50 mL Falcon tube and centrifuged (4400 rpm, 3000 xg, rt, 15 min). The sediment was suspended in EtOH (30 mL) and sonicated for 30 min. The tube was centrifuged as above, the supernatant was decanted, and the resultant sediment was dried under Ar and subsequently under N₂ and finally under high vacuum at 50 °C for 4 h. Final drying under high vacuum for 20 h at rt afforded functionalized nanoparticles (1.27 g) as a white solid: Anal. Found for (SiO₂)_nC₃H₈N: C, 3.12; H, 0.85; N, 1.10.



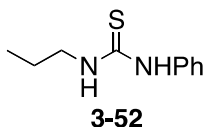
Representative procedure for phenylthiourea-functionalized silica particles (3-42).

Dried 3-aminopropyl-functionalized particles **3-51** (330 mg) were suspended in dry THF (15 mL) and stirred for 5 min. Phenylisothiocyanate (1.50 mL, 12.5 mmol) was added dropwise via syringe at rt. The reaction mixture was stirred for 25 h at rt and poured into a 50-mL Falcon tube. The tube was centrifuged (4400 rpm, 3000 xg, 10 min, rt) to give an off-white pellet (Note: the supernatant was bright yellow in color). The pellet was resuspended in EtOH, sonicated for 30 min, and centrifuged (4400 rpm, 3000 xg, 10 min, rt). The resuspension/sonication/centrifugation procedure was repeated four times. The pellet from the final washing was dried under a stream of N₂ for 3 days to afford a white powdery solid (225 mg): Anal. Found for (SiO₂)_nC₁₀H₁₃N₂S: C, 4.17; H, 0.70; N, 1.14; S, 0.94.

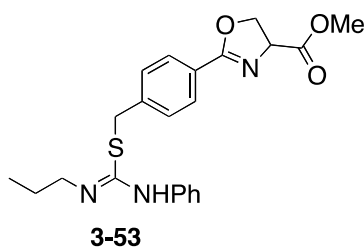
Note: Loading values were typically 0.31–0.41 mmol/g, based on %S content.



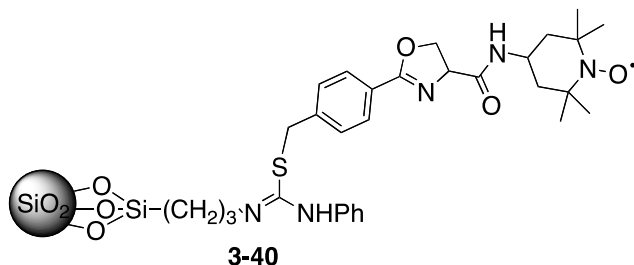
Representative procedure for fluorescein-thiourea-functionalized silica particles (3-42). Dried 3-aminopropyl-functionalized particles **3-51** (275 mg) were suspended in dry THF (15 mL) and stirred for 10 min. Fluorescein isothiocyanate (105 mg, 0.256 mmol) was added, and the bright orange suspension (which gradually became bright yellow in color) was stirred for 25 h at rt. The mixture was poured into a 50-mL Falcon tube. The tube was centrifuged (4400 rpm, 3000 xg, 10 min, rt) to give an orange pellet. The pellet was resuspended in EtOH, sonicated for 30 min, and centrifuged (4400 rpm, 3000 xg, 10 min, rt). The resuspension/sonication/centrifugation procedure was repeated four times. The pellet from the final washing was dried under a stream of N₂ for 3 days to afford bright yellow powder (172 mg): Anal. Found for (SiO₂)_nC₂₄H₂₀N₂O₅S: C, 5.61; H, 0.87; N, 1.17; S, 0.34.



1-Phenyl-3-propylthiourea (3-52).²⁶⁶ A solution of *n*-propylamine (0.700 mL, 8.51 mmol) and phenylisothiocyanate (1.00 mL, 8.35 mmol) in distilled THF (15.0 mL) was stirred at rt for 6 h. THF was removed *in vacuo*, and the residue was purified by chromatography on SiO₂ (hexanes/EtOAc, 3:1) to afford 1-phenyl-3-propylthiourea (1.62 g, quant.) as a white solid: Mp 60.9–62.8 °C (CH₂Cl₂) (lit.²⁶⁶ Mp 59–60 (EtOH)); ¹H NMR (300 MHz, CDCl₃) δ 7.71 (b, 1 H), 7.47–7.42 (m, 2 H), 7.32–7.29 (m, 1 H), 7.22–7.20 (m, 2 H), 6.02 (b, 1 H), 3.62, 3.59 (AB, *J* = 7.1 Hz, 2 H), 1.66–1.54 (m, 2 H), 0.92 (t, *J* = 7.4 Hz, 3 H).



Independent synthesis of model system: (Z)-methyl-2-(4-((N-phenyl-N'-propylcarbamimidoylthio)methyl)phenyl)-4,5-dihydrooxazole-4-carboxylate (3-53). A solution of 1-phenyl-3-propylthiourea (217mg, 1.12 mmol), DIPEA (0.130 mL, 0.787 mmol), TBAI (65 mg, 0.18 mmol), and **3-47** (109 mg, 0.430 mmol) in DMF (6.5 mL) was heated at 110 °C for 30 min. The mixture was cooled, poured into water (25 mL), and diluted with Et₂O (50 mL). The aqueous layer was extracted with Et₂O (3 x 20 mL). The combined organic layers were washed with water (3 x) and brine (once), dried (MgSO₄) and concentrated *in vacuo*. The crude residue was purified by chromatography on SiO₂ (packed using hexanes/EtOAc/Et₃N 47.5:47.5:5.0, eluted with hexanes/EtOAc, 1:1) to afford **3-53** (108 mg, 61%) as a yellow foam: ¹H NMR (300 MHz, CDCl₃) δ 7.93 (d, *J* = 8.2 Hz, 2 H), 7.38 (d, *J* = 7.1 Hz, 2 H), 7.32–7.27 (m, 4 H), 7.03 (t, *J* = 7.4 Hz, 1 H), 6.89 (d, *J* = 7.6 Hz, 2 H), 4.96 (dd, *J* = 10.6, 7.9 Hz, 1 H), 4.70 (app t, *J* = 8.3 Hz, 1 H), 4.60 (app t, 1 H), 4.46–4.35 (b, 1 H), 4.02–3.92 (b, 1 H), 3.83 (s, 3 H), 3.75–3.69 (m, 1 H), 3.23–3.16 (b, 1 H), 1.52–1.42 (m, 2 H), 1.31–1.19 (m, 2 H), 0.86 (t, *J* = 7.4 Hz, 3 H); ¹³C NMR (75 MHz, CDCl₃) δ 171.5, 165.9, 149.3, 141.9, 129.0, 128.8, 128.8, 125.8, 122.6, 122.0, 69.5, 68.5, 52.7, 44.9, 34.9, 22.8, 11.2.



Representative procedure for alkylation of thiourea-functionalized nanoparticles with 3-44 to form imidothiolate particles 3-40. An oven-dried 25-mL round-bottom flask was charged with particles **3-42** (54.9 mg), TBAI (44.1 mg, 0.119 mmol) and **3-44** (125 mg, 0.318 mmol). To the flask was added anhydrous, degassed DMF (11 mL) (degassed using freeze-pump-thaw; 3 x). DIPEA (0.13 mL, 0.75 mmol) was added, and the mixture was placed into a pre-heated oil bath and heated at 110 °C for 2 h. After cooling, the mixture was poured into a 50-mL Falcon tube containing EtOH/water, 9:1 (30 mL), and the tube was centrifuged (4400 rpm, 3000 xg, 10 min, rt). The supernatant was decanted, and the sediment was diluted with EtOH/water (9:1, 20 mL), sonicated, and centrifuged (4400 rpm, 3000 xg, 10 min, rt). This washing procedure was repeated, and the resulting sediment was resuspended in degassed DMF (10 mL), and heated at 90 °C for 20 min. After cooling, the mixture was poured into a 50-mL Falcon tube and diluted with EtOH/water, 9:1 (20 mL) and centrifuged (4400 rpm, 3000 xg, 10 min, rt). The supernatant was decanted, and the sediment was diluted with EtOH/water, 9:1 (20 mL), sonicated (20 min), and centrifuged as described above. This washing procedure was repeated two additional times, and the resulting pellet was transferred to a 15-mL Falcon tube using EtOH (7 mL), sonicated (20 min), and centrifuged as described. The supernatant was decanted, and the pellet was resuspended in absolute EtOH (7 mL), and washed using EtOH as described (3 x). The final pellet was dried under a stream of N₂ to afford pale tan-colored particles (22.6 mg).

The combined supernatants collected before resuspension in DMF were diluted with water (200 mL) and extracted with Et₂O (200 mL). The ethereal layer was washed with water and brine, dried (Na₂SO₄), and concentrated *in vacuo*. Purification by chromatography on SiO₂

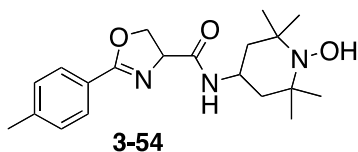
(hexanes/EtOAc, 1:2) afforded recovered **3-44** (48 mg). Anal. Found for $(\text{SiO}_2)_n\text{C}_{30}\text{H}_{35}\text{N}_5\text{O}_3\text{S}$: C, 5.69; H, 0.97; N, 1.28; S, 0.46.

Loadings were determined by elemental analysis, taking into account the loadings of the precursor and thiourea and amine nanoparticles. The combustion analysis and loading calculations are depicted in Table 4-1.

Table 4-1. Tabulated elemental analysis data for imidothiolate-functionalized silica nanoparticles.

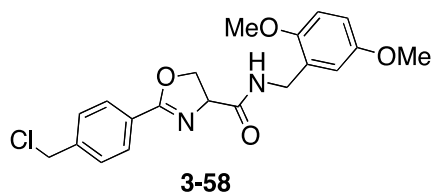
Entry	Batch	%C	%H	%N	%S	Loading based on % N (mmol/g)	Loading based on % S (mmol/g)
1	“Blank” particles	0.20	0.69	0.0	0.0		
2	Amine 3-51A	3.53	0.89	1.17	ND	0.83	
	Thiourea 3-42A	5.21	0.86	1.30	ND	0.093	ND
	Imidothiolate 3-40A	6.40	0.98	1.42	ND	0.029	ND
3	Amine 3-51A	2.23	0.68	0.72	0.0	0.51	
	Thiourea 3-42A	3.71	0.74	0.84	0.75	0.079	0.23
	Imidothiolate 3-40A	5.42	0.93	1.07	0.27	0.055	
4	Amine 3-51A	3.38	0.76	1.12	0.0	0.80	
	Thiourea 3-42A	4.17	0.70	1.1	0.84		0.26
	Imidothiolate 3-40A	5.69	0.97	1.28	0.46	0.043	

Alkylation of fluorescein-substituted thiourea-functionalized nanoparticles with 3-44 to form imidothiolate particles 3-41. The same procedure was described for formation of imiothiolate particles **3-40** was used with the following amounts of reagents: particles **3-43** (56.2 mg), TBAI (45.3 mg, 0.123 mmol), **3-44** (125 mg, 0.318 mmol), and anhydrous, degassed DMF (11 mL). Upon washing and drying under N₂, bright orange colored particles (38.5 mg) were collected. Anal. Found for (SiO₂)_nC₃₀H₃₅N₅O₃S: C, 8.02; H, 1.10; N, 1.41; S, 0.22. Recovered **3-44** (43 mg) was isolated after workup and chromatography as described in the case of imiodthiolate particles **3-40**.

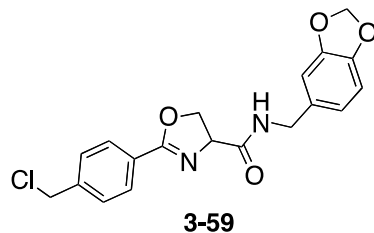


***N*-(1-hydroxy-2,2,6,6-tetramethylpiperidin-4-yl)-2-*p*-tolyl-4,5-dihydrooxazole-4-carboxamide (3-54).** A solution of **3-44** (31.5 mg, 0.0802 mmol) in THF (2.0 mL) was treated with Raney Ni (~50 mg, taken from a 50% slurry in water and washed with THF but not completely dried) and stirred for 1 h 45 min at rt. The mixture was filtered through Celite and concentrated *in vacuo*. The residue was taken up in MeOH (1.0 mL) and treated with Cu(OAc)₂•H₂O (1.4 mg, 0.0080 mmol) and stirred open to air for 1.5 h. The mixture was concentrated *in vacuo*, and the residue was taken up into CHCl₃ and washed with water. The aqueous layer was extracted with CHCl₃ (twice), and the combined organic layers were washed with water and brine, dried (Na₂SO₄) and concentrated, and dried under high vacuum overnight to afford the corresponding *N*-oxyl radical **3-57** (11.1 mg, 38%) as an orange solid. The solid was dissolved in MeOH (1 mL) and treated with excess ascorbic acid (24 mg). The solution was shaken until the orange color turned to colorless. The solution was then diluted with Et₂O and washed with saturated aqueous NaHCO₃, water, and brine, dried (MgSO₄) and concentrated *in vacuo* to afford **3-54** (9.0 mg, 31% overall) as a colorless, amorphous foam: ¹H NMR (300 MHz, CDCl₃) δ 7.87 (d, *J* = 8.1 Hz, 2 H), 7.27–7.25 (m, 2 H), 6.46 (d, *J* = 7.8 Hz, 1 H), 4.81 (dd, *J* = 10.8, 8.2 Hz, 1 H), 4.68 (dd, *J* = 10.8, 8.6 Hz, 1 H), 4.58 (t, *J* = 8.3 Hz, 1 H), 4.25–4.11 (m, 1

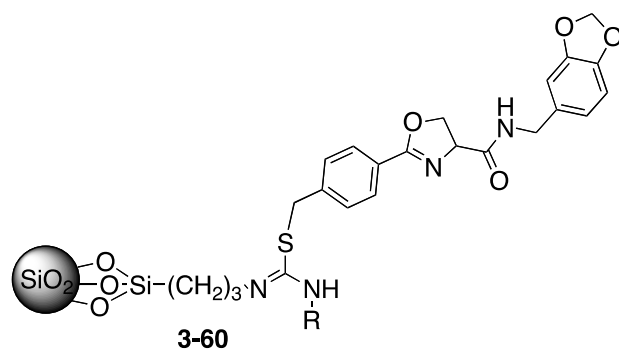
H), 2.43 (s, 3 H), 1.94 (dt, $J = 12.5, 3.5$ Hz, 1 H), 1.81 (dt, $J = 12.6, 3.5$ Hz, 1 H), 1.49–1.33 (m, 2 H), 1.23 (s, 3 H), 1.22 (s, 3 H), 1.20 (s, 3 H), 1.17 (s, 3 H).



2-(4-(Chloromethyl)phenyl)-N-(2,5-dimethoxybenzyl)-4,5-dihydrooxazole-4-carboxamide (3-58). A solution of **3-47** (308 mg, 1.21 mmol) in THF (15 mL) was treated with 1 N aqueous NaOH (1.80 mL, 1.80 mmol) and stirred for 30 min at rt. NaHCO₃ (504 mg, 6.00 mmol) was added, and THF was removed *in vacuo*. Residual water was removed by coevaporation with benzene (3 x). The residual white solid was dissolved in DMF, and a solution of 2,5-dimethoxybenzylamine (429 mg, 2.57 mmol) in DMF was added (30 mL total volume DMF). Sonication (ultrasonic bath) was employed to move the white solid from the sides of the vessel into the reaction mixture. To this solution was added DIPEA (1.00 mL, 6.05 mmol) and PyCloP (624 mg, 1.48 mmol). The reaction mixture was stirred for 1 h at rt. The mixture was diluted with EtOAc (400 mL) and washed successively with 5% aqueous NaHSO₄ (200 mL), 5% aqueous NaHCO₃, water (2 x 200 mL), and brine (100 mL), dried (MgSO₄) and concentrated *in vacuo*. Purification by chromatography on SiO₂ (hexanes/EtOAc, 1:1 to 100% EtOAc) afforded **3-58** (348 mg, 73%) as a white solid: IR (ATR) 3267, 2963, 1653, 1633, 1552, 1502, 1232, 1057 cm⁻¹; ¹H NMR (300 MHz, CDCl₃) δ 7.97 (d, $J = 8.4$ Hz, 2 H), 7.46 (d, $J = 8.5$ Hz, 2 H), 6.85–6.84 (m, 1 H), 6.78–6.77 (m, 2 H), 4.87 (dd, $J = 10.5, 8.6$ Hz, 1 H), 4.74–4.64 (m, 2 H), 4.62 (s, 2 H), 4.50 (dd, $J = 14.7, 6.2$ Hz, 1 H), 4.42 (dd, $J = 14.7, 6.0$ Hz, 1 H), 3.78 (s, 3 H), 3.74 (s, 3 H); ¹³C NMR (75 MHz, CDCl₃) δ 171.2, 165.5, 153.5, 151.8, 141.3, 128.8, 128.5, 127.1, 126.9, 115.5, 113.2, 111.3, 70.7, 69.1, 55.8, 55.7, 45.4, 39.2; HRMS (ES) m/z calc for C₂₀H₂₁ClN₂O₄Na (M+Na) 411.1088, found 411.1075.



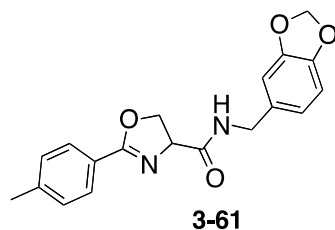
***N*-(Benzo[d][1,3]dioxol-5-ylmethyl)-2-(4-(chloromethyl)phenyl)-4,5-dihydrooxazole-4-carboxamide (3-59).** A solution of **3-47** (311 mg, 1.23 mmol) in THF (15 mL) was treated with 1 N aqueous NaOH (1.80 mL, 1.80 mmol) and stirred for 0.5 h at rt. NaHCO₃ (515 mg, 6.13 mmol) was added, and the solvent was removed *in vacuo*. Residual water was removed by coevaporation with benzene (3 x). To the white residue was added a solution of 3,4-methylenedioxybenzylamine (380 mg, 2.45 mmol) in DMF, and additional DMF was added to bring the total volume to 30 mL. The reaction vessel was sonicated (ultrasonic bath) to bring all material from the sides of the flask into solution, and DIPEA (1.00 mL, 6.13 mmol) and PyCloP (466 mg, 1.48 mmol) were added. The colorless solution was stirred for 1 h at rt. The solution was diluted with EtOAc (400 mL) and washed successively with 5% aqueous NaHSO₄ (150 mL), 5% aqueous NaHCO₃ (150 mL), water (twice), and brine, dried (Na₂SO₄) and concentrated *in vacuo*. The residue was taken up in CH₂Cl₂ and concentrated onto SiO₂, after which purification by chromatography on SiO₂ (hexanes/EtOAc, 1:1) afforded **3-59** (326 mg, 71%) as a white solid: Mp 158.8–161.4 °C; IR (ATR) 3267, 2898, 1647, 1631, 1534, 1498, 1252, 1073 cm⁻¹; ¹H NMR (300 MHz, CDCl₃) δ 7.95 (d, *J* = 8.4 Hz, 2 H), 7.45 (d, *J* = 8.5 Hz, 2 H), 6.94 (bs, 1 H), 6.79–6.75 (m, 3 H) 5.95 (s, 2 H), 4.90 (dd, *J* = 10.8, 8.6 Hz, 1 H), 4.77–4.64 (m, 2 H), 4.61 (s, 2 H), 4.47 (dd, *J* = 14.7, 6.5 Hz, 1 H), 4.30 (dd, *J* = 14.7, 5.6 Hz, 1 H); ¹³C NMR (75 MHz, CDCl₃) δ 171.5, 165.7, 147.9, 147.0, 141.3, 131.6, 128.9, 128.6, 126.9, 121.1, 108.3, 101.1, 70.6, 69.1, 45.4, 43.0; MS (EI) *m/z* (rel. intensity) 374 ([M⁺], 14), 372 ([M⁺], 40), 337 (10), 203 (100); HRMS (EI) *m/z* calc for C₁₉H₁₇ClN₂O₄ 372.0877, found 372.0870.



Nanoparticle functionalization with 3-59. A suspension of particles **3-42** (54.7 mg) in anhydrous DMF (12.5 mL) was sonicated (ultrasonic water bath) for 20 min. To the suspension was added DIPEA (0.14 mL, 0.80 mmol), TBAI (38.6 mg, 0.105 mmol) and **3-59** (119 mg, 0.319 mmol). The solution placed in a pre-heated oil bath and heated at 110 °C for 2 h. After cooling, the reaction mixture was poured into a 50-mL Falcon tube containing EtOH/water 9:1, and the tube was further diluted with EtOH/water 9:1 until the total volume reached 25 mL. The tube was centrifuged (3200 rpm, 2135 xg, 10 min, rt). The supernatant was removed *via* pipet, and the sediment was suspended in 9:1 EtOH/water (25 mL), sonicated for 15 min, and centrifuged (3000 rpm, 1877 xg, 10 min, rt). This washing process (re-suspension, sonication, centrifugation) was carried out two additional times. The sediment was then suspended in DMF (20 mL) and heated at 100 °C with stirring for 30 min. After cooling, the mixture was diluted with 9:1 EtOH/water and washed 3 x in the same manner as described above. The sediment remaining after the last wash was transferred to a 15 mL Falcon tube (using EtOH to transfer) and diluted with EtOH to the 6.5 mL mark. The tube was centrifuged (3000 rpm, 1877 xg, 5 min, rt), the supernatant was removed by pipet, and the sediment was suspended in EtOH and centrifuged under the same conditions. This washing process was repeated three times, and finally the last sediment was transferred to a clean 15 mL Falcon tube (using absolute EtOH for transfer) and dried under a stream of N₂ to afford pale orange particles (35.6 mg).

The combined supernatants from the first washes were combined and diluted with water and Et₂O. The aqueous portion was extracted with Et₂O (3 x), and the combined organic layers were washed with water and brine, dried (Na₂SO₄) and concentrated *in vacuo*. The crude residue

was purified by chromatography on SiO₂ (hexanes/EtOAc, 1:1) to afford recovered chloride **3-59** (77.6 mg), as a pale yellow solid.



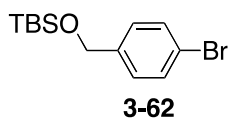
N-(Benzo[d][1,3]dioxol-5-ylmethyl)-2-p-tolyl-4,5-dihydrooxazole-4-carboxamide (3-61). A solution of **3-59** (150 mg, 0.402 mmol) in THF (45 mL) was treated with Raney Ni (3.45 g, taken from an aqueous slurry and washed with THF) and stirred at rt for 45 min. The mixture was filtered through Celite, and the Celite plug was flushed with EtOH. The filtrate was concentrated *in vacuo*, and the residue was purified by chromatography on SiO₂ (hexanes/EtOAc, 1:1) to afford **3-61** (102 mg, 75%) as a white solid: ¹H NMR (300 MHz, CDCl₃) δ 7.84 (d, *J* = 8.2 Hz, 2 H), 7.23 (d, *J* = 8.0 Hz, 2 H), 6.98 (b, 1 H), 6.79–6.75 (m, 3 H), 5.95 (s, 2 H), 4.88 (dd, *J* = 10.9, 8.5 Hz, 1 H), 4.72 (dd, *J* = 10.9, 8.7 Hz, 1 H), 4.61 (t, *J* = 8.5 Hz, 1 H), 4.47 (dd, *J* = 14.7, 6.4 Hz, 1 H), 4.30 (dd, *J* = 14.6, 5.6 Hz, 1 H), 2.41 (s, 3 H).

Procedure for “Blank” Reaction with 3-61 and particles 3-42. A solution of PITC nanoparticles **3-42** (23.5 mg) were suspended in anhydrous DMF (6.2 mL) and sonicated for 20 min (ultrasonic bath). The suspension was treated with TBAI (17.8 mg, 0.0482 mmol), DIPEA (0.065 mL, 0.37 mmol), and a solution of **3-61** (49.3 mg, 0.146 mmol). The solution was heated at 110 °C for 2 h (pre-heated oil bath). After cooling, the mixture was poured into a 50-mL Falcon tube, containing 10 mL of EtOH/water, 9:1. The tube was centrifuged (3200 rpm, 2135 xg, 10 min, rt). The supernatant was removed by pipet, and the sediment was suspended in EtOH/water 9:1 (25 mL) and sonicated for 25 min. The tube was centrifuged using the same conditions as described above, and the supernatant was removed *via* pipet. The washing procedure was repeated two additional times (3 washes total after the initial DMF dilution). The

sediment was diluted with DMF (15 mL) and transferred to a 50 mL round-bottom flask (transfer pipet), and this solution was vigorously stirred and heated at 90 °C for 20 min. The mixture was cooled and poured into a 50 mL Falcon tube and diluted with 9:1 ethanol/water (10 mL). The solution was sonicated, and subsequently centrifuged (3200 rpm, 2135 xg, 10 min, rt). The supernatant was decanted, and the particles were suspended in 9:1 EtOH/water (25 mL) and centrifuged (3200 rpm, 2135 xg, 10 min, rt). This was repeated, and the supernatant was decanted, and the particles were suspended in EtOH and transferred to a 15-mL Falcon tube (7 mL EtOH were used total). The tube was centrifuged (3200 rpm, 2135 xg, 5 min, rt), the supernatant was decanted, and the particles were suspended in EtOH (7 mL), sonicated, and centrifuged under the same conditions as above. This washing procedure was repeated four times, and finally the supernatant was decanted and the particles were suspended in EtOH (4 mL), transferred to a clean pre-weighed 15 mL Falcon tube, sonicated, and dried under N₂ to afford pale orange-colored particles (12.8 mg).

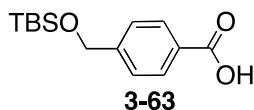
The initial supernatants were combined and diluted with water and Et₂O. The aqueous layer was extracted with Et₂O (3 x), and the combined organic layers were washed with water (3 x), and brine, dried (Na₂SO₄) and concentrated *in vacuo*. Purification by chromatography on SiO₂ (hexanes/EtOAc, 1:1) afforded recovered **3-61** (38.9 mg), as a yellow solid.

General procedure for thioether cleavage of UV-active model system 3-60. A suspension of piperonyl-labeled nanoparticles **3-60** (11.3 mg) in absolute EtOH (1.0 mL) were treated with NiCl₂ (63 mg, 0.49 mmol) and then (slowly) NaBH₄ (36 mg, 0.95 mmol), affording a black solid and much H₂ evolution. The slurry was sonicated (ultrasonic bath) for 1 h, and then filtered through a plug of Celite, flushed with EtOH (~25 mL total EtOH), and the filtrate was concentrated. The residue was taken up in distilled THF (sonication was employed to move residue from the sides of the flask into solution) and diluted to 10 mL in a volumetric flask. Aliquots of this solution were analyzed by UV/VIS at 283 nm and 264 nm. The absorbance values were correlated to a standard curve to ultimately afford loading values of 0.014 mmol/g (283 nm) and 0.011 mmol/g (264 nm).



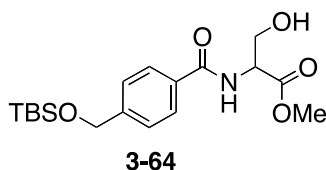
(4-Bromobenzoyloxy)(tert-butyl)dimethylsilane (3-61).^{267,268} A solution of 4-bromobenzyl alcohol (10.0 g, 52.9 mmol), TBSCl (12.1 g, 79.4 mmol), and imidazole (7.28 g, 106 mmol) in CH₂Cl₂ (110 mL) was stirred at rt for 11 h. The mixture was poured into ice-water (300 mL), and the aqueous layer was extracted with CH₂Cl₂ (3 x 100 mL). The combined organic layers were washed with saturated aqueous NaHCO₃ (150 mL), water (150 mL), and brine (150 mL), dried (Na₂SO₄) and concentrated *in vacuo*. The crude residue was purified by Kugelrohr distillation (110 °C < T < 135 °C at 2 Torr) to afford **3-61** (15.2 g, 95%) as a colorless oil: ¹H NMR (300 MHz, CDCl₃) δ 7.46 (d, *J* = 8.4 Hz, 2 H), 7.21 (d, *J* = 8.1 Hz, 2 H), 4.69 (s, 2 H), 0.95 (s, 9 H), 0.10 (s, 6 H); MS (EI) *m/z* (rel. intensity) 302 ([M⁺], 1.5), 300 ([M⁺], 1.6), 245 (98), 243 (96), 171 (58), 169 (62); HRMS (EI) *m/z* calc for C₁₃H₂₁BrOSi 300.0545, found 300.0533.

s

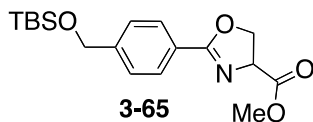


4-((tert-Butyldimethylsilyloxy)methyl)benzoic acid (3-63).²⁶⁹ A flame-dried 250-mL round-bottom flask was charged with **3-62** (5.00 g, 16.6 mmol) and THF (60 mL), and the solution was cooled to -78 °C. After stirring for 30 min at -78 °C, *n*-BuLi (9.30 mL, 18.3 mmol, *c* = 1.97 M in hexanes) was added drop-wise via syringe over a period of 25 min. The solution was stirred at -78 °C for an additional 15 min, and CO₂ was bubbled through the solution for 5 min. The mixture was quenched at -78 °C with saturated aqueous NaHSO₄ (20 mL), and the reaction vessel was warmed to rt. The mixture was diluted with water (100 mL) and EtOAc (150 mL), and the aqueous layer was extracted with EtOAc (3 x 100 mL). The combined organic layers were washed with water and brine, dried (Na₂SO₄) and concentrated *in vacuo*. Residual

water was removed by coevaporation with benzene. Upon drying under high vacuum, **3-63** (3.91 g, 88%) was obtained as a white solid: $^1\text{H NMR}$ (300 MHz, CDCl_3) δ 8.08 (d, $J = 8.3$ Hz, 2 H), 7.44 (d, $J = 8.3$ Hz, 2 H), 4.82 (s, 2 H), 0.97 (s, 9 H), 0.13 (s, 6 H); HRMS (ES) m/z calc for $\text{C}_{14}\text{H}_{22}\text{O}_3\text{SiNa}$ ($\text{M}+\text{Na}$) 289.1236, found 289.1212.



Methyl 2-(4-((tert-butyldimethylsilyloxy)methyl)benzamido)-3-hydroxypropanoate (3-64). A solution of **3-63** (2.00 g, 7.51 mmol) in CH_2Cl_2 (80 mL) was treated with *dl*-SerOMe•HCl (1.79 g, 11.3 mmol), HOBT-hydrate (1.49 g, 9.76 mmol), Et_3N (1.60 mL, 11.4 mmol), and EDC•HCl (1.58 g, 8.26 mmol). The solution was stirred at rt for 12 h and subsequently diluted with CH_2Cl_2 (150 mL). The solution was washed with 0.1 M aqueous citric acid (2 x 150 mL), saturated aqueous NaHCO_3 (150 mL), and brine (150 mL), dried (Na_2SO_4), and concentrated *in vacuo*. The crude yellow residue was purified by chromatography on SiO_2 (hexanes/EtOAc, 1:1) to afford **3-64** (2.02 g, 73%) as a colorless oil: IR (ATR) 3433, 2950, 1741, 1638, 1210, 1083 cm^{-1} ; $^1\text{H NMR}$ (300 MHz, CDCl_3) δ 7.81 (d, $J = 8.3$ Hz, 2 H), 7.40 (d, $J = 8.4$ Hz, 2 H), 7.15 (d, $J = 7.1$ Hz, 1 H), 4.87 (dt, $J = 7.2, 3.5$ Hz, 1 H), 4.79 (s, 2 H), 4.10–4.01 (m, 1 H), 3.82 (s, 3 H), 2.89 (t, $J = 5.3$ Hz, 1 H), 0.95 (s, 9 H), 0.11 (s, 6 H); $^{13}\text{C NMR}$ (75 MHz, CDCl_3) δ 171.1, 167.5, 145.8, 131.9, 127.2, 126.0, 64.4, 63.6, 55.1, 52.9, 25.9, 18.4, -5.3; MS (EI) m/z (rel. intensity) 367 (M^+ , 0.14), 310 (100), 249 (65); HRMS (EI+) m/z calc for $\text{C}_{18}\text{H}_{29}\text{NO}_5\text{Si}$ 367.1815, found 367.1821.



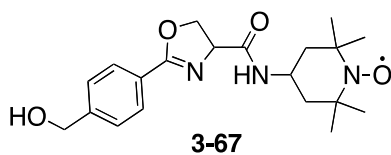
Methyl 2-(4-((tert-butyldimethylsilyloxy)methyl)phenyl)-4,5-dihydrooxazole-4-carboxylate (3-65). An oven-dried round-bottom flask was charged with a solution of **3-64** (2.53 g, 6.88 mmol) in THF (80 mL), and the solution was treated with Burgess reagent (1.97 g, 8.26 mmol) and heated at reflux for 1 h. After cooling, the reaction solution was filtered to remove a white solid, which was subsequently washed with THF. The filtrate was concentrated onto SiO₂ and purified by chromatography on SiO₂ (hexanes/EtOAc, 2:1) to afford **3-65** (1.78 mg, 74%) as a colorless oil that solidifies upon standing: Mp 49.7-52.0 °C; IR (ATR) 2950, 1735, 1640, 1210, 1083 cm⁻¹; ¹H NMR (300 MHz, CDCl₃) δ 7.95 (d, *J* = 8.4 Hz, 2 H), 7.37 (d, *J* = 8.4 Hz, 2 H), 4.95 (dd, *J* = 10.6, 7.9 Hz, 1 H), 4.78 (s, 2 H), 4.69 (dd, *J* = 8.8, 7.8 Hz, 1 H), 4.59 (dd, *J* = 10.6, 8.7 Hz, 1 H), 3.82 (s, 3 H), 0.94 (s, 9 H), 0.097 (s, 6 H); ¹³C NMR (75 MHz, CDCl₃) δ 171.7, 166.2, 145.6, 128.5, 125.7, 125.4, 69.4, 68.6, 64.5, 52.7, 25.9, 18.4, -5.3; MS (EI) *m/z* (rel. intensity) 349 ([M⁺], 17), 292 (100), 218 (38); HRMS (EI) *m/z* calc for C₁₈H₂₇NO₄Si 349.1709, found 349.1712.



2-(4-((tert-Butyldimethylsilyloxy)methyl)phenyl)-N-(1-hydroxy-2,2,6,6-tetramethylpiperidin-4-yl)-4,5-dihydrooxazole-4-carboxamide (3-66). A solution of **3-65** (300 mg, 0.858 mmol) in THF (8.5 mL) was treated with 1 N aqueous NaOH (1.30 mL, 1.30 mmol) and stirred at rt for 90 min. NaHCO₃ (354 mg, 4.21 mmol) was added, and the solvent was removed *in vacuo*. Residual water was removed by coevaporation with toluene (3 x 15 mL). To the crude white solid was added a solution of 4-amino TEMPO (300 mg, 1.75 mmol) in

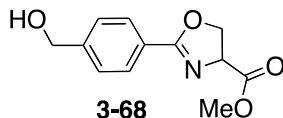
anhydrous DMF (10 mL) and residual DMF was added to bring the total volume to 17 mL. Sonication (ultrasonic bath) was employed to help with dissolution. The solution was cooled in an ice bath to ~ 0 °C and DIPEA (0.71 mL, 4.3 mmol) and DPPA (0.56 mL, 2.6 mmol) were added, and the reaction mixture was warmed to rt and stirred for 20 h. The mixture was cooled to 0 °C and quenched with saturated aqueous NaHCO₃ (12 mL) and stirred for 90 min. The mixture was poured into water (100 mL) and extracted with Et₂O (1 x 100 mL and 2 x 30 mL). The combined organic layers were washed with water (3 x 70 mL) and brine (1 x 70 mL), dried (Na₂SO₄) and concentrated *in vacuo*. Purification by chromatography on SiO₂ (hexanes/EtOAc, 1:2) afforded **3-66** (371 mg, 88%) as a peach-colored foam: IR (ATR) 3340, 2926, 1668, 1638, 1507, 1082, 833 cm⁻¹; MS (EI) *m/z* (rel. intensity) 489 (M⁺, 17), 488 (26), 431 (47), 290 (52); HRMS (EI) *m/z* calc for C₂₆H₄₂N₃O₄Si 488.2945, found 488.2939.

NMR data was carried out on the corresponding hydroxylamine (**3-66a**): a sample of **3-66** (94.5 mg) was dissolved in MeOH (5 mL), treated with ascorbic acid (88 mg) and shaken for ~ 1 min (until the solution color changed from orange to colorless). The solution was dissolved in Et₂O (20 mL) and washed twice with saturated aqueous NaHCO₃, followed by water and brine, dried (MgSO₄) and concentrated *in vacuo*. CDCl₃ (filtered through basic Al₂O₃) was added and the solution was concentrated *in vacuo* to afford (107 mg, > 100%) of the hydroxylamine. The hydroxylamine was dissolved in CDCl₃ (filtered through Al₂O₃): ¹H NMR (300 MHz, CDCl₃) δ 7.95 (d, *J* = 8.1 Hz, 2 H), 7.41 (d, *J* = 8.1 Hz, 2 H), 6.46 (b d, *J* = 8.0 Hz, 1 H), 4.85–4.78 (m, 1 H), 4.80 (s, 2 H), 4.72–4.66 (m, 1 H), 4.60 (t, *J* = 8.5 Hz, 1 H), 4.48 (bs, 1 H), 4.24–4.11 (m, 1 H), 1.93 (dt, *J* = 12.5, 3.3 Hz, 1 H), 1.80 (dt, *J* = 12.5, 3.4 Hz, 1 H), 1.46–1.25 (m, 2 H), 1.22 (s, 3 H), 1.20 (s, 3 H), 1.20 (s, 3 H), 1.16 (s, 3 H), 0.96 (s, 9 H), 0.12 (s, 6 H); ¹³C NMR (75 MHz, CDCl₃) δ 170.2, 165.3, 145.0, 127.6, 125.0, 124.6, 69.6, 68.1, 63.7, 58.1, 44.5, 40.0, 31.5, 25.0, 18.8, 17.5, -6.2.

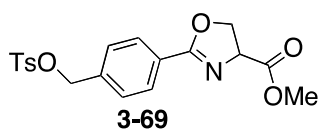


***N*-(1-oxo-2,2,6,6-tetramethylpiperidin-4-yl)-2-(4-(hydroxymethyl)phenyl)-4,5-dihydrooxazole-4-carboxamide (3-67).** A solution of **3-66** (78.3 mg, 0.160 mmol) in THF (1.10 mL) was treated with a solution of TBAF and AcOH (0.50 mL, 0.48 mmol, 0.95 mmol TBAF) and stirred at rt for 2.5 h. The reaction mixture was quenched with saturated aqueous NH₄Cl (2 mL) and water (2 mL), and the aqueous layer was extracted with EtOAc (3 x 15 mL). The combined organic layers were washed with saturated aqueous NaHCO₃ (10 mL), water (10 mL), and brine (10 mL), dried (Na₂SO₄) and concentrated *in vacuo*. The crude residue was purified by chromatography on SiO₂ (hexanes/EtOAc, 4:1 to 1:1, then 100% EtOAc) to afford **3-67** (29.3 mg, 49%) as an orange foam.

For the purpose of characterization, the material was converted to the corresponding hydroxylamine (**3-67a**). A sample was dissolved in MeOH (~2 mL), treated with ascorbic acid (15 mg), shaken until the color went from orange to colorless, and diluted with Et₂O (15 mL). The ethereal layers were washed with saturated aqueous NaHCO₃, water, and brine, dried (MgSO₄), filtered, and concentrated *in vacuo*: ¹H NMR (400 MHz, CDCl₃) δ 7.99 (d, *J* = 8.0 Hz, 2 H), 7.48 (d, *J* = 8.1 Hz, 2 H), 6.47 (d, *J* = 8.0 Hz, 1 H), 4.86–4.82 (m, 1 H), 4.82 (s, 2 H), 4.72 (dd, *J* = 10.9, 8.7 Hz, 1 H), 4.62 (t, *J* = 8.5 Hz, 1 H), 4.25–4.15 (m, 1 H), 1.95 (dt, *J* = 12.6, 3.4 Hz, 1 H), 1.82 (dt, *J* = 12.6, 3.5 Hz, 1 H), 1.48–1.42 (m, 1 H), 1.40–1.34 (m, 1 H), 1.28 (bs, 1 H), 1.24 (s, 3 H), 1.22 (s, 3 H), 1.21 (s, 3 H), 1.18 (s, 3 H); ¹³C NMR (100 MHz, CDCl₃) δ 170.7, 165.7, 144.9, 128.4, 126.4, 125.8, 70.1, 68.7, 64.4, 45.0, 40.5, 32.0, 19.4.

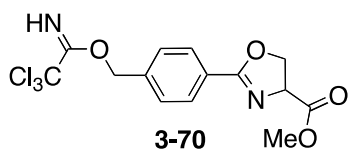


Methyl 2-(4-(hydroxymethyl)phenyl)-4,5-dihydrooxazole-4-carboxylate (3-68). A solution of **3-65** (704 mg, 2.01 mmol) in THF (14 mL) was treated with a solution of TBAF and AcOH (3.0 mL, 2.9 mmol TBAF, 1.4 mmol AcOH) at rt. The mixture was stirred for 0.5 h at rt and quenched with saturated aqueous NH₄Cl (14 mL), followed by water (14 mL) and extracted with EtOAc (3 x 30 mL). The combined organic layers were washed with brine (50 mL), dried (Na₂SO₄) and concentrated *in vacuo*. The crude residue was purified by chromatography on SiO₂ (hexanes/EtOAc, 4:1, then 100% EtOAc) to afford **3-68** (369 mg, 78%) as a white solid: Mp 86.1–87.2 °C (hexanes/EtOAc); IR 3284, 1728, 1640, 1226, 1041, 1032 cm⁻¹; ¹H NMR (300 MHz, CDCl₃) δ 7.89 (d, *J* = 8.3 Hz, 2 H), 7.35 (d, *J* = 8.4 Hz, 2 H), 4.90 (dd, *J* = 10.6, 7.9 Hz, 1 H), 4.69–4.64 (m, 3 H), 4.57 (dd, *J* = 10.6, 8.7 Hz, 1 H), 3.79 (s, 3 H), 3.09 (bs, 1 H); ¹³C NMR (75 MHz, CDCl₃) δ 171.6, 166.3, 145.3, 128.7, 126.4, 125.6, 69.5, 68.3, 64.3, 52.7; MS (EI) *m/z* (rel. intensity) 235 (M⁺, 2.3), 176 (100); HRMS (EI⁺) *m/z* calc for C₁₂H₁₃NO₄ 235.0845, found 235.0843.

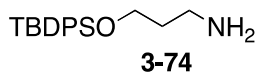


Methyl 2-(4-(tosyloxymethyl)phenyl)-4,5-dihydrooxazole-4-carboxylate (3-69). A solution of **3-68** (184 mg, 0.782 mmol) in CH₂Cl₂ (3.0 mL) was added via syringe pump (0.24 mL/min) to a solution of Ts₂O (574 mg, 1.74 mmol), Et₃N (0.24 mL, 1.71 mmol) and DMAP (10.0 mg, 0.0837 mmol) in CH₂Cl₂ (6.0 mL) maintained at 0 °C. Following completion of the addition, the reaction mixture was stirred for 2 h, gradually warming to rt. The mixture was diluted with CH₂Cl₂ (20 mL), washed with water (15 mL), and the aqueous layer was extracted with CH₂Cl₂ (10 mL). The combined organic layers were washed with water and brine, dried (Na₂SO₄), and concentrated *in vacuo* to afford a red/brown residue. The residue was purified by

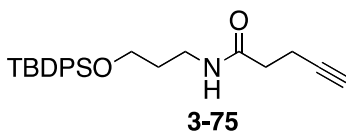
chromatography on SiO₂ (hexanes/EtOAc, 1:1) to afford **3-69** (232 mg, 76%) as a viscous yellow-tinted oil that solidifies to a white solid upon standing: Mp 87.9–90.0 °C (CH₂Cl₂); IR (ATR) 3017, 2965, 1735, 1638, 1349, 1169 cm⁻¹; ¹H NMR (300 MHz, CDCl₃) δ 7.93 (d, *J* = 8.3 Hz, 2 H), 7.80 (d, *J* = 8.3 Hz, 2 H), 7.34 (d, *J* = 8.1 Hz, 2 H), 7.30 (d, *J* = 8.4 Hz, 2 H), 5.09 (s, 2 H), 4.96 (dd, *J* = 10.6, 8.0 Hz, 1 H), 4.70 (app t, *J* = 8.4 Hz, 1 H), 4.60 (dd, *J* = 10.7, 8.8 Hz, 1 H), 3.83 (s, 3 H), 2.45 (s, 3 H); ¹³C NMR (75 MHz, CDCl₃) δ 171.5, 165.7, 145.0, 137.1, 132.9, 129.9, 128.9, 128.0, 128.0, 127.4, 70.9, 69.6, 68.6, 52.8, 21.6; MS (ES) *m/z* (rel. intensity) 412 ([M+Na]⁺), 85), 389 (M⁺, 25); HRMS (ES) *m/z* calc for C₁₉H₁₉NO₆SNa (M+Na) 412.0831, found 412.0818.



Methyl 2-(4-((2,2,2-trichloro-1-iminoethoxy)methyl)phenyl)-4,5-dihydrooxazole-4-carboxylate (3-70). A solution of **3-68** (52.4 mg, 0.223 mmol) in CH₂Cl₂ (1.3 mL) was treated with DBU (5.0 uL, 0.031 mmol) and cooled in an ice-water bath. After the solution was stirred for 10 min, trichloroacetonitrile (30 uL, 0.29 mmol) was added via syringe. The solution (which became yellow in color) was stirred for 30 min at 0 °C. The solvent was removed *in vacuo* to afford crude **3-70** as a brown residue (102 mg) which became a tan foam when placed under high vacuum. The material was used without further purification. Characteristic data are reported: ¹H NMR (300 MHz, CDCl₃) δ 8.01 (d, *J* = 8.3 Hz, 2 H), 7.49 (d, *J* = 8.2 Hz, 2 H), 5.39 (s, 2 H), 4.97 (dd, *J* = 10.6, 7.9 Hz, 1 H), 4.71 (app t, 1 H), 4.61 (dd, *J* = 10.6, 8.7 Hz, 1 H), 3.83 (s, 3 H).

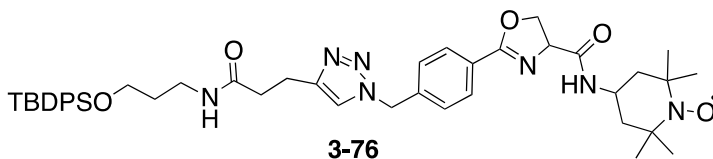


3-(*tert*-Butyldiphenylsilyloxy)propan-1-amine (3-74).²⁷⁰ A solution of 3-amino-1-propanol (1.00 mL, 12.9 mmol) and TBDPSCl (5.20 mL, 19.4 mmol) in dry CH₂Cl₂ (25 mL) was treated (slowly) with distilled Et₃N (3.60 mL, 25.6 mmol). The reaction mixture was stirred at rt for 4 h and subsequently diluted to 150 mL with CH₂Cl₂, washed with saturated aqueous NH₄Cl (100 mL), water (100 mL) and brine (100 mL), dried (MgSO₄) and concentrated. The crude residue was purified by chromatography on SiO₂ (100% CH₂Cl₂ then CH₂Cl₂/MeOH/NH₄OH (aq), 100 : 10 : 1) to afford **3-74** (2.68 g, 66%) as a viscous yellow oil: ¹H NMR (300 MHz, CDCl₃) δ 7.68 (dd, *J* = 7.0, 1.9 Hz, 4 H), 7.47–7.36 (m, 6 H), 3.75 (t, *J* = 6.0 Hz, 2 H), 2.85 (t, *J* = 6.8 Hz, 2 H), 1.70 (quint, *J* = 6.4 Hz, 2 H), 1.17 (bs, 2 H), 1.06 (s, 9 H); HRMS (ESI) *m/z* calc for C₁₉H₂₈NOSi (M+H) 314.1940, found 314.1924.



***N*-(3-(*tert*-Butyldiphenylsilyloxy)propyl)pent-4-ynamide (3-75).** A solution of **3-74** (200 mg, 0.638 mmol) and 4-pentynoic acid (63 mg, 0.64 mmol) in anhydrous DMF (5.3 mL) was treated with DIPEA (0.22 mL, 1.3 mmol) and HATU (291 mg, 0.766 mmol). The reaction mixture turned bright yellow in color upon addition of the HATU. The reaction mixture was stirred at rt for 17.5 h, and subsequently brine (20 mL) was poured into the mixture. The aqueous layer was extracted with EtOAc (3 x 30 mL), and the combined organic layers were washed with 0.5 N aqueous HCl (10 mL), water (20 mL), saturated aqueous NaHCO₃ (10 mL), water, and brine, dried (MgSO₄), and concentrated *in vacuo*. Purification by chromatography on SiO₂ (hexanes/EtOAc, 1:1) afforded **3-75** as a white solid (209 mg, 83%): Mp 70.9–72.7 °C; IR (ATR) 3326, 3280, 3071, 1963, 1637, 1547, 1429, 1099 cm⁻¹; ¹H NMR (400 MHz, CDCl₃) δ 7.73–7.66 (m, 4 H), 7.53–7.32 (m, 6 H), 5.97 (bs, 1 H), 3.78 (t, *J* = 4.2 Hz, 2 H), 3.41 (app q, *J* = 4.3 Hz, 2 H), 2.48 (ddd, *J* = 5.5, 5.5, 1.9 Hz, 2 H), 2.26 (t, *J* = 5.5 Hz, 2 H), 1.94 (t, *J* = 2.0 Hz, 1

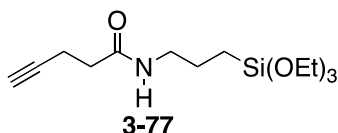
H), 1.76 (app quint, $J = 4.4$ Hz, 2 H), 1.09 (s, 9 H); ^{13}C NMR (100 MHz, CDCl_3) δ 170.6, 135.5, 133.3, 129.8, 127.8, 83.0, 69.0, 62.7, 37.7, 35.3, 31.4, 26.9, 19.1, 14.9; MS (EI) m/z (rel. intensity) 416 ($[\text{M}+\text{Na}]$, 93), 265 (100); HRMS m/z calc for $\text{C}_{24}\text{H}_{31}\text{NO}_2\text{SiNa}$ ($\text{M}+\text{Na}$) 416.2022, found 416.2009.



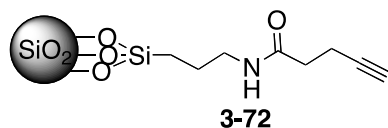
2-(4-((4-(3-(3-(*tert*-Butyldiphenylsilyloxy)propylamino)-3-oxopropyl)-1*H*-1,2,3-triazol-1-yl)methyl)phenyl)-*N*-(1-oxo-2,2,6,6-tetramethylpiperidin-4-yl)-4,5-dihydrooxazole-4-carboxamide (3-76). A flame-dried microwave vial was charged with model alkyne **3-75** (49.0 mg, 0.125 mmol), degassed toluene (2.5 mL), azide **3-50** (57.0 mg, 0.143 mmol), $\text{CuI}\cdot\text{P}(\text{OEt})_3$ (44 mg, 0.12 mmol), and DIPEA (65 μL , 0.37 mmol). The reaction mixture was stirred under N_2 atmosphere for 5 h. Additional alkyne (12.2 mg, 0.0310 mmol) was added, and the reaction mixture was stirred at rt overnight (12 h). The mixture was concentrated *in vacuo* and purified by chromatography on SiO_2 ($\text{CH}_2\text{Cl}_2/\text{MeOH}$, 95:5) to afford model triazole **3-76** (111 mg, 98%) as a pale orange foam. IR (ATR) 3502, 3335, 2930, 1642, 1540, 1105, 1085 cm^{-1} ; HRMS (ESI) m/z calc for $\text{C}_{44}\text{H}_{58}\text{N}_7\text{O}_5\text{SiNa}$ ($\text{M}+\text{Na}$) 815.4166, found 815.4177.

NMR characterization was carried out on the corresponding hydroxylamine, which was formed as follows: the analyte (94.4 mg) was dissolved in MeOH (3.0 mL) and treated with ascorbic acid (115 mg). The solution was shaken until the color change from orange to colorless was complete. The mixture dissolved in ether (10 mL) and washed with equi-volume amounts of saturated aqueous NaHCO_3 , water, and brine, dried (MgSO_4), filtered and concentrated *in vacuo*: ^1H NMR (300 MHz, CDCl_3) δ 7.95 (d, $J = 8.0$ Hz, 2 H), 7.66–7.64 (m, 4 H), 7.44–7.36 (m, 6 H), 7.30–7.27 (m, 2 H), 6.41 (d, $J = 8.0$ Hz, 1 H), 5.96 (bs, 1 H), 5.50 (s, 2 H), 4.80 (dd, $J = 10.4, 8.7$

Hz, 1 H), 4.67 (app t, 1 H), 4.59 (t, $J = 8.6$ Hz, 1 H), 4.23–4.10 (m, 1 H), 3.71 (t, $J = 5.5$ Hz, 2 H), 3.33 (bs, 2 H), 2.99 (t, $J = 6.9$ Hz, 2 H), 2.46 (t, $J = 6.9$ Hz, 2 H), 2.18 (b, 1 H), 1.92 (dt, $J = 12.5, 3.2$ Hz, 1 H), 1.78 (dt, $J = 12.5, 3.2$ Hz, 1 H), 1.73–1.64 (m, 2 H), 1.45–1.26 (m, 2 H), 1.21 (s, 3 H), 1.19 (s, 3 H), 1.18 (s, 3 H), 1.14 (s, 3 H), 1.06 (s, 9 H); ^{13}C NMR (75 MHz, CDCl_3) δ 171.3, 170.5, 165.1, 147.0, 138.5, 135.2, 133.0, 129.5, 128.9, 127.6, 127.5, 127.0, 121.3, 70.3, 68.7, 62.1, 58.6, 53.2, 45.0, 40.6, 37.1, 35.2, 32.1, 31.2, 26.6, 21.1, 19.4, 18.8.

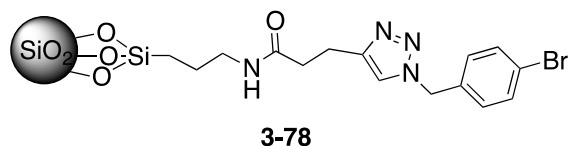


***N*-(3-(Triethoxysilyl)propyl)pent-4-ynamide (3-77).** A flame-dried 250-mL round-bottom flask was charged with 4-pentynoic acid (1.0 g, 10 mmol), CH_2Cl_2 (100 mL), (3-aminopropyl)triethoxysilane (4.80 mL, 20.5 mmol), and EDC•HCl (2.93 g, 15.3 mmol). The reaction mixture was stirred under N_2 atmosphere at rt for 18 h and concentrated *in vacuo*. The residue was purified by chromatography on SiO_2 (deactivated with 0.5% Et_3N ; hexanes/EtOAc, 1:1) to afford **3-77** (1.64 g, 53%) as a yellow oil: IR (ATR) 3292, 3286, 2971, 1644, 1545, 1074 cm^{-1} ; ^1H NMR (400 MHz, CDCl_3) δ 5.87 (bs, 1 H), 3.83 (q, $J = 7.0$ Hz, 6 H), 3.28 (dd, $J = 12.8, 6.8$ Hz, 2 H), 2.54 (ddd, $J = 7.2, 7.2, 2.6$ Hz, 2 H), 2.39 (t, $J = 7.1$ Hz, 2 H), 2.00 (t, $J = 2.6$ Hz, 1 H), 1.68–1.61 (m, 2 H), 1.24 (t, $J = 7.0$ Hz, 9 H), 0.67–0.63 (m, 2 H); ^{13}C NMR (100 MHz, CDCl_3) δ 170.7, 82.9, 69.0, 58.2, 41.7, 35.2, 22.7, 18.1, 14.7, 7.6; HRMS (ESI) m/z calc for $\text{C}_{14}\text{H}_{27}\text{NO}_4\text{SiNa}$ 324.1607, found 324.1608.

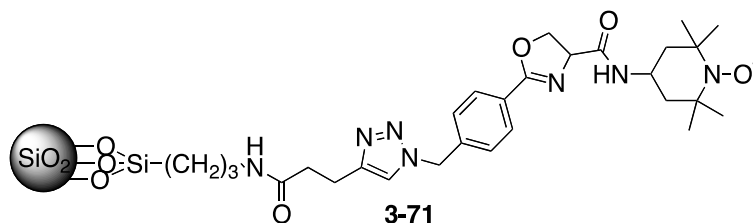


Preparation of alkyne-functionalized nanoparticles (3-72). An oven-dried 50-mL round bottom flask equipped with stir bar and condenser was charged with nanoscale SiO₂ (250 mg) and dry toluene (20 mL). (Note: SiO₂ was obtained by drying a commercial IPAST suspension under N₂ and subsequently drying the recovered particles for 24 h in a vacuum oven.) To this stirring suspension was added a solution of **3-77** (505 mg, 1.68 mmol) in dry toluene (5 mL), and the reaction mixture was heated at reflux for 3 h. The mixture was cooled to rt, and the contents were transferred to a 50-mL Falcon tube, using EtOH for transfer. Some aggregates were discarded. The tube was centrifuged (4400 rpm, 3000 xg, 30 min, rt), the supernatant was decanted, and the sediment was suspended in dry toluene, sonicated (ultrasonic bath), and centrifuged (4400 rpm, 3000 xg, 30 min, rt). This washing procedure was repeated two additional times, and the final sediment was dried under N₂, then dried under high vacuum for 24 h to afford **3-77** (200 mg) as white particles: IR (KBr) 3306, 1650, 1554 cm⁻¹; Anal. Found for (SiO₂)_nC₁₄H₂₆NO₄Si: C, 7.07; H, 1.05; N, 1.05. (Note: These particles are **3-72**, batch 1).

A separate batch of particles **3-72** was synthesized using the same protocol (**3-72**, batch 2: Anal. Found for (SiO₂)_nC₁₄H₂₆NO₄Si: C, 8.15; H, 1.26; N, 1.14).



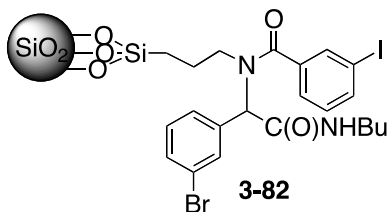
Bromide model particles (3-78). An oven-dried thick-walled vial was charged with particles **3-72** (batch 2) (35.5 mg, 0.0289 mmol based on a loading of 0.81 mmol/g) and $\text{CuI}\cdot\text{P}(\text{OEt})_3$ (12 mg, 0.034 mmol). The vial was back-filled with N_2 (3 x). Degassed toluene (1.0 mL), 4-bromobenzyl azide (15 mg, 0.071 mmol) and DIPEA (15 μL , 0.091 mmol) were added. The mixture was placed in a pre-heated oil bath and heated at 70 $^\circ\text{C}$ under N_2 atmosphere for 16 h. Upon cooling, the mixture was transferred to a 15-mL Falcon tube using additional toluene (2 mL) for transfer and dilution. The tube was centrifuged (4400 rpm, 3000 xg, 15 min, rt). The colorless supernatant was removed via pipet. The sediment was suspended in toluene (3 mL), sonicated (ultrasonic bath) for 30 min, and centrifuged (4400 rpm, 3000 xg, 15 min, rt). This washing procedure was repeated, and the sediment was suspended in dry toluene (3 mL) and heated at reflux for 20 min. Upon cooling, the mixture was centrifuged, and the sediment was suspended in anhydrous THF (3 mL), sonicated for 20 min, and centrifuged (4400 rpm, 3000 xg, 15 min, rt). The supernatant was removed, and the sediment was suspended in absolute EtOH (4 mL), sonicated for 5 min, and centrifuged (4400 rpm, 3000 xg, 15 min, rt). The particles were suspended in EtOH (4 mL) and centrifuged under the same conditions, the supernatant was decanted, and the particles were dried under N_2 , then in a vacuum oven at 100 $^\circ\text{C}$ for 2 days to afford model particles **3-78** (15.3 mg) as white particles: Anal. Found for $(\text{SiO}_2)_n\text{C}_{15}\text{H}_{19}\text{BrN}_4\text{O}$: C, 9.67; H, 1.17; N, 2.31; Br, 2.26.



TEMPO-functionalized nanoparticles (3-71, Batch A). An oven-dried thick-walled vial was charged with particles **3-72** (batch 1) (73.1 mg, 0.0548 mmol based on a loading of 0.75 mmol/g), azide **3-50** (40.1 mg, 0.100 mmol), and $\text{CuI}\cdot\text{P}(\text{OEt})_3$ (28.0 mg, 0.0785 mmol). The tube was back-filled with N_2 (3 x). Degassed toluene (1.0 mL) was added followed by DIPEA (35 μL , 0.21 mmol). The mixture was stirred for 15 h at rt under a N_2 atmosphere. The reaction mixture was transferred to a 15-mL Falcon tube using additional toluene (3 mL) for transfer and dilution. The tube was centrifuged (4400 rpm, 3000 xg, 10 min, rt). The supernatant was removed via pipet. The sediment was suspended in toluene (4 mL), sonicated (ultrasonic bath) for 20 min, and centrifuged (4400 rpm, 3000 xg, 10 min, rt). This washing procedure was repeated, and the sediment was suspended in dry toluene (4 mL) and heated at reflux for 20 min. Upon cooling, the mixture was centrifuged, the supernatant removed, and the sediment was suspended in anhydrous THF (4 mL), sonicated for 20 min, and centrifuged (4400 rpm, 3000 xg, 15 min, rt). The supernatant was removed, and the sediment was suspended in absolute EtOH (4 mL), sonicated for 20 min, and centrifuged (4400 rpm, 3000 xg, 15 min, rt). The EtOH wash was repeated, and the particles were dried under N_2 , then under high vacuum (2 mmHg) at 60 $^\circ\text{C}$ for 12 h to afford **3-71** (Batch A) (56.6 mg) as pale orange colored particles: Anal. Found for $(\text{SiO}_2)_n\text{C}_{28}\text{H}_{39}\text{N}_7\text{O}_4$: C, 9.21; H, 1.24; N, 1.60.

TEMPO-functionalized nanoparticles (3-71 Batch B). The analogous procedure for synthesis of **3-71 Batch A** was used with the following amounts of reactants/reagents: particles **3-72** (batch 1) (34 mg, 0.026 mmol based on a loading of 0.75 mmol/g), azide **3-50** (40.1 mg, 0.100 mmol), and complex $\text{CuI}\cdot\text{P}(\text{OEt})_3$ (14.0 mg, 0.0393 mmol), degassed toluene (1.0 mL), and DIPEA (20 μL , 0.12 mmol). Instead of stirring at rt, the mixture was placed in a pre-heated oil bath and stirred under N_2 atmosphere at 70 $^\circ\text{C}$ for 16 h. After using the washing protocol

described in the case of **3-71 Batch A**, the particles were dried under N₂, then in a vacuum oven at 100 °C for 2 days to afford particles **3-71 Batch B** (22.6 mg) as orange particles: Anal. Found for (SiO₂)_nC₂₈H₃₉N₇O₄: C, 9.67; H, 1.29; N, 1.95.

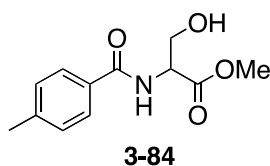


Procedure for model Ugi functionalization of nanoparticles (**3-82**).

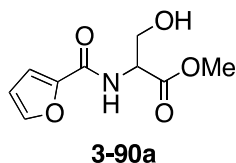
A flame-dried thick-walled vial equipped with stir bar was charged with particles (**3-51**) (100 mg) and distilled THF (1.3 mL). To the vigorously stirring suspension was added distilled 3-bromobenzaldehyde (29 μL, 0.25 mmol), and the mixture was stirred at rt under N₂ atmosphere for 90 min. 3-Iodobenzoic acid (62 mg, 0.25 mmol) was added, followed by *n*-butylisocyanide (52 μL, 0.50 mmol). The reaction mixture was stirred at rt for 1 h and then at 60 °C for 24 h. Upon cooling, the reaction mixture was transferred via pipet to a 15-mL Falcon tube, using additional EtOH (1 mL) to help transfer particles. The tube was centrifuged (4400 rpm, 3000 xg, 10 min). The supernatant was removed via pipet, and the collected sediment was dried under N₂ overnight. The dried particles were transferred to an eppendorf nylon 0.22 μm centrifugal filter, and EtOH was placed on top of the filter. The tube was centrifuged (6000 rpm, 3000 xg, 1h, rt). Additional EtOH was added to fill the top of the filter, and the tube was centrifuged under the same conditions. This wash was repeated twice, and the particles were collected and dried in the vacuum oven (44 h, -10 in Hg, 100 °C) to afford functionalized particles **3-82** (17 mg) as a pale yellow powder: Anal. Found for (SiO₂)_nC₂₂H₂₅BrIN₂O₂: C, 5.85; H, 0.93; N, 0.73; Br, 0.41; I, 2.73.

General procedure for the preparation of β -hydroxy amides 3-84 and 3-90a-e using the corresponding carboxylic acids (Procedure A). A solution of acid (1.0 equiv) and *dl*-serine methyl ester hydrochloride (1.5 equiv) in dry CH_2Cl_2 (*ca.* 0.1 M) was treated with HOBT-hydrate (1.3 equiv) and Et_3N (1.5 equiv). The solution was cooled to 0 °C and treated with EDC•HCl (1.1 equiv). The mixture was stirred overnight and diluted with CH_2Cl_2 and washed with 0.1 M aqueous citric acid, saturated aqueous NaHCO_3 , and brine, dried (Na_2SO_4), and concentrated *in vacuo*.

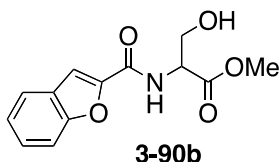
General procedure for the preparation of β -hydroxy amides 3-90a-e using the corresponding acid chlorides (Procedure B). A slurry of *dl*-serine methyl ester hydrochloride (1.6 equiv) and Et_3N (1.6 equiv) in CH_2Cl_2 (0.2 M in acid chloride) was cooled to 0 °C and treated with acid chloride (1.0 equiv). The reaction mixture was warmed to rt and stirred at rt overnight. The mixture was diluted with CH_2Cl_2 and washed with 5% aqueous NaHSO_4 and brine, dried (Na_2SO_4), and concentrated *in vacuo*.



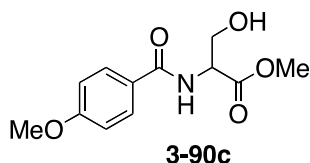
Methyl 3-hydroxy-2-(4-methylbenzamido)propanoate (3-84).²⁷¹ Following General procedure A, *p*-toluic acid (1.00 g, 7.34 mmol) was converted to **3-84**. After purification on SiO_2 (hexanes/ EtOAc , 1:1 then 1:2) **3-84** (1.15 g, 66%) was obtained as a white solid: ^1H NMR (300 MHz, CDCl_3) δ 7.74 (d, $J = 8.3$ Hz, 2 H), 7.26 (d, $J = 8.0$ Hz, 2 H), 7.07 (bd, $J = 6.4$ Hz, 1 H), 4.88 (dt, $J = 7.0, 3.6$ Hz, 1 H), 4.08 (dd, $J = 5.9, 3.6$ Hz, 2 H), 3.84 (s, 3 H), 2.58 (t, $J = 5.9$ Hz, 1 H), 2.41 (s, 3 H).



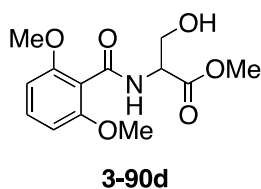
Methyl 2-(furan-2-carboxamido)-3-hydroxypropanoate (3-90a).²⁷² Following General procedure **B**, 2-furoyl chloride (0.500 mL, 4.98 mmol) was converted to **3-90a**. After purification by chromatography on SiO₂ (hexanes/EtOAc, 1:1 then 100% EtOAc) **3-90a** (478 mg, 45%) was obtained as a white solid: ¹H NMR (300 MHz, CDCl₃) δ 7.50 (m, 1 H), 7.24 (bs, 1 H), 7.17 (d, *J* = 3.3 Hz, 1 H), 6.53 (dd, *J* = 3.6, 1.8 Hz, 1 H), 4.85 (dt, *J* = 7.4, 3.6 Hz, 1 H), 4.12–4.02 (m, 2 H), 3.84 (s, 3 H), 2.44 (bs, 1 H).



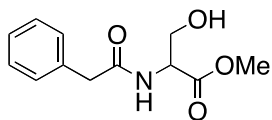
Methyl 2-(benzofuran-2-carboxamido)-3-hydroxypropanoate (3-90b). Following General procedure **A**, 2-benzenefurancarboxylic acid (500 mg, 3.02 mmol) was converted to **3-90b** (615 mg, 77%), which was isolated as an analytically pure yellow solid and used without further purification: Mp 82.1–84.0 °C; IR (ATR) 3412, 3303, 2958, 1748, 1630, 1594, 1513, 1438, 1177 cm⁻¹; ¹H NMR (300 MHz, CDCl₃) δ 7.71–7.68 (m, 1 H), 7.56–7.52 (m, 3 H), 7.48–7.42 (m, 1 H), 4.92 (dt, *J* = 7.5, 3.5 Hz, 1 H), 4.19–4.05 (m, 2 H), 3.87 (s, 3 H), 2.42 (bt, *J* = 4.5 Hz, 1 H); ¹³C NMR (100 MHz, CDCl₃) δ 170.6, 159.0, 154.8, 147.8, 127.3, 127.2, 123.7, 122.7, 111.9, 111.2, 63.2, 54.6, 52.9; MS (ES) *m/z* (rel. intensity) 286 ([M+Na], 95), 268 (100); HRMS (ES) *m/z* calc for C₁₃H₁₃NO₅Na 286.0691, found 286.0695.



Methyl 3-hydroxy-2-(4-methoxybenzamido)propanoate (3-90c).²⁷³ Following General procedure **B**, *p*-methoxybenzoyl chloride (0.500 mL, 3.69 mmol) was converted to **3-90c**. Purification by chromatography on SiO₂ (hexanes/EtOAc, 1:1, then 100% EtOAc) afforded **3-90c** (0.286 g, 31%) as an amorphous white solid: ¹H NMR (300 MHz, CDCl₃) δ 7.8 (d, *J* = 8.9 Hz, 2 H), 7.03 (bd, *J* = 6.5 Hz, 1 H), 6.93 (d, *J* = 8.9 Hz, 2 H), 4.87 (dt, *J* = 7.0, 3.6 Hz, 1 H), 4.06 (bt, *J* = 3.9 Hz, 2 H), 3.86 (s, 3 H), 3.83 (s, 3 H), 2.73 (bt, *J* = 5.3 Hz, 1 H).



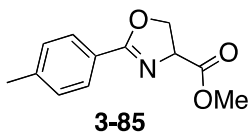
Methyl 2-(2,6-dimethoxybenzamido)-3-hydroxypropanoate (3-90d). Following General procedure **B**, 2,6-dimethoxybenzoyl chloride (1.0 g) was converted to **3-90d** (1.18 g, 84%), which was isolated as a white solid and used without further purification: ¹H NMR (300 MHz, CDCl₃) δ 7.31 (t, *J* = 8.4 Hz, 1 H), 6.69 (d, *J* = 6.7 Hz, 1 H), 6.59 (d, *J* = 8.4 Hz, 2 H), 4.87 (dt, *J* = 6.8, 3.4 Hz, 1 H), 4.27 (dd, *J* = 11.4, 3.4 Hz, 1 H), 3.98 (dd, *J* = 11.4, 3.3 Hz, 1 H), 3.84 (s, 6 H), 3.83 (s, 3 H), 2.64 (bs, 1 H).



3-90e

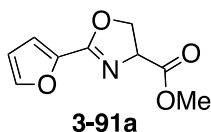
Methyl 3-hydroxy-2-(2-phenylacetamido)propanoate (3-90e). Following General procedure A, phenyl acetic acid (808 mg, 5.93 mmol) was converted to **3-90e** (840 mg, ~60%) which was isolated as a (crude) viscous yellow oil and used without further purification: ^1H NMR (300 MHz, CDCl_3) δ 7.41–7.28 (m, 5 H), 6.40 (bs, 1 H), 4.65 (dt, $J = 7.2, 3.7$ Hz), 4.00–3.86 (m, 2 H), 3.76 (s, 3 H), 3.64 (s, 2 H), 2.47 (bs, 1 H).

General procedure for conversion of β -hydroxy amides to the corresponding oxazolines using Burgess Reagent. A solution of β -hydroxy amides (1.0 equiv) in distilled THF (0.1 M) was treated with Burgess reagent (1.2 equiv) and heated at reflux for 1 h. Upon cooling, the mixture was concentrated onto SiO_2 and purified by chromatography on SiO_2 .

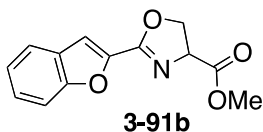


3-85

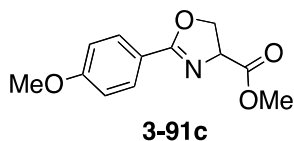
Methyl 2-*p*-tolyl-4,5-dihydrooxazole-4-carboxylate (3-85).²⁷¹ Following the general procedure, **3-84** (995 mg, 4.19 mmol) was converted to **3-85**. Purification by chromatography on SiO_2 (hexanes/EtOAc, 2:1) afforded **3-85** (704 mg, 77%) as a white solid: ^1H NMR (300 MHz, CDCl_3) δ 7.87 (d, $J = 8.2$ Hz, 2 H), 7.22 (d, $J = 8.0$ Hz, 2 H), 4.95 (dd, $J = 10.6, 7.9$, 1 H), 4.69 (app t, $J = 8.3$ Hz, 1 H), 4.59 (dd, $J = 10.6, 8.7$ Hz, 1 H), 3.82 (s, 3 H), 2.40 (s, 3 H).



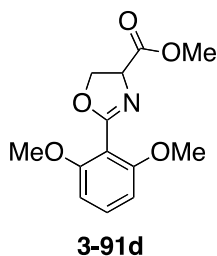
Methyl 2-(furan-2-yl)-4,5-dihydrooxazole-4-carboxylate (3-91a). Following the general procedure, **3-90a** (470 mg, 2.20 mmol) was converted to **3-91a**. Purification by chromatography on SiO₂ (hexanes/EtOAc, 1:1 then 100% EtOAc) afforded crude **3-91a** (284 mg, 66%) as a viscous yellow oil: ¹H NMR (300 MHz, CDCl₃) δ 7.57–7.56 (m, 1 H), 7.04 (d, *J* = 3.4 Hz, 1 H), 6.50 (dd, *J* = 3.5, 1.8 Hz, 1 H), 4.95 (dd, *J* = 10.4, 7.9 Hz, 1 H), 4.69 (t, *J* = 8.6 Hz, 1 H), 4.56 (dd, *J* = 10.4, 8.7 Hz, 1 H), 3.81 (s, 3 H).



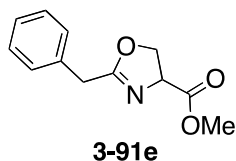
Methyl 2-(benzofuran-2-yl)-4,5-dihydrooxazole-4-carboxylate (3-91b). Following the general procedure, **3-90b** (508 mg, 1.93 mmol) was converted to **3-91b**. Purification by chromatography on SiO₂ (hexanes/EtOAc, 2:1 then 1:1) to afforded crude **3-91b** as a white solid (215 mg, ~45%): ¹H NMR (300 MHz, CDCl₃) δ 7.68–7.57 (m, 1 H), 7.45–7.39 (m, 1 H), 7.38 (s, 1 H), 7.33–7.26 (m, 1 H), 5.03 (dd, *J* = 10.5, 8.0 Hz, 1 H), 4.77 (t, *J* = 8.4 Hz, 1 H), 4.65 (dd, *J* = 12.3, 8.7 Hz, 1 H), 3.84 (s, 3 H).



Methyl 2-(4-methoxyphenyl)-4,5-dihydrooxazole-4-carboxylate (3-91c).²⁷⁴ (DAST was used instead of Burgess Reagent). A flame-dried round-bottom flask cooled under N₂ atmosphere was charged with a solution of **3-90c** (257 mg, 1.01 mmol) in dry CH₂Cl₂ (6 mL). The solution was cooled to -78 °C and stirred for 10 min. DAST (0.15 mL, 1.1 mmol) was added drop-wise *via* syringe, and the solution was stirred at -78 °C for 1 h. Anhydrous K₂CO₃ (210 mg, 1.52 mmol) was added, and the solution was warmed to rt and stirred for 2 h. Saturated aqueous NaHCO₃ (6 mL) was slowly added, and the solution was diluted with water (~10 mL) and CH₂Cl₂ (15 mL). The layers were separated, and the organic layer was washed twice with brine, dried (MgSO₄) and concentrated *in vacuo* to afford **3-91c** (172 mg, 72%) as a white solid: ¹H NMR (300 MHz, CDCl₃) δ 7.96–7.91 (m, 2 H), 6.94–6.89 (m, 2 H), 4.93 (dd, *J* = 10.5, 7.8 Hz, 1 H), 4.67 (dd, *J* = 8.6, 8.0 Hz, 1 H), 4.57 (dd, *J* = 10.5, 8.7 Hz, 1 H), 3.86 (s, 3 H), 3.82 (s, 3 H).

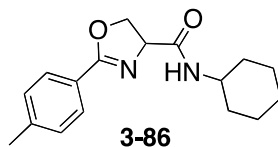


Methyl 2-(2,6-dimethoxyphenyl)-4,5-dihydrooxazole-4-carboxylate (3-91d). Following the general procedure, **3-90d** (890 mg, 3.14 mmol) was converted to **3-91d**. Purification by chromatography on SiO₂ (hexanes/EtOAc, 1:1, then 100% EtOAc) to afforded **3-91d** (566 mg, 68%) as a viscous yellow oil that foams upon drying under vacuum.

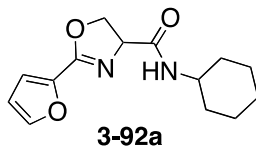


Methyl 2-benzyl-4,5-dihydrooxazole-4-carboxylate (3-91e). Following the general procedure, **3-90e** was converted to **3-91**. Purification by chromatography on SiO₂ (hexanes/EtOAc, 1:1) afforded crude **3-91e** (381 mg, 49%) as a pale yellow oil: ¹H NMR (300 MHz, CDCl₃) δ 7.36–7.29 (m, 5 H), 4.76 (dd, *J* = 10.3, 8.1 Hz, 1 H), 4.50 (app t, *J* = 8.3 H), 4.40 (dd, *J* = 10.5, 8.8 Hz, 1 H), 3.80 (s, 3 H), 3.69–3.68 (m, 2 H).

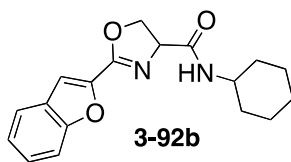
General procedure for conversion of oxazoline methyl esters to the corresponding *N*-cyclohexylamides. A solution of ester (1.0 equiv) in distilled THF (0.1 M) was treated with 1 M aqueous NaOH (1.5 equiv). The solution was stirred at rt for 20 min. NaHCO₃ (5.0 equiv) was added, and the solvent was removed *in vacuo*. Residual water was removed by coevaporation of the residue with toluene (3 x). Anhydrous DMF (0.05 M) was added, and the solution was placed under Ar atmosphere and treated with DIPEA (5.0 equiv). The solution was cooled to 0 °C, and DPPA (3.0 equiv) was added. The reaction mixture was warmed to rt and stirred at rt overnight. The mixture was cooled to 0 °C and quenched with saturated aqueous NaHCO₃ (1.5 x reaction volume) and stirred for 1 h. The mixture was poured into water and diluted with EtOAc. The layers were separated, and the aqueous layer was extracted with EtOAc (2 x). The combined organic layers were washed with water (3 x) and brine, dried (Na₂SO₄) and concentrated *in vacuo*.



***N*-Cyclohexyl-2-*p*-tolyl-4,5-dihydrooxazole-4-carboxamide (3-86)** Following the general procedure, **3-85** (302 mg, 1.38 mmol) was converted to **3-86**. Subsequent purification by chromatography on SiO₂ (hexanes/EtOAc, 2:1, then 1:1) afforded crude **3-86** (392 mg, 99%) as a white solid: IR (ATR) 3281, 2932, 1638, 1551, 1234, 1079 cm⁻¹; ¹H NMR (300 MHz, CDCl₃) δ 7.88–7.85 (m, 2 H), 7.27–7.24 (m, 2 H), 6.57 (bd, *J* = 7.7 Hz, 1 H), 4.80 (dd, *J* = 10.9, 8.3 Hz, 1 H), 4.68 (dd, *J* = 10.8, 8.5 Hz, 1 H), 4.57 (t, *J* = 8.4 Hz, 1 H), 3.86–3.72 (m, 1 H), 2.42 (s, 3 H), 2.00–1.93 (m, 1 H), 1.87–1.81 (m, 1 H), 1.76–1.59 (m, 3 H), 1.45–1.32 (m, 2 H), 1.24–1.07 (m, 3 H); ¹³C NMR (75 MHz, CDCl₃) δ 170.9, 166.2, 142.5, 129.2, 128.4, 124.3, 70.6, 69.0, 47.9, 33.0, 32.9, 25.5, 24.8, 24.8, 21.6.

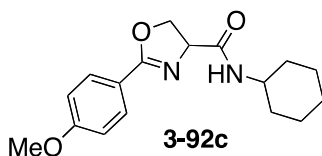


***N*-Cyclohexyl-2-(furan-2-yl)-4,5-dihydrooxazole-4-carboxamide (3-92a)**. Following the general procedure, **3-91a** (280 mg, 1.43 mmol) was converted to **3-92a**. Purification by chromatography on SiO₂ (hexanes/EtOAc, 1:1) afforded crude **3-92a** (298 mg, 79%) as a white solid: ¹H NMR (300 MHz, CDCl₃) δ 7.59 (dd, *J* = 1.7, 0.8 Hz, 1 H), 7.02 (dd, *J* = 3.5, 0.6 Hz, 1 H), 6.53 (dd, *J* = 3.5, 1.7 Hz, 1 H), 4.83 (dd, *J* = 12.3, 5.5 Hz, 1 H), 4.67 (dd, *J* = 10.8, 8.6 Hz, 1 H), 4.57 (t, *J* = 8.6 Hz, 1 H), 3.83–3.72 (m, 1 H).



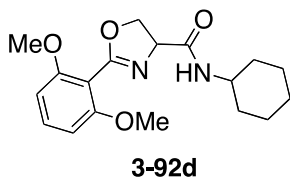
2-(Benzofuran-2-yl)-N-cyclohexyl-4,5-dihydrooxazole-4-carboxamide (3-92b).

Following the general procedure, **3-91b** (215 mg, 0.877 mmol) was converted to **3-92b**. Purification by chromatography on SiO₂ (hexanes/EtOAc, 1:1) afforded crude **3-92b** (187 mg, 68%) as a white solid: ¹H NMR (400 MHz, CDCl₃) δ 7.68 (d, *J* = 5.9 Hz, 1 H), 7.62 (d, *J* = 6.3 Hz, 1 H), 7.44 (t, *J* = 6.2 Hz, 1 H), 7.37 (s, 1 H), 7.30 (t, *J* = 5.5 Hz, 1 H), 6.59 (bd, *J* = 5.9 Hz, 1 H), 4.92 (dd, *J* = 8.1, 6.5 Hz, 1 H), 4.75 (dd, *J* = 8.1, 6.5 Hz, 1 H), 4.67 (t, *J* = 6.5 Hz, 1 H), 3.84–3.70 (m, 1 H), 1.99–1.92 (m, 1 H), 1.89–1.84 (m, 1 H), 1.77–1.58 (m, 3 H), 1.43–1.29 (m, 2 H), 1.27–1.08 (m, 3 H).



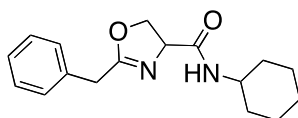
N-Cyclohexyl-2-(4-methoxyphenyl)-4,5-dihydrooxazole-4-carboxamide (3-92c). An alternative procedure was used in this case: A solution of **3-91c** (172 mg, 0.731 mmol) in THF (7 mL) was treated with 1 N aqueous NaOH (1.1 mL, 1.1 mmol) and stirred at rt for 30 min. NaHCO₃ (307 mg, 3.66 mmol) was added, and the solvent was removed in *vacuo*. Residual water was removed by coevaporation with toluene (3 x 10 mL). To the white residue was added anhydrous DMF (14 mL), cyclohexylamine (0.170 mL, 1.47 mmol), DIPEA (0.61 mL, 3.6 mmol) and PyBroP (413 mg, 0.877 mmol). The mixture was stirred at rt for 1 h 45 min, and diluted with EtOAc (150 mL). This solution was washed with 5% aqueous NaHSO₄ (100 mL), 5% aqueous NaHCO₃ (100 mL), water (2 x 100 mL) and brine, dried (Na₂SO₄), and concentrated *in vacuo*. The crude residue was dissolved in CH₂Cl₂ and concentrated onto SiO₂. Subsequent

purification by chromatography on SiO₂ (hexanes/EtOAc, 1:1) afforded **3-92c** (100 mg, 45%) as a white solid: IR (ATR) 3428, 3284, 2932, 1643, 1611, 1515 cm⁻¹; ¹H NMR (400 MHz, CDCl₃) δ 7.94–7.91 (m, 2 H), 6.96–6.93 (m, 2 H), 6.57 (bd, 1 H), 4.80 (dd, *J* = 8.2, 6.2 Hz, 1 H), 4.68 (dd, *J* = 8.2, 6.5 Hz, 1 H), 4.56 (t, *J* = 6.3 Hz, 1 H), 3.87 (s, 3 H), 3.83–3.73 (m, 1 H), 1.99–1.96 (m, 1 H), 1.86–1.83 (m, 1 H), 1.75–1.59 (m, 3 H), 1.44–1.30 (m, 2 H), 1.24–1.06 (m, 3 H); ¹³C NMR (100 MHz, CDCl₃) δ 171.0, 165.9, 126.6, 130.2, 119.5, 113.8, 70.6, 69.1, 55.4, 47.9, 33.0, 32.9, 25.5, 24.8, 24.8; MS (ES) *m/z* (rel. intensity) 325 ([M+Na]⁺, 80), 303 (M⁺, 100), 221 (75); HRMS (ES) *m/z* calc for C₁₇H₂₂N₂O₃Na 325.1528, found 325.1529.



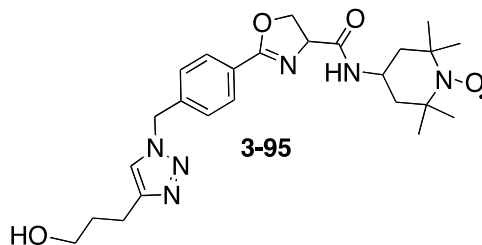
***N*-cyclohexyl-2-(2,6-dimethoxyphenyl)-4,5-dihydrooxazole-4-carboxamide (3-92d).**

Following the general procedure, **3-91d** (560 mg, 2.11 mmol) was converted to **3-92d**. Purification by chromatography on SiO₂ (100% EtOAc) afforded **3-92d** (564 mg, 80%): ¹H NMR (300 MHz, CDCl₃) δ 7.35 (t, *J* = 8.4 Hz, 1 H), 6.67 (d, *J* = 8.1 Hz, 2 H), 6.60 (d, *J* = 8.5 Hz, 2 H), 4.85 (dd, *J* = 10.4, 6.9 Hz, 1 H), 4.69–4.56 (m, 2 H), 3.84 (s, 6 H), 2.05–1.93 (m, 2 H), 1.93–1.61 (m, 2 H), 1.40–1.25 (m, 3 H), 1.21–0.93 (m, 3 H).



3-92e

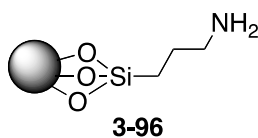
2-Benzyl-N-cyclohexyl-4,5-dihydrooxazole-4-carboxamide (3-92e). Following the general procedure, **3-91e** (370 mg, 1.69 mmol) was converted to **3-92e**. Purification by chromatography on SiO₂ (hexanes/EtOAc, 1:1) afforded (crude) **3-92e** (245 mg, 51%) as a white solid: ¹H NMR (300 MHz, CDCl₃) δ 7.38–7.28 (m, 5 H), 6.39 (bd, *J* = 7.4 Hz, 1 H), 4.62 (app t, *J* = 9.5 Hz, 1 H), 4.52–4.42 (m, 1 H), 3.80–3.69 (m, 1 H), 3.66 (s, 2 H), 1.91 (d, *J* = 11.5 Hz, 1 H), 1.80 (d, *J* = 12.9 Hz, 1 H), 1.71–1.65 (m, 3 H), 1.71–1.65 (m, 3 H), 1.42–1.30 (m, 2 H), 1.22–1.04 (m, 3 H).



3-95

N-(1-Oxy-2,2,6,6-tetramethylpiperidin-4-yl)-2-((4-(3-hydroxypropyl)-1H-1,2,3-triazol-1-yl)methyl)phenyl)-4,5-dihydrooxazole-4-carboxamide (3-95). An oven-dried 25-mL round-bottom flask was charged with **3-50** (280 mg, 0.701 mmol), dry toluene (13.5 mL), 4-pentyn-1-ol (83 μL, 0.90 mmol), and DIPEA (0.37 mL, 2.1 mmol). The solution was degassed (3 freeze-pump-thaw cycles) and CuI•POEt₃ (250 mg, 0.70 mmol) was added. The solution was stirred at rt under Ar atmosphere for 24 h, and solvent was concentrated *in vacuo*. Purification by chromatography on SiO₂ (10% MeOH/CH₂Cl₂) afforded **3-95** (228 mg, 67%) as an orange foam: IR (ATR) 3409, 2934, 1640, 1514, 1361 cm⁻¹; HRMS (ESI) *m/z* calc for C₂₅H₃₆N₆O₄ (M+H) 484.2798, found 484.2799. NMR data were obtained after reduction to the corresponding hydroxylamine:

***N*-(1-hydroxy-2,2,6,6-tetramethylpiperidin-4-yl)-2-(4-((4-(3-hydroxypropyl)-1*H*-1,2,3-triazol-1-yl)methyl)phenyl)-4,5-dihydrooxazole-4-carboxamide (3-95a).** A solution of **3-95** (73.0 mg, 0.151 mmol in dry MeOH (1.5 mL) was treated with (*L*)-ascorbic acid (27 mg, 0.15 mmol). The solution was stirred under an Ar atmosphere at rt for 30 min. The solution was diluted with EtOAc (30 mL) and washed with saturated aqueous NaHCO₃ (3 mL), water (3 mL), and brine (3 mL), dried (MgSO₄), filtered, and concentrated *in vacuo*. The concentrate was coevaporated with CDCl₃ (filtered through basic Al₂O₃) to afford the corresponding hydroxylamine (62.3 mg, 85%) as a white foam: ¹H NMR (500 MHz, CDCl₃) δ 7.98 (d, *J* = 8.2 Hz, 2 H), 7.32 (d, *J* = 8.1 Hz, 2 H), 7.27 (s, 1 H), 6.40 (d, *J* = 7.9 Hz, 1 H), 5.56 (s, 2 H), 4.81 (dd, *J* = 11.0, 8.5 Hz, 1 H), 4.70 (dd, *J* = 10.9, 8.8 Hz, 1 H), 4.61 (t, *J* = 8.6 Hz, 1 H), 4.20–4.11 (m, 1 H), 3.71 (t, *J* = 6.0 Hz, 2 H), 2.83 (t, *J* = 7.2 Hz, 2 H), 1.96–1.91 (m, 3 H), 1.80 (dt, *J* = 12.5, 3.4 Hz, 1 H), 1.42 (t, *J* = 12.4 Hz, 1 H), 1.34 (t, *J* = 12.4 Hz, 1 H), 1.22 (s, 3 H), 1.20 (s, 3 H), 1.19 (s, 3 H), 1.15 (s, 3 H); ¹³C NMR (125 MHz, CDCl₃) δ 170.3, 165.0, 147.8, 138.3, 128.8, 127.5, 126.9, 120.6, 70.1, 68.6, 61.4, 53.2, 44.8, 40.4, 31.5, 21.7, 19.3.



Representative procedure for preparation of (3-aminopropyl)-functionalized CPG (3-96).²⁴⁴ A microwave tube (2–5 mL size) was charged with native controlled pore glass (120–200 mesh/500 Å pore, 616 mg) and (3-aminopropyl)triethoxysilane (3.0 mL). The tube was sealed and subjected to microwave heating (Biotage reactor) at 100 °C for 2 x 1 min then 1 x 5 min. The contents were filtered using a medium-sized fritted funnel, and the solids were washed with toluene (2 x 20 mL), MeOH (2 x 20 mL), CH₂Cl₂ (2 x 20 mL), and distilled hexanes (2 x 20

mL). The solid (616 mg) was removed and placed into a 20 mL scintillation vial covered in punched aluminum foil for storage in a dessicator.

Representative procedure for determination of the loading of (3-aminopropyl)-functionalized CPG via trityl analysis.²⁴⁵

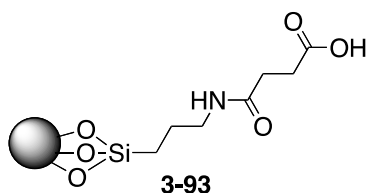
Preparation of DMT reagent. DMTCI (423 mg, 1.25 mmol) was placed in a 15-mL polypropylene Falcon tube, followed by distilled THF (2.5 mL), AgNO₃ (211 mg, 1.25 mmol) and distilled pyr (0.50 mL). The tube was capped with a septum and Ar balloon and mixed on the vortex for 4 min. The tube was centrifuged (2000 rpm, 5 min).

Protocol for loading determination. A sample of 3-aminopropyl functionalized porous glass **3-96** (20-50 mg) was added to a 1-dram vial and dried under high vacuum overnight. To the vial was added the DMT reagent solution (0.50 mL). The vial was flushed with Ar and shaken (200 rpm) for 20 min. The functionalized CPG was collected by filtration onto a medium-sized fritted funnel and washed at least three times each with DMF, THF, and Et₂O. The bright pink beads were transferred to a 1 dram vial and dried under high vacuum. A portion of the sample (6-8 mg) was weighed directly into a 50-mL volumetric flask. The sample was diluted to the line with a 3% Cl₃CCO₂H/CH₂Cl₂ w/v solution and analyzed from 600 nm to 400 nm (UV/VIS). Due to high absorbance values, 5-fold dilutions of the sample was made using 3% Cl₃CCO₂H/CH₂Cl₂ w/v, and the diluted solution was analyzed from 600 nm to 400 nm (UV/VIS). Concentrations (and consequent loadings) were calculated based on the absorbance values at 504 nm using an extinction coefficient of 76 mLcm⁻¹μmol⁻¹. Measurements were made in triplicate. Loadings were typically in the range of 100–150 μmol/g. Representative data from loading determination after several batch functionalizations are depicted in Table 4-2.

Table 4-2. Loadings of 3-aminopropyl functionalized CPG.

Entry	Batch of CPG 3-96	Loading ($\mu\text{mol/g}$)
1	3-96A	125 ^a
2 ^c	3-96B	130 \pm 20
3 ^d	3-96C	77 ^b \pm 4
4	3-96D	114 \pm 11
5	3-96E	153 ^a
6	3-96F	150 ^a \pm 50

^aSingle measurement. ^bMean \pm standard deviation (n = 3 trials). ^cFunctionalization conditions were as follows: μ wave 1 x 1 min, then 5 min. ^dFunctionalization conditions were as follows: μ wave, 5 min.



Representative procedure for preparation of succinylated CPG (3-93).²⁴⁴ A microwave vial was charged with 3-aminopropyl functionalized CPG **3-96** (512 mg, based on a loading = 144 $\mu\text{mol/g}$) followed by a solution of succinic anhydride (1.25 g, 12.5 mmol) and DMAP (150 mg, 1.23 mL) in anhydrous DMF (3.5 mL). The vial was subjected to heating in the Biotage microwave reactor at 100 $^{\circ}\text{C}$ (2 x 1 min, then 1 x 5 min). The solid CPG was collected by filtration through a medium-sized fritted funnel. The solid was washed with MeOH (3 x 15 mL), CH_2Cl_2 (3 x 15 mL), EtOAc (3 x 15 mL), and hexanes (3 x 15 mL). The solids were

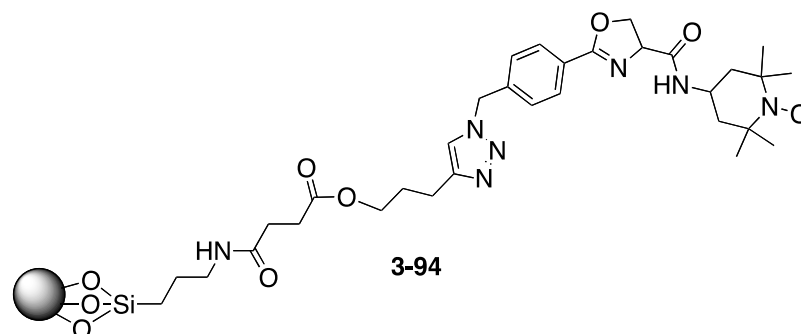
collected into a 20 mL scintillation vial, capped with foil (with punched holes) and stored in the dessicator for 4 days.

Representative procedure for determination of the loading of succinylated CPG.²⁴³

A sample of succinylated CPG (75.7 mg) was dried under high vacuum overnight in a 1-dram vial. To the vial was added 4-nitrophenol (9 mg, 0.07 mmol) EDC (11 mg, 0.06 mmol), distilled pyr (0.50 mL), and distilled Et₃N (40 μL, 0.1 mmol). The vial was shaken (200 rpm) at rt overnight. The solid was collected by filtration through a medium-sized fritted funnel and washed with pyridine, MeOH, and CH₂Cl₂ and dried under high vacuum to afford esterified CPG (62.4 mg). A sample of the esterified porous glass (11–13 mg) was weighed directly into a 25-mL volumetric flask. The flask was filled to the line with 0.1 M aqueous NaOH and analyzed from 600 nm to 300 nm (UV/VIS). Concentrations (and consequent loading) was calculated based on the absorbance values at 400.5 nm using an extinction coefficient of 15.7 mLcm⁻¹μmol⁻¹. Loadings from the respective precursor amine batches are shown in Table 4-3.

Table 4-3. Loadings of succinylated CPG.

Entry	Batch of precursor 3-96 (loading)	Batch of CPG 3-93	Loading (μmol/g)
1	3-96B (130 ± 20)	3-93B	85
2	3-96C (77 ± 4)	3-93C	56
3	3-96D (114 ± 11)	3-93D	139
4	3-96E (153)	3-93E	156
5	3-96F (150 ± 50) _–	3-93F	101
6	3-96G (ND)	3-93G	142
7	3-96H (ND)	3-93H	150



Representative procedure for esterification of succinylated CPG with triazole 3-95 (3-94). A 20-mL scintillation vial was charged with succinylated particles (456 mg, 0.0648 mmol, loading =150 $\mu\text{mol/g}$) and treated with a solution of alcohol **3-95** (147 mg, 0.304 mmol), DMAP (8.0 mg, 0.065 mmol) and anhydrous DMF (2.5 mL). Et_3N (45 μL , 0.32 mmol) and EDC $\cdot\text{HCl}$ (66 mg, 0.34 mmol) were added. The vial was capped, sealed, and shaken (100 rpm) on a platform shaker at rt overnight (15 h). The solids were collected by filtration on a medium-sized fritted funnel and washed with CH_2Cl_2 (3 x 30 mL), MeOH (3 x 30 mL) and hexanes (3 x 30 mL). The very pale orange beads were dried under high vacuum, and CPG (490 mg) was collected.

To recover unreacted triazole **3-95**, the filtrate (prior to washing) was diluted with CH_2Cl_2 (10 mL) and washed with water (2 x 5 mL) and brine (5 mL), dried (MgSO_4), filtered, and concentrated *in vacuo*. The residue was purified by chromatography (ISCO, 4 g SiO_2 cartridge, 0–20% MeOH/ CH_2Cl_2) to afford recovered **3-95** (72.6 mg).

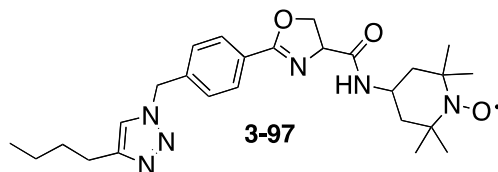
Representative procedure for determination of loading via saponification of nitroxide-functionalized CPG. A sample of functionalized CPG **3-94** (16.0 mg) was weighed into a 1-dram vial. The CPG was treated with 0.1 M aqueous NaOH/MeOH (1:1, v/v) (1.0 mL), and the vial was shaken (200 rpm) for 6 h at rt. The solution was transferred to a 25-mL volumetric flask, and the flask was filled to the mark with the 0.1 M aqueous NaOH/MeOH (1:1, v/v). The sample was analyzed from 400 nm to 200 nm (UV/VIS). The concentration (and consequent loading) was calculated based on the absorbance at 249 nm using an extinction

coefficient of $17 \text{ mLcm}^{-1}\mu\text{mol}^{-1}$. Note: the extinction coefficient was calculated based on a previously generated calibration curve generate from solutions of triazole **3-95** in 0.1 M aqueous NaOH/MeOH, 1:1.

Loadings were typically 100–150 $\mu\text{mol/g}$. Loadings from different batches of esterified CPG **3-94** are tabulated in Table 4-4.

Table 4-4. Loadings of CPG esterified with triazole **3-95**.

Entry	Batch of precursor 3-93 (loading, $\mu\text{mol/g}$)	Batch of CPG 3-94	Loading ($\mu\text{mol/g}$)
1	3-93D (139)	3-94A	100 ± 10
2	3-93E (156)	3-94B	110
3	3-93E (156)	3-94C	118
4	3-96E (156)	3-94D	153
5	3-96H (150)_	3-94E	156



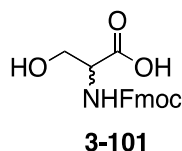
2-(4-((4-Butyl-1H-1,2,3-triazol-1-yl)methyl)phenyl)-N-(1-oxy-2,2,6,6-tetramethylpiperidin-4-yl)-4,5-dihydrooxazole-4-carboxamide (3-97). An oven-dried thick-walled vial was charged with a solution of **3-50** (50 mg, 0.13 mmol) in toluene (0.83 mL), followed by additional toluene (1.7 mL). 1-Hexyne (17 μ L, 0.15 mol) and DIPEA (65 μ L, 0.38 mmol) were added. The solution was degassed using the freeze-pump-thaw method (three cycles). Upon warming to rt and flushing with N₂, CuI•P(OEt)₃ (45 mg, 0.13 mmol) was quickly added. The solution was stirred at rt for 51 h. The reaction mixture was concentrated *in vacuo*, and the residue was purified by chromatography on SiO₂ (hexanes/EtOAc, 1:2 to 100% EtOAc) to afford **3-97** (40 mg, 67%) as an orange foam: HRMS (ESI) *m/z* calc for C₂₆H₃₈N₆O₃ (M+H) 482.3005, found 482.3021.

For NMR characterization, a sample of **3-97** was converted to the corresponding hydroxylamine (**3-97a**): A sample of **3-97** (11.1 mg) was dissolved in MeOH (0.5 mL) and shaken with ascorbic acid (5 mg) until the solution was colorless. The solution was dissolved in Et₂O (~3 mL) and washed with minimal amounts of saturated aqueous NaHCO₃ and brine, filtered through a small plug of MgSO₄, and concentrated *in vacuo* to afford the corresponding hydroxylamine **3-97a** (8.0 mg): ¹H NMR (400 MHz, CDCl₃) δ 7.97 (d, *J* = 8.2 Hz, 2 H), 7.31 (d, *J* = 8.2 Hz, 2 H), 7.22 (s, 1 H), 6.39 (d, *J* = 8.0 Hz, 1 H), 5.56 (s, 2 H), 4.81 (dd, *J* = 10.9, 8.4 Hz, 1 H), 4.70 (dd, *J* = 10.2, 6.6 Hz, 1 H), 4.60 (t, *J* = 6.4 Hz, 1 H), 4.22–4.12 (m, 1 H), 2.71 (t, *J* = 7.6 Hz, 2 H), 1.93 (dt, *J* = 12.6, 3.4 Hz, 1 H), 1.80 (dt, *J* = 12.5, 3.4 Hz, 1 H), 1.68–1.60 (m, 2 H), 1.45–1.31 (m, 5 H), 1.22 (s, 3 H), 1.20 (s, 3 H), 1.19 (s, 3 H), 1.15 (s, 3 H), 0.92 (t, *J* = 7.4 Hz, 3 H); ¹³C NMR (100 MHz, CDCl₃) δ 170.5, 165.2, 148.9, 138.7, 128.9, 127.6, 127.0, 120.3, 70.3, 68.7, 53.2, 44.9, 40.5, 31.9, 31.2, 29.3, 25.1, 22.0, 19.4, 13.5.

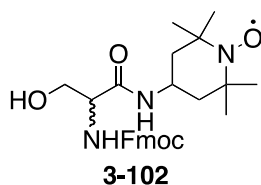
Procedure for covalency test of CPG. An oven-dried 1-dram vial was charged with succinylated particles **3-93** (100 mg, loading ~139 $\mu\text{mol/g}$). A second oven-dried vial was charged with triazole **3-97** (20 mg, 0.040 mmol), DMAP (15 mg, 0.12 mmol) and anhydrous DMF (0.50 mL). This solution was transferred to the vial containing the succinylated CPG under Ar atmosphere. Et_3N (10 μL , 0.070 mmol) was added, followed by EDC $\cdot\text{HCl}$ (13 mg, 0.070 mmol). The vial was capped, sealed, and shaken (100 rpm) on a platform shaker at rt overnight (19 h). The solids were collected on a medium-sized fritted funnel and washed with CH_2Cl_2 (3 x 15 mL), MeOH (3 x 15 mL), and hexanes (3 x 15 mL). The white solid CPG (98 mg) was collected in a 1-dram vial and dried under high vacuum for 5 h.

Three samples (17 mg each) of the CPG were weighed into 1-dram vials and treated with 0.1 M aqueous NaOH/MeOH (1:1 v/v) (1.0 mL) and shaken (200 rpm) at rt overnight. The contents of each vial were transferred to a 25-mL volumetric flask, and each flask was filled to the mark with 0.1 M aqueous NaOH/MeOH (1:1 v/v). The samples were analyzed from 400 nm to 200 nm, and the absorbance at 248 nm (0.051, 0.052, 0.071) would correspond to loadings of 4-6 $\mu\text{mol/g}$ assuming triazole **3-97** has the same extinction coefficient as triazole **3-95** (17 $\text{mLcm}^{-1}\mu\text{mol}^{-1}$). Note: The extinction coefficient of triazole **3-97** in 0.1 M aqueous NaOH/MeOH, 1:1 was determined to be 15.4 $\text{mLcm}^{-1}\mu\text{mol}^{-1}$.

Due to having some absorbance at 248 nm, succinylated particles **3-93** (16.6 mg) were treated with 0.1 M aqueous NaOH/MeOH (1:1 v/v) (1.0 mL) and shaken (200 rpm) at rt overnight. The contents of the vial were transferred to a 25-mL volumetric flask, and each flask was filled to the mark with 0.1 M aqueous NaOH/MeOH (1:1 v/v). The sample was analyzed from 400 nm to 200 nm, and absorbance (with a maximum at 259.6 nm) was observed. The absorbance was confirmed to be adsorbed DMAP after analyzing an independently prepared DMAP standard.

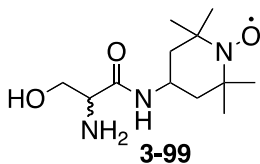


***N*-(9-Fluorenylmethoxycarbonyl)-*DL*-serine (3-101).**²⁴⁶ *DL*-Serine (1.0 g, 9.5 mmol) was suspended in 10% aqueous Na₂CO₃ (17 mL) and 1,4-dioxane (8 mL) and cooled to 0 °C. A solution of Fmoc-OSu (3.2 g, 9.5 mmol) in 1,4-dioxane (15 mL) was added over a period of 30 min using an addition funnel. The reaction mixture was stirred overnight, and the solvent was removed *in vacuo*. Water (75 mL) was added, the suspension was washed with Et₂O, and the aqueous layer was acidified with 1 M aqueous citric acid to pH ~3–4. The aqueous layer was extracted with EtOAc (3 x 70 mL), and the combined EtOAc layers were dried (MgSO₄), filtered and concentrated. Coevaporation of the crude residue with CH₂Cl₂ afforded a white foam (3.7 g). The crude product was recrystallized from hot CH₂Cl₂ (~60 mL) and hexanes (~30 mL, added after boiling the crude product in CH₂Cl₂). After standing for 2 h, **3-101** was isolated (1.71 g, 55%). The mother liquor was concentrated *in vacuo*, and this first crop of material was combined with the mother liquor. Boiling CH₂Cl₂ (~50 mL) was added. Upon cooling, **3-101** (2.74 g, 88%) precipitated as a white powder: ¹H NMR (400 MHz, MeOD) δ 7.79 (d, *J* = 7.5 Hz, 2 H), 7.68 (t, *J* = 6.4 Hz, 2 H), 7.38 (t, *J* = 7.4 Hz, 2 H), 7.30 (t, *J* = 7.2 Hz, 2 H), 4.38 (dd, *J* = 10.4, 7.0 Hz, 1 H), 4.34–4.22 (m, 3 H), 3.84 (dddd, *J* = 11.3, 11.3, 11.3, 5.0 Hz, 2 H); HRMS (ESI) *m/z* calc for C₁₈H₁₆NO₅ (M-H) 326.1028, found 326.1059.



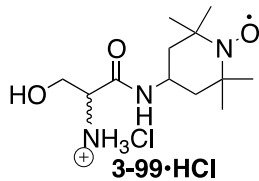
(9*H*-Fluoren-9-yl)methyl 3-hydroxy-1-(1-hydroxy-2,2,6,6-tetramethylpiperidin-4-ylamino)-1-oxopropan-2-ylcarbamate (3-102). A suspension of **3-101** (50 mg, 0.15 mmol) in

CH₂Cl₂ (1.0 mL) was cooled to 0 °C and treated with a solution of 4-amino TEMPO (39 mg, 0.23 mmol) in CH₂Cl₂ (0.50 mL) followed by HOBT (23 mg, 0.17 mmol), DMAP (21 mg, 0.17 mmol) and EDC•HCl (35 mg, 0.18 mmol). The reaction mixture was warmed to rt and stirred for 21 h. The mixture was diluted with CH₂Cl₂ (10 mL) and washed with 0.1 M aqueous citric acid (2 x 5 mL), saturated aqueous NaHCO₃ (5 mL), and brine (5 mL), dried (MgSO₄), and concentrated *in vacuo*. Purification by chromatography on SiO₂ (hexanes/EtOAc, 1:1 to 1:2 to 1:3) afforded **3-102** (43.4 mg, 59%) as an orange foam. LCMS data were obtained using an Agilent (Varian HPLC) Pursuit XRs Ultra 2.8 C18 column (50 x 2.0 mm) (R_t 9.20 min, 0.50 mL/min, 20% to 100% MeCN/water over 5 min): MS (ESI) *m/z* 503.3 (M+Na). The corresponding hydroxylamine was also detected as a minor product by LCMS (R_t 8.34 min): MS (ESI) *m/z* 504.2.



2-Amino-3-hydroxy-N-(1-oxy-2,2,6,6-tetramethylpiperidin-4-yl)propanamide (3-99).

An oven-dried 10-mL flask was charged with **3-102** (121 mg, 0.252 mmol) followed by 20% piperidine/CH₂Cl₂ (2.5 mL). The mixture was stirred at rt for 30 min. The mixture was concentrated onto SiO₂ and purified by chromatography on SiO₂ (CHCl₃/MeOH, 95:5 to CHCl₃/MeOH, 90:10 to CHCl₃/MeOH/aqueous NH₄OH 90:9:1) to afford **3-99** (56.6 mg, 87%) as an orange foam. The product **3-99** was taken on directly to the following step.



+ hydroxylamine (**3-99-HCl**a)

2-Amino-3-hydroxy-N-(1-oxy-2,2,6,6-tetramethylpiperidin-4-yl)propanamide hydrochloride salt (3-99•HCl). A solution of free amine **3-99** (56.6 mg, 0.219 mmol) in dry 1,4-dioxane (2.5 mL) was treated with a solution of HCl in 1,4-dioxane (0.11 mL, 0.44 mmol, $c = 4.0$ M in 1,4-dioxane). The orange solution quickly turned to a turbid, yellow suspension. After 30 min of stirring, the mixture was filtered (fritted funnel) and the yellow solids were washed with dry Et₂O. Upon drying under high vacuum overnight **3-99•HCl** (60.3 mg, 93%) was collected as a bright yellow solid^a: IR (ATR) 3545, 2947, 1664, 1459, 1385 cm⁻¹; ¹H NMR (400 MHz, MeOD) δ 4.35 (t, $J = 11.9$ Hz, 1 H), 3.94–3.92 (m, 2 H), 3.87–3.82 (m, 1 H), 2.19–2.16 (m, 2 H), 2.02 (t, $J = 13.1$ Hz, 2 H), 1.52 (s, 6 H), 1.50 (s, 6 H); ¹³C NMR (100 MHz, MeOD) 167.8, 69.8, 61.7, 56.2, 42.6, 42.5, 41.0, 28.2, 20.4.

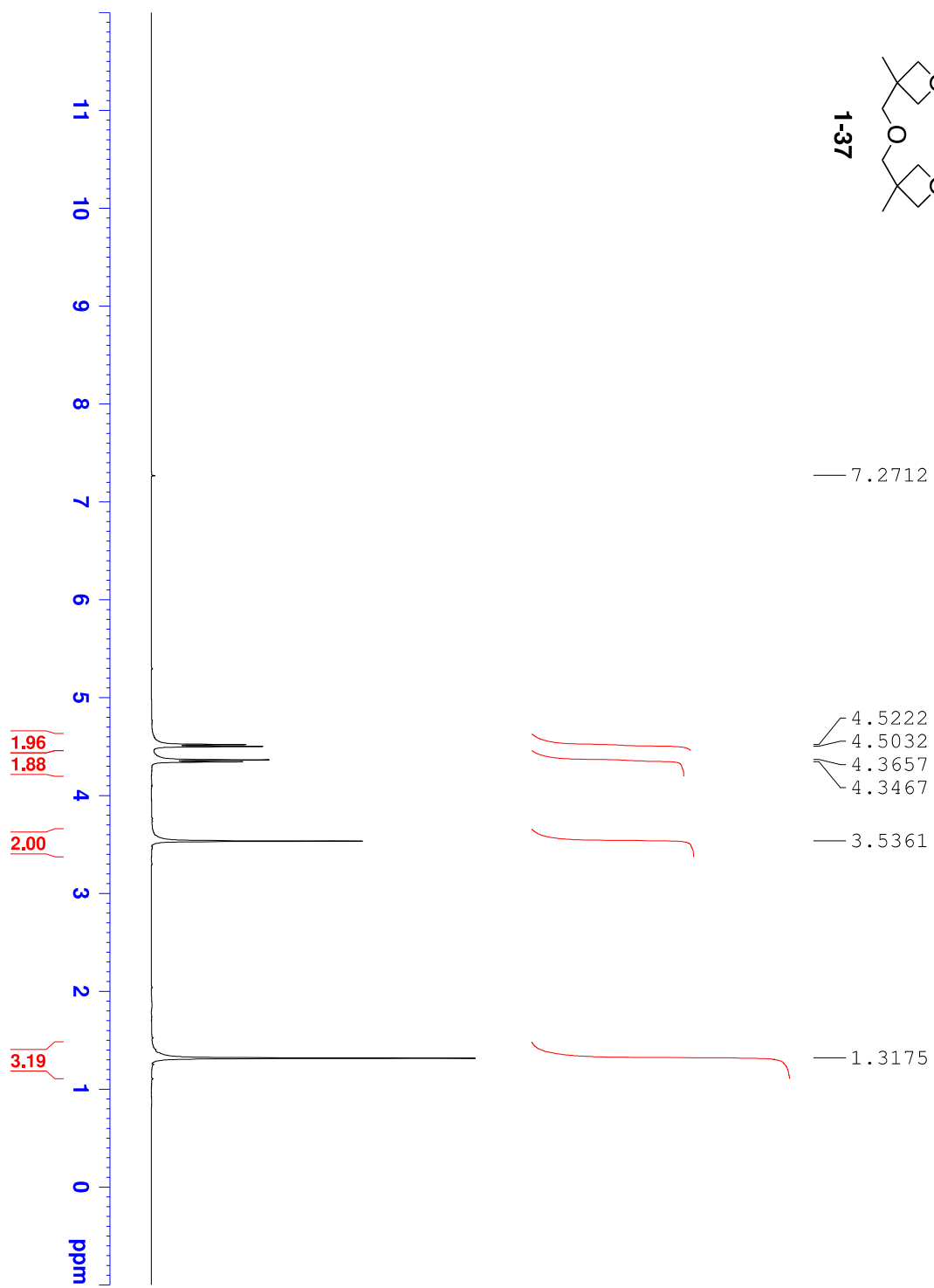
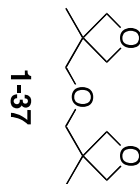
Both the nitroxide **3-99** and the corresponding hydroxylamine **3-99a** were detected by LCMS using an analytical C18 column (150 mm x 4.6 mm) (R_t **3-99** 2.38 min, R_t **3-99a** 2.02 min, 0.50 mL/min, 3% MeCN/water for 5 min, then 3% MeCN/water to 95% MeCN/water to 12 min, 0.50 mL/min):

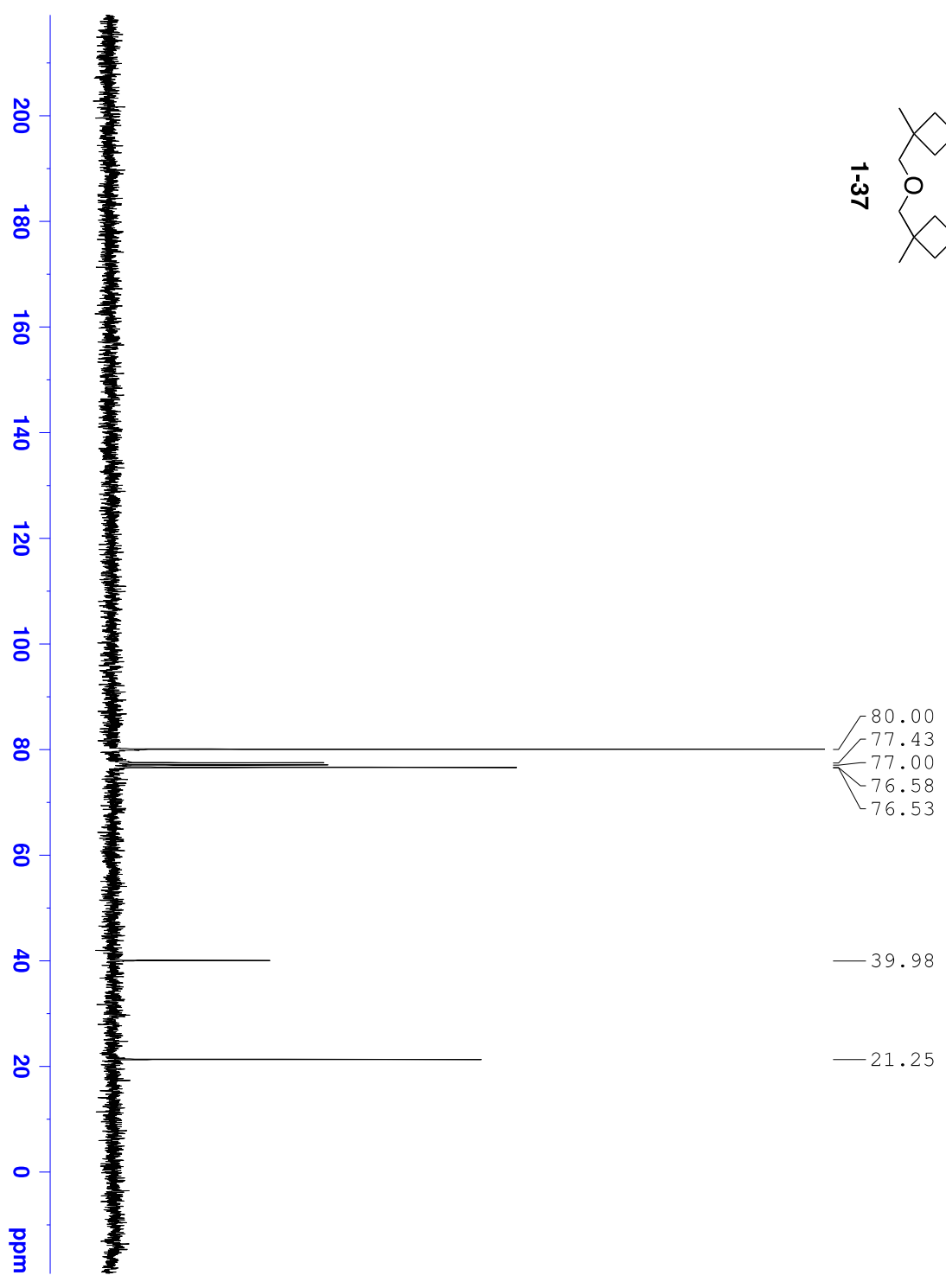
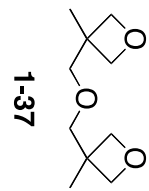
3-99: HRMS (HESI) m/z calc for C₁₂H₂₅O₃N₃ (M+H) 259.1890, found 259.1876.

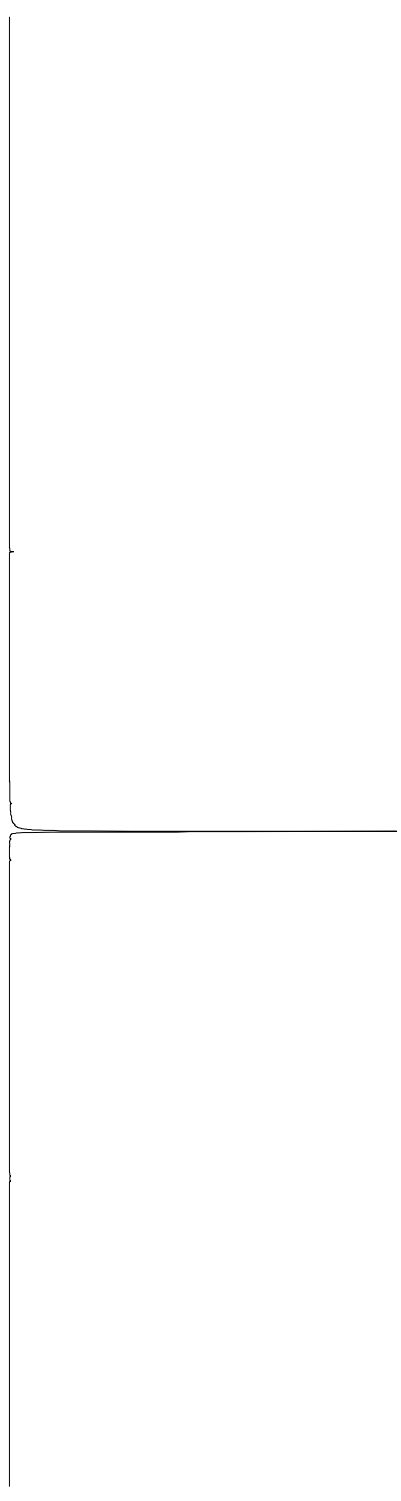
3-99a: HRMS (HESI) m/z calc for C₁₂H₂₆O₃N₃ (M+H) 260.1969, found 260.1953.

^aNote: Upon coevaporation of the solid with MeOD, the solid became a pale orange color.

APPENDIX A: SELECTED ^1H NMR AND ^{13}C NMR SPECTRA

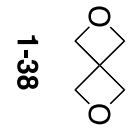






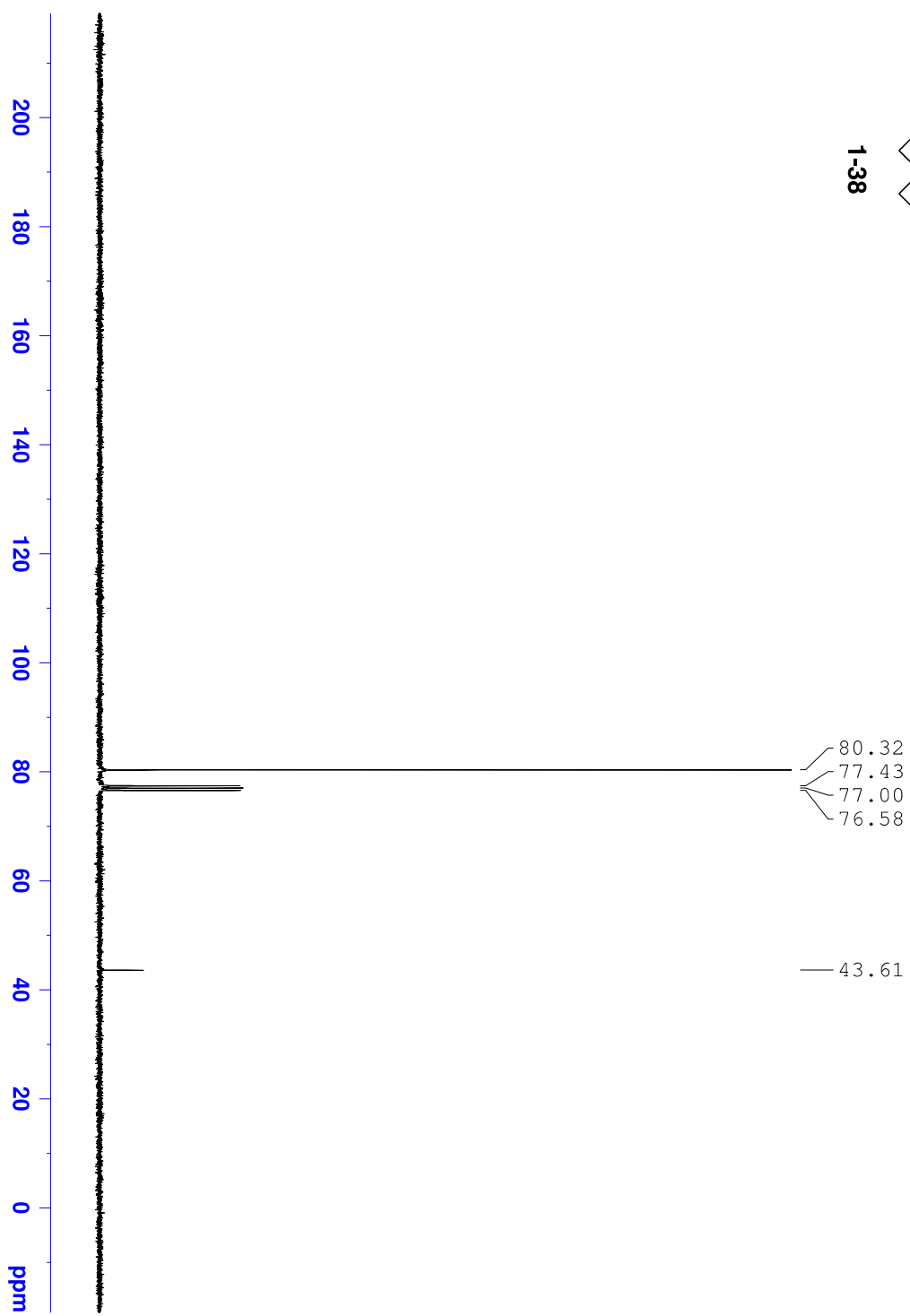
— 7.2744

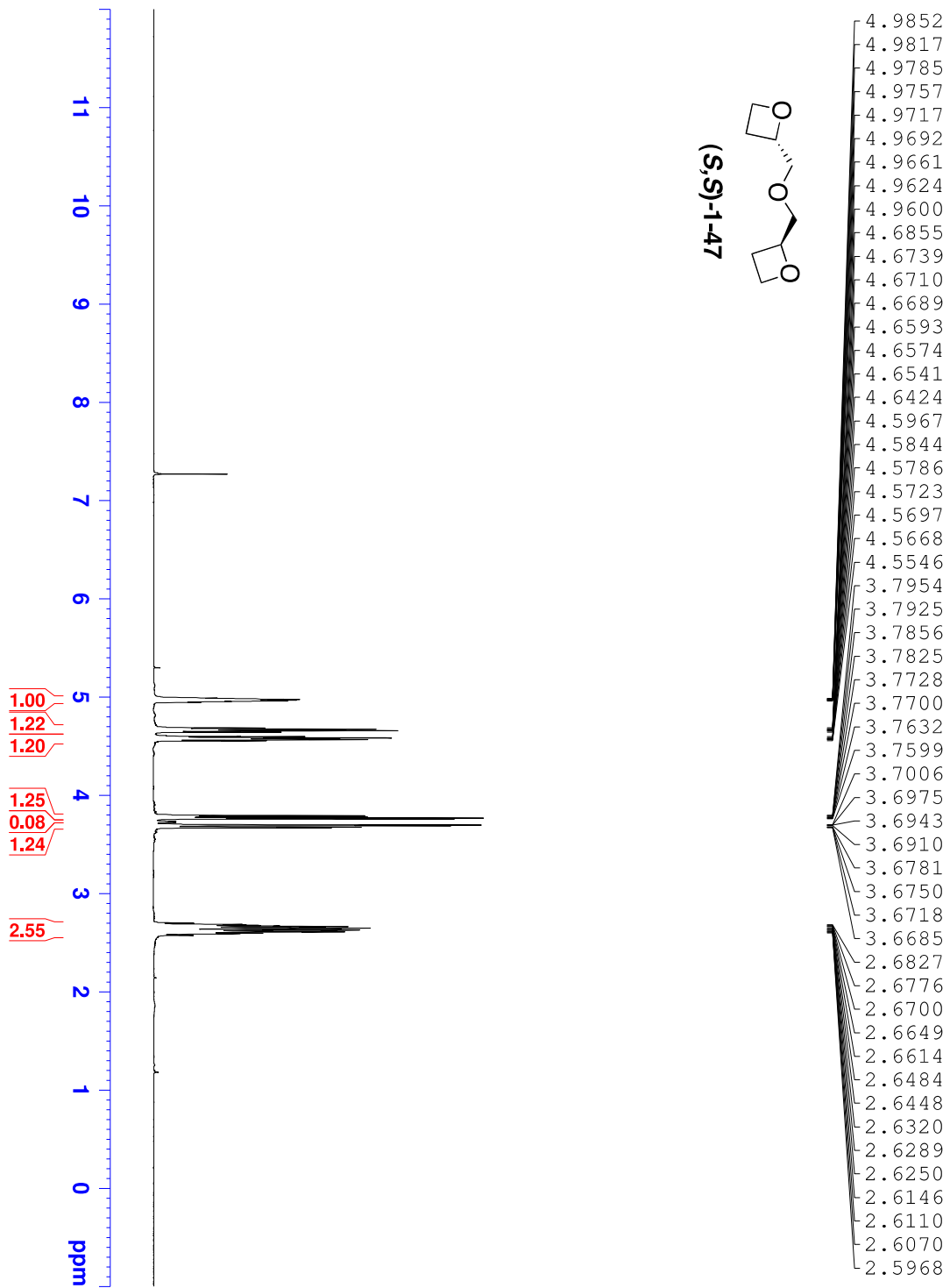
— 4.8027

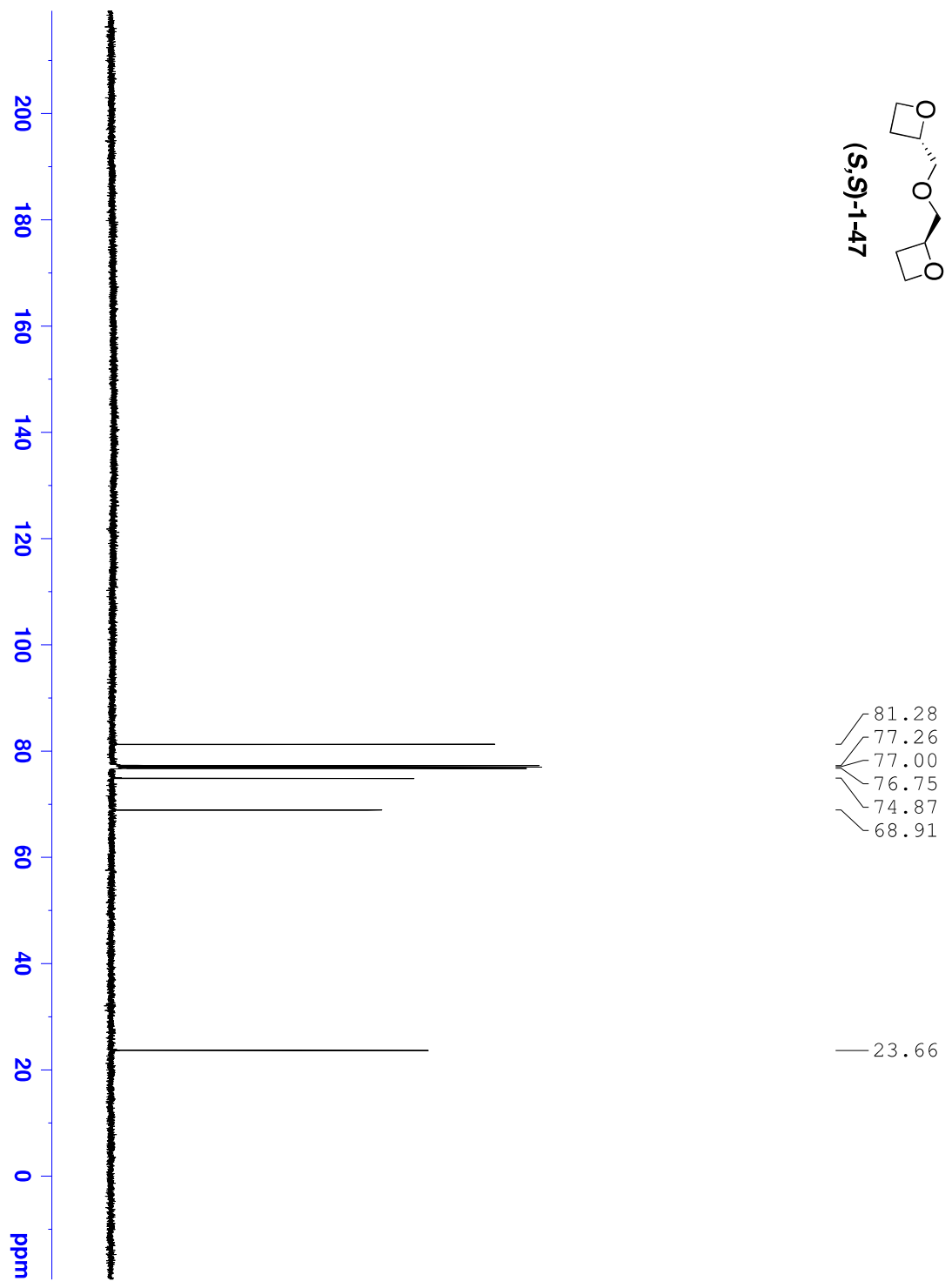
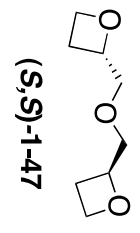


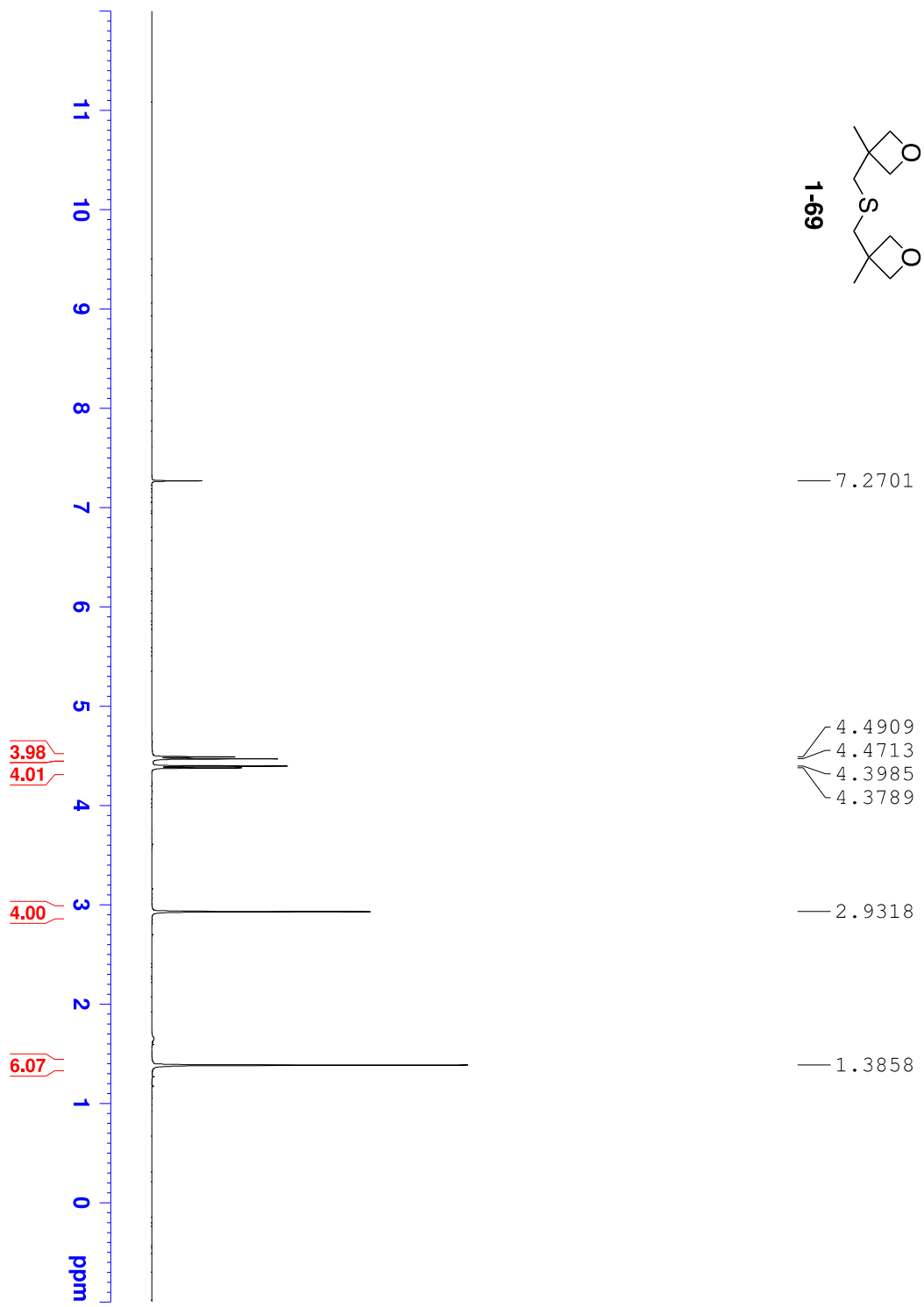


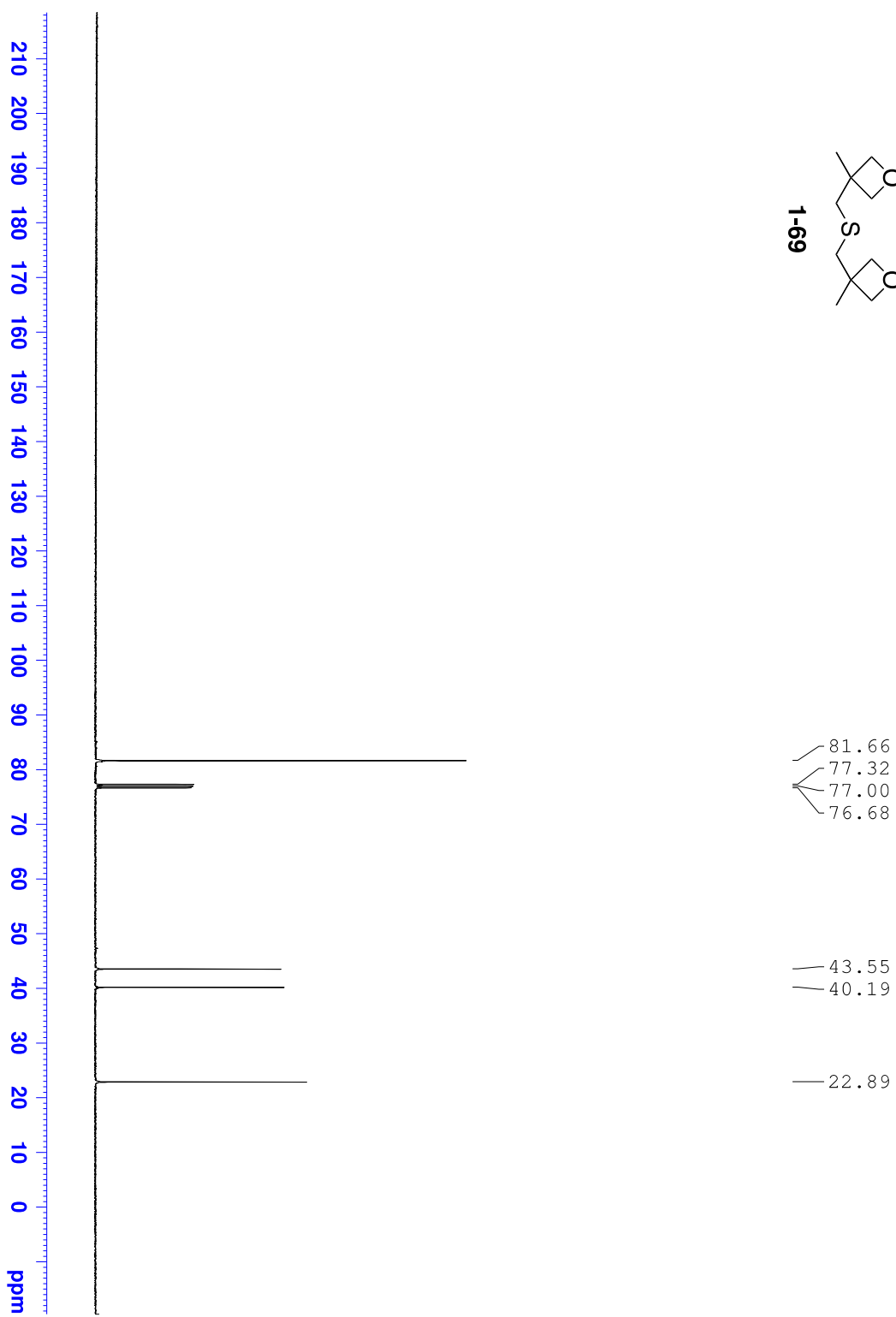
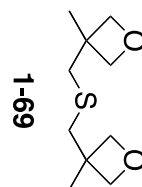
1-38

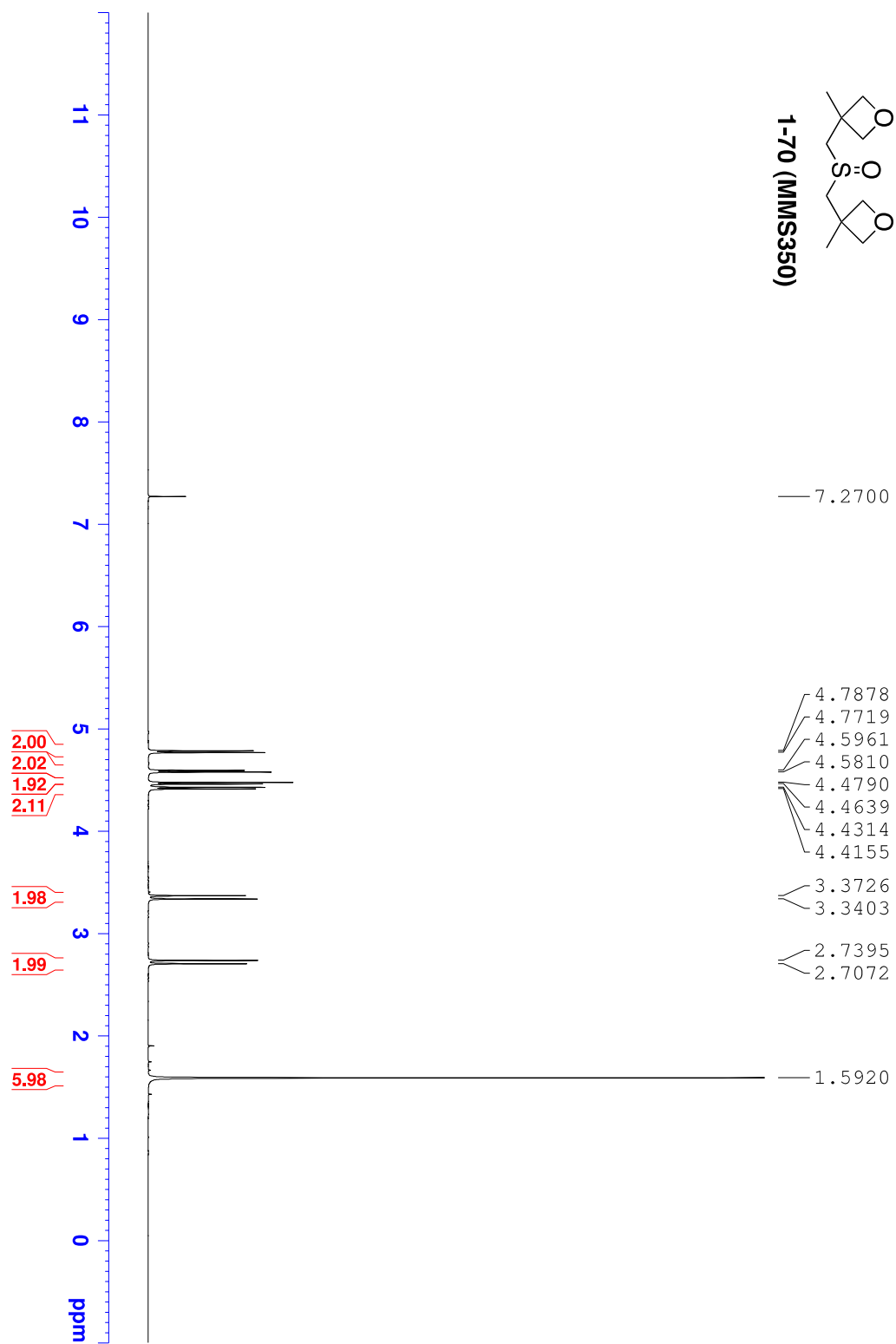


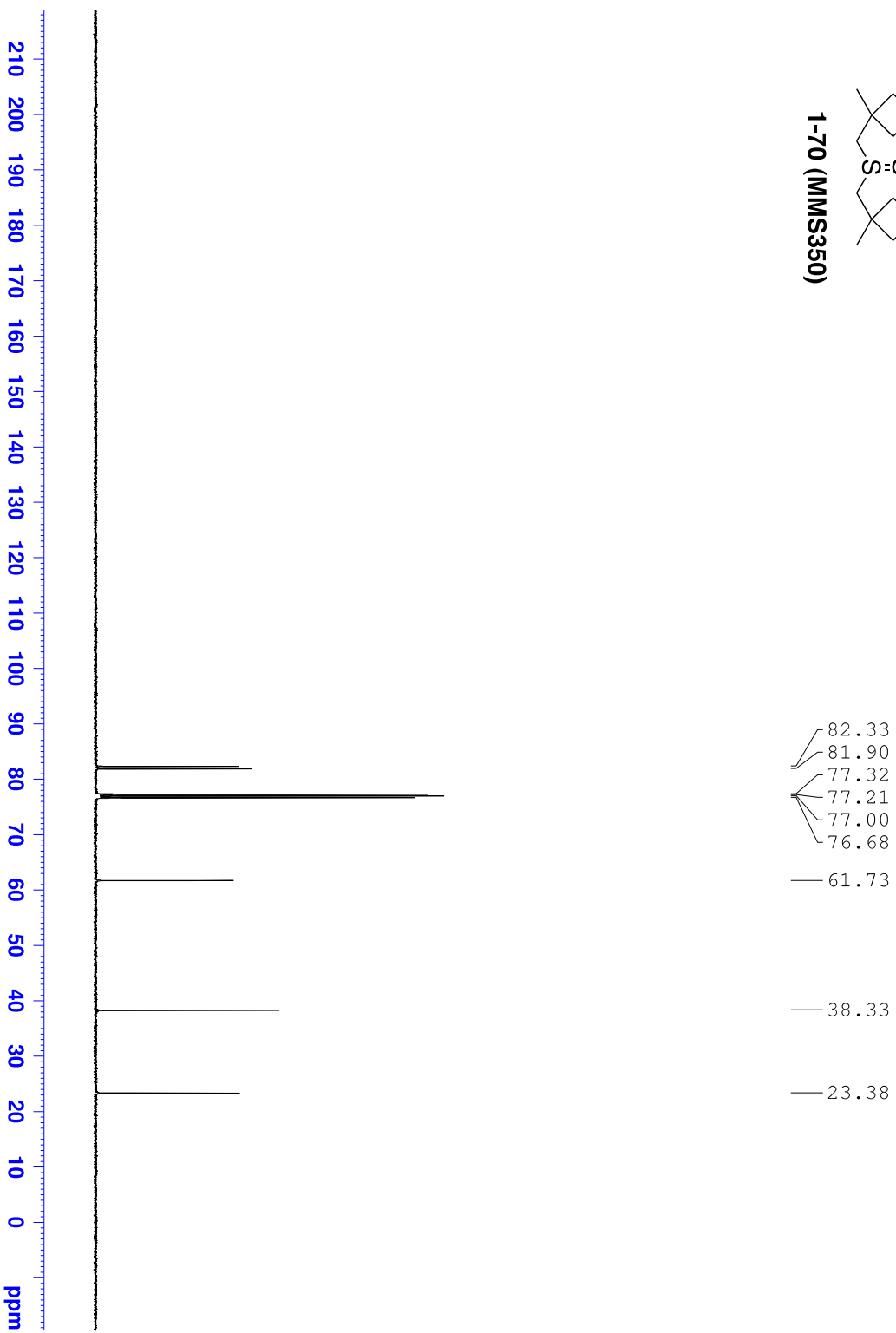
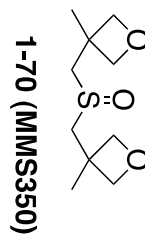


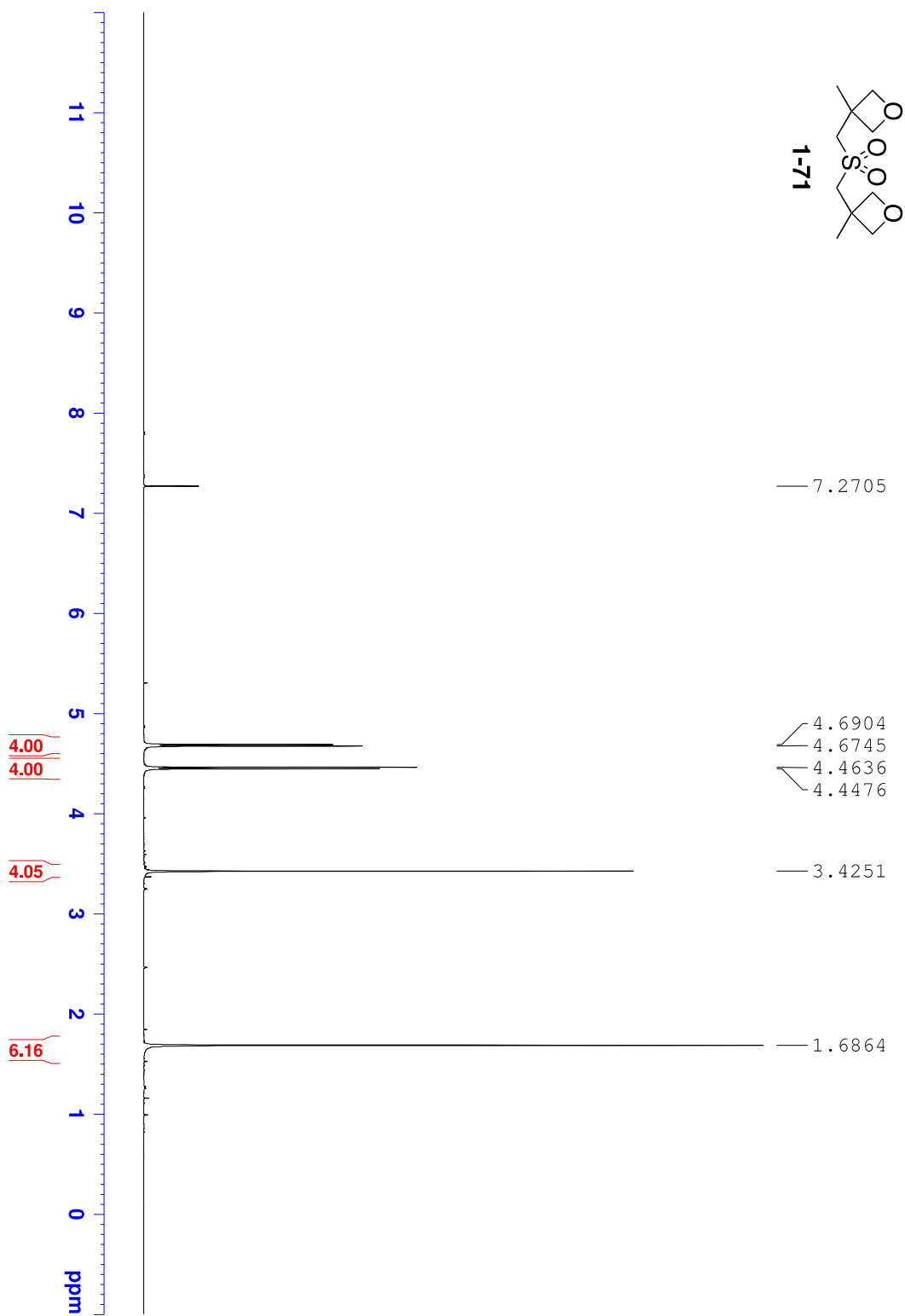


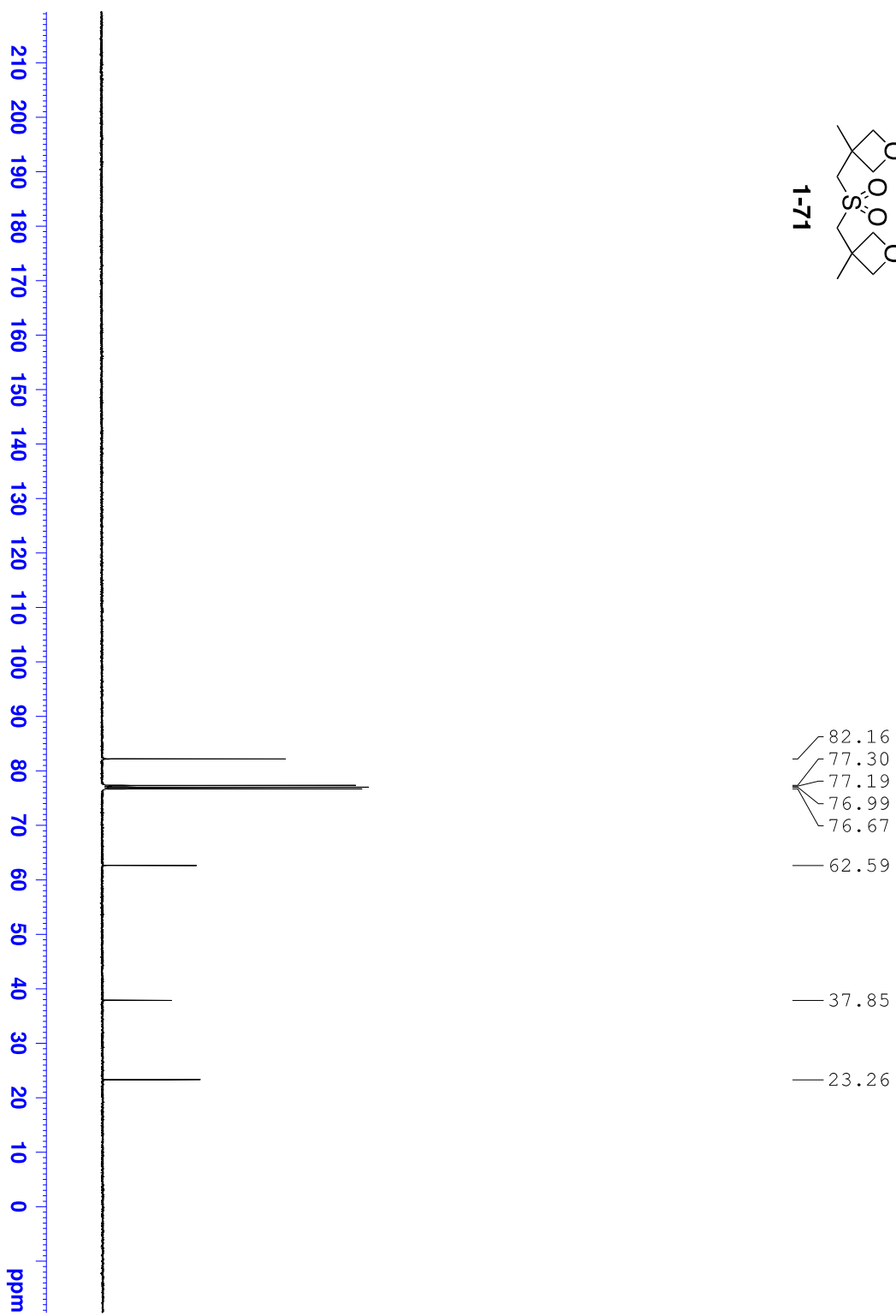
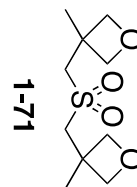


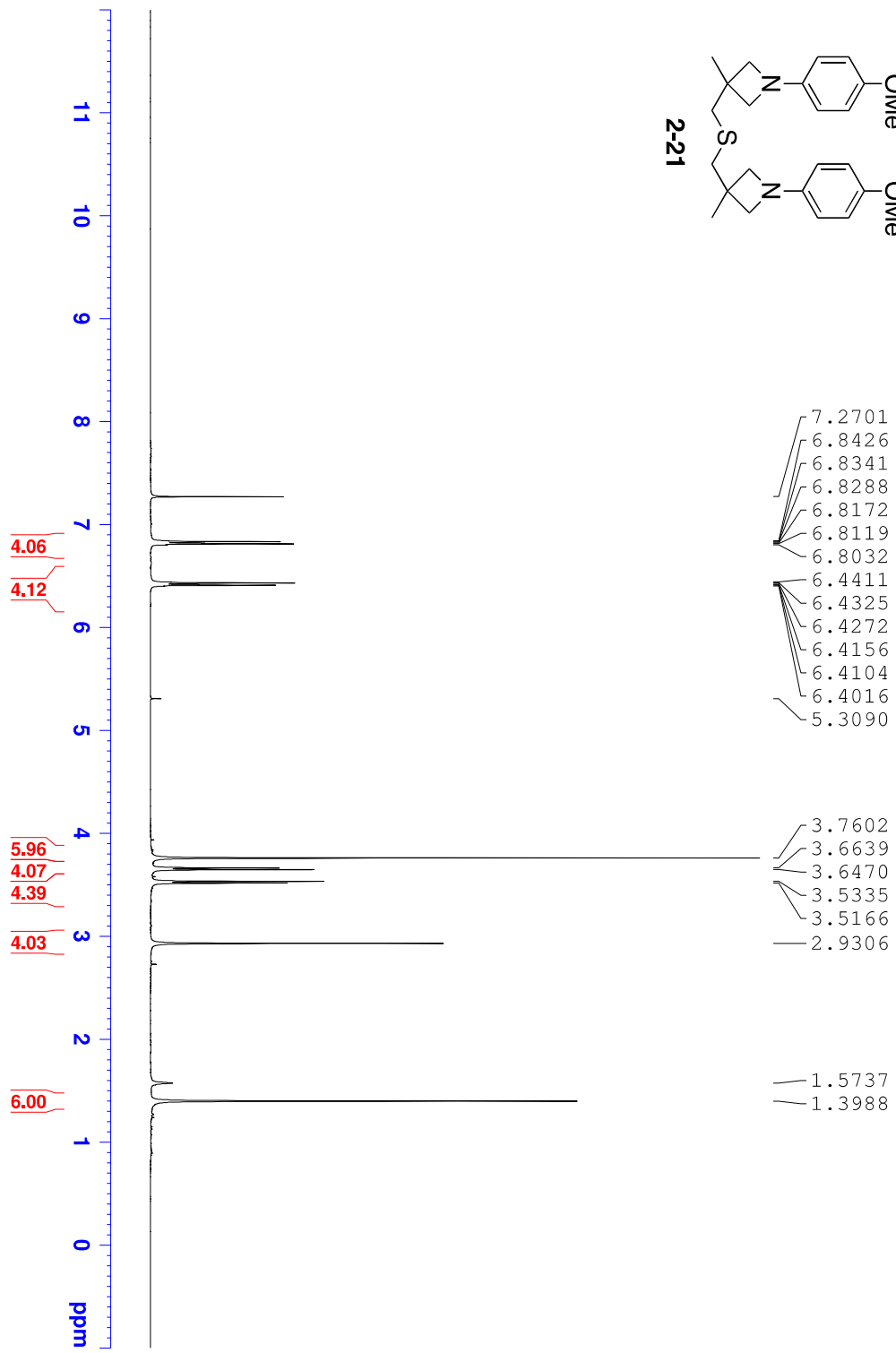
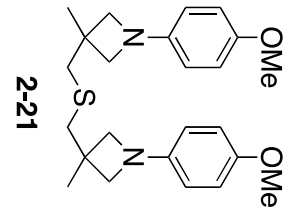


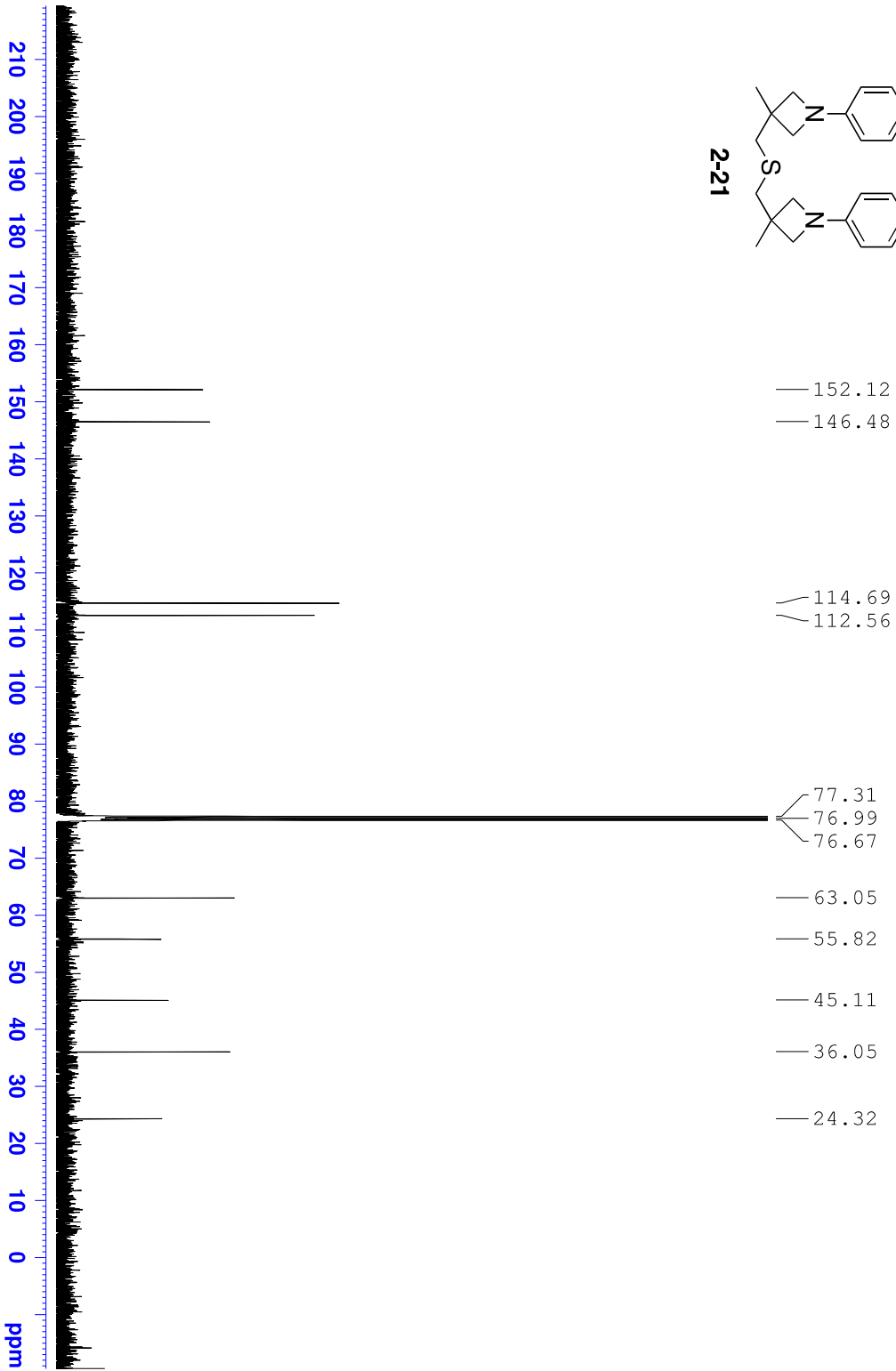
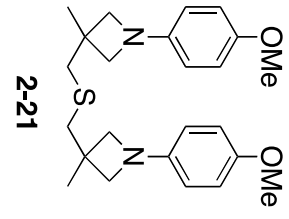


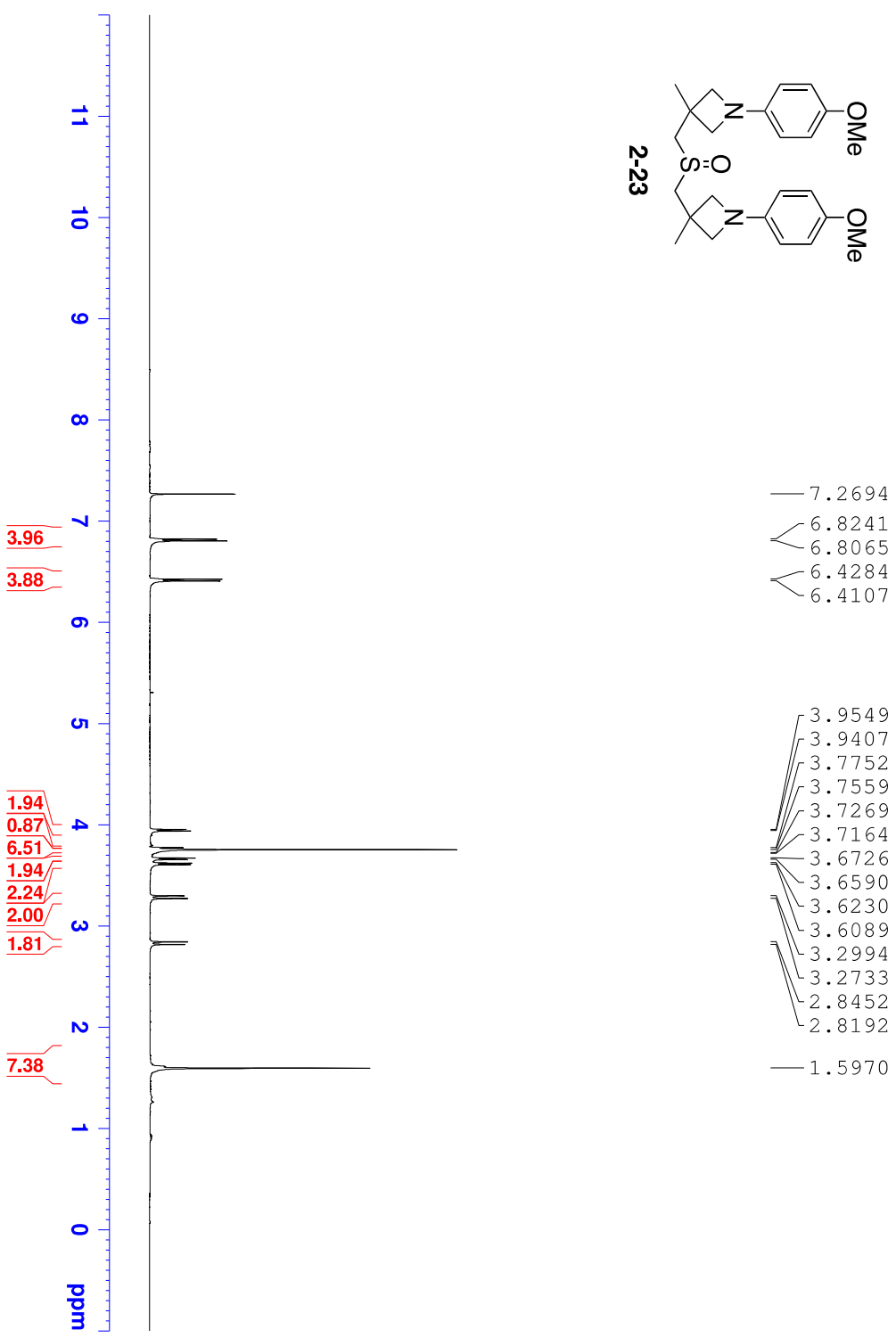
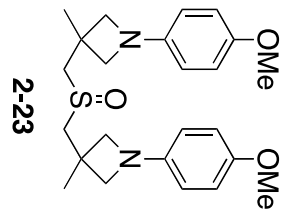


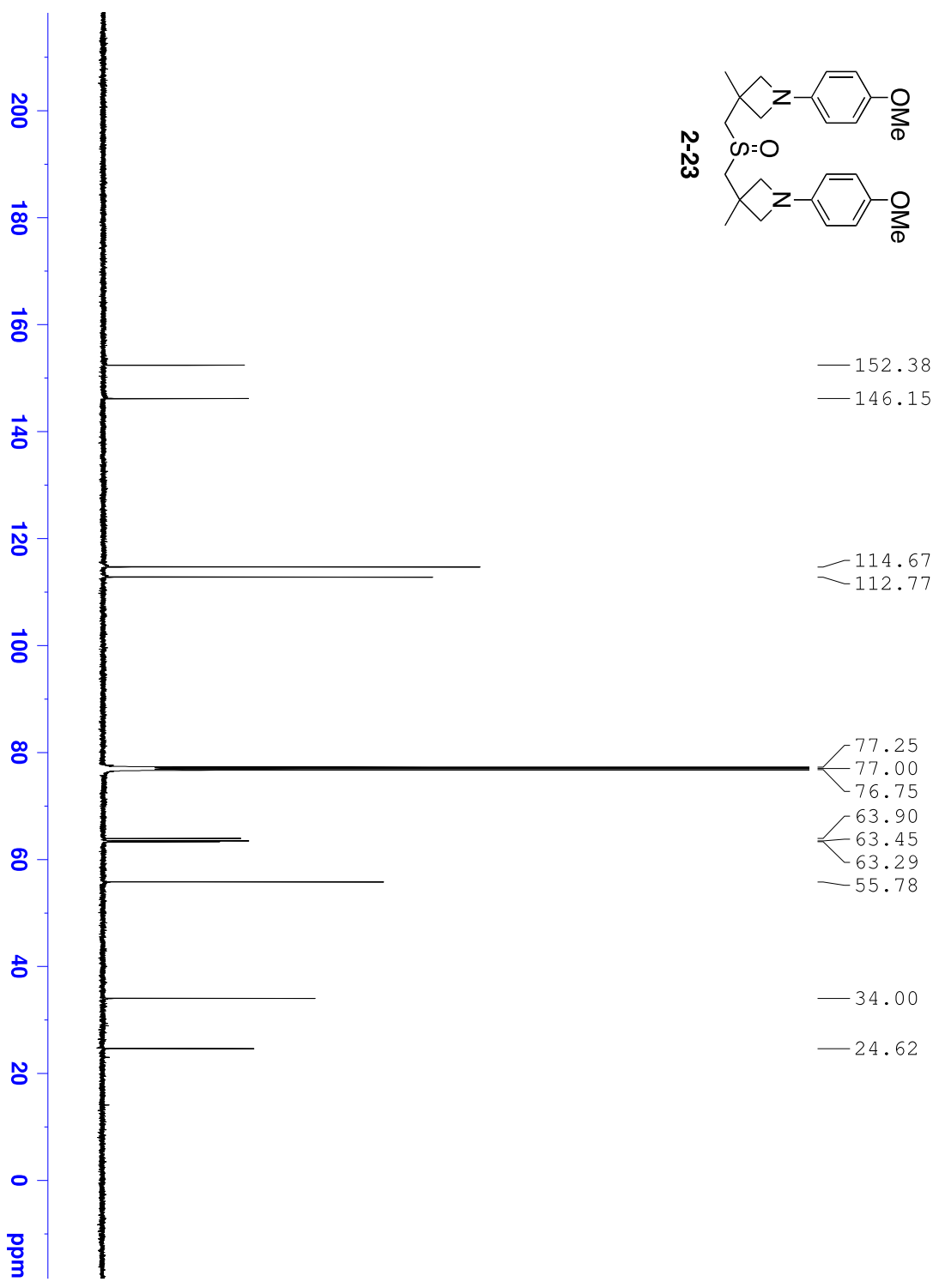


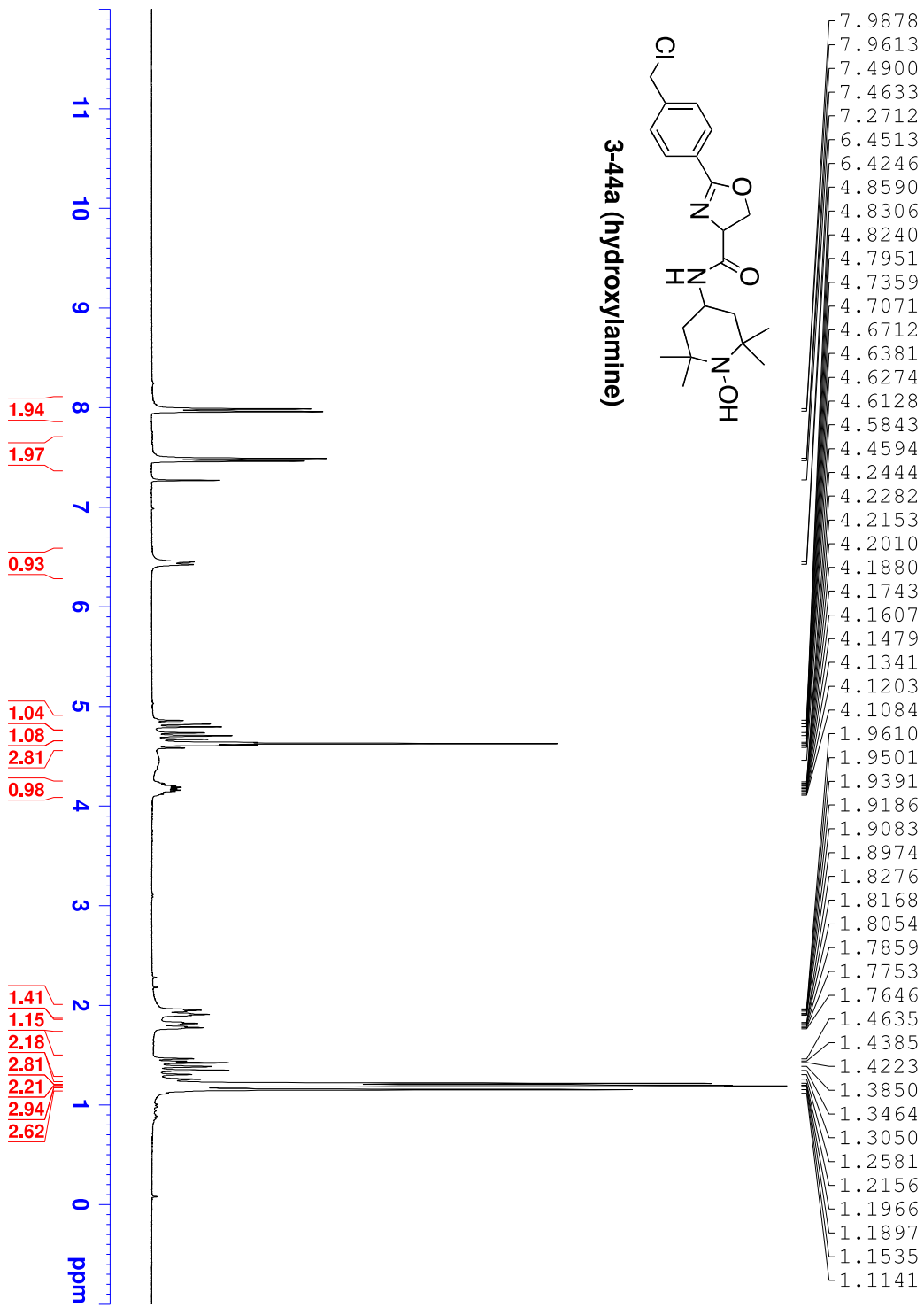


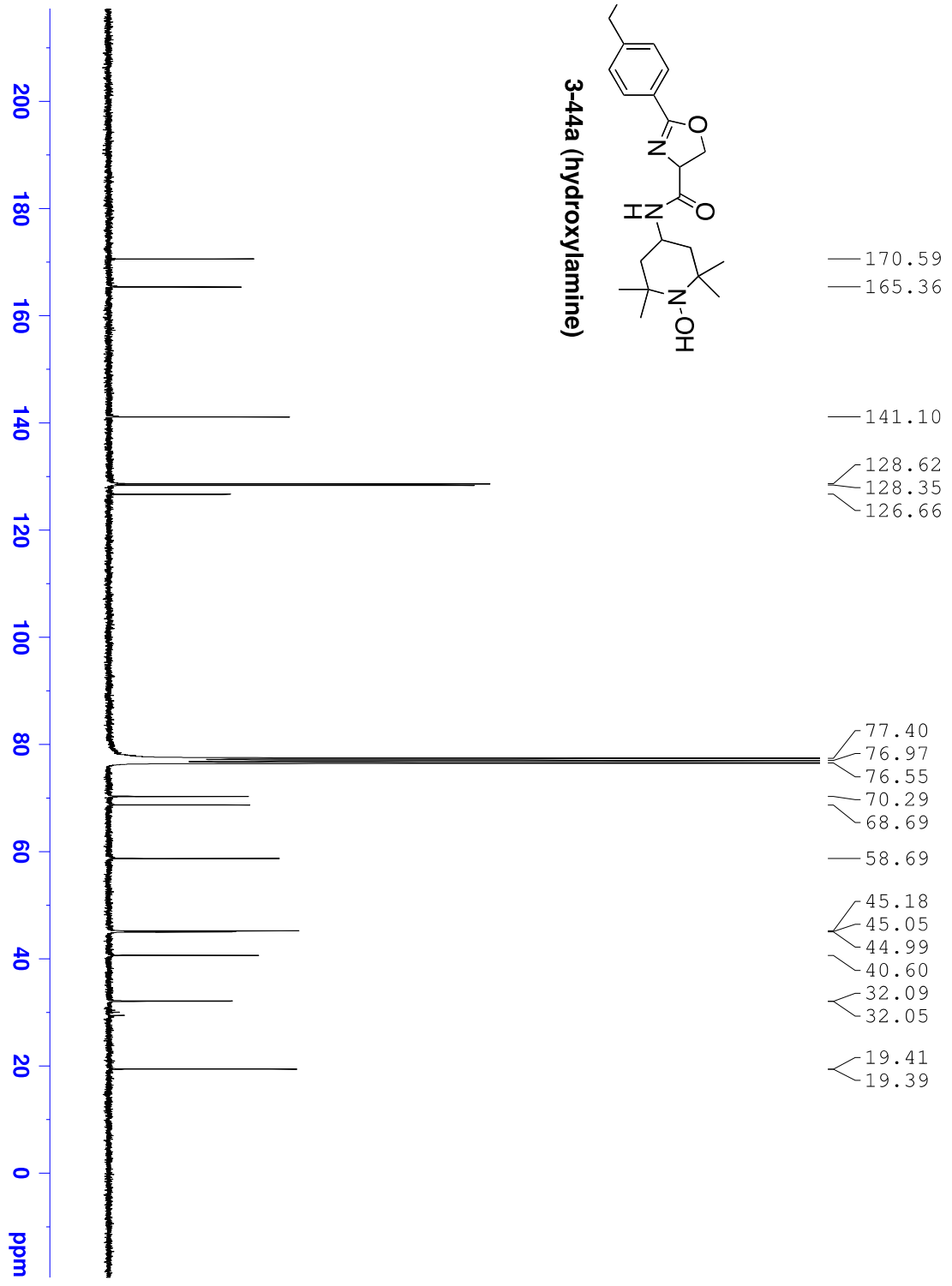
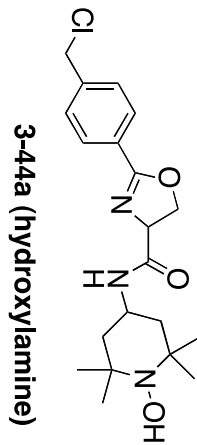


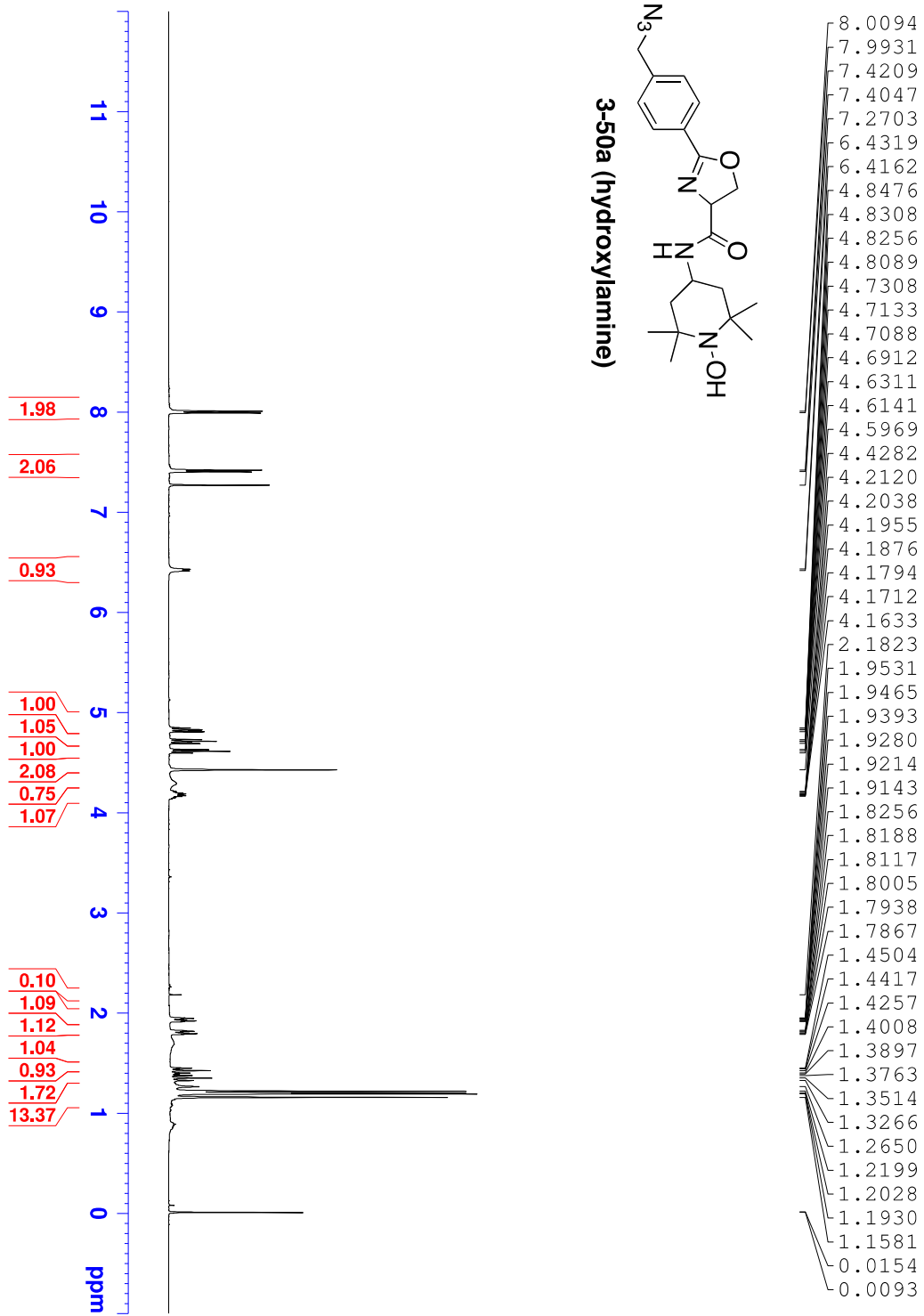
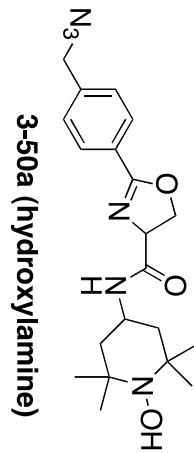


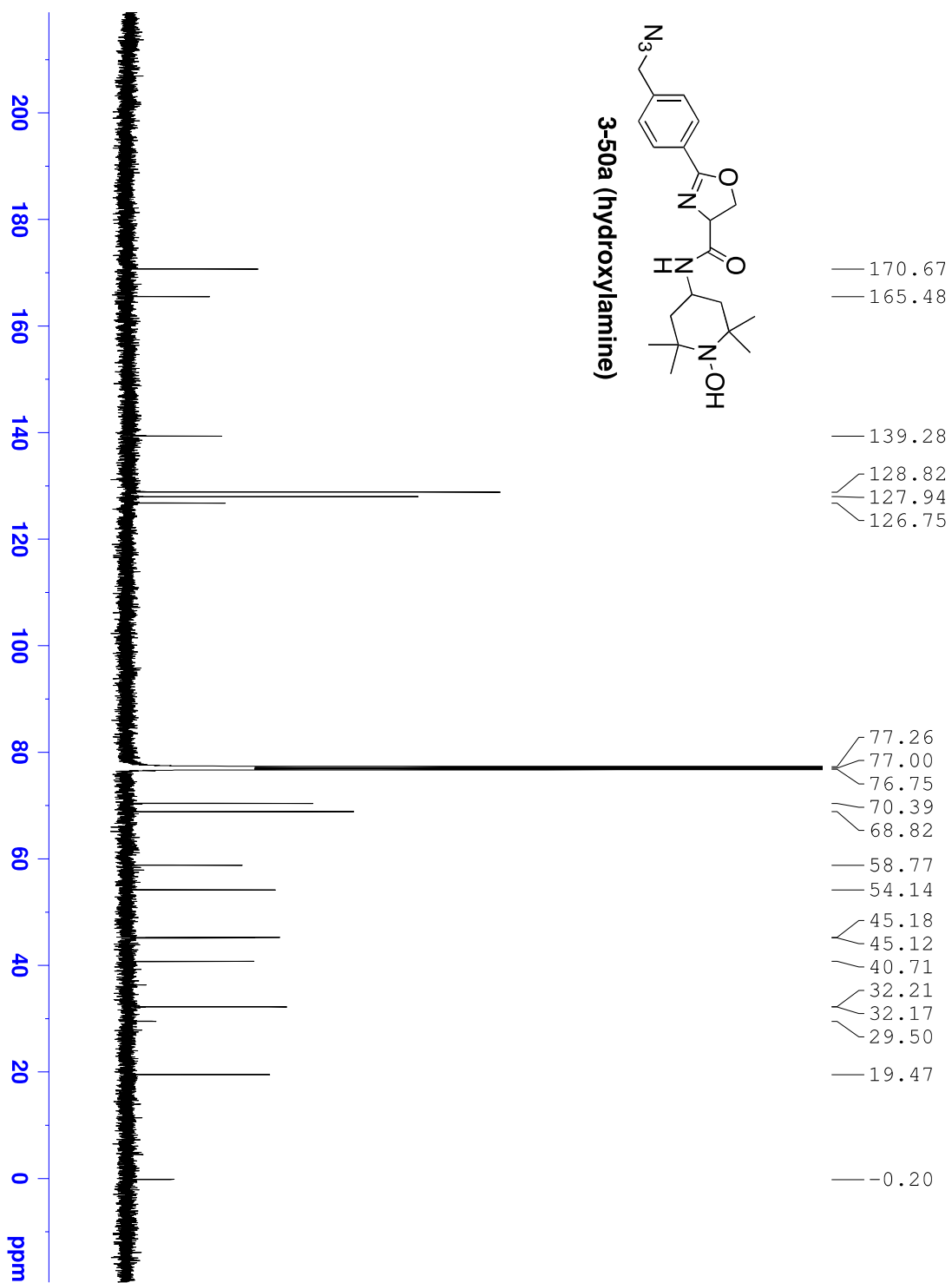


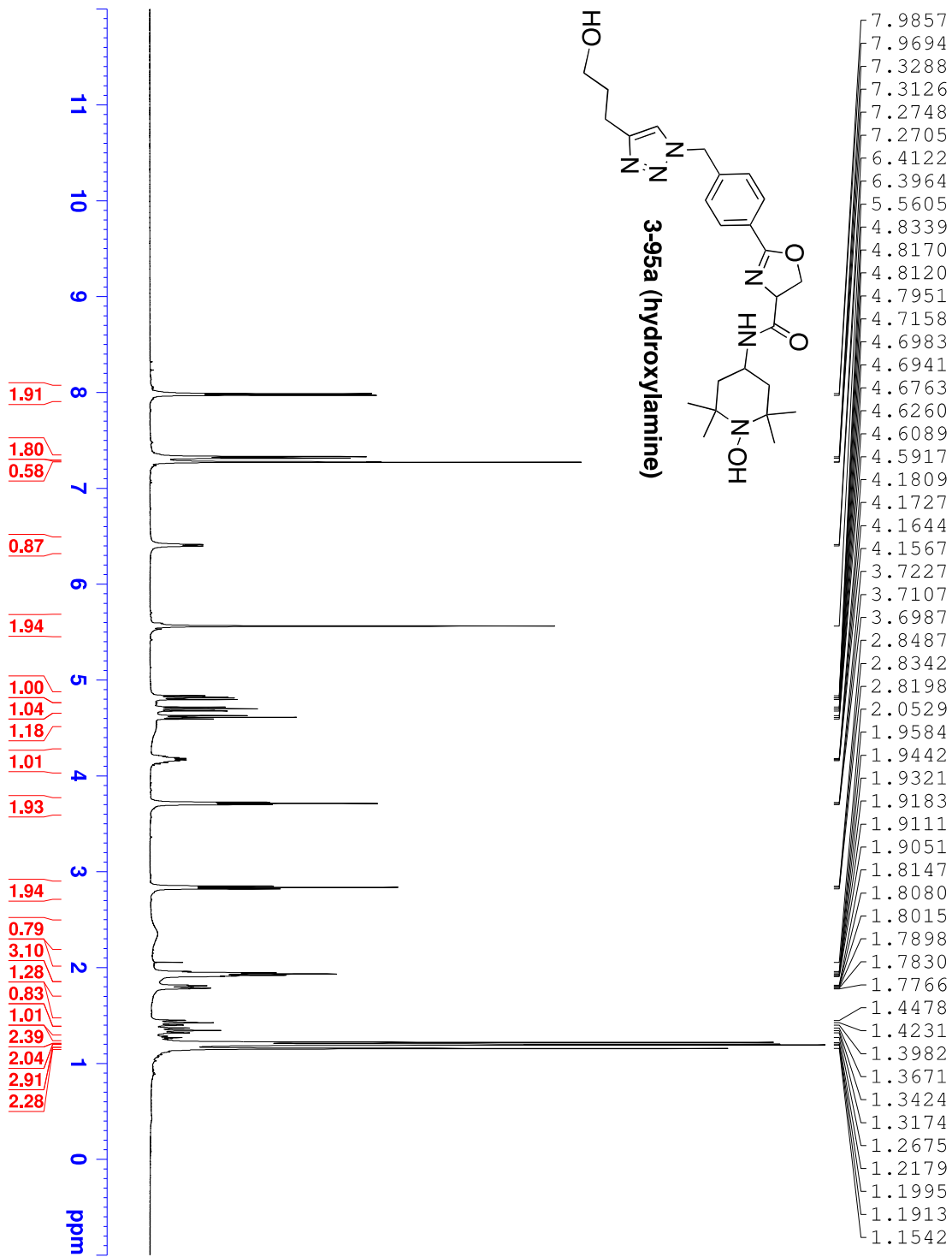


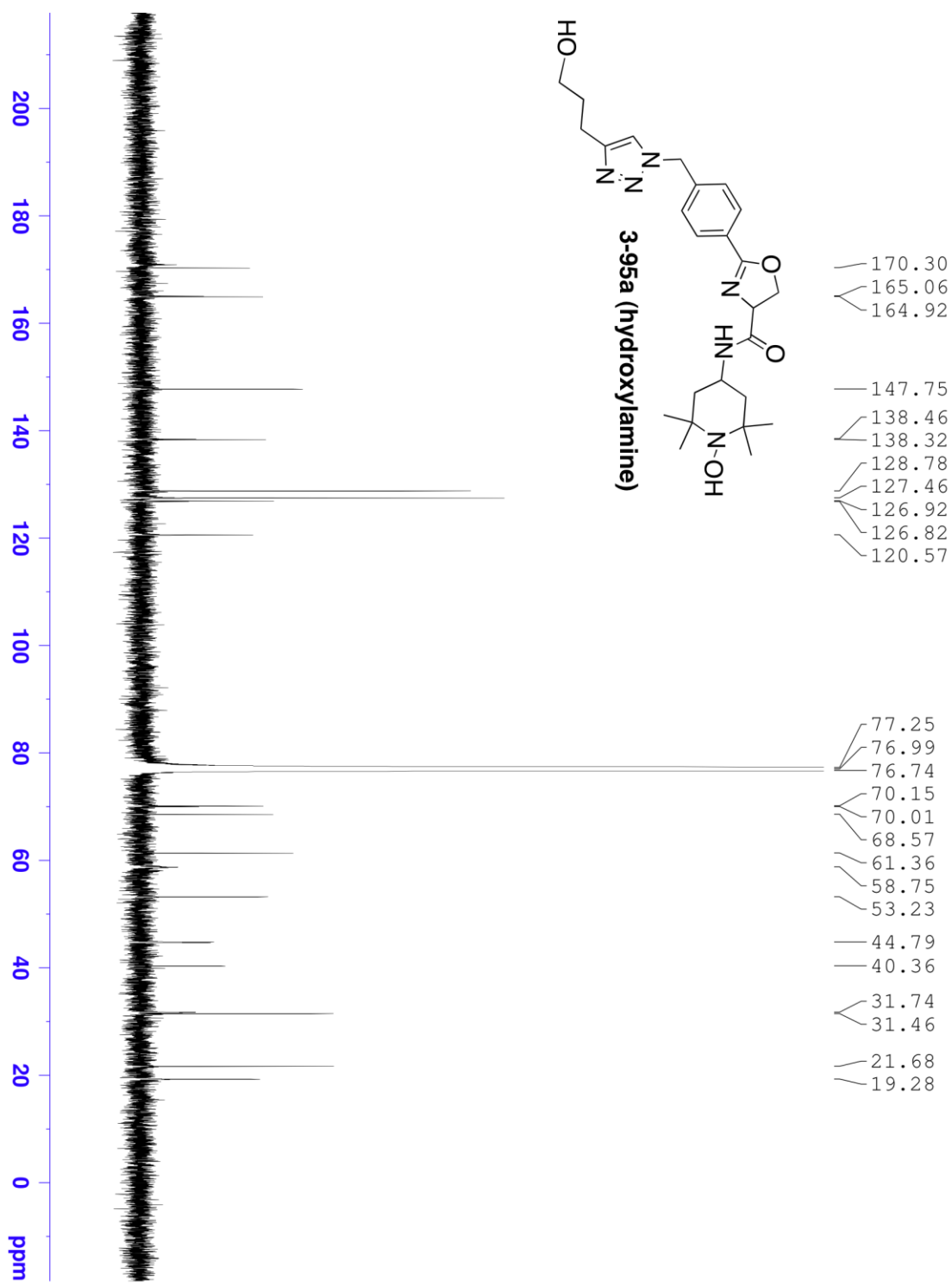












APPENDIX B: X-RAY DATA FOR MMS350

Table B-1. Crystal data and structure refinement for MMS350.

Identification code	sprach3a	
Empirical formula	C ₁₀ H ₁₈ O ₃ S	
Formula weight	218.30	
Temperature	100(2) K	
Wavelength	1.54178 Å	
Crystal system	Monoclinic	
Space group	P 21/c	
Unit cell dimensions	a = 21.605(5) Å	a = 90°.
	b = 9.786(3) Å	b = 90°.
	c = 10.348(3) Å	g = 90°.
Volume	2188.0(10) Å ³	
Z	8	
Density (calculated)	1.325 Mg/m ³	
Absorption coefficient	2.484 mm ⁻¹	
F(000)	944	
Crystal size	? x ? x ? mm ³	
Theta range for data collection	2.04 to 72.69°.	
Index ranges	-26<=h<=26, -12<=k<=12, -12<=l<=12	
Reflections collected	22534	
Independent reflections	3848 [R(int) = 0.1174]	
Completeness to theta = 72.69°	88.3 %	
Absorption correction	None	
Refinement method	Full-matrix least-squares on F ²	
Data / restraints / parameters	3848 / 0 / 253	
Goodness-of-fit on F ²	4.403	
Final R indices [I>2sigma(I)]	R1 = 0.2702, wR2 = 0.6295	

R indices (all data)

R1 = 0.4840, wR2 = 0.6681

Largest diff. peak and hole

1.860 and -2.106 e.Å⁻³

Table B-2. Atomic coordinates ($\times 10^4$) and equivalent isotropic displacement parameters ($\text{Å}^2 \times 10^3$) for MMS350. $U(\text{eq})$ is defined as one third of the trace of the orthogonalized U^{ij} tensor.

	x	y	z	U(eq)
S(1)	-4363(1)	2371(6)	3691(3)	87(2)
O(1)	-4360(5)	3324(14)	4690(9)	115(5)
C(1)	-3674(4)	2648(15)	2685(12)	57(4)
S(2)	640(1)	2708(5)	3798(3)	71(2)
C(2)	-3086(5)	2590(20)	3452(12)	75(5)
O(2)	-2358(4)	3870(12)	3838(9)	77(3)
O(3)	-6264(5)	4243(16)	3355(14)	137(6)
C(3)	-2968(6)	3760(20)	4335(17)	84(6)
O(4)	638(4)	1575(12)	2757(9)	77(3)
C(4)	-2506(6)	3021(12)	2715(14)	71(5)
O(5)	-1280(4)	733(12)	4091(10)	89(4)
C(5)	-2999(6)	1070(17)	4118(14)	77(5)
C(6)	-4931(6)	2680(20)	2503(13)	88(5)
O(6)	2658(5)	1244(13)	3697(12)	89(4)
C(7)	-5590(7)	2630(20)	3063(15)	103(7)
C(8)	-5769(8)	3780(20)	4090(30)	130(10)
C(9)	-6093(6)	3396(19)	2216(14)	96(6)
C(10)	-5779(8)	1170(20)	3590(20)	111(8)
C(11)	62(5)	2257(18)	5031(12)	82(5)
C(12)	-583(5)	2430(30)	4423(11)	89(6)
C(13)	-781(7)	1422(18)	3301(18)	82(6)
C(14)	-1093(5)	1551(14)	5263(11)	57(4)
C(15)	-767(7)	3960(20)	3994(18)	97(6)
C(16)	1313(4)	2412(15)	4858(11)	54(3)

C(17)	1894(6)	2570(20)	4059(12)	75(5)
C(18)	2475(6)	2120(30)	4747(14)	120(10)
C(19)	2042(5)	1410(20)	3230(15)	92(7)
C(20)	1999(5)	4010(16)	3347(12)	62(4)

Table B-3. Bond lengths [Å] and angles [°] for MMS350.

S(1)-O(1)	1.393(10)
S(1)-C(6)	1.763(13)
S(1)-C(1)	1.837(12)
C(1)-C(2)	1.499(11)
C(1)-H(1A)	0.9900
C(1)-H(1B)	0.9900
S(2)-O(4)	1.546(10)
S(2)-C(16)	1.845(10)
S(2)-C(11)	1.839(15)
C(2)-C(3)	1.49(2)
C(2)-C(4)	1.527(18)
C(2)-C(5)	1.65(2)
O(2)-C(3)	1.418(16)
O(2)-C(4)	1.465(15)
O(3)-C(8)	1.39(2)
O(3)-C(9)	1.488(19)
C(3)-H(3A)	0.9900
C(3)-H(3B)	0.9900
C(4)-H(4A)	0.9900
C(4)-H(4B)	0.9900
O(5)-C(14)	1.509(14)
O(5)-C(13)	1.511(17)
C(5)-H(5A)	0.9800
C(5)-H(5B)	0.9800
C(5)-H(5C)	0.9800
C(6)-C(7)	1.54(2)

C(6)-H(6A)	0.9900
C(6)-H(6B)	0.9900
O(6)-C(19)	1.426(13)
O(6)-C(18)	1.44(2)
C(7)-C(10)	1.58(3)
C(7)-C(9)	1.584(16)
C(7)-C(8)	1.60(2)
C(8)-H(8A)	0.9900
C(8)-H(8B)	0.9900
C(9)-H(9A)	0.9900
C(9)-H(9B)	0.9900
C(10)-H(10A)	0.9800
C(10)-H(10B)	0.9800
C(10)-H(10C)	0.9800
C(11)-C(12)	1.538(14)
C(11)-H(11A)	0.9900
C(11)-H(11B)	0.9900
C(12)-C(13)	1.58(2)
C(12)-C(15)	1.61(3)
C(12)-C(14)	1.65(2)
C(13)-H(13A)	0.9900
C(13)-H(13B)	0.9900
C(14)-H(14A)	0.9900
C(14)-H(14B)	0.9900
C(15)-H(15A)	0.9800
C(15)-H(15B)	0.9800
C(15)-H(15C)	0.9800
C(16)-C(17)	1.511(15)
C(16)-H(16A)	0.9900
C(16)-H(16B)	0.9900
C(17)-C(19)	1.46(2)
C(17)-C(18)	1.510(17)
C(17)-C(20)	1.61(2)
C(18)-C(19)	1.96(2)

C(18)-H(18A)	0.9900
C(18)-H(18B)	0.9900
C(19)-H(19A)	0.9900
C(19)-H(19B)	0.9900
C(20)-H(20A)	0.9800
C(20)-H(20B)	0.9800
C(20)-H(20C)	0.9800

O(1)-S(1)-C(6)	114.0(9)
O(1)-S(1)-C(1)	108.6(7)
C(6)-S(1)-C(1)	98.3(6)
C(2)-C(1)-S(1)	112.4(8)
C(2)-C(1)-H(1A)	109.0
S(1)-C(1)-H(1A)	109.1
C(2)-C(1)-H(1B)	109.2
S(1)-C(1)-H(1B)	109.2
H(1A)-C(1)-H(1B)	107.9
O(4)-S(2)-C(16)	107.7(5)
O(4)-S(2)-C(11)	108.1(7)
C(16)-S(2)-C(11)	94.9(5)
C(1)-C(2)-C(3)	116.0(14)
C(1)-C(2)-C(4)	114.7(9)
C(3)-C(2)-C(4)	87.2(11)
C(1)-C(2)-C(5)	110.8(13)
C(3)-C(2)-C(5)	114.8(11)
C(4)-C(2)-C(5)	111.5(11)
C(3)-O(2)-C(4)	92.5(10)
C(8)-O(3)-C(9)	93.6(13)
O(2)-C(3)-C(2)	89.6(12)
O(2)-C(3)-H(3A)	113.7
C(2)-C(3)-H(3A)	113.8
O(2)-C(3)-H(3B)	113.7
C(2)-C(3)-H(3B)	113.7
H(3A)-C(3)-H(3B)	111.0

O(2)-C(4)-C(2)	86.6(11)
O(2)-C(4)-H(4A)	114.2
C(2)-C(4)-H(4A)	114.2
O(2)-C(4)-H(4B)	114.2
C(2)-C(4)-H(4B)	114.2
H(4A)-C(4)-H(4B)	111.4
C(14)-O(5)-C(13)	90.4(9)
C(2)-C(5)-H(5A)	109.5
C(2)-C(5)-H(5B)	109.5
H(5A)-C(5)-H(5B)	109.5
C(2)-C(5)-H(5C)	109.4
H(5A)-C(5)-H(5C)	109.5
H(5B)-C(5)-H(5C)	109.5
C(7)-C(6)-S(1)	112.1(10)
C(7)-C(6)-H(6A)	109.2
S(1)-C(6)-H(6A)	109.2
C(7)-C(6)-H(6B)	109.2
S(1)-C(6)-H(6B)	109.2
H(6A)-C(6)-H(6B)	107.9
C(19)-O(6)-C(18)	86.2(10)
C(6)-C(7)-C(10)	113.3(16)
C(6)-C(7)-C(9)	114.3(14)
C(10)-C(7)-C(9)	116.1(15)
C(6)-C(7)-C(8)	116.9(17)
C(10)-C(7)-C(8)	110.4(15)
C(9)-C(7)-C(8)	82.5(13)
O(3)-C(8)-C(7)	92.8(15)
O(3)-C(8)-H(8A)	113.1
C(7)-C(8)-H(8A)	113.2
O(3)-C(8)-H(8B)	113.1
C(7)-C(8)-H(8B)	113.1
H(8A)-C(8)-H(8B)	110.5
O(3)-C(9)-C(7)	89.7(10)
O(3)-C(9)-H(9A)	113.7

C(7)-C(9)-H(9A)	113.7
O(3)-C(9)-H(9B)	113.7
C(7)-C(9)-H(9B)	113.7
H(9A)-C(9)-H(9B)	110.9
C(7)-C(10)-H(10A)	109.5
C(7)-C(10)-H(10B)	109.5
H(10A)-C(10)-H(10B)	109.5
C(7)-C(10)-H(10C)	109.5
H(10A)-C(10)-H(10C)	109.5
H(10B)-C(10)-H(10C)	109.5
C(12)-C(11)-S(2)	107.7(10)
C(12)-C(11)-H(11A)	110.1
S(2)-C(11)-H(11A)	110.2
C(12)-C(11)-H(11B)	110.2
S(2)-C(11)-H(11B)	110.2
H(11A)-C(11)-H(11B)	108.5
C(11)-C(12)-C(13)	118.4(15)
C(11)-C(12)-C(15)	116.2(15)
C(13)-C(12)-C(15)	108.1(12)
C(11)-C(12)-C(14)	109.3(13)
C(13)-C(12)-C(14)	83.0(11)
C(15)-C(12)-C(14)	117.8(13)
O(5)-C(13)-C(12)	94.3(13)
O(5)-C(13)-H(13A)	112.8
C(12)-C(13)-H(13A)	112.9
O(5)-C(13)-H(13B)	112.9
C(12)-C(13)-H(13B)	112.9
H(13A)-C(13)-H(13B)	110.3
O(5)-C(14)-C(12)	91.9(9)
O(5)-C(14)-H(14A)	113.3
C(12)-C(14)-H(14A)	113.3
O(5)-C(14)-H(14B)	113.3
C(12)-C(14)-H(14B)	113.3
H(14A)-C(14)-H(14B)	110.6

C(12)-C(15)-H(15A)	109.4
C(12)-C(15)-H(15B)	109.5
H(15A)-C(15)-H(15B)	109.5
C(12)-C(15)-H(15C)	109.5
H(15A)-C(15)-H(15C)	109.5
H(15B)-C(15)-H(15C)	109.5
C(17)-C(16)-S(2)	108.2(8)
C(17)-C(16)-H(16A)	110.0
S(2)-C(16)-H(16A)	110.1
C(17)-C(16)-H(16B)	110.1
S(2)-C(16)-H(16B)	110.0
H(16A)-C(16)-H(16B)	108.4
C(19)-C(17)-C(18)	82.4(14)
C(19)-C(17)-C(16)	114.9(15)
C(18)-C(17)-C(16)	113.7(11)
C(19)-C(17)-C(20)	112.6(12)
C(18)-C(17)-C(20)	110.9(13)
C(16)-C(17)-C(20)	117.3(16)
O(6)-C(18)-C(17)	92.7(11)
O(6)-C(18)-C(19)	46.6(7)
C(17)-C(18)-C(19)	47.8(9)
O(6)-C(18)-H(18A)	113.2
C(17)-C(18)-H(18A)	113.1
C(19)-C(18)-H(18A)	135.0
O(6)-C(18)-H(18B)	113.2
C(17)-C(18)-H(18B)	113.2
C(19)-C(18)-H(18B)	114.5
H(18A)-C(18)-H(18B)	110.5
O(6)-C(19)-C(17)	95.2(11)
O(6)-C(19)-C(18)	47.1(7)
C(17)-C(19)-C(18)	49.9(9)
O(6)-C(19)-H(19A)	112.7
C(17)-C(19)-H(19A)	112.7
C(18)-C(19)-H(19A)	114.1

O(6)-C(19)-H(19B)	112.7
C(17)-C(19)-H(19B)	112.7
C(18)-C(19)-H(19B)	135.7
H(19A)-C(19)-H(19B)	110.2
C(17)-C(20)-H(20A)	109.5
C(17)-C(20)-H(20B)	109.5
H(20A)-C(20)-H(20B)	109.5
C(17)-C(20)-H(20C)	109.5
H(20A)-C(20)-H(20C)	109.5
H(20B)-C(20)-H(20C)	109.5

Symmetry transformations used to generate equivalent atoms:

Table B-4. Anisotropic displacement parameters ($\text{\AA}^2 \times 10^3$) for MMS350. The anisotropicdisplacement factor exponent takes the form: $-2p^2 [h^2 a^{*2} U^{11} + \dots + 2 h k a^* b^* U^{12}]$

	U11	U22	U33	U23	U13	U12
S(1)	61(2)	145(5)	54(3)	29(3)	-27(2)	2(3)
O(1)	144(9)	159(13)	44(7)	-51(8)	-12(6)	-21(8)
C(1)	54(7)	44(7)	72(9)	-1(8)	-31(6)	-10(6)
S(2)	64(2)	97(4)	50(2)	-4(2)	-24(2)	-5(2)
C(2)	37(6)	141(16)	45(8)	48(10)	-10(5)	-1(8)
O(2)	59(6)	112(9)	61(6)	20(7)	-12(5)	-24(5)
O(3)	124(9)	172(15)	114(10)	-60(10)	-67(8)	13(9)
C(3)	49(8)	121(16)	84(12)	-25(12)	3(8)	-18(9)
O(4)	81(6)	100(8)	52(6)	-15(6)	-16(5)	4(5)
C(4)	76(9)	40(8)	98(11)	-12(8)	-57(8)	6(6)
O(5)	88(7)	116(10)	63(7)	-1(7)	-7(5)	-37(6)
C(5)	77(9)	96(14)	57(10)	49(9)	-4(7)	17(8)
C(6)	86(10)	117(14)	60(10)	3(11)	-13(8)	-31(10)
O(6)	83(7)	115(10)	69(8)	-4(8)	-2(6)	24(6)
C(7)	95(12)	147(18)	66(10)	8(13)	-52(9)	52(12)
C(8)	78(11)	104(16)	210(30)	-72(19)	-5(14)	39(11)
C(9)	94(10)	136(17)	60(10)	-4(10)	-50(8)	-13(9)
C(10)	86(11)	87(15)	160(20)	45(15)	28(13)	8(10)
C(11)	74(8)	104(12)	69(10)	-45(10)	-31(8)	25(9)
C(12)	63(8)	183(19)	22(7)	-36(10)	-14(6)	-13(11)
C(13)	58(9)	85(13)	101(15)	-20(12)	8(9)	-10(8)
C(14)	41(6)	78(10)	50(8)	2(7)	-15(5)	5(6)
C(15)	79(10)	114(15)	98(14)	30(14)	-3(9)	38(10)
C(16)	58(7)	65(8)	38(7)	-31(7)	-2(5)	20(7)
C(17)	72(9)	129(15)	24(7)	0(9)	-18(6)	-24(9)
C(18)	63(9)	260(30)	37(9)	0(14)	-11(7)	13(12)
C(19)	40(7)	172(19)	63(11)	-27(12)	-25(7)	8(9)
C(20)	51(7)	96(12)	38(7)	24(8)	-13(6)	-5(7)

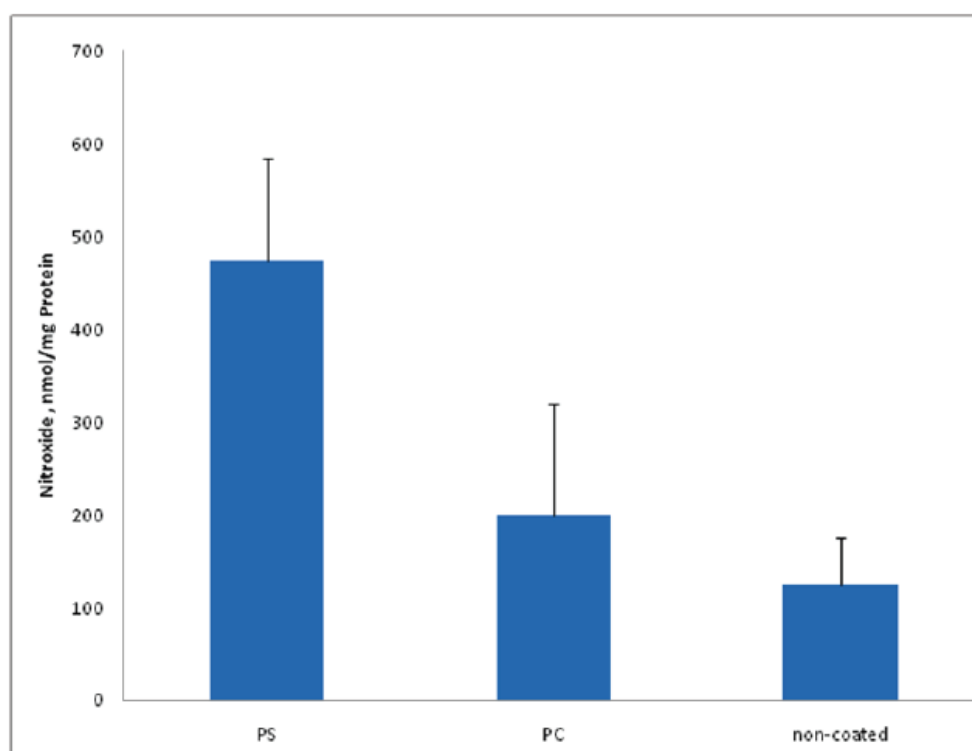
Table B-5. Hydrogen coordinates ($\times 10^4$) and isotropic displacement parameters ($\text{\AA}^2 \times 10^3$)

for MMS350.

	x	y	z	U(eq)
H(1A)	-3661	1944	1998	68
H(1B)	-3705	3553	2262	68
H(3A)	-3230	4572	4152	101
H(3B)	-2984	3521	5263	101
H(4A)	-2208	2272	2555	86
H(4B)	-2591	3545	1915	86
H(5A)	-3379	819	4580	115
H(5B)	-2652	1096	4728	115
H(5C)	-2915	392	3444	115
H(6A)	-4859	3588	2112	105
H(6B)	-4893	1986	1811	105
H(8A)	-5896	3408	4938	155
H(8B)	-5442	4482	4204	155
H(9A)	-5915	3929	1492	116
H(9B)	-6431	2795	1909	116
H(10A)	-5674	476	2940	167
H(10B)	-6225	1148	3756	167
H(10C)	-5553	980	4389	167
H(11A)	121	1300	5315	99
H(11B)	105	2862	5793	99
H(13A)	-947	1902	2533	98
H(13B)	-445	789	3045	98
H(14A)	-904	988	5953	68
H(14B)	-1433	2119	5616	68
H(15A)	-428	4359	3493	145
H(15B)	-843	4514	4765	145
H(15C)	-1142	3928	3464	145

H(16A)	1313	3080	5576	64
H(16B)	1294	1481	5231	64
H(18A)	2770	2874	4906	144
H(18B)	2391	1613	5557	144
H(19A)	1778	601	3408	110
H(19B)	2027	1637	2299	110
H(20A)	2387	3981	2855	92
H(20B)	2022	4740	3993	92
H(20C)	1653	4187	2757	92

**APPENDIX C: DATA FOR MACROPHAGE UPTAKE OF IMIDOTHIOULATE
FUNCTIONALIZED SILICA NANOPARTICLES**



RAW 264.7 macrophages were incubated with phospholipids coated SiO₂-Tempo (50µg/million cells) for 2hr, the intracellular nitroxide signal was detected by ESR, with addition of K₃Fe(CN)₆.

Figure C-1. Macrophage uptake by imidothiolate-functionalized silica nanoparticles.

REFERENCES

- (1) Reichardt, C. *Solvents and Solvent Effects in Organic Chemistry*; 3 ed.; Wiley-VCH: Weinheim, 2003.
- (2) Constable, D. J. C.; Jiménez-González, C.; Henderson, R. K. *Org. Process Res. Dev.* **2007**, *11*, 133-137.
- (3) Mukhopadhyay, T.; Seebach, D. *Helv. Chim. Acta* **1982**, *65*, 385-391.
- (4) Capello, C.; Fischer, U.; Hungerbühler, K. *Green Chem.* **2007**, *9*, 927-934.
- (5) Jessop, P. G. *Green Chem.* **2011**, *13*, 1391-1398.
- (6) Wuitschik, G.; Carreira, E. M.; Wagner, B.; Fischer, H.; Parrilla, I.; Schuler, F.; Rogers-Evans, M.; Müller, K. *J. Med. Chem.* **2010**, *53*, 3227-3246.
- (7) Burkhard, J. A.; Wuitschik, G.; Rogers-Evans, M.; Müller, K.; Carreira, E. M. *Angew. Chem. Int. Ed.* **2010**, *49*, 9052-9067.
- (8) Reichardt, C. In *Solvents and Solvent Effects in Organic Chemistry*; 3 ed.; Wiley-VCH: Weinheim, 2003, p 162-237.
- (9) Gutmann, V. *The Donor-Acceptor Approach to Molecular Interactions*; Plenum Press: New York, 1978.
- (10) Maria, P.-C.; Gal, J.-F. *J. Phys. Chem.* **1985**, *89*, 1296-1304.
- (11) *Handbook of Chemistry and Physics*; 84 ed.; CRC Press: New York, 2003-2004.
- (12) Rauk, A.; Hunt, I. R.; Keay, B. A. *J. Org. Chem.* **1994**, *59*, 6808-6816.
- (13) McLaughlin, D. E.; Tamres, M.; Searles, S., Jr. *J. Am. Chem. Soc.* **1960**, *82*, 5621-5625.
- (14) Paquette, L. A.; Tae, J.; Hickey, E. R.; Trego, W. E.; Rogers, R. D. *J. Org. Chem.* **2000**, *65*, 9160-9171.
- (15) Bellon, L. *J. Org. Chem.* **1980**, *45*, 1166-1168.
- (16) Abraham, M. H.; Duce, P. P.; Prior, D. V. *J. Chem. Soc., Perkin Trans. 2* **1989**, 1355-1378.
- (17) Bordejé, M. C.; Mó, O.; Yáñez, M.; Herreros, M.; Abboud, J.-L. M. *J. Am. Chem. Soc.* **1993**, *115*, 7389-7396.
- (18) Banks, H. D. *J. Org. Chem.* **2003**, *68*, 2639-2644.

- (19) Giota, G.; Lillocci, C. *J. Phys. Org. Chem.* **1993**, *6*, 187-192.
- (20) Eigenmann, H. K.; Golden, D. M.; Benson, S. W. *J. Phys. Chem.* **1973**, *77*, 1687-1691.
- (21) Aue, D. H.; Webb, H. M.; Bowers, M. T. *J. Am. Chem. Soc.* **1974**, *97*, 4137-4139.
- (22) Moriarty, R. M. In *Topics in Stereochemistry*; Eliel, E. L., Allinger, N. L., Eds.; John Wiley & Sons: New York, 1974; Vol. 8, p 273-421.
- (23) Lucht, B. L.; Collum, D. B. *J. Am. Chem. Soc.* **1995**, *117*, 9863-9874.
- (24) Reich, H. J.; Kulicke, K. J. *J. Am. Chem. Soc.* **1996**, *118*, 273-274.
- (25) Henegar, K. E.; Muchnij, J. A.; Maleczka Jr., R. E. In *Encyclopedia of Reagents for Organic Synthesis*; John Wiley & Sons: 2007; Vol. 7, p 5207-5208.
- (26) Seebach, D.; Corey, E. J. *J. Org. Chem.* **1975**, *40*, 231-237.
- (27) Wuitschik, G.; Carreira, E. M.; Rogers-Evans, M.; Müller, K. In *Process Chemistry in the Pharmaceutical Industry: Challenges in an Ever Changing Climate*; Gadamasetti, K., Braish, T., Eds.; CRC Press: Boca Raton, 2008; Vol. 2, p 217-229.
- (28) Wuitschik, G.; Rogers-Evans, M.; Müller, K.; Fischer, H.; Wagner, B.; Schuler, F.; Polonchuk, L.; Carreira, E. M. *Angew. Chem. Int. Ed.* **2006**, *45*, 7736-7739.
- (29) Lajunen, M.; Koskinen, J.-M. *Acta Chem. Scand.* **1994**, *48*, 788-791.
- (30) Searles, S.; Lutz, E. F.; Tamres, M. *J. Am. Chem. Soc.* **1959**, *82*, 2932-2935.
- (31) Searles, S.; Tamres, M. *J. Am. Chem. Soc.* **1951**, *73*, 3704-3706.
- (32) Zaugg, H. E.; Horrom, B. W.; Borwardt, S. *J. Am. Chem. Soc.* **1960**, *82*, 2895-2903.
- (33) Zaugg, H. E.; Ratajczyk, J. F.; Leonard, J. E.; Schaefer, A. D. *J. Org. Chem.* **1972**, *37*, 2249-2253.
- (34) Hünig, S.; Wehner, G. *Chem. Ber.* **1980**, *113*, 302-323.
- (35) Sikorski, W. H.; Reich, H. J. *J. Am. Chem. Soc.* **2001**, *123*, 6527-6535.
- (36) Cohen, T.; Abraham, W. D.; Myers, M. *J. Am. Chem. Soc.* **1987**, *109*, 7923-7924.
- (37) Ostrowski, P. C.; Kane, V. *Tetrahedron Lett.* **1977**, *40*, 3549-3552.
- (38) Seebach, D. *Angew. Chem. Int. Ed. Engl.* **1988**, *27*, 1624-1654.
- (39) Cassel, S.; Debaig, C.; Benvegna, T.; Chaimbault, P.; Lafosse, M.; Plusquellec, D.; Rollin, P. *Eur. J. Org. Chem.* **2001**, *5*, 875-896.
- (40) Arnett, E. M.; Palmer, C. A. *J. Am. Chem. Soc.* **1990**, *112*, 7354-7360.
- (41) Rutherford, J. L.; Collum, D. B. *J. Am. Chem. Soc.* **2001**, *123*, 199-202.

- (42) Rutherford, J. L.; Collum, D. B. *J. Am. Chem. Soc.* **1999**, *121*, 10198-10202.
- (43) Wailes, P. C.; Wiegold, H. *J. Organomet. Chem.* **1970**, *24*, 405-411.
- (44) Hart, D. W.; Schwartz, J. *J. Am. Chem. Soc.* **1974**, *96*, 8115-8116.
- (45) Schwartz, J.; Labinger, J. A. *Angew. Chem. Int. Ed. Engl.* **1976**, *15*, 333-340.
- (46) Wipf, P.; Jahn, H. *Tetrahedron* **1996**, *52*, 12853-12910.
- (47) Endo, J.; Koga, N.; Morokuma, K. *Organometallics* **1993**, *12*, 2777-2787.
- (48) Spletsoer, J. T.; White, J., M.; Tunoori, A. R.; Georg, G. I. *J. Am. Chem. Soc.* **2007**, *129*, 3408-3419.
- (49) Ashby, E. C.; Duke, R. B.; Neumann, H. M. *J. Am. Chem. Soc.* **1967**, *89*, 1964-1965.
- (50) Lewis, R. N.; Wright, J. R. *J. Am. Chem. Soc.* **1952**, *74*, 1253-1257.
- (51) Patwardhan, N. N.; Gao, M.; Carlier, P. R. *Chem. Eur. J.* **2011**, *17*, 12250-12253.
- (52) Krasovskiy, A.; Straub, B., F.; Knochel, P. *Angew. Chem. Int. Ed.* **2006**, *45*, 159-162.
- (53) Wuitschik, G.; Rogers-Evans, M.; Buckl, A.; Bernasconi, M.; Märki, M.; Godel, T.; Fischer, H.; Wagner, B.; Parrilla, I.; Schuler, F.; Schneider, J.; Alker, A.; Schweizer, W. B.; Müller, K.; Carreira, E. M. *Angew. Chem. Int. Ed.* **2008**, *47*, 4512-4515.
- (54) Reboul, M. *Ann. Chim. (Paris)* **1878**, *14*, 496.
- (55) Noller, C. R. *Org. Synth.* **1949**, *29*, 92-93.
- (56) Pruckmayr, G.; Dreyfuss, P.; Dreyfuss, M. P. In *Kirk-Othmer Encyclopedia of Chemical Technology*; John Wiley & Sons: 2000; Vol. 6, p 1-30.
- (57) Taboada, R.; Ordonio, G. G.; Ndakala, A. J.; Howell, A. R.; Rabien, P. R. *J. Org. Chem.* **2003**, *68*, 1480-1488.
- (58) Bach, T.; Eilers, F. *J. Org. Chem.* **1999**, *64*, 8041-8044.
- (59) Dvorak, C. A.; Dufour, C.; Iwasa, S.; Rawal, V. H. *J. Org. Chem.* **1998**, *63*, 5302-5303.
- (60) Bach, T.; Kather, K.; Krämer, O. *J. Org. Chem.* **1998**, *63*, 1910-1918.
- (61) Fredriksen, S. B.; Dale, J. *Acta Chem. Scand.* **1992**, *46*, 574-588.
- (62) Dale, J.; Fredriksen, S. B. *Acta Chem. Scand.* **1992**, *46*, 271-277.
- (63) Nicolauo, K. C.; Ueno, H.; Liu, J.-J.; Nantermet, P. G.; Yang, Z.; Renaud, J.; Paulvannan, K.; Chadha, R. *J. Am. Chem. Soc.* **1995**, *117*, 653-659.
- (64) Kusama, H.; Hara, R.; Kawahara, S.; Nishimori, T.; Kashima, H.; Nakamura, N.; Morihira, K.; Kuwajima, I. *J. Am. Chem. Soc.* **2000**, *122*, 3811-3820.

- (65) Holton, R. A.; Kim, H.-B.; Somoza, C.; Liang, F.; Biediger, R. J.; Boatman, P. D.; Shindo, M.; Smith, C. C.; Kim, S.; Nadizadeh, H.; Suzuki, Y.; Tao, C.; Vu, P.; Tang, S.; Zhang, P.; Murthi, K. K.; Gentile, L. N.; Liu, J. H. *J. Am. Chem. Soc.* **1994**, *116*, 1599-1600
- (66) Ducton, M. A. J.; Estiarte, M. A.; Tan, D.; Kaub, C.; O'Mahony, D. J. R.; Jonson, R., J.; Cox, M.; Edwards, W. T.; Wan, M.; Kincaid, J.; Kelly, M. G. *Org. Lett.* **2008**, *10*, 3259-3262.
- (67) Baum, K.; Berkowitz, P. T.; Grakauskas, V.; Archibald, T. G. *J. Org. Chem.* **1983**, *48*, 2953-2956.
- (68) Delmond, B.; Pommier, J.-C.; Valade, J. *J. Organomet. Chem.* **1973**, *47*, 337-350.
- (69) Wojtowicz, J. A.; Polak, R. J.; Zaxlowsky, J. A. *J. Org. Chem.* **1971**, *36*, 2232-2236.
- (70) Farthing, A. C. *J. Chem. Soc.* **1955**, 3648-3654.
- (71) Xianming, H.; Kellogg, R. M. *Synthesis* **1995**, 533-538.
- (72) Leclercq, P. P.; Bats, J.-P.; Moulines, J. *Synthesis* **1981**, 550-551.
- (73) Abdul-Rahman, A.-N.; Issidorides, C. H. *J. Org. Chem.* **1962**, *27*, 67-70.
- (74) Searles, S.; Nicerson, R. G.; Witsiepe, W. K. *J. Org. Chem.* **1960**, *24*, 1839-1844.
- (75) Behrendt, J. M.; Bala, K.; Golding, P.; Hailes, H. C. *Tetrahedron Lett.* **2005**, *46*, 643-645.
- (76) Christlieb, M.; Davies, J. E.; Eames, J.; Hooley, R.; Warren, S. *J. Chem. Soc. Perkin Trans. 1* **2001**, 2983-2996.
- (77) Pattison, D. B. *J. Am. Chem. Soc.* **1957**, *79*, 3455-3456.
- (78) Porco, J. A., Jr.; Schreiber, S. L. In *Comp. Org. Synth.*; Trost, B. M., Fleming, I., Eds.; Pergamon: Oxford, 1991; Vol. 5, p 151-192.
- (79) Okuma, K.; Tanaka, Y.; Kaji, S.; Ohta, H. *J. Org. Chem.* **1983**, *48*, 5133-5134.
- (80) Fitton, A. O.; Hill, J.; Jane, D. E.; Millar, R. *Synthesis* **1987**, *12*, 1140-1142.
- (81) Eigenmann, H. K.; Golden, D. M.; Benson, S. W. *J. Phys. Chem.* **1973**, *77*, 1687-1691.
- (82) Dickens, F.; Jones, H. E. H. *Br. J. Cancer* **1963**, *17*, 100-108.
- (83) Druckrey, H.; Kruse, H.; Preussmann, R.; Ivankovic, S. *Z. Krebsforsch.* **1970**, *74*, 241-270.

- (84) Gómez-Bombarelli, R.; Brito Palma, B.; Martins, C.; Kranendonk, M.; Rodrigues, A. S.; Calle, E.; Rueff, J.; Casado, J. *Chem. Res. Toxicol.* **2010**, *23*, 1275-1281.
- (85) Adaligil, E.; Davis, B. D.; Hilmey, D. G.; Shen, Y.; Spruell, J. M.; Brodbelt, J. S.; Houk, K. N.; Paquette, L. A. *J. Org. Chem.* **2007**, *72*, 6215-6223.
- (86) Rose, N. G. W.; Blaskovich, M. A.; Evindar, G.; Wilkinson, S.; Luo, Y.; Fishlock, D.; Reid, C.; Lajoie, G. A. *Org. Synth.* **2002**, *79*, 216-221.
- (87) Corey, E. J.; Raju, N. *Tetrahedron Lett.* **1983**, *24*, 5571-5574.
- (88) Zhdanko, A. G.; Nenajdenko, V. G. *J. Org. Chem.* **2009**, *74*, 884-887.
- (89) Seebach, D.; Henning, R.; Mukhopadhyay, T. *Chem. Ber.* **1982**, *115*, 1705-1720.
- (90) O'Neil, I. A.; Lai, J. Y. Q.; Wynn, D. *Chem. Commun.* **1999**, 59-60.
- (91) Hogen-Esch, T. E.; Smid, J. *J. Am. Chem. Soc.* **1966**, *88*, 307-318.
- (92) Hogen-Esch, T. E.; Smid, J. *J. Am. Chem. Soc.* **1966**, *88*, 318-324.
- (93) Kwon, D. W.; Kim, Y. H. *J. Org. Chem.* **2002**, *67*, 9488-9491.
- (94) Gurjar, M. K.; Sarma, B. V. N. B. S.; Sadalapure, K.; Adhikari, S. *Synthesis* **1998**, *10*, 1424.
- (95) Harnden, M., R.; Wyatt, P. G.; Boyd, M., R.; Sutton, D. *J. Med. Chem.* **1990**, *33*, 187-196.
- (96) Skarzewski, J. *Tetrahedron* **1989**, *45*, 4593-4598.
- (97) Byrne, B.; Karras, M. *Tetrahedron Lett.* **1987**, *28*, 769-772.
- (98) Wilk, B. K.; Helom, J. L.; Coughlin, C. W. *Org. Process Res. Dev.* **1998**, *2*, 407-411.
- (99) Kloetzing, R. J.; Krasovskiy, A.; Knochel, P. *Chem. Eur. J.* **2007**, *13*, 215-227.
- (100) Wang, X.-J.; Zhang, L.; Sun, X.; Xu, Y.; Krishnamurthy, D.; Senanayake, C. H. *Org. Lett.* **2005**, *7*, 5593-5595.
- (101) Wang, X.-J.; Sun, X.; Zhang, L.; Xu, Y.; Krishnamurthy, D.; Senanayake, C. H. *Org. Lett.* **2006**, *8*, 305-307.
- (102) Da, C.-S.; Wang, J.-R.; Yin, X.-G.; Fan, X.-Y.; Liu, Y.; Yu, S.-L. *Org. Lett.* **2009**, *11*, 5578-5581.
- (103) Liu, Y.; Da, C.-S.; Yu, S.-L.; Yin, X.-G.; Wang, J.-R.; Fan, X.-Y.; Li, W.-P.; Wang, R. *J. Org. Chem.* **2010**, *75*, 6869-6878.

- (104) Harutyunyan, S. R.; López, F.; Browne, W. R.; Correa, A.; Peña, D.; Badorrey, R.; Meetsma, A.; Minnaard, A. J.; Feringa, B. L. *J. Am. Chem. Soc.* **2006**, *128*, 9103-9118.
- (105) White, J. D.; Shin, H.; Kim, T.-S.; Cutshall, N. S. *J. Am. Chem. Soc.* **1997**, *119*, 2404-2419.
- (106) Macrae, C. F.; Bruno, I. J.; Chisholm, J. A.; Edgington, P. R.; McCabe, P.; Pidcock, E.; Rodriguez-Monge, L.; Taylor, R.; van de Streek, J.; Wood, P. A. *J. Appl. Cryst.* **2008**, *41*, 466-470.
- (107) Kürti, L.; Czakó, B. *Strategic Applications of Named Reactions in Organic Synthesis*; Academic Press, 2005.
- (108) De Luca, L.; Giacomelli, G.; Porcheddu, A. *J. Org. Chem.* **2001**, *66*, 7907-7909.
- (109) Janzen, W. P.; Popa-Burke, i. G. *J. Biomol. Screening* **2009**, *14*, 444-451.
- (110) Zitha-Bovens, E.; Maas, P.; Wife, D.; Tijhuis, J.; Hu, Q.-H.; Kleinöder, T.; Gasteiger, J. *J. Biomol. Screening* **2009**, *14*, 557-565.
- (111) Kozikowski, B. A.; Burt, T. M.; Tirey, D. A.; Williams, L. E.; Kuzmak, B. R.; Stanton, D. T.; Morand, K. L.; Nelson, S. L. *J. Biomol. Screening* **2003**, *8*, 205-209.
- (112) Waybright, T. J.; Britt, J. R.; McCloud, T. G. *J. Biomol. Screening* **2009**, *14*, 708-715.
- (113) Stegemann, S.; Leveiller, F.; Franchi, D.; de Jong, H.; Lindén, H. *Eur. J. Pharm. Sci.* **2007**, *31*, 249-261.
- (114) Di, L.; Kerns, E. H. *Curr. Opin. Drug Discovery Dev.* **2005**, *8*, 495-504.
- (115) Di, L.; Fish, P. V.; Mano, T. *Drug Discovery Today* **2012**, *17*, 486-495.
- (116) Yalkowsky, S. H. *Solubility and Solubilization in Aqueous Media*; Oxford University Press: New York, 1999.
- (117) Strickley, R. G. *Pharm. Res* **2004**, *21*, 201-230.
- (118) Sanghvi, R.; Narazaki, R.; Machatha, S. G.; Yalkowsky, S. H. *AAPS PharmSciTech* **2008**, *9*, 366-376.
- (119) Pitha, J.; Szente, A.; Greenberg, J. *J. Pharm. Sci.* **1983**, *72*, 665-668.
- (120) Kurien, B. T.; Scofield, R. H. *Trends Pharmacol. Sci.* **2009**, *30*, 334-335.
- (121) Kurien, B. T.; Singh, A.; Matsumoto, H.; Scofield, R. H. *Assay Drug Dev. Technol.* **2007**, *5*, 567-576.
- (122) Sprachman, M. M.; Wipf, P. *Assay Drug Dev. Technol.* **2012**, *10*, 269-277.

- (123) Yu, X.; Li, Y.; Wu, D. *J. Mol. Catal. B: Enzym.* **2004**, *30*, 69-73.
- (124) Shareef, A.; Angove, M. J.; Wells, J. D.; Johnson, B. B. *J. Chem. Eng. Data* **2006**, *51*, 879-881.
- (125) Yalkowsky, S. H.; He, Y. *Handbook of Aqueous Solubility Data*; CRC Press: New York, 2003.
- (126) Wipf, P.; Miller, C. P. *J. Am. Chem. Soc.* **1992**, *114*, 10975-10977.
- (127) Uch, A. S.; Hesse, U.; Dressman, J. B. *Pharm. Res.* **1999**, *16*, 968-971.
- (128) Bravo-Altamirano, K.; George, K. M.; Frantz, M.-C.; LaValle, C. R.; Tandon, M.; Leimgruber, S.; Sharlow, E. R.; Lazo, J. S.; Wang, Q. J.; Wipf, P. *ACS Med. Chem. Lett.* **2011**, *2*, 154-159.
- (129) George, K. M.; Frantz, M.-C.; Bravo-Altamirano, K.; LaValle, C. R.; Tandon, M.; Leimgruber, S.; Sharlow, E. R.; Lazo, J. S.; Wang, Q. J.; Wipf, P. *Pharmaceutics* **2011**, *3*, 186-228.
- (130) Sharlow, E. R.; Giridhar, K. V.; LaValle, C. R.; Chen, J.; Leimgruber, S.; Barrett, R.; Bravo-Altamirano, K.; Wipf, P.; Lazo, J. S.; Wang, Q. J. *The Journal of Biological Chemistry* **2008**, *283*, 33516-33526.
- (131) Li, D. B.; Rogers-Evans, M.; Carreira, E. M. *Org. Lett.* **2011**, *13*, 6134-6136.
- (132) Cheng, X.; Hochlowski, J.; Tang, H.; Hepp, D.; Beckner, C.; Kantor, S.; Schmitt, R. *J. Biomol. Screening* **2003**, *8*, 292-304.
- (133) Prinsep, M. R.; Moore, R. E.; Levine, I. A.; Patterson, G. M. L. *J. Nat. Prod.* **1992**, *55*, 140-142.
- (134) Diao, T.; Stahl, S. S. *J. Am. Chem. Soc.* **2011**, *133*, 14566-14569.
- (135) Donnelly, E. H.; Nemhauser, J. B.; Smith, J. M.; Kazzi, Z. N.; Farfán, E. B.; Chang, A. S.; Naem, S. F. *South. Med. J.* **2010**, *103*, 541-544.
- (136) Jiang, J.; Belikova, N. A.; Hoyer, A. T.; Zhao, Q.; Epperly, M. W.; Greenberger, J. S.; Wipf, P.; Kagan, V. E. *Int. J. Rad. Biol. Phys.* **2008**, *70*, 816-825.
- (137) Rwigema, J.-C. M.; Beck, B.; Wang, W.; Doemling, A.; Epperly, M. W.; Shields, D.; Goff, J. P.; Franicola, D.; Dixon, T.; Frantz, M.-C.; Wipf, P.; Tyurina, Y.; Kagan, V. E.; Wang, H.; Greenberger, J. S. *Int. J. Radiat. Oncol. Biol. Phys.* **2011**, *80*, 860-868.

- (138) Greenberger, J. S.; Clump, D.; Kagan, V.; Bayir, H.; Lazo, J. S.; Wipf, P.; Li, S.; Gao, X.; Epperly, M. W. *Front. Oncol.* **2012**, *1*:59, 10.3389/fonc.2011.00059.
- (139) Mitchell, J. B.; Russo, A.; Kuppusamy, P.; Krishna, M. C. *Ann. N.Y. Acad. Sci.* **2000**, *899*, 28-43.
- (140) Hoye, A. T.; Davoren, J. E.; Wipf, P.; Fink, M. P.; Kagan, V. E. *Acc. Chem. Res.* **2008**, *41*, 87-97.
- (141) Kagan, V. E.; Bayir, H. A.; Belikova, N. A.; Kapralov, O.; Tyurina, Y. Y.; Tyurin, V. A.; Jiang, J.; Stoyanovsky, D. A.; Wipf, P.; Kochanek, P. M.; Greenberger, J. S.; Pitt, B.; Shvedova, A. A.; Borisenko, G. *Free Radical Biol. Med.* **2009**, *46*, 1439-1453.
- (142) Kagan, V. E.; Tyurin, V. A.; Jiang, J.; Tyurina, Y. Y.; Ritov, V. B.; Amoscato, A. A.; Osipov, A. N.; Belikova, N. A.; Kapralov, A. A.; Kini, V.; Vlasova, I. I.; Zhao, Q.; Zou, M.; Di, P.; Svistunenko, D. A.; Kurnikov, I. V.; Borisenko, G. G. *Nat. Chem. Biol.* **2005**, *1*, 223-232.
- (143) Kagan, V. E.; Wipf, P.; Stoyanovsky, D.; Greenberger, J. S.; Borisenko, G.; Belikova, N. A.; Yanamala, N.; Samhan Arias, A. K.; Tungekar, M.; Jiang, J.; Tyurina, Y. Y.; Ji, J.; Klein-Seetharaman, J.; Pitt, B. R.; Shvedova, A. A.; Bayir, H. *Adv. Drug Delivery Rev.* **2009**, *61*, 1375-1385.
- (144) Yin, H.; Zhu, M. *Free Radical Res.* **2012**, *46*, 959-974.
- (145) Frantz, M.-C.; Wipf, P. *Environ. Mol. Mutagen.* **2010**, *51*, 462-475.
- (146) Williams Jr., C. H. *Eur. J. Biochem.* **2000**, *267*, 6101.
- (147) Culotta, V. C.; Yang, M.; O'Halloran, T. V. *Biochim. Biophys. Acta* **2006**, *1763*, 747-758.
- (148) Kurtz Jr., D. M. *Acc. Chem. Res.* **2004**, *37*, 902-908.
- (149) Bernard, M. E.; Kim, H.; Berhane, H.; Epperly, M. W.; Franicola, D.; Zhang, X.; Houghton, F.; Shields, D.; Wang, H.; Bakkenist, C. J.; Frantz, M.-C.; Forbeck, E. M.; Goff, J. P.; Wipf, P.; Greenberger, J. S. *Radiat. Res.* **2011**, *176*, 603-612.
- (150) Frantz, M.-C.; Pierce, J. G.; Pierce, J. M.; Kangying, L.; Qingwei, W.; Johnson, M.; Wipf, P. *Org. Lett.* **2011**, *13*, 2318-2321.
- (151) Kanai, A.; Zabbarova, I.; Amoscato, A.; Epperly, M.; Xiao, J.; Wipf, P. *Org. Biomol. Chem.* **2007**, *5*, 307-309.

- (152) Wipf, P.; Xiao, J.; Jiang, J.; Belikova, N. A.; Tyurin, V. A.; Fink, M. P.; Kagan, V. E. *J. Am. Chem. Soc.* **2005**, *127*, 12460-12461.
- (153) Blinco, J. P.; Hodgson, J. L.; Morrow, B. J.; Walker, J. R.; Will, G. D.; Coote, M. L.; Bottle, S. E. *J. Org. Chem.* **2008**, *73*, 6763-6771.
- (154) Epperly, M. W.; Gretton, J. E.; Sikora, C. A.; Jefferson, M.; Berarding, M.; Nie, S.; Greenberger, J. S. *Radiat. Res.* **2003**, *160*, 568-578.
- (155) Epperly, M. W.; Gretton, J. E.; Defillippi, S. J.; Sikora, C. A.; Liggitt, D.; Koe, G.; Greenberger, J. S. *Radiat. Res.* **2001**, *155*, 2-14.
- (156) Schlüter, T.; Struy, H.; Schönfeld, P. *FEBS Lett.* **2000**, *481*, 42-46.
- (157) Murphy, M. P.; Smith, R. A. *J. Annu. Rev. Pharmacol. Toxicol.* **2007**, *47*, 629-656.
- (158) Wipf, P.; Xiao, J. *Org. Lett.* **2005**, *7*, 103-106.
- (159) Solubilities were determined by Ms. Kayla Lloyd and Dr. Joshua Sacher.
- (160) Ashwood-Smith, M. J. *Int. J. Rad. Biol.* **1961**, *3*, 41-48.
- (161) Littlefield, L. G.; Joiner, E. E.; Colyer, S. P.; Sayer, A. M.; Frome, E. L. *Int. J. Rad. Biol.* **1988**, *53*, 875-890.
- (162) Vos, O.; Kaalen, M. C. A. C. *Int. J. Rad. Biol.* **1962**, *5*, 609-621.
- (163) Veltwisch, D.; Janata, E.; Asmus, K.-D. *J. Chem. Soc., Perkin Trans. 2* **1980**, 146-153.
- (164) Herscu-Kluska, R.; Masarwa, A.; Saphier, M.; Cohen, H.; Meyerstein, D. *Chem. Eur. J.* **2008**, *14*, 5880-5889.
- (165) Li, B.; Gutierrez, P. L.; Amstad, P.; Blough, N. V. *Chem. Res. Toxicol.* **1999**, *12*, 1042-1049.
- (166) Watanabe, M.; Suzuki, M.; Suzuki, K.; Hayakawa, Y.; Miyazaki, T. *Radiat. Res.* **1990**, *124*, 73-78.
- (167) Ueda, T.; Toyoshima, Y.; Kushihashi, T.; Hishida, T.; Yasuhara, H. *J. Toxicol. Sci.* **1993**, *18*, 239-244.
- (168) Personal communication: Epperly, M. W.; Shields, D.; Dixon, T. M.; Cao, S.; Goff, J. P.; Greenberger, J. S., MMS350: a novel bifunctional sulfoxide with radiation protection and mitigation properties.

- (169) Goff, J. P.; Shields, D.; wang, H.; Skoda, E. M.; Sprachman, M. M.; Wipf, P.; Atkinson, J.; London, B.; Lazo, J. S.; Kagan, V.; Epperly, M.; Greenberger, J. S. *Exp. Hematol.* **2012**, *Manuscript Submitted for Publication*.
- (170) Personal communication: Goff, J. P.; Epperly, M. W.; Dixon, T. M.; Zhang, X.; Greenberger, J. S., Live Imaging of Luciferase Positive Bone Marrow Stromal Cell Migration to Form Radiation Pulmonary Fibrosis.
- (171) Personal communication: Kalash, R.; Epperly, M.; Greenberger, J. S., MMS350 is downregulating the expression of VEGF and vWF Specifically in Pulmonary Endothelial Cells.
- (172) Epperly, M. W.; Kalash, R.; Dixon, T.; Sprachman, M. M.; Zhang, X.; Shields, D.; Cao, S.; Wipf, P.; Berhane, H.; Greenberger, J. S. *Radiat. Res.* **2012**, *Manuscript submitted*.
- (173) Burkhard, J. A.; Wagner, B.; Fischer, H.; Schuler, F.; Müller, K.; Carreira, E. M. *Angew. Chem. Int. Ed.* **2010**, *49*, 3524-3527.
- (174) Eicher, T.; Hauptmann, S. *The Chemistry of Heterocycles*; WILEY-VCH GmbH & Co. KGaA: Weinheim, 2003.
- (175) Dorofeeva, O. V.; Mastryukov, V. S. *J. Mol. Struct.* **1981**, *75*, 225-240.
- (176) López, J. C.; Blanco, S.; Lesarri, A.; Alonso, J. L. *J. Chem. Phys.* **2001**, *114*, 2237-2250.
- (177) Verkade, J. M. M.; van Hemert, L. J. C.; Quaedflieg, P. J. L. M.; Alsters, P. L.; van Delft, F. L.; Rutjes, F. P. J. T. *Tetrahedron Lett.* **2006**, *47*, 8109-8113.
- (178) Burkhard, J.; Carreira, E. M. *Org. Lett.* **2008**, *10*, 3525-3526.
- (179) Burkhard, J. A.; Guérot, C.; Knust, H.; Rogers-Evans, M.; Carreira, E. M. *Org. Lett.* **2010**, *12*, 1944-1947.
- (180) Druzhilovsky, D. S.; Filimonov, D. A.; Liao, C.; Peach, M.; Nicklaus, M.; Poroikov, V. V. *Biochemistry (Moscow) Supplement Series B: Biomedical Chemistry* **2010**, *4*, 59-67.
- (181) Ioakimidis, L.; Thoukydidis, L.; Mirza, A.; Naeem, S.; Reynisson, J. *QSAR Comb. Sci.* **2008**, 445-456.
- (182) Yazdanian, M.; Glynn, S. L.; Wright, J. L.; Hawi, A. *Pharm. Res.* **1998**, *15*, 1490-1494.
- (183) Irvine, J. D.; Takahshi, L.; Lockhart, K.; Cheong, J.; Tolan, J. W.; Selick, H. E.; Grove, J. R. *J. Pharm. Sci.* **1999**, *88*, 28-33.

- (184) Asefa, T.; Tao, Z. *Chem. Res. Toxicol.* **2012**, doi. 10.1021/tx300166u.
- (185) Yoshitomi, T.; Suzuki, R.; Mamiya, T.; Matsui, M.; Hirayama, A.; Nagasaki, Y. *Bioconjugate Chem.* **2009**, *20*, 1792-1798.
- (186) Faraji, A. H.; Wipf, P. *Bioorg. Med. Chem.* **2009**, *17*, 2950-2962.
- (187) Barreto, J. A.; O'Malle, W.; Kubell, M.; Graham, B.; Stephan, H.; Spiccia, L. *Adv. Mater.* **2011**, *23*, H18-H40.
- (188) Huynh, N. T.; Roger, E.; Lautram, N.; Benoit, J.-P.; Passirani, C. *Nanomedicine* **2010**, *5*, 1415-1433.
- (189) Jafarzadeh, M.; Rahman, I. A.; Sipaut, C. S. *J Sol-Gel Sci. Technol.* **2009**, *50*, 328-336.
- (190) Stöber, W.; Fink, A.; Bohn, E. *J. Colloid Interface Sci.* **1968**, *26*, 62-69.
- (191) Pang, J.; Luan, Y.; Yang, X.; Jiang, Y.; Zhao, L.; Zong, Y.; Li, Z. *Mini Rev. Med. Chem.* **2012**, *12*, 775-788.
- (192) Napierska, D.; Thomassen, L. C. J.; Rabolli, V.; Lison, D.; Gonzalez, L.; Kirsch-Volders, M.; Martens, J. A.; Hoet, P. H. *Small* **2009**, *5*, 846-853.
- (193) Tao, Z.; Toms, B. B.; Goodisman, J.; Asefa, T. *Chem. Res. Toxicol.* **2009**, *22*, 1869-1880.
- (194) Lin, Y.-S.; Haynes, C. L. *J. Am. Chem. Soc.* **2010**, *132*, 4834-4842.
- (195) Chang, J.-S.; Chang, K. L. B.; Hwang, D.-F.; Kon, Z.-L. *Environ. Sci. Technol.* **2007**, *41*, 2064-2068.
- (196) Singh, N.; Karambelkar, A.; Gu, L.; Lin, K.; Miller, J. S.; Chen, C. S.; Sailor, M. J.; Bhatia, S. N. *J. Am. Chem. Soc.* **2011**, *133*, 19582-19585.
- (197) Veeranarayanan, S.; Poulouse, A. C.; Mohamed, S.; Aravind, A.; Nagaoka, Y.; Yoshida, Y.; Maekawa, T.; Kumar, D. S. *J. Fluoresc.* **2012**, *22*, 537-548.
- (198) Barandeh, F.; Nguyen, P.-L.; Kumar, R.; Iacobucci, G. J.; Kuznicki, M. L.; Kosterman, A.; Bergey, E. J.; Prasad, P. N.; Gunawardena, S. *PLoS One* **2012**, *7*, 1-15.
- (199) Hu, L.; Mao, Z.; Zhang, Y.; Gao, C. *J. Nanosci. Lett.* **2011**, *1*, 1-16.
- (200) He, X.; Nie, H.; Wang, K.; Tan, W.; Wu, X.; Zhang, P. *Anal. Chem.* **2008**, *80*, 9597-9603.
- (201) Huang, X.; Li, L.; Liu, T.; Hao, N.; Liu, H.-L.; Chen, D.; Tang, F. *ACS Nano* **2011**, *5*, 5390-5399.

- (202) He, Q.; Zhang, Z.; Gao, F.; Li, Y.; Shi, J. *Small* **2011**, *7*, 271-280.
- (203) Lu, J.; Liong, M.; Li, Z.; Zink, J. I.; Tamanoi, F. *Small* **2010**, *6*, 1794-1805.
- (204) Serda, R. E.; Mack, A.; van de Ven, A. L.; Ferrati, S.; Dunner Jr., K.; Godin, B.; Chiappini, C.; Landry, M.; Brousseau, L.; Liu, X.; Bean, A. J.; Ferrari, M. *Small* **2010**, *6*, 2691-2700.
- (205) Sharpe, E.; Andreescu, D.; Andreescu, S. In *Oxidative Stress: Diagnostics, Prevention, and Therapy*; American Chemical Society: Washington, DC, 2011, p 235-253.
- (206) Heckert, E. G.; Karakoti, A. S.; Seal, S.; Self, W. T. *Biomaterials* **2008**, *29*, 2705-2709.
- (207) Korsvik, C.; Patil, S.; Seal, S.; Self, W. T. *Chem. Commun.* **2007**, 1056-1058.
- (208) Nie, Z.; Liu, K. J.; Zhong, C.-J.; Wang, L.-F.; Yang, Y.; Tian, Q.; Liu, Y. *Free Radical Biol. Med.* **2007**, *43*, 1243-1254.
- (209) Yen, F.-L.; Wu, T.-H.; Tzeng, C.-W.; Lin, L.-T.; Lin, C.-C. *J. Agric. Food Chem* **2010**, *58*, 7376-7382.
- (210) Kumari, A.; Yadav, S. K.; Pakade, Y. B.; Singh, B.; Yadav, S. C. *Colloids Surf., B* **2010**, *80*, 184-192.
- (211) Yoshitomi, T.; Hirayama, A.; Nagasaki, Y. *Biomaterials* **2011**, *32*, 8021-8028.
- (212) Qiu, L.; Zheng, C.; Zhao, Q. *Mol. Pharmaceutics* **2012**, *9*, 1109-1117.
- (213) Miyata, K.; Oba, M.; Nakanishi, M.; Fukushima, S.; Yamasaki, Y.; Koyama, H.; Nishiyama, N.; Kataoka, K. *J. Am. Chem. Soc.* **2008**, *130*, 16287-16294.
- (214) He, Q.; Gao, Y.; Zhang, L.; Bu, W.; Chen, H.; Li, Y.; Shi, J. *J. Mater. Chem.* **2011**, *21*, 15190-15192.
- (215) Lu, D.; Wen, x.; Liang, J.; Gu, Z.; Zhang, X.; Fan, Y. *J. Biomed. Mat. Res. Part B: Appl. Biomaterials* **2008**, *89*, 177-183.
- (216) Sung, H.-W.; Sonaje, K.; Liao, Z.-X.; Hsu, L.-W.; Chuang, E.-Y. *Acc. Chem. Res.* **2012**, *45*, 619-629.
- (217) Ke, C.-J.; Su, T.-Y.; Chen, H.-L.; Liu, H.-L.; Chiang, W.-L.; Chu, P.-C.; Xia, Y.; Sung, H.-W. *Angew. Chem. Int. Ed.* **2011**, *50*, 8086-8089.
- (218) Gan, Q.; Lu, X.; Yuan, Y.; Qian, J.; Zhou, H.; Lu, X.; Shi, J.; Liu, C. *Biomaterials* **2011**, *32*, 1932-1942.

- (219) Aznar, E.; Marcos, M. D.; Martinez-Mañez, R.; Sancenón, F.; Soto, J.; Amorós, P.; Guillem, C. *J. Am. Chem. Soc.* **2009**, *131*, 6833-6843.
- (220) Yoshitomi, T.; Nagasaki, Y. *Nanomedicine* **2011**, *6.3*, 509.
- (221) Wipf, P.; Wang, C. *Org. Lett.* **2006**, *8*, 2381-2384.
- (222) Wipf, P.; Venkatraman, S. *J. Org. Chem.* **1995**, *60*, 7224-7229.
- (223) Wipf, P.; Uto, Y. *J. Org. Chem.* **2000**, *65*, 1037-1049.
- (224) Hargaden, G. C.; Guiry, P. J. *Chem. Rev.* **2009**, *109*, 2505-2550.
- (225) Desimoni, G.; Faita, G.; Jørgensen, K. A. *Chem. Rev.* **2011**, *111*, PR284-PR437.
- (226) Moraski, G. C.; Chang, M.; Villegas-Estrada, A.; Franzblau, S. G.; Möllmann, U.; Miller, M. J. *Eur. J. Med. Chem.* **2010**, *45*, 1703-1716.
- (227) Bundgaard, H.; Johansen, M. *Int. J. Pharm.* **1982**, *10*, 165-175.
- (228) Burr, A.; Bundgaard, H. *Int. J. Pharm.* **1988**, *46*, 159-167.
- (229) Kempe, K.; Lobert, M.; Hoogenboom, R.; Schubert, U. S. *J. Comb. Chem.* **2009**, *11*, 274-280.
- (230) Mohammadpoor-Baltork, I.; Khosropour, A. R.; Hojati, S. F. *Synlett* **2005**, 2747-2750.
- (231) Wipf, P.; Venkatraman, S. *Tetrahedron Lett.* **1996**, *37*, 4659-4662.
- (232) Wipf, P.; Miller, C. P. *Tetrahedron Lett.* **1992**, *33*, 907-910.
- (233) Phillips, A. J.; Uto, Y.; Wipf, P.; Reno, M. J.; Williams, D. R. *Org. Lett.* **2000**, *2*, 1165-1168.
- (234) Boissnard, S.; Neuville, L.; Bois-Choussy, M.; Zhu, J. *Org. Lett.* **2000**, *2*, 2459-2462.
- (235) Wipf, P.; Miller, C. P. *J. Org. Chem.* **1993**, *58*, 1575-1578.
- (236) Colwell, A. R.; Duckwall, L. R.; Brooks, R.; McManus, S. P. *J. Org. Chem.* **1981**, *46*, 3097-3102.
- (237) Coste, J.; Frérot, E.; Jouin, P. *J. Org. Chem.* **1994**, *59*, 2437-2446.
- (238) Personal communication with Dr. Valerian E. Kagan and Dr. Wei Hong Feng.
- (239) Personal communication: Feng, W. H. K., V. E., Silica nanoparticle project update.
- (240) Gujadhur, R.; Venkataraman, D.; Kintigh, J. T. *Tetrahedron Lett.* **2001**, *42*, 4791-4793.
- (241) Ziegler, F. E.; Fowler, K. W.; Rodgers, W. B.; wester, R. T. *Org. Synth.* **1987**, *65*, 108.
- (242) Tyurin, V. A.; Kagan, V. E., Personal communication: SiO₂ Nanoparticle progress report.

- (243) Pon, R. T. *Curr. Protoc. Nucleic Acid Chem.* **2000**, *3*, 3.2.1-3.2.23.
- (244) Iyer, R. P.; Padmanabhan, S.; Coughlin, J. E. **2005**, *3*, 3.13.1-3.13-18.
- (245) Damha, M. J.; Giannaris, P. A.; Zabarylo, S. V. *Nucleic Acids Res.* **1990**, *18*, 3813-3821.
- (246) Brimble, M. A.; Kowalczyk, R.; Harris, P. W. R.; Dunbar, P. R.; Muir, V. J. *Org. Biomol. Chem.* **2008**, *6*, 112-121.
- (247) Dzygiel, P.; Monti, C.; Piarulli, U.; Gennari, C. *Org. Biomol. Chem.* **2007**, *5*, 3464-3471.
- (248) Schaus, S. E.; Brandes, B. D.; Larrow, J. F.; Tokunaga, M.; Hansen, K. B.; Gould, A. E.; Furrow, M. E.; Jacobsen, E. N. *J. Am. Chem. Soc.* **2002**, *124*, 1307-1315.
- (249) Burgess, E. M.; Penton, H. R.; Taylor, E. A.; Williams, W. M.; Nottke, J. E.; Benson, R. E. *Org. Synth.* **1977**, *56*, 40-42.
- (250) Öhrlein, R.; Schwab, W.; Ehrler, R.; Jäger, V. *Synthesis* **1986**, 535-538.
- (251) Silva, P. C.; Costa, J. S.; Pereira, V. L. P. *Synth. Commun.* **2001**, *31*, 595-600.
- (252) O'Neil, I. A.; Bhamra, I.; Gibbons, P. D. *Chem. Commun.* **2006**, *43*, 4545-4547.
- (253) Buchwald, S. L.; LaMaire, S. J.; Nielsen, R. B.; Watson, B. T.; King, S. M. *Org. Synth.* **1993**, *71*, 77-80.
- (254) Brugat, N.; Duran, J.; Polo, A.; Real, J.; Álvarez-Larena, Á.; Piniella, J. F. *Tetrahedron: Asymmetry* **2002**, *13*, 569-577.
- (255) Gurjar, M. K.; Sarma, B. V. N. B. S.; Sadalapure, K.; Adhikan, S. *Synthesis* **1998**, *10*, 1424.
- (256) Weber, E. *J. Org. Chem.* **1982**, *47*, 3478-3486.
- (257) Niu, T.; Zhang, W.; Huang, D.; Xu, C.; Wang, H.; Hu, Y. *Org. Lett.* **2009**, *11*, 4474-4477.
- (258) Bartroli, J.; Turmo, E.; Algueró, M.; Boncompte, E.; Vericat, M. L.; García-Rafanell, J.; Forn, J. *J. Med. Chem.* **1995**, *38*, 3918-3932.
- (259) Ueno, S.; Shimizu, R.; Kuwano, R. *Angew. Chem. Int. Ed.* **2009**, *48*, 4543-4545.
- (260) da Ribeiro, R. S.; Esteves, P. M.; Mattos, M. C. S. *Synthesis* **2011**, *5*, 739-744.
- (261) Baret, P.; Beaujolais, V.; Béguin, C.; Gaude, D.; Pierre, J.-L.; Serratrice, G. *Eur. J. Inorg. Chem.* **1998**, 613-619.

- (262) He, P.; Dong, C.-G.; Hu, Q.-S. *Org. Lett.* **2007**, *9*, 343-346.
- (263) Evans, D. A.; Michael, F. E.; Tedrow, J. S.; Campos, K. R. *J. Am. Chem. Soc.* **2003**, *125*, 3534-3543.
- (264) Biswas, S.; Maiti, S.; Jana, U. *Eur. J. Org. Chem.* **2010**, *15*, 2861-2866.
- (265) Meyer, B. N.; Ferrigni, N. R.; Putnam, J. E.; Jacobsen, L. B.; Nichols, D. E.; McLaughlin, J. L. *Planta Med.* **1982**, *45*, 31-34.
- (266) Ottanà, R.; Maccari, R.; Barreca, M. L.; Bruno, G.; Rotondo, A.; Rossi, A.; Chiricosta, G.; Di Paola, R.; Sautebin, L.; Cuzzocrea, S.; Vigorita, M. G. *Bioorg. Med. Chem.* **2005**, *13*, 4243-4252.
- (267) Lehnher, D.; McDonald, R.; Ferguson, M. J.; Tykwinski, R. R. *Tetrahedron* **2008**, *64*, 11449-11461.
- (268) Sessler, J. L.; Wang, B.; Harriman, A. *J. Am. Chem. Soc.* **1995**, *117*, 704-714.
- (269) Kita, Y.; Akai, S.; Ajimura, N.; Yoshigi, M.; Tsugoshi, T.; Yasuda, H.; Tamura, Y. *J. Org. Chem.* **1986**, *51*, 4150-4158.
- (270) McCarthy, O.; Musso-Buendia, A.; Kaiser, M.; Brun, R.; Ruiz-Perez, L. M.; Johansson, N. G.; Pacanowska, D. G.; Gilbert, I. H. *Eur. J. Med. Chem.* **2009**, *44*, 678-688.
- (271) Diéguez, M.; Parnies, O. *Chem.-Eur. J.* **2008**, *14*, 3653-3669.
- (272) Ferreira, P. M. T.; Monteiro, L. S.; Pereira, G. *Eur. J. Org. Chem.* **2008**, 4676-4683.
- (273) Ferreira, P. M., T.; Monteiro, L. S.; Pereira, G. *Eur. J. Org. Chem.* **2008**, 4676-4683.
- (274) Fukuhara, T.; Hasegawa, C.; Hara, S. *Synthesis* **2007**, 1528-1534.